EFFECT OF EARTHQUAKES ON PERFORMANCE-BASED DESIGN

EFFECT OF EARTHQUAKE CHARACTERISTICS ON PERFORMANCE-BASED DESIGN

By

NOHA ABDELAZIZ, B.Sc.

A Thesis

Submitted to the School of Graduate Studies

in Partial Fulfillment of the Requirements

for the Degree

Master of Applied Science

McMaster University

MASTER OF APPLIED SCIENCE — McMaster University

(Civil Engineering) — Hamilton, Ontario

TITLE: Effect of Earthquake Characteristics on Performance-based Design

AUTHOR: Noha Abdelaziz, B.Sc. (Ain Shams University, Cairo, Egypt)

SUPERVISOR: Dr. A. Ghobarah

NUMBER OF PAGES: xiii, 152, A.30, B.30.

ABSTRACT

Building codes are undergoing a conceptual transition stage. Codes now are directed towards utilizing the concept of performance-based design engineering. Performance-based seismic engineering expresses the design criteria in terms of achieving certain performance objectives when the structure is subjected to defined seismic hazard levels. Recent seismic events highlighted the significance of applying multiple performance objectives in the design criteria of the structure.

The objective of this study is to investigate the development of design yield spectra and to evaluate the various factors that affect its general characteristics. The study addresses the effect of near-fault (NF) and far-field (FF) earthquakes, the magnitude of the earthquake, the directivity effect and the effect of different types of soils on the yield spectra using actual earthquake ground-motion records. Permissible design regions representing the different earthquake hazards are formed in order to develop design spectra suitable for code application.

Actual earthquake records are used in this study to conduct realistic analysis and make valid response comparisons. Records are classified according to the points of investigation. For the analysis, a SDOF system is subjected to the chosen set of ground motions scaled to different peak ground acceleration levels. Linear and nonlinear dynamic analyses of the system are performed. The yield spectra are formed using the analysis results. The effect of each of the classification categories on the spectra formation is investigated.

To attain multiple performance objectives in the yield spectra method, a graphical procedure is formed to develop an admissible design region plot in which the combinations of strength and stiffness serve these multiple objectives.

The yield spectra (YS) design procedure is outlined. An example for using the YS design procedure in combination with the admissible design region plot is illustrated. An investigation of the effectiveness of this procedure, and where it lies within the spectrum of available methods is discussed.

ACKNOWLEDGEMENTS

I would like to express my gratitude to many people who have made my graduate studies meaningful and who have given me numerous hours of support during my Master's program at McMaster University. First, I would like to thank Dr. A. Ghobarah, my senior supervisor during the course of this work, for his guidance and for giving me the opportunity for academic advancement. Without his careful supervision, encouragement, assistance and feedback, this thesis would not have been completed.

Next, I wish to thank my family for their encouragement and support in my academic pursuits. I would also like to extend my love and appreciation to my husband Ahmed Fakhr for his constant support in the pursuit of my dreams.

My acknowledgements would not be complete without expressing my thanks towards Allah, who has given me the strength to overcome all the difficulties in my life. I feel very fortunate to have had the opportunity to study this amazing world from the point of engineering. Without his love and guidance through the years, I would not have had the courage to pursue graduate studies.

TABLE OF CONTENTS

LIST OF TABLES

LIST OF FIGURES

1. INTRODUCTION

CHAPTER 1

INTRODUCTION

1.1 LITERATURE REVIEW

One of the major developments in seismic design through the last decade is the evolution of Performance-Based Engineering (PBE). Conventional Seismic design has been entirely force-based, with a final check on the structural displacements for serviceability requirements. The primary design parameter of codes is the period of structure. Performance was considered a secondary issue that often related to strength. However, recent earthquakes demonstrated the difference between the performance and strength and showed that increasing strength may not improve the performance of the structure nor reduce the damage. This focused the need for a fundamental change in seismic design and pointed the research towards the new concept of performance-based design.

1.1.1 PERFORMANCE-BASED DESIGN

The objective of the performance-based design is to design the structure to achieve multiple performance objectives. In other words, the structure is required to meet several stated levels of performance given various expected levels of seismic ground motion. The performance targets may be a level of stress not to be exceeded, a load, a displacement, a limit state or target damage state (Ghobarah 2001). Generally, the performance of the structure is related to the level of damage, hence the maximum displacement (drift) is a good indicator of the structure damage level. This may explain

the use of the terminology Displacement–based design (DBD) as a sub item of Performance-based design. Performance-based engineering is a much broader approach that includes performance-based design, construction and lifelong maintenance of the structure.

1.1.2 FORCE-BASED AND DISPLACEMENT-BASED DESIGN

Bommer and Elnashai (1998) explained the basic difference between the force-based and the displacement-based methods of design. The primary input to the force-based design is a set of forces with a check on the level of the corresponding deformation to verify whether it is equal to or higher than the acceptable serviceability limits. Meanwhile, the primary design quantity in the displacement-based approach is a target displacement. If the level of damping corresponding to the target displacement of an equivalent linear system is known, the period of the structure may be estimated. Knowing the required period of vibration, the designer can dimension the structure with the stiffness, strength and ductility that ensure achieving the target displacement.

Priestley and Kowalsky (2000) discussed the incorporation of foundation flexibility in the displacement-based design procedure. Flexible foundation effects will increase the elastic period of the structure, hence imply reduced seismic design forces. It will also reduce the displacement ductility, and hence reduce the force-reduction factors. The relation between the seismic intensity and the base shear is fundamentally different in the two methods (displacement-based and force-based design procedures). The required base shear is proportional to the square of the seismic intensity in the displacement-based procedure, whereas in force-based design the relation is linear.

Priestly and Kowalsky showed that the displacement-based design approach is simple to apply and should result in uniform levels of seismic risk. Significant differences in seismic performance can be expected from structures designed to the displacement-based design procedure when compared with conventional force-based design approach.

1.1.3 PERFORMANCE OBJECTIVES

Vision 2000 (SEAOC, 1995) defines the performance objective as "an expression of the desired performance level for each earthquake design level". Ghobarah (2001) defined four performance levels with the acceptable damage state and the allowable drift limits as summarized in Table 1.1. Performance Levels are associated with earthquake hazard and design levels as given by Table 1.2.

1.1.4 DISPLACEMENT-BASED DESIGN PROCEDURES

Different DBD procedures have been proposed in recent years but only few of them were developed to a point suitable for implementation in design codes. These methods are discussed subsequently with a final comparison between them based on various aspects such as simplicity and completeness. The design procedures are summarized in the form of flowcharts.

1.1.4.1 DEFORMATION CONTROLLED SEISMIC DESIGN (Panagiotakos and Faradis 1999)

The approach is to perform elastic analysis for a "serviceability" earthquake (equivalent to EQ-I). The reinforcement in the structure is determined based on the resulting forces. The final longitudinal and transverse reinforcement in the member

critical sections are such that the peak inelastic deformation of the member does not exceed the allowable deformations under "Life safety" seismic action (equivalent to EQ-IV). The general procedure is illustrated in the flowchart shown in Figure 1.1.

The use of the uncracked model of structure in the initial elastic design to EQ-I gives higher design forces and moments when compared to other methods. Other methods recommend the use of section properties modified to allow for cracking observed in structures at the point of yield.

Further investigation of the design procedure is still required. The method does not recommend expressions for allowable ultimate rotations of wall structures. The proposed procedure does not provide recommendations for designing structures with flexible foundations. The inelastic rotation amplification factors for estimating upper chord-rotation demands are given. However, when applying the procedure to various case studies, it is not clear that the amplification factors still apply to these cases as in case of wall structures.

1.1.4.2 PROPORTIONING OF RC STRUCTURES DESIGN (Browning 2001)

The premise of this method is that controlling the mass-stiffness relationship in the building period will control the lateral drift since the expected drift of a structure is a function of its mass and stiffness and their distribution (Browning 2001). This explains that it is a target period method that aims to achieve a certain drift limit. The general procedure is illustrated in the flowchart shown in Figure 1.2. In the flowchart T_t refers to the maximum target period, T_i is the structure period, V_b is the base shear and C_y is the minimum base shear strength coefficient. This method is generally easy to apply.

However, it requires a number of iterations to satisfy its target. The method doesn't address the inelastic rotation demands and ductility limits.

According to Sullivan (2002) the method provides strength that is more than 5 times that of other design methods. He attributed this to the use of gross uncracked section properties in determining the structural period that is used with acceleration response spectra to obtain the design base shear coefficient. He suggested also that the larger design strength might be due to the use of an acceleration amplification factor intended to allow for a wide range of ground motions.

1.1.4.3 YIELD POINT SPECTRA DESIGN (Aschheim and Black 2000)

The yield point spectra (YPS) method is a new spectral representation of seismic demand. It aims to use the capacity curve in conjunction with YPS to constrain the combinations of strength and stiffness to target drift limits and ductility values to satisfy a number of performance objectives. Permissible design regions for the different earthquakes can be plotted on the same axes of the YPS. Knowing the structure's yield displacement, the strength required to satisfy all ductility and drift limits can be obtained from the graph in one-step. The general procedure is illustrated in the flowchart shown in Figure 1.3. The YPS plot the yield points for oscillators having constant displacement ductility for a range of oscillator periods on the axes representing the yield strength coefficient and the yield displacement.

The yield displacement is relatively stable as the base shear strength is modified. This makes it easy to determine the base shear strength required to satisfy multiple

performance objectives. The method provides acceptable drift and ductility values. It provides low base shear and thus cost effective design in comparison with other methods. In the flowchart, C_y is the yield strength coefficient, Δ_y is the yield displacement, μ is the ductility and Δ_T is the target displacement.

1.1.4.4 SEISMIC DESIGN WITH ADVANCED ANALYTICAL TECHNIQUES (Kappos and Manafpour 2000)

Kappos and Manafpour developed a different design model in that it uses force-based design approach to establish a basic strength level of the structure for an elastic response to EQ-I. A model is then constructed in which the beams are modeled as yielding members to exhibit inelastic behaviour. Two time-history analyses of the model are conducted for EQ-II (occasional earthquake) and EQ-IV to check the drift and ductility limits and detailing of members. The general procedure is illustrated in the flowchart shown in Figure 1.4.

This method uses a partial inelastic model of the structure. This means that moderate amount of cracking is considered rather than being fully cracked as in other procedures. According to Kappos, using fully cracked section for the entire member might lead to underestimation of the ductility demands. The proposed procedure accounts explicitly for higher mode effects in the inelastic structure. It addresses non-uniform yielding of beams, and fluctuation of the axial loading. The process deals with many of the uncertainties regarding the strength level at the beam-column joints through the model used for the dynamic time history analysis.

Unlike other procedures, no need exists for reducing the structure to an "equivalent" SDOF system. The basic analytical model directly provides design forces and moments for all members. However, the method may be considered as time consuming since multiple time history analyses are required.

1.1.4.5 DBD USING INELASTIC DESIGN SPECTRA (Chopra and Goel 2001)

In this method, a target yield displacement and design ductility are estimated. Introducing these parameters into the inelastic design spectra, a period and initial stiffness are established. Knowing the initial stiffness and the yield displacement, the required yield strength can be determined. The general procedure is illustrated in the flowchart shown in Figure 1.5.

The method includes the drift limits within the design limits while providing only a low level of strength (Sullivan 2002). However, the method is not complete as a design tool as it only addresses SDOF systems. It does not provide recommendation for the distribution of the base shear along the height of the structure and it does not deal with structures with flexible foundation. In the flowchart, h is the height of the structure, T_n is the fundamental period of the structure, M is the mass, and f_y is the yield strength.

1.1.4.6 CAPACITY SPECTRUM METHOD (Freeman 1998)

In the method proposed by Freeman (1998), the capacity spectrum for the structure is superimposed onto a group of demand spectra for different ductility/damping levels to check the building performance. The general procedure is explained in the flowchart

shown in Figure 1.6. In the flowchart S_a is the spectral acceleration, and S_d is the spectral displacement.

The procedure performs well since target design parameters are not exceeded and the required strength is not excessive. However, Freeman does not recommend a particular method to develop demand spectra for different levels of damping. Freeman does not provide a recommended procedure for the design of new structures for which the initial strength is unknown. He does not address which risk events should be checked or what an appropriate target displacement should be. In addition, no recommendation is made as to how the base shear should be distributed along the height of the structure (Sullivan 2002).

This indicates that Freeman's method requires further research to clear the above points to decrease the uncertainties in the estimations that has to be taken into account by the designer. At this time, Freeman's method is best suited for checking the performance of existing structures for which the initial strength is already known.

1.1.4.7 DIRECT DISPLACEMENT-BASED DESIGN (Priestley and Kowalsky 2000)

Priestley and Kowalsky (2000) proposed a relatively simple and fast method to design the structure to achieve a specified acceptable level of damage under a design earthquake. The limit is defined as a displacement profile related to limit material strains or to code specified drift limits. The elastic properties of the structure are the end products of the design rather than the starting point. The general procedure is explained in the flowchart shown in Figure 1.7.

Priestley and Kowalsky investigated the incorporation of the foundation flexibility effects. The foundation flexibility increases the system yield displacement from Δ_y to $\Delta_f+\Delta_y$ (where Δ_y is the structure yield displacement for a rigid base, and Δ_f is the displacement due to foundation flexibility). This will increase the elastic period of the structure. The displacement ductility capacity (μ) will decrease due to flexibility of foundation, hence; will reduce the force-reduction factors.

They studied the influence of the seismic intensity on base shear. The sensitivity of base shear to building height was investigated. It showed that design base shear force is independent of the number of stories. This pointed the way towards possible design simplification. Time history analysis was performed and showed excellent agreement with the target displacement profiles.

1.1.4.8 DISPLACEMENT-BASED DESIGN (SEAOC 1999)

This method is relatively fast and easy to apply to obtain the design base shear. However, several assumptions have to be made by the designer. The method designs for target drift values but ductility demands are not controlled. Four different risk events and drift limits may be considered for design depending on the performance objective. The base shear is distributed over the height of the structure with respect to the displaced shape or the code distribution with respect to mass and height (Sullivan 2002). The general procedure is illustrated in the flowchart shown in Figure 1.8. In the flowchart, DRS refers to the displacement response spectra, and the ADRS refers to acceleration-displacement response spectra.

The method performs well giving cost efficient design and in general maintaining the target design parameters. On the other hand, the method does not identify an approximate yield displacement for the structure. Checking whether the structure yield displacement is within the target displacements for the design drift limits can ensure the reliability of the effective stiffness. The effective stiffness can be adjusted if necessary. The procedure doesn't address the design of structures with flexible foundations.

1.1.5 COMPARISON BETWEEN DBD METHODS

Sullivan (2002) studied the various displacement-based design procedures discussed above, by comparing five case studies. The first case study examines 8 storey building with walls of equal dimensions in a regular layout on a rigid foundation. The second case study examines 8-storey building similar to that of case 1 but with flexible foundation. The third case examines 8-storey building with walls arranged in an irregular layout. The fourth case study examines a 7-storey regular moment resisting frame building. The fifth case study examines 8-storey frame building with vertical irregularities.

A chart is developed to highlight the strengths and weaknesses of each of the methods. The chart compares the different approaches based on simplicity, versatility, performance and completeness. The various aspects of each method are evaluated on a scale from 1 to 5, 1 being very poor and 5 being excellent. The results of this assessment are shown in Figure 1.9. It can be concluded that these displacement-based design procedures are developed to a standard suitable for implementation in the code although

further research is required to enhance the simplicity and the completeness of some of the design procedures.

One of the interesting and effective design methods is the "Yield Point Spectra" method introduced by Aschheim and Black (2000). The method allows the design to several limit states in one-step. Once the spectra are constructed, with the drift and ductility limits imposed, the procedure provides low base shear and consequently cost effective design in relation to other methods [Sullivan 2002]. However, further research is needed to develop yield spectra suitable for code applications, and study the different factors that affect its formation. Some of these factors include the effect of the near-fault and far-field earthquakes on the characteristics of the spectra, the effect of rupture directivity and the effect of different types of soils that might have significant effect on the yield displacement and hence affects the spectra as well.

1.1.6 SPECIAL FEATURES OF NEAR-FAULT EARTHQUAKES

The particular characteristics of ground motion in the near-fault zone and their potential to damage structures is a subject of considerable current interest. Near-fault effects were found to be significant within distances of 20 km of the fault. Structures designed according to current codes in the near-fault were observed to suffer significant damage during recent earthquakes. This indicated that improved representation of near-fault ground motions in seismic codes is required.

Ground motions recorded within the near-fault region of an earthquake are qualitatively quite different from the usual far-field earthquake ground motions. A long period pulse in the acceleration history that appears as a coherent pulse in the velocity

and the displacement time histories does not exist in ground motion records away from the near-fault region (Chopra and Chintanapakdee, 2001).

The large amplitude long duration velocity pulses recorded in near-fault regions may be the cause of significant damage particularly to long period structures. These pulses transmit large amount of energy to the structure in a short time. High-energy dissipation is likely being concentrated in the weakest parts of the structural system. The result is large inelastic deformations with related structural damage as a consequence (Mollaioli et al, 2002)

1.1.7 DIRECTIVITY EFFECT

Strong-motion seismologists have recognized the effects of rupture directivity on near-fault ground motions for few decades. Long period pulses were observed in recent near-fault records such as the 1992 Landers (California) earthquake, the 1994 Northridge (California) earthquake, the 1995 Kobe (Japan) earthquake, and the 1999 Chi-Chi (Taiwan) earthquake. These pulses are strongly influenced by the type of the fault, the location of the epicenter, the direction of slip on the fault and the location of the recording station relative to the fault. The location of the recording station relative to the fault is the cause of 'directivity effect' due to the propagation of the rupture toward or away from the recording site. The propagation of fault rupture toward a site at a velocity close to the shear wave velocity causes most of the seismic energy from the rupture to arrive in a single large long-period pulse of motion that occurs at the beginning of the record (Somerville et al., 1997). When the recording station is located in the direction of rupture, the seismic waves due to fault rupture arrive at the recording site at the same

time creating the long period pulse in the fault normal direction. The fault parallel component is normally of smaller magnitudes.

For the same peak ground acceleration (PGA) and duration of shaking, ground motions with directivity pulses can generate higher base shears, inter-story drift, and roof displacements in high-rise and long period buildings. In addition, ductility demand can be higher as well (Malhotra 1999).

1.2 OBJECTIVES

The objective of this study is to investigate the development of design yield spectra and to evaluate the various factors that affect its general characteristics. The study will address the effect of near-fault (NF) and far-field (FF) earthquakes, the directivity effect and the effect of different types of soils on the yield spectra using actual earthquake ground motion records. Permissible design regions representing the different earthquake hazards will be formed in order to develop design spectra suitable for code application.

1.3 SCOPE OF WORK

To achieve the outlined study objectives, the scope of the investigation is summarized in the following steps:

The available literature on related topics is reviewed in Chapter One. Available methods of performance-based design are discussed. The difference between near-fault and far-field earthquake characteristics and the directivity effect concept are reviewed. A general survey of various earthquakes from different sources and their classification

according to the directivity effect and the type of soil is presented in Chapter two. The earthquake records selected for this study are categorized.

Chapter Three outlines the spectrum analysis and the steps of the formation of the spectra are introduced. A single degree of freedom system is subjected to the chosen set of ground motions scaled to different peak ground acceleration levels. Linear and nonlinear dynamic analyses of the system are performed. For each ground motion, three relationships are established: force modification factor versus period for different ductility values, yield strength coefficient versus period for different ductility values and finally the yield spectrum of this particular record. Chapter Four represents the results of the analysis by taking average of each of the three graphs discussed in Chapter three for the different scales of ground accelerations for constant ductility factors. The yield spectra are presented, discussions are provided to highlight the various effects of the type of the ground motion chosen whether NF or FF earthquake records and the rupture directivity effect as well as the type of soil; whether it is rock or soil.

The formation of the graph representing the performance objectives for the different earthquake hazard levels is discussed in Chapter Five. The final admissible design region is emphasized by considering the design of a three and twelve storey concrete frame buildings for the different hazard levels. The admissible design region graph is superimposed over the yield spectra. An application of the yield spectra design procedure is presented. An example for using the combined graph of the admissible design region plot and the yield spectrum is illustrated. Investigation of the effectiveness

of this procedure is discussed. The conclusions of the study and recommendations for future research work are presented in Chapter Six.

Table 1.1 Performance levels, corresponding damage state and drift limits (Ghobarah 2001)

Performance level	Damage state	Drift
Fully operational, immediate occupancy	No damage	<0.2%
Operational, damage control moderate	Repairable	<0.5%
Life safe – Damage state	Irreparable	<1.5%
Near collapse, limited safety, hazard reduced	Severe	<2.5%
Collapse		>2.5%

Table 1.2 Proposed earthquake hazard levels (Ghobarah 2001)

Earthquake frequency	Return period in years	Probability of exceedance
Frequent (EQ-I)	43	50% in 30 years
Occasional	72	50% in 50 years
Rare	475	10% in 50 years
Very rare (EQ-IV)	970	5% in 50 years or 10% in 100 years
Extremely rare	2475	2% in 50 years

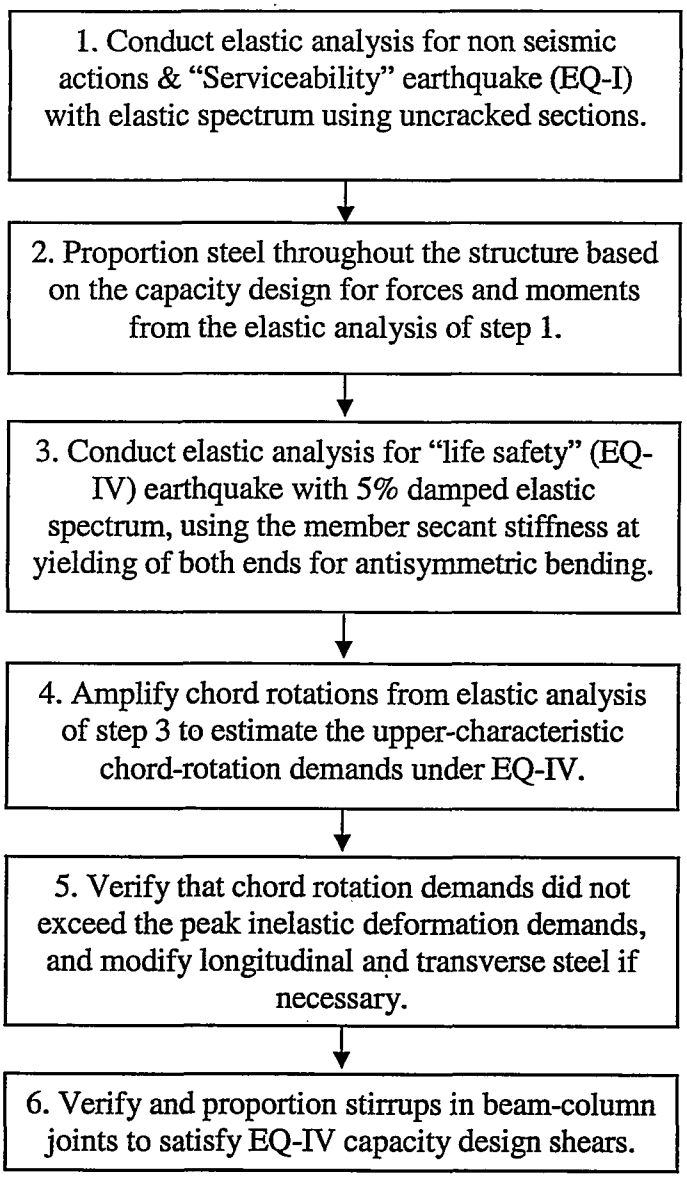

Figure 1.1 Flowchart of Panagiotakos and Fardis method

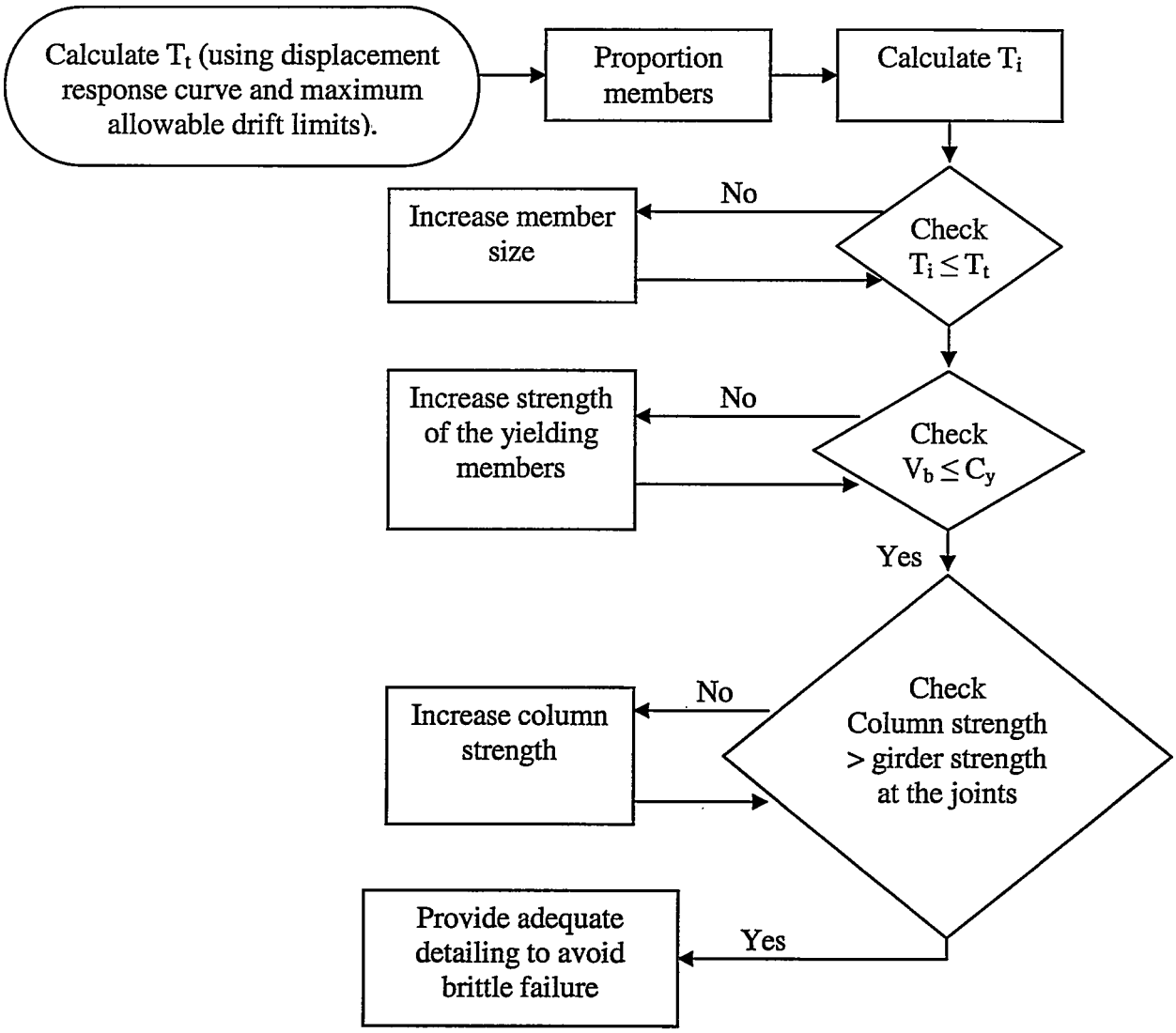

Figure 1.2 Flowchart of Browning method

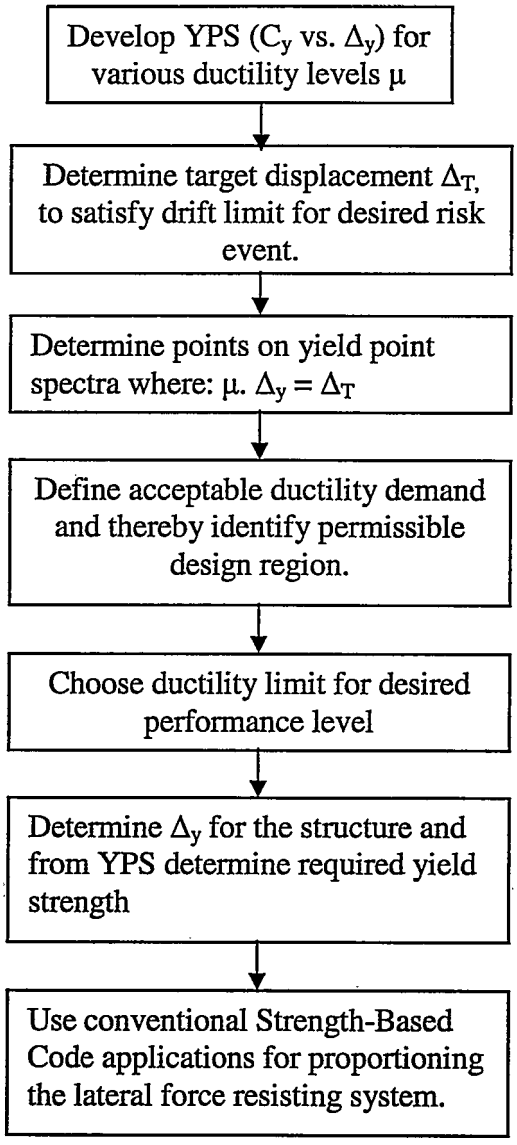

Figure 1.3 Flowchart of Aschheim and Black method (Sullivan 2002)

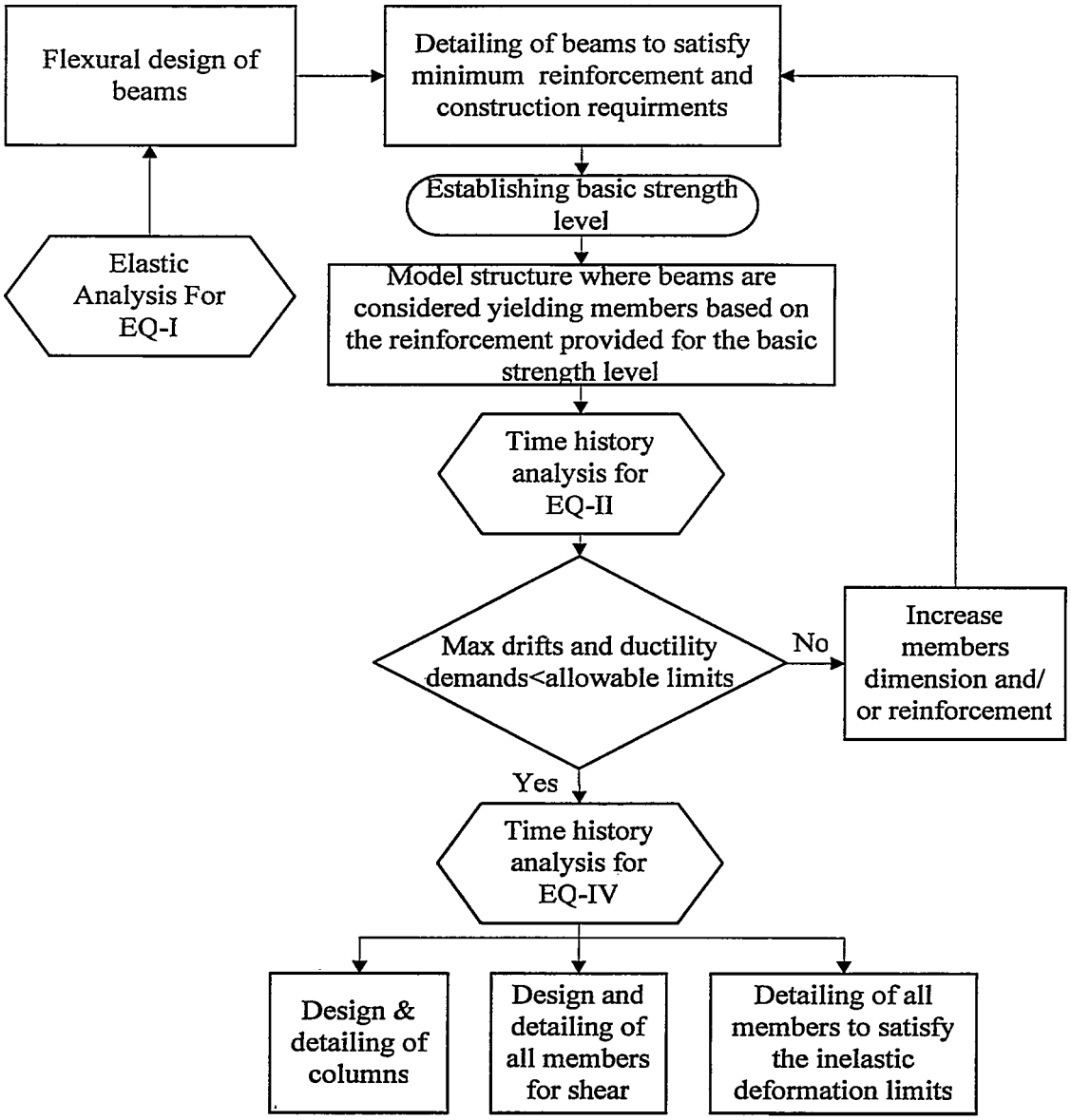

Figure 1.4 Flowchart of Kappos and Manafpour method

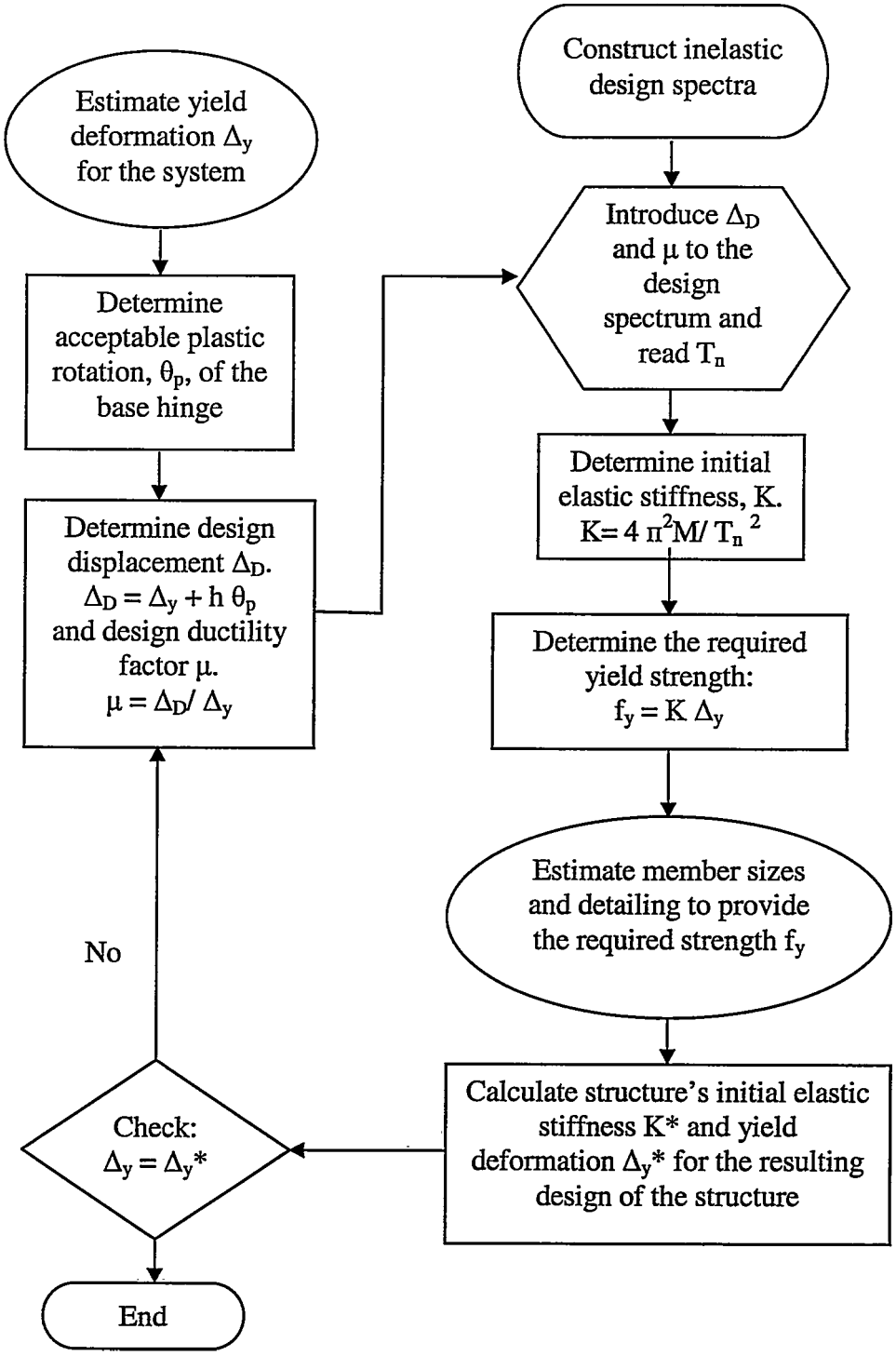

Figure 1.5 Flowchart of Chopra and Goel method

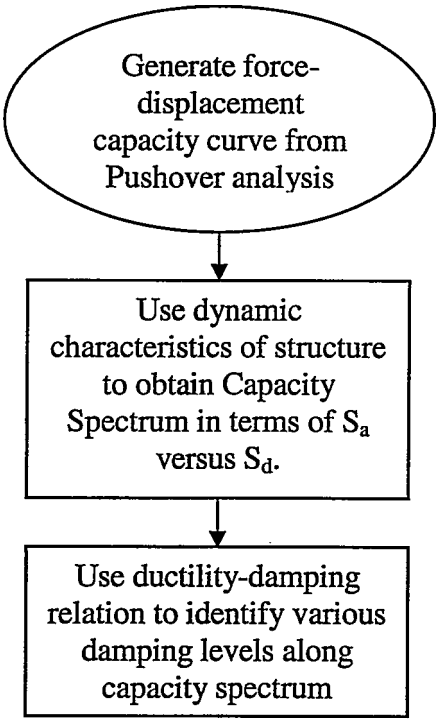

Figure 1.6 Flowchart of Freeman method (Sullivan 2002)

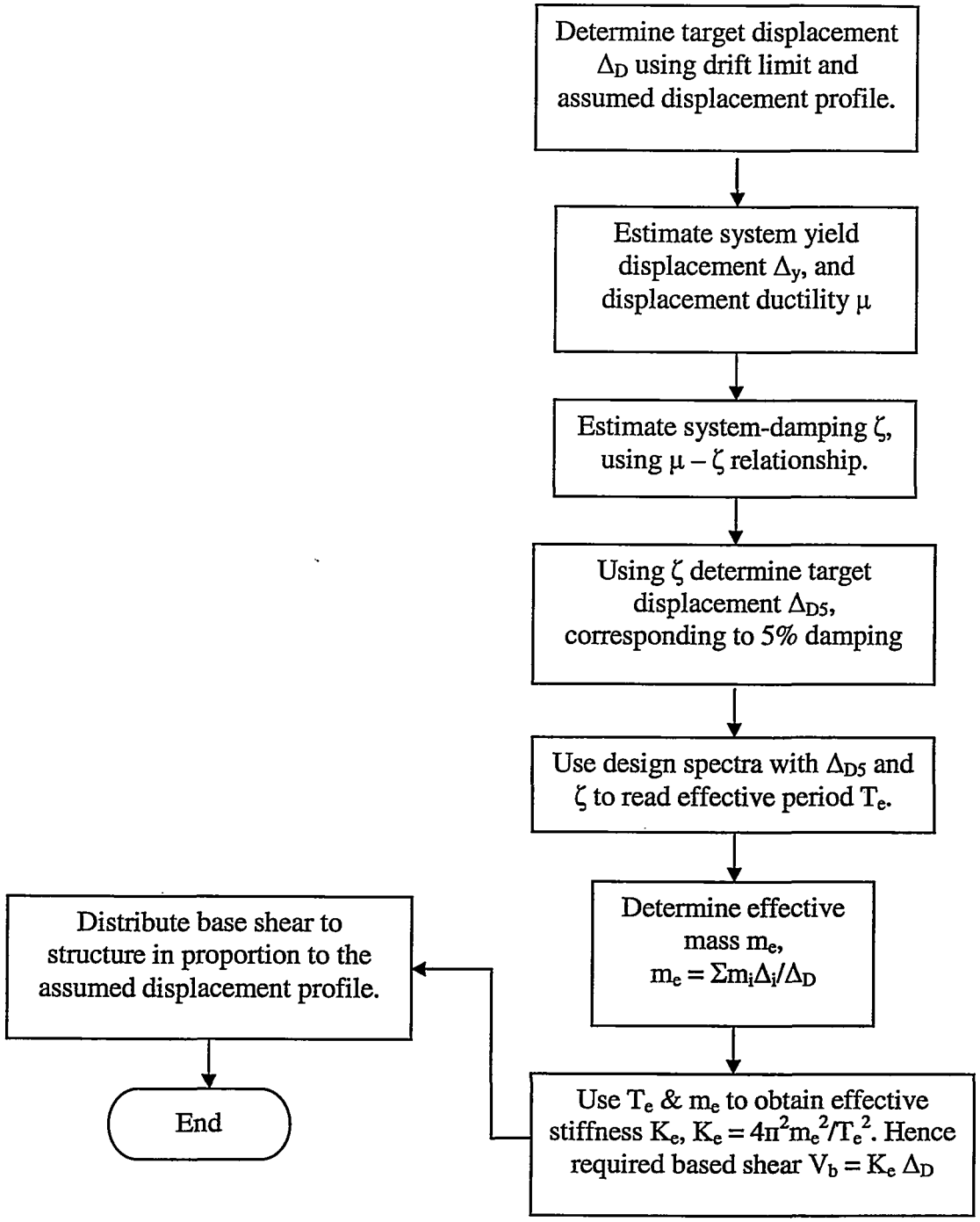

Figure 1.7 Flowchart of Priestly and Kowalsky method

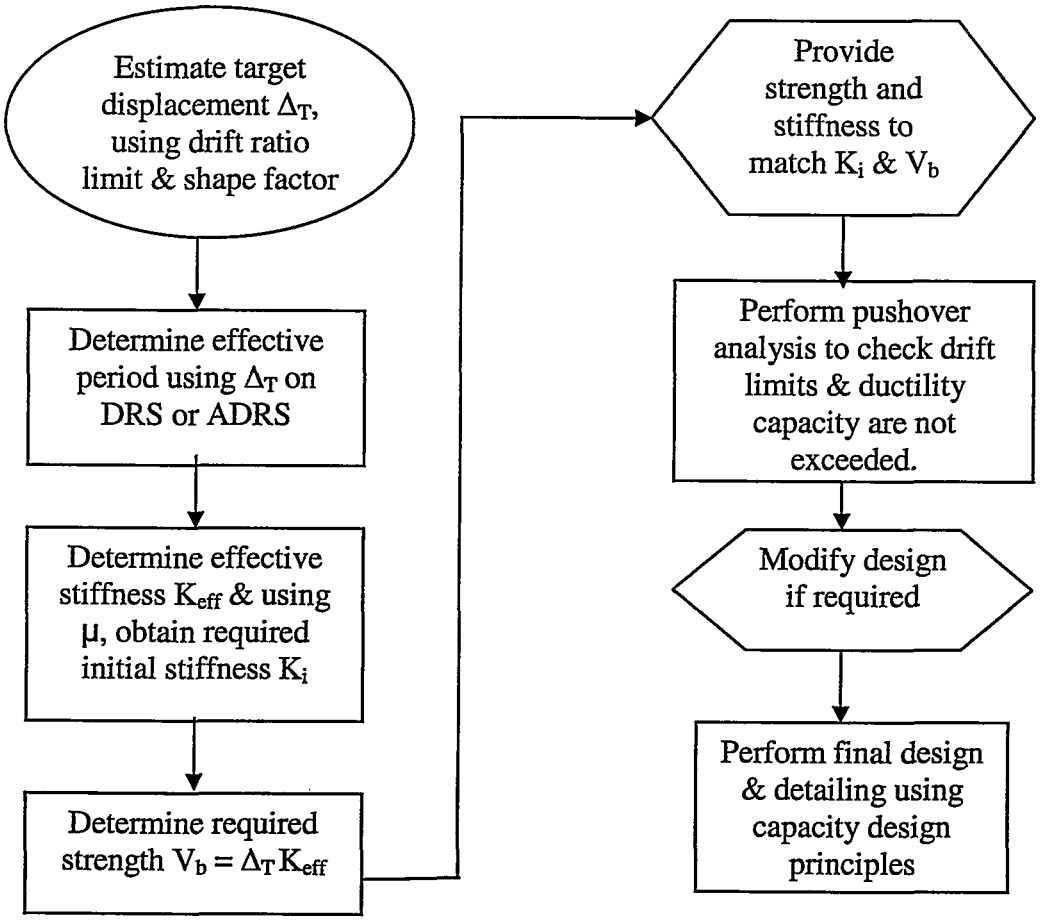

Figure 1.8 Flowchart of SEAOC method (Sullivan 2002)

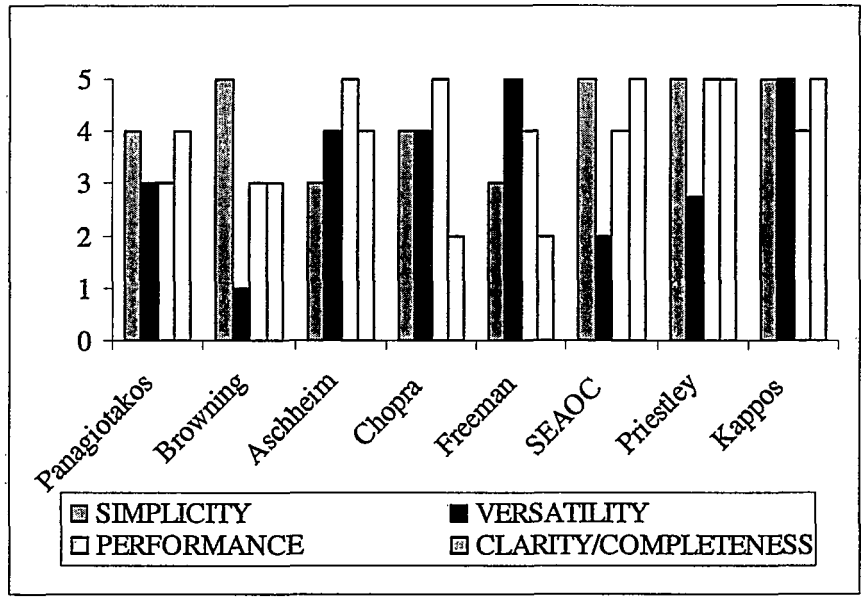

Figure 1.9 Assessment of the displacement based design procedures (Sullivan 2002)

2. EARTHQUAKE RECORDS

CHAPTER 2

EARTHQUAKE RECORDS

2.1 INTRODUCTION

Several major earthquakes occurred in the recent past that resulted in damage to structures that cost millions of dollars as well as substantial loss of life. The target of current research in earthquake engineering is not only to reduce the loss of life, but also to limit financial loss that is a function of the damage to the structure in accordance with certain allowable limits for various seismic hazards. Inherently, the performance based design concept implies the definition of multiple target performance (damage) levels, which are expected to be achieved, or at least not exceeded, when the structure is subjected to earthquake ground motion of specified intensity.

Actual records of earthquakes are needed since they are important sources of data. They allow the evaluation of seismic hazards and the more accurate predictions concerning the likely location and magnitude of future earthquakes. Characterization of these records can help establish accurate design criteria. Actual value parameters can be introduced in the design procedure rather than being assumed by the designer.

In order to conduct realistic analyses and make valid response comparisons, actual earthquake records were collected from various sources and classified to represent different points of investigation that are of specific interest to this study. The classified earthquake record information is summarized in tables to show the relevant data for each

earthquake. Some earthquakes that signify the points of the study were chosen for spectrum analysis formation.

2.2 SOURCES OF EARTHQUAKE RECORDS

Information systems have improved vastly in the last 25 years and statistical data are now more readily available. Several organizations provide a means of gathering and documenting open source data. For this study, sufficient data was required to cover all the points of investigation discussed later in the chapter. A large set of earthquake records was gathered from various sources to form a wide earthquake database that covers several parts of the world where earthquakes are frequent, as well as destructive.

An example of active seismic zones with intense earthquake events is western US. The area is well instrumented and a large number of records are obtained during each event. The intense seismic activities in western US can be attributed to the presence of active faults such as the San-Andreas Fault. The fault has been the cause of destructive earthquakes in the past, and will be the source of future destructive shocks.

Western US earthquake records as well as the central and eastern database records were studied to cover all the United States. The records are available from the US Geological Survey USGS (2003). In addition, Canadian earthquake records were obtained from the National Geological Survey of Canada (2003).

Japan is another area of high seismicity. All of Japan lies in one of the most seismically active regions of the world. Heavily populated areas are often subject to strong earthquakes. The island nation is surrounded by major offshore faults and is crisscrossed by many active faults. There are two networks of strong motion instruments

that are managed by the Earthquake Research Institute, University of Tokyo (2003), and the Earthquake Information at the Kanto-Tokai district, Japan (2003). Broad-band seismic Japanese databases such as F-net (2003) (Full-range seismograph network), Kik-net (2003) (KIBAN Kyoshin network) which is a subset of the Hi-net and K-net (Kyoshin network) were accessed.

Records of European earthquakes, the Mediterranean area and the Middle East were obtained from the European Strong-Motion Database CD (Ambraseys et al. 2000). Generally, strong motion instrumentation and recording in Europe and the Middle East started much later than in the United States and Japan. The number of records available for investigation is small relative to US and Japanese records.

As an example of destructive earthquakes, two major main events and their aftershocks occurred in Turkey in 1999. The two events are of special interest since they were large earthquakes that affected a large urban environment. The U.S. Geological Survey provided a CD with sufficient information about these two events and their aftershocks (Celebi et al. 2001). The CD included eight sources of data; two of them were from Turkey: ITU (Istanbul Technical University) and ERD (Earthquake Research Department of the ministry of Public works and reconstruction, Ankara).

According to recent studies, when comparing the relative seismicity of Japan, California and the rest of the world, based on shallow events (less than 60 kilometers deep), for corrected magnitude (Ms) equal to or greater than 7. The data is for the period of 90 years from 1900 to 1989. Earthquakes in California (and western Nevada), present approximately 1% of the world data for events with magnitudes equal to or greater than

5.0. It was observed that the percentage of the earthquakes that occurred in Japan and western United States, particularly, was consistent in comparison with the rest of the countries in the world.

The number of shallow and potentially damaging earthquakes (M5 to M8.9) in Japan is about a factor of 6 to 7 greater than in the California region. Japanese earthquakes represent about 6% to 7% of the world's potentially damaging shallow earthquakes (EQE 2003). This comparison is shown in Table 2.1.

2.3 CATEGORIZATION OF DATA

The intent of this study is to investigate the formation of the yield spectra, and to evaluate the degree to which more detailed information can improve the design procedure. Incorporation of the factors that can affect the earthquake intensity will help in the detailed study of the spectra to make it suitable for code implementation. Acquired data has been investigated, homogenized and assembled according to various aspects that influence the earthquake severity and damage potential.

2.3.1 EARTHQUAKE CHARACTERISTICS

In the development of current codes, no distinction is made between near-fault and far-field earthquakes. Codes were historically based on the experience of the recorded motion not sufficiently close to the causative fault. During the last 15 years, an ever-increasing database of recorded earthquakes has indicated that the characteristics of ground motion can vary significantly with the distance from the fault.

Studies have shown that a structure in the near-fault region (defined to be within a distance of 20 km from the fault rupture) may experience a dynamic response that is twice or more of a similar structure located at some distance from the fault. Structures at this zone suffer significant damage when designed according to currently available design approaches.

The ground motion in the near-fault region has large amplitude long duration velocity pulse at the beginning of the record. These pulses transmit a large amount of energy to the structure in a short time causing damage. The critical condition, according to Singh (2003) occurs when a long duration pulse has an average acceleration that is of the same order as the yield resistance seismic coefficient of the structure. The yield resistance seismic coefficient is obtained by dividing the base shear capacity with the structure effective weight.

When further investigating the dynamic response of structures subjected to both near-fault and far-field records, results have shown that higher force demand and higher ductility demand are expected when the structure is subjected to near-fault excitations (Liao et al. 2001).

It is important to consider the near-fault effects in the development of design methods. Remarkably, these features of near-fault ground motion have not yet been well documented and are generally not considered in seismic design. There is a lack of a database for identified near-fault earthquakes. Categorization of the collected earthquake records is conducted to summarize the significant information for various near-fault records. In addition, yield resistance seismic coefficient, ductility demand and force

demands of the structure are all factors that influence the development of the yield spectra as will be explained in the following chapters. The special characteristics of the near-fault earthquakes are evaluated and classified.

2.3.2 DIRECTIVITY EFFECT

Examining the near-fault time histories, the effect of the rupture directivity is clearly recognized. Two distinct directivity effects are observed: forward and backward directivity. In the near-fault zone, some records are characterized by a long pulse in the acceleration history that appears as a coherent pulse in the velocity and displacement histories (Chopra and Chintanapakdee 2001). The location of the recording station relative to the fault is the cause of the directivity effect due to the propagation of the rupture towards or away from the recording site.

Forward directivity is when the propagation of the seismic waves is in the direction of the site. Generally, the rupture propagates at a velocity close to the shear wave velocity causing most of the seismic energy of the rupture to arrive at the site in a single large pulse of motion that occur at the beginning of the record with a relatively short duration (Somerville et al. 1997). Backward directivity occurs when the rupture propagates away form the site, it gives rise to opposite effect: long duration motions having low amplitudes.

Singh (2003) explained the cause of the presence of the high peak short duration pulse in the forward directivity near-fault records and the long duration low intensity pulse in the backward directivity records, assuming the velocity of rupture is nearly as large as the shear wave velocity. This is illustrated in Figure 2.1.

Somerville et al. (1997) illustrated the differences in the velocity time histories at Lucerne (forward directivity) and Joshua Tree (backward directivity) recording stations. Data are from 1992 Landers earthquake in Southern California as shown in Figure 2.2.

Furthermore, for the same PGA and duration of shaking, ground motions with directivity pulses can generate high base shears, inter-storey drifts, and roof displacements in high-rise and long period structures. In addition, ductility demands can be higher as well (Malhorta 1999). In view of the fact that these are important aspects for the development of the Yield Spectra, further categorization of the near-fault records according to the directivity effect is made to evaluate the effect on the spectra.

2.3.3 SITE EFFECTS

The type of soil at the site is known to influence the ground motion that the structure is subjected to. Soil amplification effects have been documented in several major recent earthquakes. For sites at the same distance from the rupture fault, the amplification may vary by 10 times. In the 1995 Kobe earthquake, peak ground accelerations as high as 0.8 g were recorded in the near-fault region on alluvial sites, while, the recordings at near-fault rock sites were typically of significantly lower magnitudes of PGA (i.e. about 0.3g). Site amplification effects of soft soil and recently constructed near-shore islands caused severe damage and loss of life.

In some situations, a resonance can occur in deep soil layers, markedly increasing the ground shaking resulting from an earthquake. This causes more damage than in adjacent areas. Soft soil overlying hard bedrock tends to amplify the ground motion, which may cause excessive damage. The reason is that as the seismic waves pass from

harder to softer rock layers and slow down, the amplitude increases for the waves to carry the same amount of energy. Thus, shaking tends to be stronger at sites with softer surface layers, where the seismic waves move more slowly (SCEC 2003).

This demonstrates that structures on different soil sites, even if they are within the same distance from the fault, can be subjected to significantly different ground motion with different PGA and different response. Structures prone to this amplified ground motion should be designed to higher values of base shear and roof displacement as well as interstorey drifts. This explains the importance of studying the site effects on the design spectra.

In terms of soil conditions, the majority of the sites from the available records can only be described at best in very general terms such as 'Soil' or 'Rock'. This is due to the lack of detailed information about the site soil. For example, the detail whether the site soil is 'soft rock' or 'very soft soil' or 'stiff soil' is often not available. Further subdivision of the collected data separates the records on rock sites from those on soil sites, to study their influence on the spectra independently.

2.3.4 MAGNITUDE EFFECT

The most widely accepted indicators of the size of an earthquake are its magnitude and intensity. The magnitude is a measure of an earthquake in terms of the released energy. The most popular scale is the Richter scale proposed by Charles F. Richter in 1934. Public, scientists, engineers and technicians have recognized this scale as a measure of the relative size of an earthquake. The Richter magnitude is calculated

from the amplitude of the largest seismic wave recorded for the earthquake, regardless what type of wave was the strongest.

In this study, categorization of earthquakes was based on the magnitude values of the earthquakes rather than intensities. This is because the magnitude of an earthquake is a unique indicator for the size of the earthquake. On the other hand, each earthquake is characterized with various intensities, depending on the location of the particular site.

The Richter scale is logarithmic. It starts from zero upwards, an increase in magnitude of one unit corresponds to a tenfold increase in the size of an earthquake. Thus, an earthquake of magnitude 6 is ten times larger than one of magnitude 5, and a hundred times larger than one of magnitude 4. The effect of the earthquakes with different magnitudes is shown in Table 2.2.

In this study, the earthquakes records will be classified as greater or less than magnitude 6. This is because earthquakes greater than M=6 can be regarded as significant, with the likelihood of causing damage and loss of life. In addition, in nuclear power plant siting studies, locations near faults causing possible magnitudes 6 or larger earthquakes are avoided. However, it is likely that existing nuclear installations may be subjected to near fault earthquakes of magnitude less than 6.

While compiling the data, it was noticed that for a single earthquake, magnitude values given by different seismological observatories may vary. This may be attributed to the use of several different methods to estimate the magnitude. The uncertainty in an estimate of the magnitude is about ± 0.3 units. Therefore, the magnitude values of the closest seismological organization to the earthquake source were adopted in this study.

2.4 RECORDS CHOSEN FOR THE STUDY

In this study, a two-stage procedure is followed for earthquake classification and selection. First, all near-fault earthquakes from available records are identified and classified. Second, few representative earthquake records are selected for the analysis. The classification of the records is performed according to the flowchart shown in Figure 2.3.

Tables 2.3 to 2.6 summarize the relevant information for the categorized data where the near-fault records are assembled under forward directivity rupture records and backward directivity ones. Table 2.3 represents the information about near-fault, forward directivity earthquake records with magnitude greater than 6 for rock and soil sites. Table 2.4 summarizes the near-fault, forward directivity earthquake records with magnitude less than 6 for rock and soil sites. Similarly, Table 2.5 sums up the near-fault, backward directivity rupture records of magnitude more than 6 and Table 2.6 summarizes the near-fault, backward directivity rupture earthquake records of magnitude less than 6 for various rock and soil sites.

For analysis purposes, 30 representative records are selected from the collected data to represent each of the factors discussed previously; ten earthquakes are chosen to represent the forward directivity effect with magnitude greater than 6, five of them represent the rock sites and five represent the soil sites. Similarly, 10 earthquakes represent the forward directivity but with magnitude less than 6 for both rock and soil effects. The selected earthquake records for the analyses are identified by the check mark

(√) shown in tables 2.3 to 2.6. Fault mechanism was not explicitly considered in selecting those earthquakes.

For the purpose of this study, ten far-field earthquake records as listed in Table 2.7 are selected for the development of yield spectra.

Table 2.1 Average number of shallow earthquakes in 90 years in Japan, California and world wide (EQE 2003)

Richter magnitude	World	California and W. Nevada	Japan
8.0 – 9.0	45	1	4
7.0 – 7.9	775	7	45
6.0 – 6.9	7,100	75	450
5.0 – 5.9	70,000	730	4,500

Table 2.2 Earthquake effects for different Richter magnitudes (PGC 2003)

Description	Richter magnitudes	Earthquake effects
Very minor	1- 3	Generally, not felt
Minor	3- 4	Often felt, no damage
Moderate	5-5.9	Felt widely, slight damage near epicenter
Strong	6-6.9	Damage to poorly constructed buildings and other structures within 10's km.
Major	7-7.9	Cause serious damage up to 100 km
Great	8	Great destruction, loss of life over several 100 km
Rare	9	Rare great earthquakes, major damage over a large region over 1000 km

Table 2.3 Near-fault, forward directivity rupture earthquake records of magnitude greater than 6

	Earthquake event	Date	Magnitude (ML)	Station name & component	Epicenter Distance (km)	PGA (g)	Site soil
	Gazli, USSR	17/5/1976	7.3	Karakyr,GAZ090	3	0.718	Rock
✓	Morgan Hill, California	24/4/1984	6.2	Gilroy array #6, G06-UP	11.8	0.405	Rock
	Morgan Hill, California	24/4/1984	6.2	Coyote Lake Dam, CYC285	0.1	1.298	Rock
	Morgan Hill, California	24/4/1984	6.2	Gilroy Gavilan Coll.,GIL067	14	0.114	Rock
	Cape Mendocino, California	25/4/1992	7.1	Cape Mendocino,CPM000	8.5	1.497	Rock
	Landers, California	28/6/1992	7.3	Lucerne, LCN345	1.1	0.785	Rock
✓	Northridge, California	17/1/1994	6.6	Pacomia Kagel Canyon, PKC360	8.2	0.433	Rock
	Northridge, California	17/1/1994	6.6	Pacoima Dam, PUL104	8	1.585	Rock
✓	Izumi, Japan	26/3/1997	6.3	KGS002,0	13.2	0.727	Rock
	Miyanojoh, Japan	26/3/1997	6.3	KGS005, 90	14.8	0.493	Rock
	Akune, Japan	13/5/1997	6.2	KGS004,0	12.8	0.156	Rock
	Ikumonaka, Japan	25/6/1997	6.1	YMG003,90	20	0.136	Rock
	Susa, Japan	25/6/1997	6.1	YMG001,90	19.5	0.14	Rock
✓	Tsuwano, Japan	25/6/1997	6.1	SMN014,0	14.5	0.421	Rock
	Kocaeli, Turkey	17/8/1999	7.4	Arcelik, 000	17	0.298	Rock
	Kocaeli, Turkey	17/8/1999	7.4	Gebze,000	17	0.401	Rock
	Chi-chi, Taiwan	20/9/1999	7.3	TCU045, N	20	0.512	Rock
✓	Chi-chi, Taiwan	20/9/1999	7.3	TCU095, N	17	0.712	Rock
	Chi-chi, Taiwan	20/9/1999	7.3	CHY080-W	14.93	0.968	Rock
	Nigata Prefecture, Japan	16/6/1964	7.5	Kawagishi-cho, EW	0	0.171	Soil

Table 2.3 Near-fault, forward directivity rupture earthquake records of magnitude greater than 6 (continued)

	Earthquake event	Date	Magnitude (ML)	Station name & component	Epicenter Distance (km)	PGA (g)	Site soil
	San Fernando, California	2/9/1971	6.6	Pacoima Dam, PCD164	2.8	1.226	Soil
✓	Imperial Valley, California	15/10/1979	6.6	El Centro array #6, VL	1.3	1.665	Soil
	Imperial Valley, California	15/10/1979	6.6	El Centro array #7, VL	0.6	0.544	Soil
	Loma Prieta, California	18/10/1989	7.0	Gilroy Array #6, GO6000	19.9	0.126	Soil
✓	Loma Prieta, California	18/10/1989	7.0	Corralitos, CLS000	5.1	0.644	Soil
	Cape Mendocino, California	25/4/1992	7.1	Petrolia, PET090	9.5	0.662	Soil
✓	Kobe, Japan	16/1/1995	7.0	Takarazuka, TAZ090	1.2	0.694	Soil
✓	Erzican, Turkey	18/8/1999	6.9	Erzican, ERZ-EW	17	0.619	Soil
✓	Duzce, Turkey	11/12/1999	7.2	Bolu, BOL090	17.6	0.822	Soil

✓ Represent selected earthquake records for analysis

Table 2.4 Near-fault, forward directivity rupture earthquake records of magnitude less than 6

	Earthquake event	Date	Magnitude (ML)	Station name & component	Epicenter Distance (km)	PGA (g)	Site soil
	Iwate Prefecture, Japan	1/4/1970	5.8	Miyako Harbor, Ns	17	0.189	Rock
✓	New Madrid Missiouri, US	31/12/1988	2.2	Ridgely, Tennessee, HL	10	0.009	Rock
	Knoxville Tennessee, US	12/2/1989	2.4	Corryton, HL(N0)	9.8	0.005	Rock
✓	Miramichi, Canada	31/03/1982	5	Mitchell Lake Rd.,N28 (HL)	3.9	0.193	Rock
	Whitter Narrows, California	10/1/1987	5.9	Transmitter Hill, GRV330	12.1	0.457	Rock
	Whitter Narrows, California	10/1/1987	5.9	San Gabriel - Egrand Av, GRV180	9	0.304	Rock
	Helena, Montana	31/10/1987	5.5	Carroll College,HMC270	8	0.173	Rock
✓	Massena New York	8/9/1988	2.3	MSNA_NCEER,N335 (HL)	10	0.009	Rock
✓	Massena New York	19/7/1989	2.7	MSNA_NCEER,N335 (HL)	7.5	0.003	Rock
	Hinoemata, Japan	2/6/1996	4.3	FKS029,90	13.7	0.35	Rock
	Naruko, Japan	13/8/1996	5	MYG005,90	11	0.708	Rock
✓	Atami, Japan	3/3/1997	5	SZO001,90	18.9	0.127	Rock
	Itohi, Japan	26/4/1998	4.7	SZO002, 90	10.7	0.356	Rock
	Atami, Japan	26/4/1998	4.7	SZO001,90	19.4	0.07	Rock
	Ibaraki Prefecture, Japan	14/11/1964	5.1	Atomic Energy Research Insitu, NS	8	0.202	Soil
✓	Japanese	28/5/1966	5.3	Matsushiro-C, NS	4	0.38	Soil
	Japanese	30/3/1968	5	Wakayama Harbor, EW	5	0.442	Soil
	Lytle Creek	9/12/1970	5.4	Wrightwood, WTW205	15.4	0.2	Soil

Table 2.4 Near-fault, forward directivity rupture earthquake records of magnitude less than 6 (continued)

	Earthquake event	Date	Magnitude (ML)	Station name & component	Epicenter Distance (km)	PGA (g)	Site soil
✓	Livermore, California	27/1/1980	5.8	Eastman Kodak, KOD180	17.6	0.301	Soil
	Chalfant Valley, California	21/7/1986	5.9	Zack Brothers Ranch, ZAK270	11	0.143	Soil
	Chiba Prefecture, Japan	11/10/1997	5.2	Kashima Harbor Works, EW	12	0.128	Soil
✓	Duzce Turkey aftershock	12/11/1999	5.4	496,EW	17.9	0.739	Soil
✓	Duzce Turkey aftershock	12/11/1999	5.4	492, NS	17.7	0.306	Soil
	Duzce Turkey aftershock	12/11/1999	5.4	487, EW	16.9	0.289	Soil
	Duzce Turkey aftershock	12/11/1999	5.4	498, EW	17.5	0.206	Soil

✓ Represent selected earthquake records for analysis

Table 2.5 Near-fault, backward directivity rupture earthquake records of magnitude greater than 6

Earthquake event	Date	Magnitude (ML)	Station name & component	Epicenter Distance (km)	PGA (g)	Site soil
Parkfield, California	28/6/1966	6.1	Temblor pre-1969, TMB205	9.9	0.357	Rock
Monte Negro,Yugoslavia	15/4/1979	7	Albatros Hotel, Ulcinj, N00E	17	0.171	Rock
Banja Luka, Yugoslavia	13/8/1981	6.1	Seism. Station, N90W	8.5	0.074	Rock
Coalinga, California	7/9/1983	6	Oil City, OLC270	8.2	0.866	Rock
Coalinga, California	7/9/1983	6	Palmer Ave., PLM270	12.2	0.272	Rock
Coalinga, California	7/9/1983	6	Transmitter Hill, TSM360	9.2	1.083	Rock
Nahanni, Canada	23/12/1985	6.9	Site 1, Iverson, long.	7.5	1.101	Rock
Loma Prieta, California	18/10/1989	7	LGP090	6.1	0.605	Rock
Loma Prieta, California	18/10/1989	7	BRN090	10.2	0.501	Rock
Kocaeli, Turkey	17/8/1999	7.4	Izmit, 180	7.7	0.401	Rock
Kobe, Japan	16/1/1995	7	KNMA, KJM000	0.6	0.821	Soil
Kocaeli, Turkey	17/8/1999	7.4	Yarimca, YPT-UP	17	0.463	Soil
Kocaeli, Turkey	17/8/1999	7.4	Duzce,DZC-UP	17	0.613	Soil

Table 2.6 Near-fault, backward directivity rupture earthquake records of magnitude less than 6

Earthquake event	Date	Magnitude (ML)	Station name & component	Epicenter Distance (km)	PGA (g)	Site soil
Honshu, Japan	5/4/1966	5.4	Honshia-A, N00E	4	0.27	Rock
Japanese	28/5/66	5.4	Susobana dam, NS	13	0.052	Rock
Monte Negro, Yougoslavia	9/4/1979	5.4	Albatros Hotel, Ulcinj, N00E	12.5	0.042	Rock
Coalinga, California	7/9/1983	5.3	ATC360	12.6	0.673	Rock
Coalinga, California	7/9/1983	5.3	Anticline Ridge Pad, ATP270	12.6	0.452	Rock
Miramichi, Canada	12/2/1989	5	Indian Brook II ,N231(HL)	0.8	0.335	Rock
Miramichi, Canada	12/2/1989	5	Holmes Lake N18 (HL)	6	0.14	Rock
River Ebo, Japan	14/2/1956	5.7	Eq. Institute, Tokyo, NS	14	0.074	Soil
Japanese	12/11/1966	5.5	Ariake Sea Embakment, N40E	19	0.119	Soil
Japanese	3/8/1966	5.3	Matsushiro-C, NS	7	0.22	Soil
Japanese	28/8/1966	5.3	Matsushiro-C, NS	9	0.187	Soil
Etorofu Is	4/5/1966	5.4	Ochial Bridge,NS	12	0.274	Soil
Japanese	20/5/1966	4.9	Matsushiro-C, NS	4	0.234	Soil

Table 2.7 Far-field earthquake records selected for analysis

Earthquake event	Date	Magnitude (ML)	Station name & component	Epicenter Distance (km)	A/V ratio	PGA (g)	Site soil
Long Beach, California	9/2/1971	6.3	L.A. Subway Terminal, N51W	59	0.41	0.095	Rock
San Fernando, California	21/7/1952	6.4	445 Figueroa st., S38W	41	0.69	0.119	Rock
Monte Negro, Yugoslavia	15/4/1979	7.0	Albatros hotel, N00E	30	0.88	0.171	Rock
Kern County, California	10/3/1933	7.6	Taft Lincoln school tunnel, S69E	56	1.01	0.179	Rock
San Fernando, California	9/2/1971	6.4	Lake Hughes, array station 4, CAL. , S21W	26	1.72	0.143	Rock
Honshu, Japan	11/5/1972	7.9	Muroran harbor, N00E	290	0.68	0.226	Soil
San Fernando, California	9/2/1971	6.4	222 Figueroa st., S37W	41	0.69	0.129	Soil
San Fernando, California	18/5/1940	6.4	Hollywood Storage P.E. lot, N90E	35	1.00	0.206	Soil
Imperial Valley, California	16/5/1968	6.6	El Centro, S00E	27	1.04	0.348	Soil
Honshu, Japan	9/2/1971	5.8	Kushiro central wharf, N00E	33	2.43	0.146	Soil

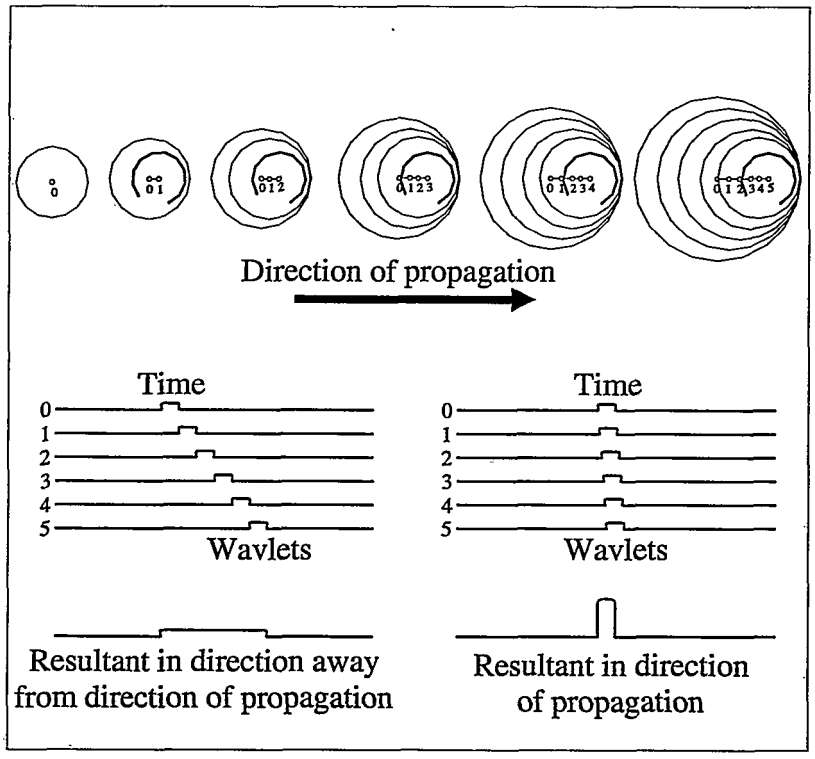

Figure 2.1 Directivity effect (Singh 2003)

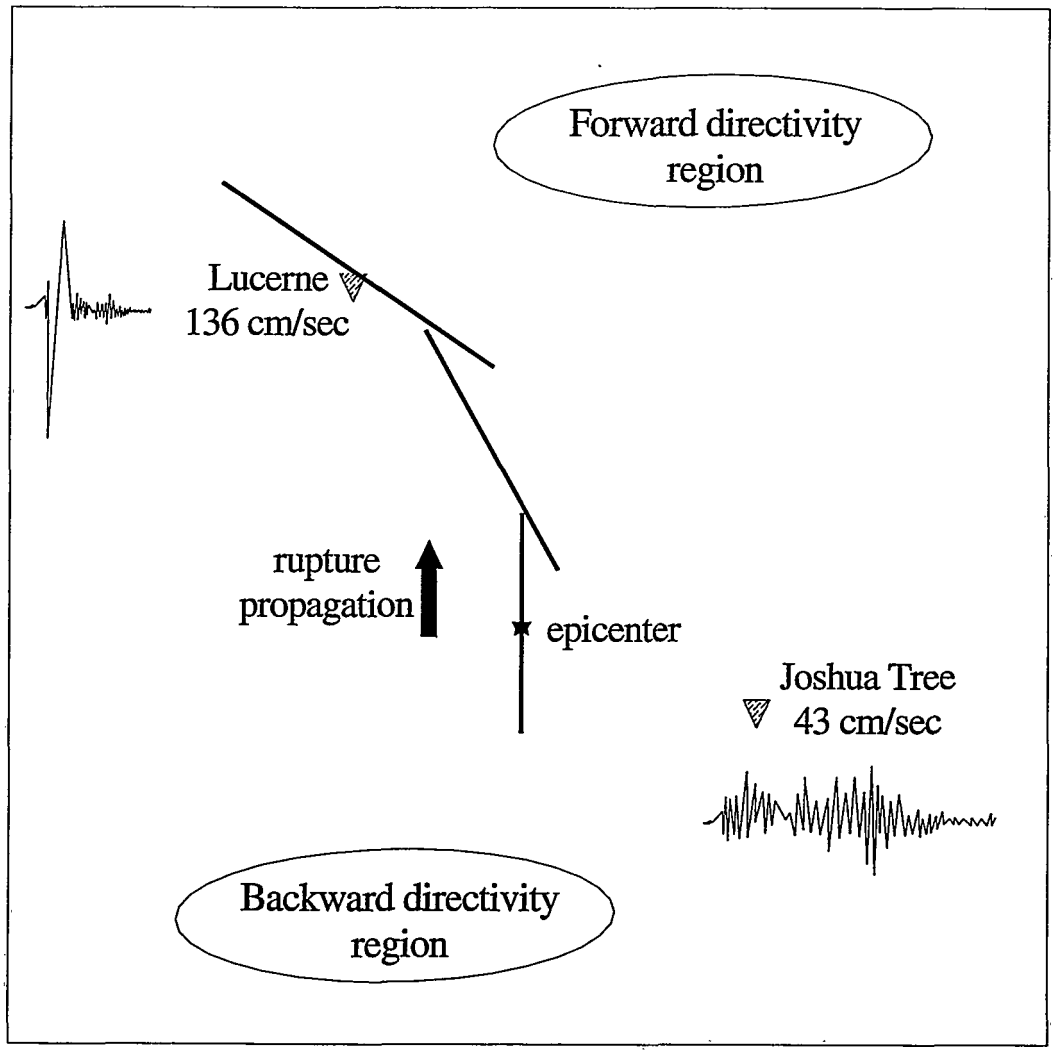

Figure 2.2 Differences between Forward and Backward directivity (Somerville et al. 1997)

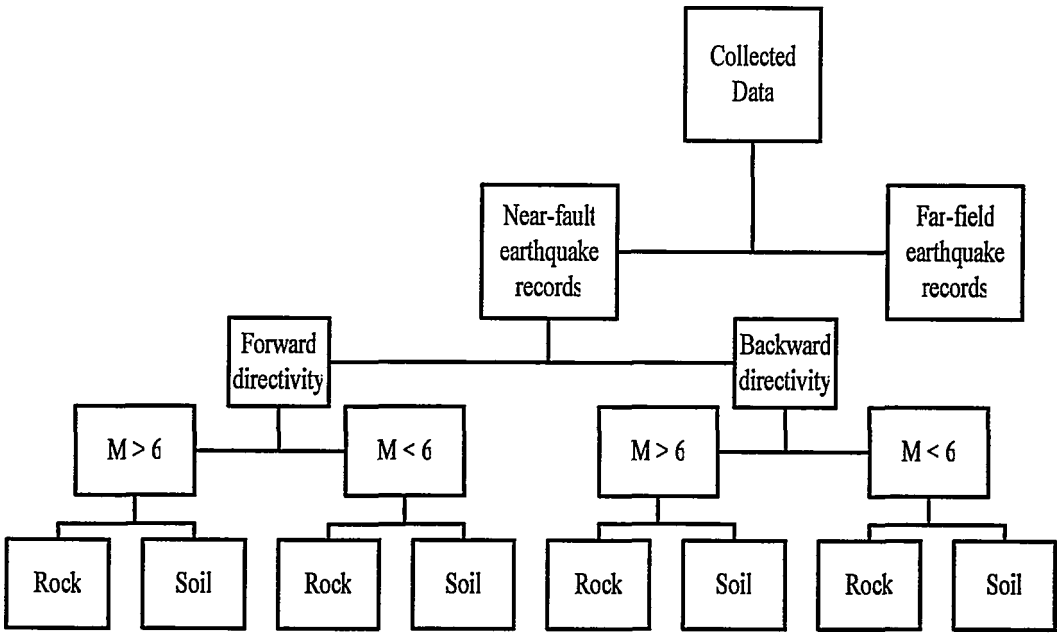

Figure 2.3 Categorization of data for this study

3. YIELD SPECTRUM DESIGN PROCEDURE

CHAPTER 3

YIELD SPECTRUM DESIGN PROCEDURE

3.1 INTRODUCTION

Traditional seismic design has focused on the strength of the structure rather than its performance. Design methods have been force/strength approaches. These methods used the period of the structure as the primary design parameter. In the performance-based design approach, the performance of the structure is the main target of the design process. Since structural damage is directly related to the deformation of the structure, displacement or drift may be used as the performance criteria.

Recent earthquakes around the world highlighted the need for performance-based seismic design with the consideration of both structural and non-structural damage, multiple performance objectives, specific quantification of performance criteria, and consideration of inelastic deformation of structures (Xue and Chen 2003). The yield spectrum method (YS) is a simple and effective method that is compatible with performance based design approach. It presents a stable graphical method that satisfies the target of multiple performance criteria. Performing linear and nonlinear analyses in the formation of the spectra ensures the consideration of both elastic and inelastic deformation of the structure.

In this chapter, the advantages of using the yield displacement as a primary design parameter for the yield spectra method are explained. The definition of the yield spectra and the methodology of its formation are discussed. The program used in the analysis of

the data is demonstrated and the steps of the calculation process are explained. The outcome graphs of the calculation process including the yield spectrum are presented.

3.2 YIELD DISPLACEMENT AS A PRIMARY DESIGN PARAMETER

The force-based procedures are based on the idea that the period of the structure can be estimated early in the design process, given the dimensions of the structure and the preliminary structural concept. At the end of the design processes, the actual period of the structure may vary significantly, especially if changes in the strength and stiffness of the members of the structure are made. Thus, it is difficult to accurately estimate the final period of the design process at early stages of the design.

The yield displacement is a more stable and useful parameter to be used in the seismic design of structures. The stability of the yield displacement was illustrated with four examples (Aschheim 2002). The examples were of moment resisting frames, each designed to limit roof drift for a specific ground motion using an equivalent SDOF system with the yield point spectra. The yield displacement was stable and consistent while the fundamental periods required to meet the performance objective varied significantly.

Aschheim and Black (2000) illustrated an example to support the choice of the yield displacement as a relatively stable parameter. They showed the base shear versus the roof displacement for two four-story steel moment resisting frames. The two buildings were similar in geometry but differed in the stiffness and strength by using different steel sections in the beams and columns. A bilinear curve fitted to the resulting capacity curves for the first mode shape. The changes in the yield spectra were negligible

between the two systems. The base shear coefficients were 0.3 and 0.56, and the periods were 1.13 and 0.81 s, respectively. The stability of the yield displacement relative to the change in the base shear strengths, stiffness and the fundamental period changes is illustrated in Figure 3.1.

The yield displacement of the structure is a function of the yield strain of the material, the height of the structure, the depth of the yielding members, the shape of the predominant mode of response, and the distribution of the mass and stiffness throughout the structure. These factors are known early in the design process, allowing early, accurate and relatively stable estimate of the yield displacement. On the other hand, the period is seen to be a consequence of the choices made in the design process to satisfy the performance objective. Thus, a major difference is that the yield displacement is independent of the strength of the structure while the fundamental period is totally dependent on it. This explains that the reliability of the yield displacement should be higher than that on the fundamental period of the structure in the design procedure.

3.3 METHODOLOGY FOR DETERMINING THE YIELD SPECTRA

3.3.1 ANALYSIS PROGRAM

The idealized bilinear load- displacement behaviour of SDOF oscillator is shown in Figure 3.2. There is a characteristic point on the load-deformation curve that defines the yield point of a SDOF system. For a bilinear load deformation relationship, some important points are defined for the calculation process of the yield spectra formation. The characteristic yield point is given by the yield displacement, Δ_y, and the yield

strength, V_y, of the oscillator. The ratio of V_y to the weight of the structure, W, is the yield strength coefficient, C_y. The peak displacement (ultimate) of the oscillator is defined by Δ_u, where the ratio of the ultimate displacement to the yield displacement gives the ductility value of the oscillator, $\mu = \Delta_u/\Delta_y$.

In this study, to determine the yield spectra the "Nonlin version 6.01" program is used (FEMA 2002). This program is a windows based application for nonlinear dynamic time history analysis of single degree of freedom systems. Using the program, both linear and nonlinear analyses are performed on SDOF systems. The dynamic loading is input as an earthquake accelerogram acting on the base of the structure. Actual earthquake records discussed in Chapter 2 are used for the analysis. Nonlin program uses a step-by-step method to solve the nonlinear equations of motion based on the structural dynamics solution techniques.

3.3.2 INITIAL INPUT REQUIRED

The structure is idealized as a SDOF system. For linear analysis, the following properties are required: weight (W), damping (β), and initial stiffness (K_1). For nonlinear analysis, two additional properties are required: secondary stiffness (K_2), and yield strength (F_y). The general units used for the analysis are: for length units centimeter (cm) is used, and for the force units the kilo Newton (kN) is used.

The weight of the system (W) is taken to be 1000 kN. The damping of the system (β) is taken to be 5% of the critical damping. The initial stiffness (K_1) is the slope of the pre-yield segment of the force-displacement response of a structure. Figure 3.3 illustrates the definition of the initial stiffness. The initial stiffness is calculated for each value of the

chosen range of periods for the calculation process (T= 0.1, 0.2, 0.3, 0.4, 0.5, 0.75, 1.0, 1.5, and 2.0 s) using the following equation:

$$T = 2\pi\sqrt{\frac{M}{K}} \tag{3.1}$$

where, M is the mass of the structure.

$$\therefore T = 2\pi\sqrt{\frac{1000}{g.K}} \tag{3.2}$$

where, g is the gravity acceleration with a value of 980.7 cm/s^2.

The secondary stiffness (K_2) is the first of two properties required for nonlinear analysis. The secondary stiffness is the slope of the post-yielding portion of the force-displacement response of a structure. K_2 is illustrated in Figure 3.3. Generally, K_2 is taken 5% of the initial stiffness. Table 3.1 shows the values of K_1, K_2 used in the calculation process. The calculated stiffness values are only dependent on the period of the structure for a given system mass.

The yield strength (F_y) is the force at which the yielding occurs. For a constant yield displacement, the yield strength value varies with the change in period. Figure 3.4a illustrates the definition for the case of a bilinear behaviour, where the yield strength is well defined. However, for a general nonlinear behaviour, the yield strength is defined by the intersection of the two tangents as illustrated in Figure 3.4b.

The SDOF system is subjected to ground acceleration in the form of ground motion acceleration time history. Records chosen in Chapter 2 are used after scaling to the required PGA.

3.3.3 ANALYSIS PROCEDURE

Having selected 30 earthquakes for this study, a calculation process is performed for each record. Eight periods are chosen to cover a wide range of practical frequencies (T= 0.1, 0.2, 0.3, 0.4, 0.5, 0.75, 1.0, 1.5, and 2.0 s). To study the effect of the PGA on the results, the earthquake records are scaled to four values of PGA (0.1g, 0.2g, 0.3g, and 0.4g). Thus, for each earthquake record and each period, the subsequent steps of calculation are followed:

a) LINEAR ANALYSIS

The linear analysis is the first step towards the formation of the yield spectra. The initial inputs of the SDOF system required for linear analysis are the system mass, damping, and initial stiffness according to the values in Table 3.1. Linear elastic analysis gives the force variation with displacement for the duration of the record (F_e) and the corresponding maximum displacement (Δ_e) stored as illustrated in Table 3.2.

b) NONLINEAR ANALYSIS

To conduct the nonlinear analysis, two additional system properties are needed: the secondary stiffness (K_2) and the force modification factor. The secondary stiffness is set according to the values stated in Table 3.1. For setting the yield strength for the nonlinear analysis, there are four levels of force modification factor chosen for this study (R= 2, 3, 4, and 8). The F_y value is calculated by dividing the value of F_e from the linear elastic analysis by the R values. The result of the nonlinear analysis, at each R-value, is

the maximum displacement of the system (Δ_{max}) and the maximum force carried by the system (F_{max}). These values are stored for further calculations as illustrated in Table 3.3.

c) CALCULATED PARAMETERS

For each period, few simple calculations are made from the linear and nonlinear analysis results. For a given R-value, the corresponding ductility value μ is calculated. The ductility is equal to the peak displacement Δ_{max} multiplied by the R-value and divided by the elastic displacement Δ_e.

$$\mu = \frac{\Delta_{max} R}{\Delta_e} \tag{3.3}$$

The yield displacement Δ_y is calculated as the ratio of the Δ_{max} by the ductility value.

$$\Delta_y = \Delta_{max}/\mu \tag{3.4}$$

The yield strength coefficient C_y is calculated as the ratio of the maximum force (base shear) to the weight of the structure.

$$C_y = \frac{F_{max}}{1000} \tag{3.5}$$

A new force modification factor R_{new} can now be calculated as the ratio between the elastic force to the maximum force.

$$R_{new} = \frac{F_e}{F_{max}} \tag{3.6}$$

The quantities obtained using formulas 3.3 to 3.6 are stored as demonstrated in the example in Table 3.3. The table summarizes the calculations for the 1994 Northridge earthquake, Pacoima dam ground motion, scaled to PGA 0.3g.

3.3.4 ASSESSMENT OF RESULTS

The described steps of the analysis were conducted using all the selected earthquake records. The results as shown in Table 3.3 are plotted. For each period, the calculated results are curve fitted to obtain corresponding values for specific required ductility levels (μ = 1, 2, 3, 4, and 8). Thus, for each ductility value, there is a calculated value for R_{new} factor, C_y factor, and Δ_y.

Using the calculated values of various parameters, three different graphs are plotted. The R-μ-T graph is plotted using the R_{new} values corresponding to the required ductility level. The relationship between the force modification factor and the period of the structure for the constant ductility levels is plotted. As example, Figure 3.5 presents the R-μ-T graph for Northridge earthquake, Pacoima dam ground motion, scaled to PGA 0.3g.

The force modification factor R is implied by the codes as a factor assigned for an acceptable damage level. These values are assigned to various structural systems based on experience and judgment. Investigating the R_{new} values leads to having accurate R-values. Knowing the period of the structure and the required ductility, the required force modification factor can be easily obtained.

The second graph is the C_y-μ-T graph. This graph represents the relationship between the yield strength coefficients and the period of the structure for different ductility levels. The C_y factor is a significant factor for the design process of the structure since it gives the design base shear. Figure 3.6 illustrates an example C_y-μ-T graph for Northridge earthquake, Pacoima dam ground motion, scaled to PGA 0.3g. The yield

strength coefficient divided by the R factor gives the base shear force of the structure. Given the base shear, normal force based design of the structure can be conducted to proportion the member's strengths, and proportion the lateral force resisting systems.

The third graph is the yield spectra. The yield displacement for oscillators with constant ductility is plotted with the yield strength coefficient (C_y). Figure 3.7 presents the yield spectra for the 1994 Northridge earthquake, Pacoima Dam ground motion, scaled to PGA 0.3g, for ductility values μ=1, 2, 3, 4, and 8.

The yield spectra shown in Figure 3.7 provide the relationship between the yield strength coefficient and the yield displacement for constant ductility values for a specific ground motion. Knowing the yield displacement of the oscillator and the required ductility value for the structure, an estimate of the yield strength coefficient can be made. This allows the estimation of the base shear forces and the start of the design process of the structure.

As an example to illustrate the design procedure consider an oscillator with yield displacement of 5 mm, and the required ductility of μ=2. From the yield spectrum, the yield displacement of 5 mm and the curve for ductility 2 gives C_y value of 0.2. The weight of the building is 1000 kN, the base shear force value is 1000 x 0.2 = 200 kN. The base shear can be distributed along the height of the structure giving the required design forces. The simplicity of this graph helps to consider the influence of changes in stiffness and strength on the yield displacement and ductility values, thus their effect on the C_y factor is take into account directly in a single step.

The described calculation procedure is repeated to determine the yield spectra for the chosen earthquake records scaled to different PGA levels. From the yield spectra of a large number of earthquakes, a realistic design spectrum can be determined. Averages are taken for records on rock sites and records on soil sites to investigate the soil effect on the yield spectra. Another general averages are formed for records on all site soils. Using the resulting graphs, comparisons are made to analyze the influence of various factors on the spectra. Studying the effect of the site soil type, the epicentral distance and the magnitude of the earthquake on the spectra gives actual and realistic values for some parameters utilized in the design process. These parameters used to be assumed by the designer.

Table 3.1 Stiffness values for the SDOF oscillators

Period (s)	K1 (kN/cm)	K2 (kN/cm)
0.1	4028.40	201.42
0.2	1007.1.	50.35
0.3	447.60	22.38
0.4	251.60	12.58
0.5	161.14	8.06
0.75	71.65	3.58
1.0	40.28	2.01
1.5	17.89	0.89
2.0	10.07	0.50

Table 3.2 Example of linear analysis results for the Northridge earthquake 17/1/1994 (Pacoima dam, upper left abutment 104) scaled to PGA 0.3g

Period (s)	F_e (kN)	Δ_e (mm)
0.1	164.13	0.41
0.2	189.99	1.89
0.3	204.05	4.60
0.4	151.99	6.04
0.5	143.60	8.91
0.75	63.91	8.92
1.0	35.85	8.90
1.5	13.40	7.49
2.0	4.97	4.94

Table 3.3 Example of nonlinear analysis results for the Northridge earthquake 17/1/1994 (Pacoima dam, upper left abutment 104) scaled to PGA 0.3g

T (s)	R	F_{max} (kN)	Δ_{max} (mm)	R_{new}	μ	C_y	Δ_y (mm)
0.1	1.0	164.132	0.410	1.000	1.000	0.164	0.410
	2.0	88.778	0.540	1.849	2.634	0.089	0.205
	3.0	69.121	0.850	2.375	6.220	0.069	0.137
	4.0	61.670	1.130	2.661	11.024	0.062	0.103
	8.0	57.045	1.860	2.877	36.293	0.057	0.051
0.2	1.0	189.992	1.890	1.000	1.000	0.190	1.890
	2.0	102.170	2.370	1.860	2.508	0.102	0.945
	3.0	72.465	2.440	2.622	3.873	0.072	0.630
	4.0	57.632	2.480	3.297	5.249	0.058	0.473
	8.0	39.305	3.330	4.834	14.095	0.039	0.236
0.3	1.0	204.046	4.600	1.000	1.000	0.204	4.600
	2.0	104.544	3.410	1.952	1.483	0.105	2.300
	3.0	71.162	2.930	2.867	1.911	0.071	1.533
	4.0	56.552	3.620	3.608	3.148	0.057	1.150
	8.0	33.786	4.270	6.039	7.426	0.034	0.575
0.4	1.0	151.986	6.040	1.000	1.000	0.152	6.040
	2.0	79.305	5.650	1.916	1.871	0.079	3.020
	3.0	52.505	3.480	2.895	1.728	0.053	2.013
	4.0	42.335	4.970	3.590	3.291	0.042	1.510
	8.0	23.667	4.470	6.422	5.921	0.024	0.755
0.5	1.0	143.602	8.910	1.000	1.000	0.144	8.910
	2.0	73.313	6.330	1.959	1.421	0.073	4.455
	3.0	50.193	5.860	2.861	1.973	0.050	2.970
	4.0	38.229	5.120	3.756	2.299	0.038	2.228
	8.0	21.684	5.750	6.622	5.163	0.022	1.114
0.75	1.0	63.913	8.920	1.000	1.000	0.064	8.920
	2.0	32.722	6.590	1.953	1.478	0.033	4.460
	3.0	22.865	7.330	2.795	2.465	0.023	2.973
	4.0	18.474	9.200	3.460	4.126	0.018	2.230
	8.0	10.474	8.050	6.102	7.220	0.010	1.115

Table 3.3 Example of nonlinear analysis results (continued)

T (s)	R	F_{max} (kN)	Δ_{max} (mm)	R_{new}	μ	C_y	Δ_y (mm)
1.0	1.0	35.848	8.900	1.000	1.000	0.036	8.900
	2.0	19.087	10.220	1.878	2.297	0.019	4.450
	3.0	13.693	11.630	2.618	3.920	0.014	2.967
	4.0	10.298	8.860	3.481	3.982	0.010	2.225
	8.0	5.527	6.310	6.486	5.672	0.006	1.113
1.5	1.0	13.399	7.490	1.000	1.000	0.013	7.490
	2.0	7.063	7.800	1.897	2.083	0.007	3.745
	3.0	4.939	7.780	2.713	3.116	0.005	2.497
	4.0	3.958	8.670	3.385	4.630	0.004	1.873
	8.0	2.163	6.400	6.195	6.836	0.002	0.936
2.0	1.0	4.972	4.940	1.000	1.000	0.005	4.940
	2.0	2.720	7.110	1.828	2.879	0.003	2.470
	3.0	1.990	8.440	2.498	5.126	0.002	1.647
	4.0	1.555	7.440	3.197	6.024	0.002	1.235
	8.0	0.892	5.990	5.574	9.700	0.001	0.618

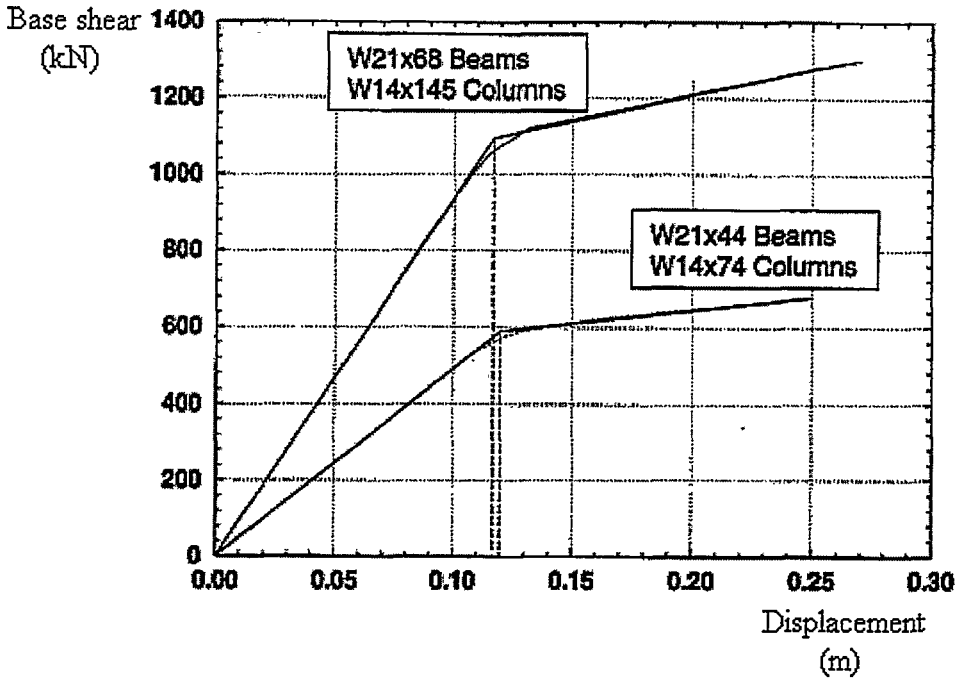

Figure 3.1 The yield displacement of frames with different lateral stiffness (Aschheim and Black 2000)

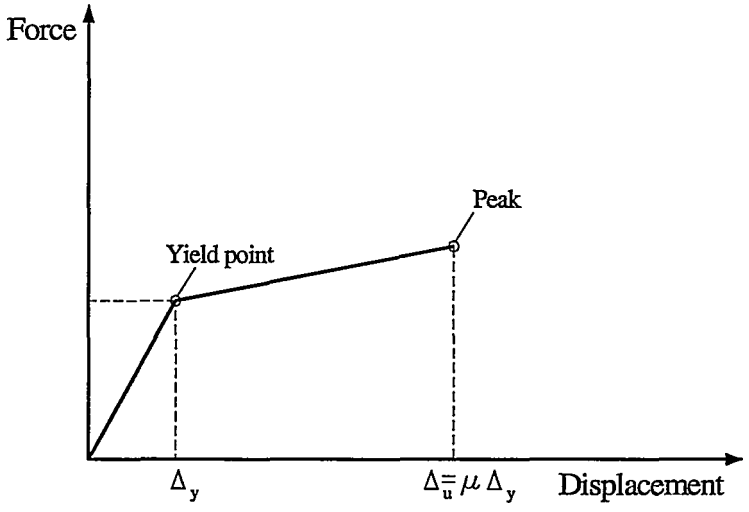

Figure 3.2 Force-displacement response of a SDOF system

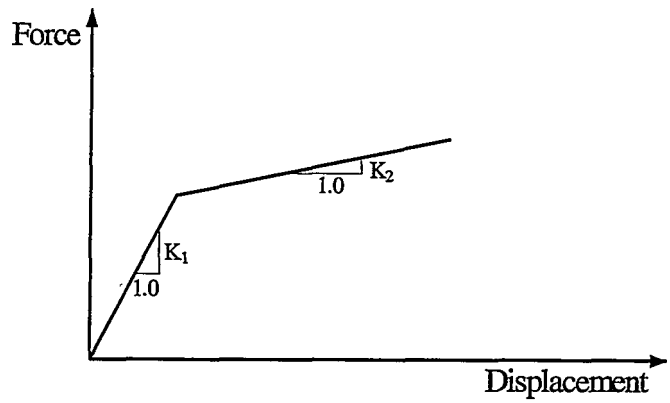

Figure 3.3 Force-displacement relation of a SDOF system showing K_1, K_2 definitions

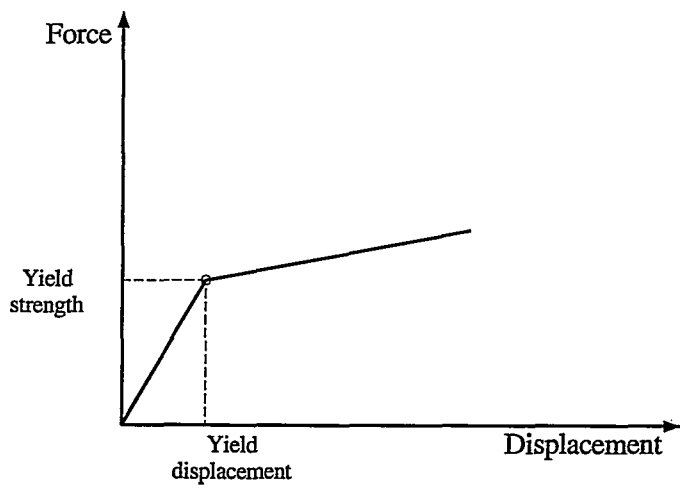

Figure 3.4a Well defined yield point in case of bilinear behaviour

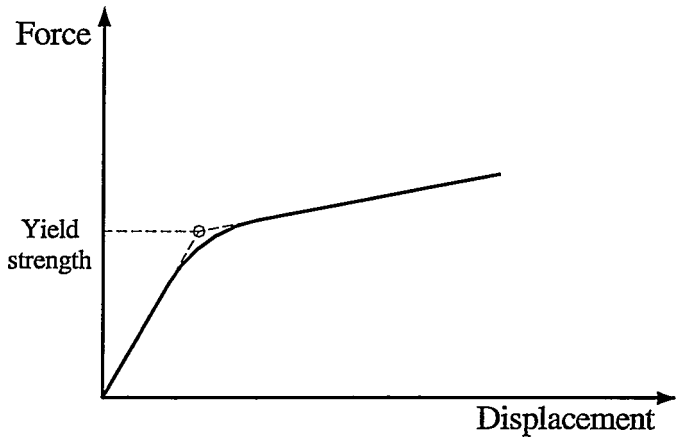

Figure 3.4b Yield strength definition in case of a general non-linear behaviour

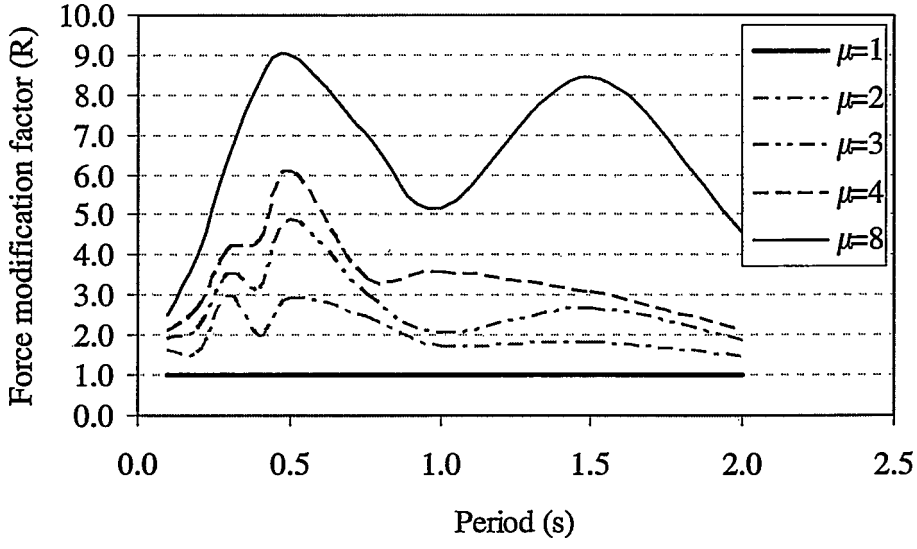

Figure 3.5 R-μ-T graph for the 1994 Pacoima dam, Northridge earthquake for PGA 0.3g

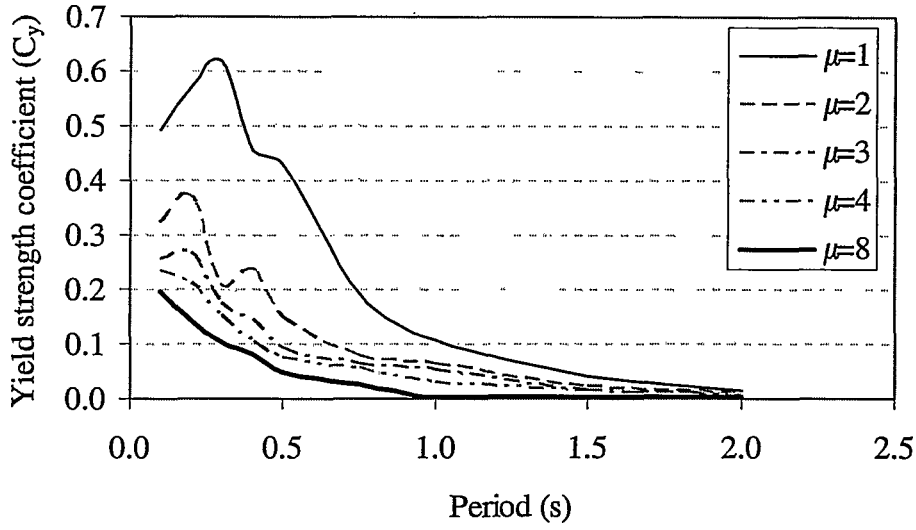

Figure 3.6 C_y-μ-T graph for the 1994 Pacoima dam, Northridge earthquake for PGA 0.3g

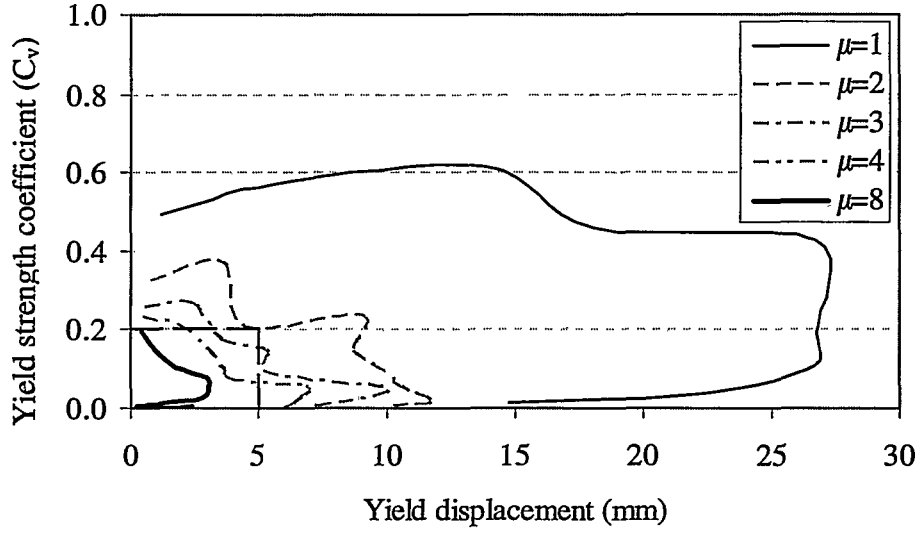

Figure 3.7 Yield spectra for the 1994 Pacoima dam, Northridge earthquake for PGA 0.3g

4. EVALUATION OF RESULTS

CHAPTER 4

EVALUATION OF RESULTS

4.1 INTRODUCTION

Developing an efficient and effective general methodology for the design of structures to multiple performance and hazard levels is the major target of present earthquake engineering research. The Yield spectra procedure, as discussed in Chapter 3 is a simple and effective method that allows the design for several limit states in one-step. Further investigation is required to study the unresolved issues concerning the quantitative understanding of site-specific characteristics, their likely effects on structures, and some aspects of near-fault effects (Ghobarah 2001).

In previous chapters, different sets of earthquake records were selected. A SDOF system was subjected to these ground motions scaled to different peak ground accelerations. Linear and nonlinear dynamic analyses of the system were conducted. For each record, three relationships were established: force modification factor variation with the period for different ductility levels, yield strength coefficient variation with the period for different ductility values, and the yield spectrum for the record (yield strength coefficient variation with yield displacement for different ductility values).

In this chapter, averages of each of these relationships for the different values of scaled peak ground accelerations at constant ductility values are presented. Each relationship has an average graph for the earthquake records on rock sites, an average graph for the records on soil sites, and a general graph for records on both rock and soil

sites. These plots will help to investigate the effect of the site soil on the results. The different graphs are plotted for records with magnitude greater and less than 6 for the near-fault records to study the magnitude effect on the results. In addition, similar graphs are plotted for the far-field earthquake records, thus highlighting the effect of the fault distance on the yield spectra. Scaling the records to different values of PGA helps to investigate the effect of the PGA of the ground motion on the yield spectra. This will show the difference in the design values for the structure when subjected to ground motion scaled to different PGA values.

Evaluating the effect of various parameters on the design spectrum, results in some important conclusions that will help improve the development of the design method. Investigation of the effect of various parameters will help reduce the uncertainties in the design procedure and will enhance the yield spectra method to be suitable for code applications.

4.2 FORCE MODIFICATION FACTOR (R-μ-T) GRAPH

Current codes assign a level of acceptable damage implied by the R-factor (Force modification factor). The R-factor values differ for various structural systems at the life-safety performance level. These values are qualitative and judgmental in general; however, they are widely accepted and used in seismic design.

Researchers have considered the R-factor to consist of components associated with system ductility (R_μ) and overstrength (R_s), where $R = R_\mu R_s$. Aschheim and Black concluded that the system ductility limits at the life safety level should correspond

approximately to the R_μ implicit in current codes, while the associated R_s factors would be applicable to the required lateral strength. Hence, investigation of the R-values using nonlinear analysis is important to validate design assumptions and to ensure that performance objectives are satisfied.

4.2.1 METHODOLOGY

To investigate the R-factor, an analysis procedure was applied to each earthquake record. The procedure is as follows: first, a SDOF system is subjected to the earthquake record and a linear analysis of the system is conducted. The maximum elastic force (F_e) and the maximum elastic displacement (Δ_e) from the linear analysis are recorded for different period values (T = 0.1, 0.2, 0.3, 0.4, 0.5, 0.75, 1.0, 1.5, 2.0 s). Knowing Fe, four levels of R are selected (R = 2, 3, 4, 8). This range of R-values was selected because the highest R-values are 4 and 8 in the Canadian and U.S. practice, respectively. Using the selected R-value, F_e and Δ_e are reduced to get F_y, and Δ_y where ($F_y = F_e/R$, $\Delta_y = \Delta_e/R$), F_y being the yield force and Δ_y being the yield displacement of the structure. Finally, for each level of F_y an inelastic analysis of the SDOF is conducted to evaluate the maximum force (F_{max}), and the maximum displacement demand (Δ_{max}). Thus, the force modification factor is recalculated as $R = F_e/F_{max}$, and the ductility demand is $\mu_d = \Delta_{max}/\Delta_y$.

Using these results, the relationship between the R-factor and the period for different ductility levels is established for each earthquake record. As the records are scaled to different PGA, for each PGA value, average of this relationship is taken for earthquake records on rock sites, records on soil sites, and a general average for both soil and rock together. These graphs are grouped according to the magnitude of the

earthquake and the distance from the fault. The classification of the graphs is performed according to the flowchart shown in Figure 4.1.

4.2.2 DISCUSSION OF RESULTS

From studying the values of the recalculated R-factors resulting from the inelastic analysis, it was found that for short period structures, the R-factors must be reduced to maintain constant ductility responses. Similar observation was made by Aschheim and Black (2000). The values of the new R-factors are smaller than the selected R_μ factors for nonlinear analysis procedures, for the chosen periods. This is because for short period systems, R_μ applies as a system ductility limit, thus the actual strength reduction factor will be smaller than the R_μ factor.

Comparing the average graphs in Figures 4.2 and 4.3, shows that R-factor value for near-fault earthquake records with magnitude less than 6 are higher than that for the records with magnitude higher than 6 for the periods in range 0.1s-1.5s. This can be attributed to the site soil effect. Although the magnitude of these earthquakes is less than 6, which includes minor to moderate earthquakes, the R-μ-T graph for each of the chosen 5 records has a very high R-factor. This is true especially at high ductility values. In addition, there is no specific range of periods where those peaks are present; this explains why the R-factor value is high all over the period range from 0.1s to 1.5s in Figure 4.3. The R-factor values for each record scaled to PGA 0.1g is shown in Appendix A.

For the rock graph, the peak values occur at periods of 0.5s then the value of the R-factor becomes nearly constant or decreases with period as shown in Figure 4.2. Investigating the soil graph in Figure 4.2, the R-factor tends to increase in value with the

increase in the period. This explains the reason for higher values of R-factor at periods greater than 1.5s.

Evaluating the rock and soil graphs in Figures 4.2 and 4.3 individually, for the same period, the R-factor varies for rock and soil sites. For example, if similar buildings with similar conditions (e.g. T=0.4s and μ=4) were built on rock and soil sites where earthquakes with magnitude higher than 6 are expected. The building on the rock site will have high R-factor of 6.3 while that on the soil site will have R-factor of 2.9. This illustrates how the soil site affects the force modification factor.

The far-field earthquake records show different variation of the force modification factor with the periods as shown in Figure 4.4. The influence of the soil becomes clear in the graphs. Soft soil magnifies the ground motion. This may explain the high R-factor that is calculated for the records, especially for periods equal to 0.3s and 1s. Examining the rock behaviour, the values are much lower in the far-field than in the near-fault region. Although the earthquake ground motion attenuates with distance away from the fault, the presence of soil even in the far-field tends to magnify the effect of the earthquake.

The effect of scaling the records to different PGA (0.1g, 0.2g, 0.3g, 0.4g) shows that: the R-factor for the same earthquake record under the same conditions remains similar under the various PGA values. This can be clearly shown in Figures 4.2, 4.5, 4.6 and 4.7 for near-fault forward directivity earthquakes with magnitude greater than 6, Figures 4.3, 4.8, 4.9 and 4.10 for near-fault forward directivity earthquakes with magnitudes less than 6, and Figures 4.4, 4.11, 4.12 and 4.13 for far-field earthquakes.

A general observation is that for rock sites, the structures with periods in the range 0.1s-0.75s have higher R-factor in comparison with the other periods for the same ductility values. This applies to all cases studied. While for the soil sites, the behaviour varies with varying the conditions of the site, the magnitude of the earthquake and the distance from the fault. Thus, further investigation of the soil characteristics and its effect on the R-factor is required.

4.3 YIELD STRENGTH COEFFICIENT (C_Y-μ-T) GRAPH

The basic idea of the yield spectra design procedure is to calculate the base shear force then distribute it over the height of the building. The base shear coefficient, defined as base shear/weight of the structure, is used in the design of member strength, allowing conventional strength-based design procedure to be used in performance-based approaches for designing the lateral force resisting system (Aschheim and Black 2000). The base shear coefficient for a building is $\alpha_1 C_y$ (α_1 is the mass participation factor; C_y is the yield strength coefficient defined as the base shear divided by the weight of the structure).

The yield strength coefficient versus period graph shows the variation of the C_y factor with the period of structures at different ductility values. This indicates that the periods with higher yield strength coefficient correspond to higher base shear forces.

4.3.1 METHODOLOGY

The C_y factor is calculated using the procedure explained earlier in section 4.2.1. The yield strength coefficient equals the base shear force (V) divided by the weight of the

building (W), C_y=V/W. The base shear force is the calculated F_{max}. To simplify numerical calculations, the weight of the building is taken to be 1000 kN. A value of the C_y is computed in the linear analysis of the SDOF system. In the nonlinear analysis, for each selected R-value, at the various selected periods, C_y values are determined.

Using these results, the second relationship between the C_y factor and the period for different ductility values is established for each earthquake record. Similar to the R-μ-T graph, for each PGA, average of this relationship is taken for earthquake records on rock sites, records on soil sites, and a general average for rock and soil together. These graphs are grouped according to the magnitude of the earthquake and the epicentral distance. The classification of the graphs is according to the flowchart shown in Figure 4.14.

4.3.2 DISCUSSION OF RESULTS

The C_y values tend to be higher for very small periods for all ductility levels. The C_y values decrease with the increase in periods until it becomes nearly constant with very small value at longer periods. This behaviour is typical regardless of the magnitude of the earthquake, type of soil, and epicentral distance. The behaviour of C_y with the period is shown in Figures 4.15, 4.16 and 4.17 for NFE with magnitude greater than 6, NFE with magnitude less than 6 and FFE, respectively.

Investigating the effect of magnitude of the earthquake shown in Figures 4.15 and 4.16, the C_y values tend to be slightly higher for earthquake records with magnitude greater than 6 than the earthquake records with magnitude less than 6. This is attributed to the slightly higher C_y values of the earthquake records on both the rock and soil sites.

The behaviour is reasonable since it is expected that with the increase in magnitude of an earthquake, the base shear forces increase, hence increase the yield strength coefficient.

Comparing the rock and soil graphs in Figure 4.15, for the same period and ductility value, the C_y value is higher for the soil site when compared to the rock sites. This indicates higher base shear for structures constructed on soil sites. Similar conclusion is observed when studying Figure 4.16, but the values are much higher in the soil sites than that of the rock especially for periods up to 1.0s. This illustrates the importance of the soil type in magnification of the ground motion effect.

Studying the effect of the fault distance on the C_y values, shown in Figure 4.17, the C_y values for the far-field records are of higher values than those for the near-fault records for both rock and soil sites. This means that short period structures in the far-field region will have higher base shear forces than that in the near-fault region, at the same PGA level. Investigating the soil graph in the figure, higher C_y values are due to the magnification effect of the soil regardless of the distance. In addition, at far distances, it is expected that the high frequencies tend to be filtered and low frequencies of the ground motion remain. These observations are made within the limitations of the PGA scaling procedure and the specific small number of records selected.

The influence of scaling the PGA of the records shows that the C_y factor increases with the increase in the PGA value. For example, the values of C_y for PGA of 0.2g, 0.3g, 0.4g are twice, three times, and four times the value of 0.1g, respectively. This explains the relationship between the values of the C_y factor when scaling the record to different peak ground accelerations. Thus, one can predict the base shear force for designing the

structure. This is clearly shown in Figures 4.15, 4.18 and 4.19 for near-fault forward directivity records with magnitude greater than 6, Figures 4.16, 4.21, 4.22, and 4.23 for near-fault forward directivity records with magnitude less than 6, and Figures 4.17, 4.24, 4.25, and 4.26 for far-field records. Figures 4.15 to 4.26 were replotted in the form of a separate graph for ductility level with the response for all PGA level on the same plot. These plots are in Figures B.1 to B.16 in Appendix B.

4.4 YIELD DISPLACEMENT (YIELD SPECTRA)

Aschheim and Black (2000) showed that the yield displacement is a relatively stable parameter even with changes in the base shear, strength, lateral stiffness, and periods of vibration. This highlighted the idea of approaching the seismic design from the perspective of constant yield displacement rather than by the traditional approach of constant period.

Quantifying performance objectives in terms directly related to the design process is necessary for ease of application. Aschheim and Black adopted the peak drift as a design parameter that is directly related to the response and damage of the non-structural components. A more appropriate parameter in design is the maximum interstorey drift as it takes into account the distribution of damage along the height of the structure. The ductility is a useful index as well; it is directly related to the structural damage associated with inelastic response. Controlling the drift and ductility of the system will achieve the desired performance objectives. Examples of recommended drift limits are proposed in the Vision 2000 (1995). System ductility limits can be also related to acceptable levels of structural damage.

4.4.1 METHODOLOGY

The procedure was explained in sections 4.2.1, and 4.3.1. In the linear and nonlinear analysis steps, a value for the maximum displacement demand (Δ_{max}) and a value for the yield strength coefficient C_y are calculated. For each ductility value, the C_y factor is plotted against the displacement. This is the third relationship established from the calculation process. Similar to the previous relationships, for each PGA, average behaviours were calculated for earthquake records on rock sites, records on soil sites, and a general average for both soil sites. These graphs are grouped according to the magnitude of the earthquake and the distance from the fault. The classification of the graphs is performed according to the flowchart shown in Figure 4.27.

4.4.2 DISCUSSION OF RESULTS

The recommended drift limit and the system ductility related to the required performance objective are first established. Using the yield spectra, the yield strength coefficient can be obtained allowing the design of the members and the structure using the calculated base-shear force distribution.

In Figures 4.28, 4.29 and 4.30, the structures with low ductility values should be designed to higher C_y values. There is a general trend for the relationship between the ductility, peak displacement demand, and the C_y factor. The higher the ductility level, the higher the peak displacement limit, and thus the lower the C_y values.

Studying near-fault earthquake records with magnitude greater than 6, Figure 4.28 shows that the yield displacements for the soil sites are larger than those of the rock sites.

This shows that structures built on soil sites and subjected to earthquakes with magnitude greater than 6 have high peak displacement limit as compared to those built on rock sites.

In Figure 4.29, for near-fault records with magnitude less than 6, the behaviour is different, both rock and soil sites have relatively small yield displacements. Even for very small displacements, the C_y factors for the soil sites are still larger than those for the rock sites. In a general, comparison between the average graphs shown in Figures 4.28 and 4.29 indicates the effect of the magnitude of the earthquake record. The yield displacements and C_y factor are larger with the higher magnitudes (greater than 6). Thus the greater the magnitudes, the larger the required displacement limit, C_y factor, and finally base shear forces.

In Figure 4.30 for far-field earthquake records, the yield displacements and C_y factor have higher values than those for the near-fault records. It is observed that rock and soil sites give very close values for the C_y factor. Figure 4.17 shows that for similar periods the C_y values was nearly the same for both site soils. This can be attributed to the low frequency content of the records at the far-field, which makes the behaviour of the structure on rock and soil similar.

Similar to the variation of C_y with the period, the influence of changing the PGA of the records shows that the values of the C_y factor and the yield displacement increase with the increase in the PGA value. For example, the values of C_y for PGA 0.2g, 0.3g, 0.4g are almost twice, three times, and four times the value of 0.1g respectively. This is shown in Figures 4.28, 4.31, 4.32, and 4.33 for near-fault forward directivity records with magnitude greater than 6, Figures 4.29, 4.34, 4.35, and 4.36 for near-fault forward

directivity records with magnitude less than 6, and Figures 4.30, 4.37, 4.38, and 4.39 for far-field records. Figures 4.28 to 4.39 were replotted in the form of a separate graph for each ductility level with response for all PGA levels on the same plot. These plots are in Figures B.17 to B.31 in Appendix B.

4.5 SUMMARY

From the previous discussions of the R-μ-T graphs, the C_y-μ-T graphs, and the yield spectra, some of the important aspects of the behaviour are summarized.

The effect of the site soil for near-fault records is evaluated using the variation of the R-factor values with changing the soil type (rock, soil). This is shown when comparing the response of structures having the same period, under the same ground motion, but on different site soils. The difference in the response of the structures on rock and soil sites at near-fault distances is quite significant.

Comparing the rock and soil C_y-μ-T graphs illustrated the influence of the soil factor. Structures of periods up to 1.0s on soil sites have higher C_y factor than those on rock sites when subjected to same ground motion and within the same broad epicentral distance classification. This illustrates the contribution of the soil to magnifying the ground motion, leading to higher base shear forces, thus higher C_y factors. Similar result is achieved by studying the yield spectra, the rock sites have small yield displacements and low C_y factor. While the records on soil sites showed higher yield displacement values and higher C_y values.

Studying the behaviour of structures to far-field records leads to different results from those under the effect of near-fault. The response to the records on the rock and soil

sites is close with the possibility of having higher responses in either of them. For the rock sites, the earthquake ground motion is characterized by high frequency content, thus the responses remains high even with varying distance from the fault. For the soil sites, however, although the high frequencies attenuate with the wave travel, the soil at the site of the structure magnifies the ground motion. This explains the predicted response of structure on soil and rock sites in the far-field.

The type of the site soil appears to be an important factor influencing the seismic design of structures in near-fault region. Studying the far-field and the near-fault effects shows that near-fault effect should be addressed in design codes.

The behaviour of structure on rock is generally consistent in having the peak response at short period structures in the interval from 0.1s to 0.75s. On the other hand, the soil sites have a wide peak response interval. The peak response varied with the magnitude and the epicentral distance. This indicates that further sub-categorization of the soil sites is required (for example: stiff soil, soft soil).

Scaling of the earthquake record was found to have no effect on the R-factor values. This is true regardless of the soil type and the epicentral distance. The PGA scaling of the records indicate that the ratio between the responses at the different PGA is directly proportional to the ratio between the PGA values. This behaviour is illustrated in the Figures from B.1 to B.16, which presents the C_y-T relationship. These graphs show the relationship between the C_y factor and the period at constant ductility levels for the chosen PGA (0.1g, 0.2g, 0.3g, and 0.4g). Figures B.16 to B.31 show the relationship

between the C_y factor and the yield displacement at constant ductility levels for the chosen PGA.

The force modification factor increases with the increase in the ductility of the structure. This agrees with the code's approach, although the relationship is not linear as generally assumed. This is illustrated by Figures 4.2 to 4.13. The C_y factor decreases with the increase in the ductility levels as demonstrated by Figures 4.15 to 4.26 to present the C_y-μ-T relationship, and by Figures 4.28 to 4.39 to present the yield spectra. As expected, this indicates that the base shear force decreases as the ductility level increases.

The validity of the observations made in this investigation is limited by the relatively small number of ground motions selected for the analysis as well as the limitations of the PGA scaling approach.

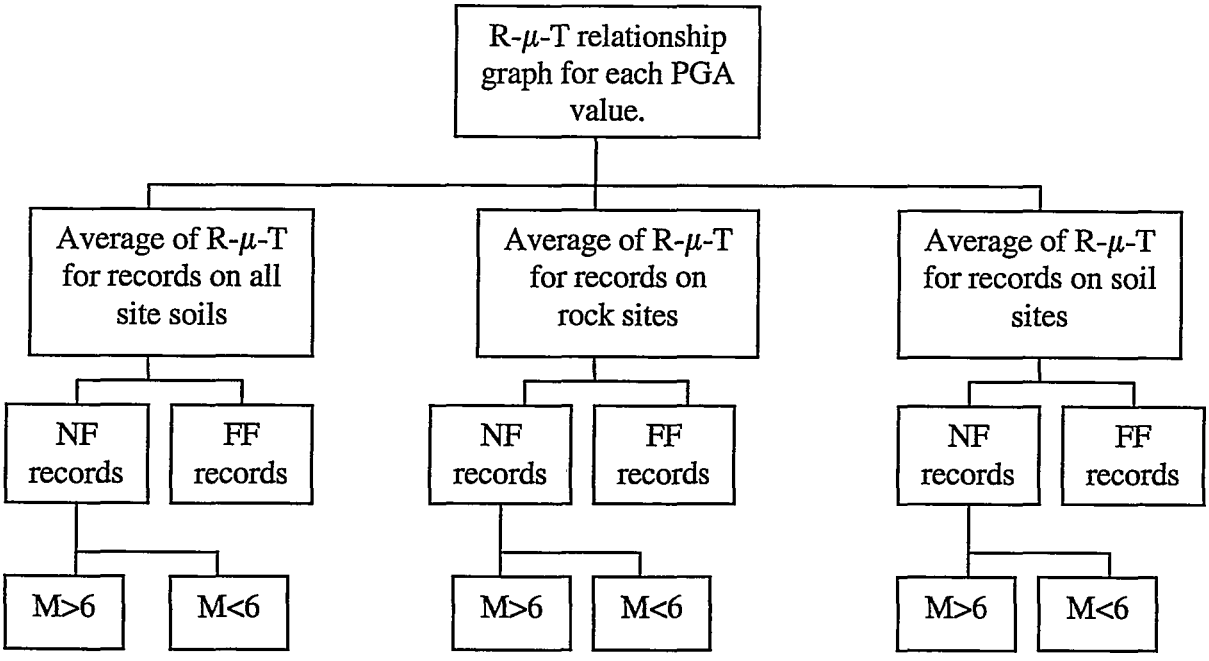

Figure 4.1 Classification of the R-μ-T graph

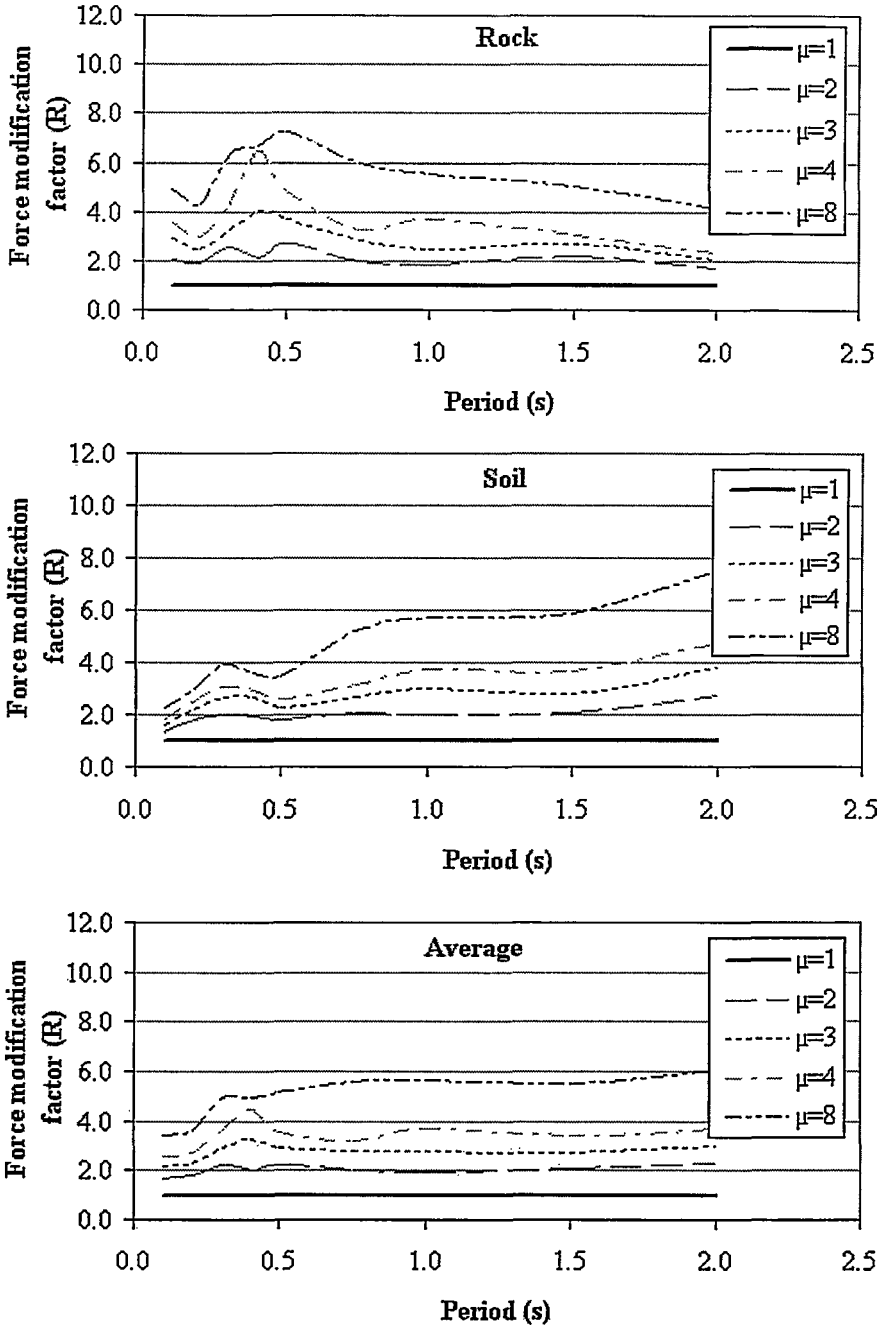

Figure 4.2 Force modification factor variation with period for NFE with magnitude >6 with PGA = 0.1g

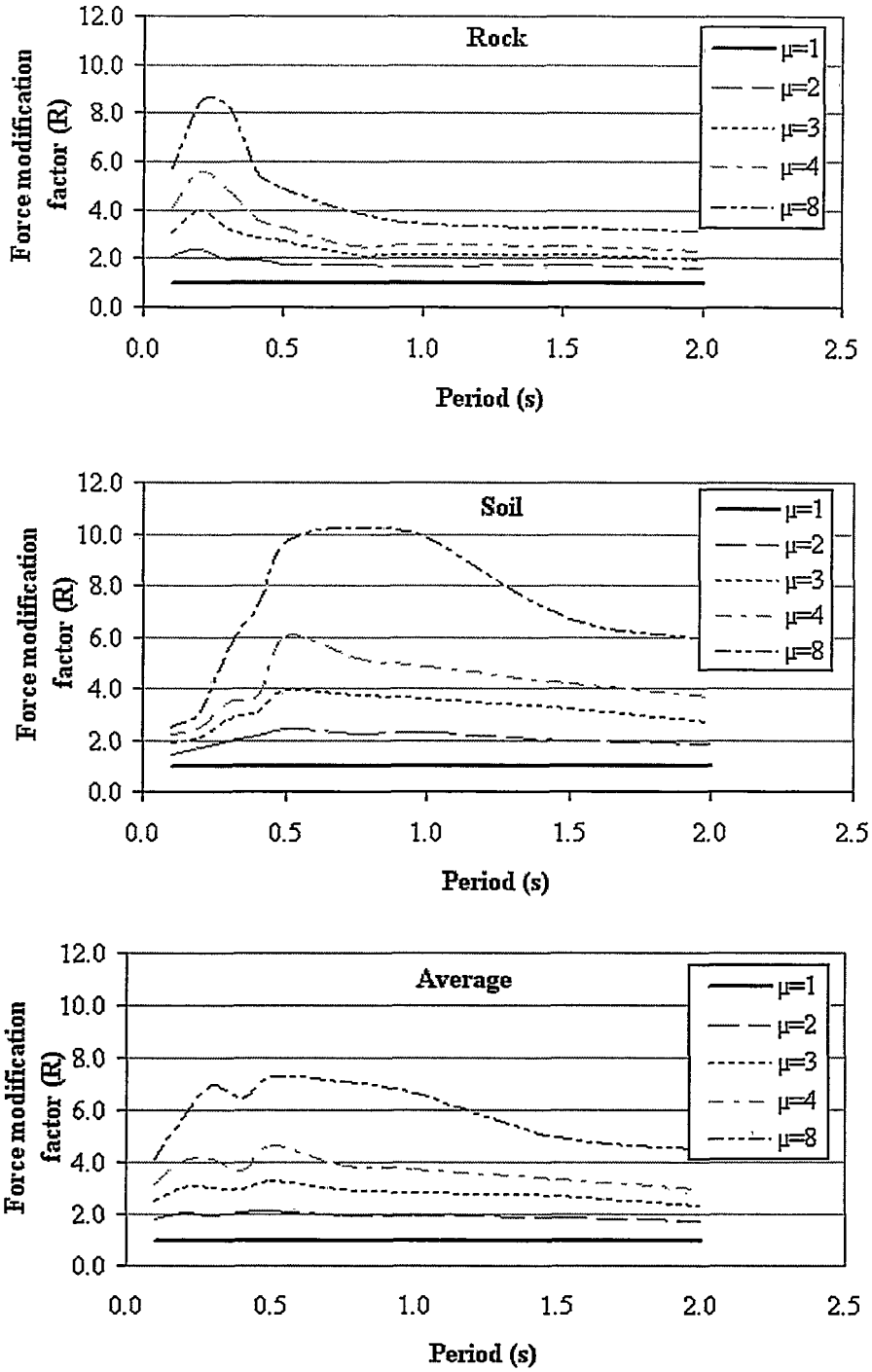

Figure 4.3 Force modification factor variation with period for NFE with magnitude <6 with PGA = 0.1g

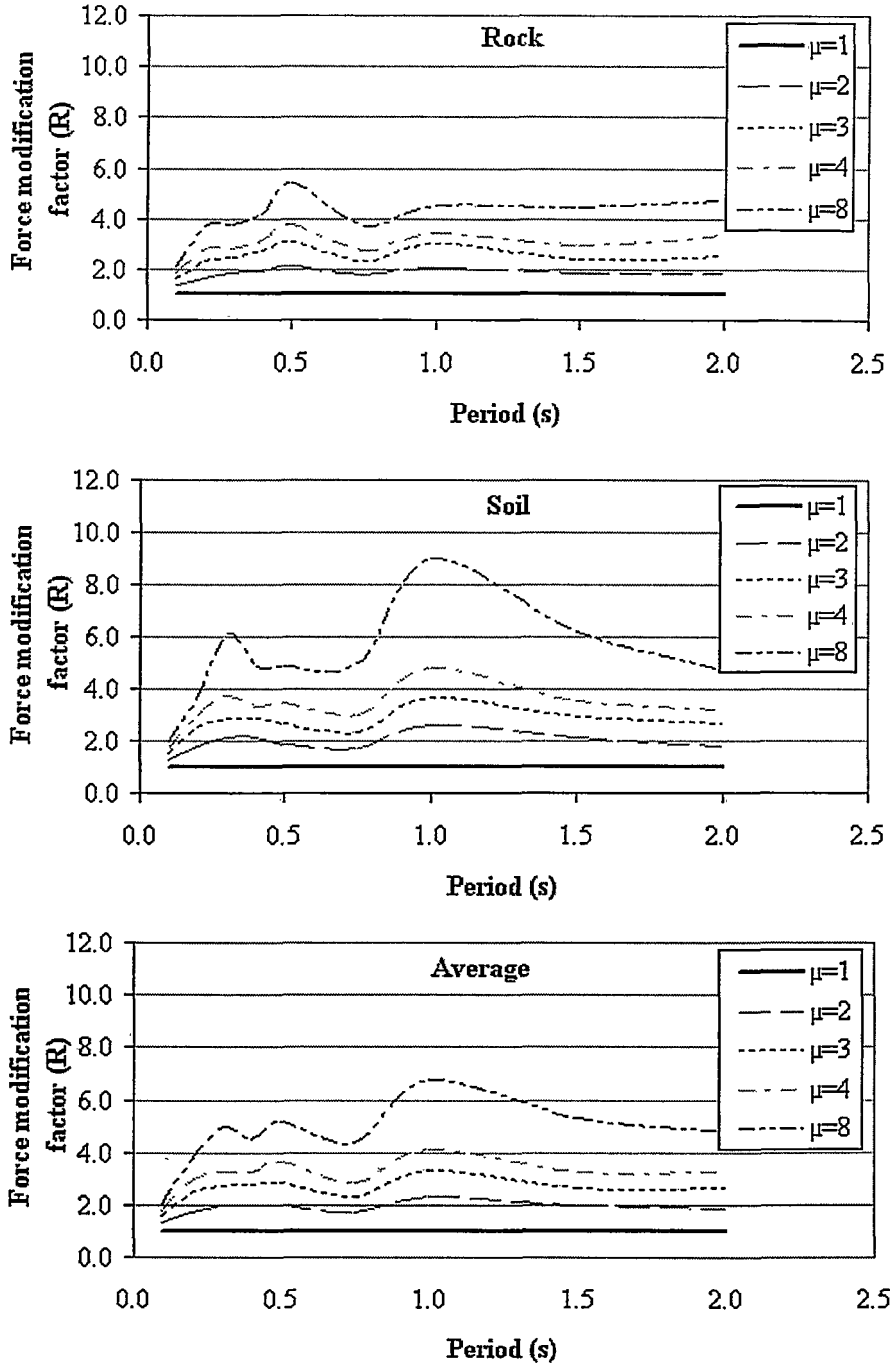

Figure 4.4 Force modification factor variation with period for FFE with PGA = 0.1g

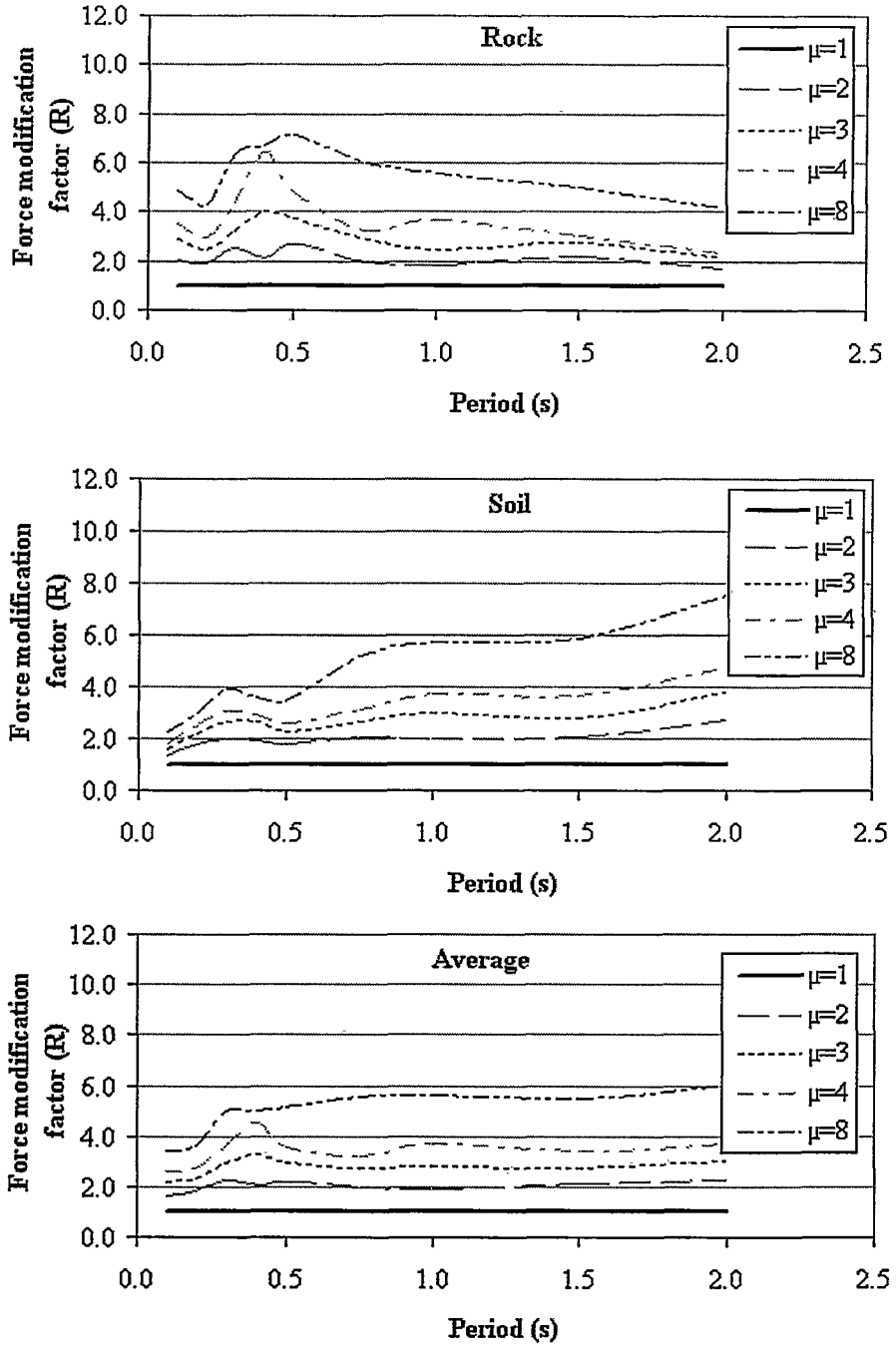

Figure 4.5 Force modification factor variation with period for NFE with magnitude >6 with PGA = 0.2g

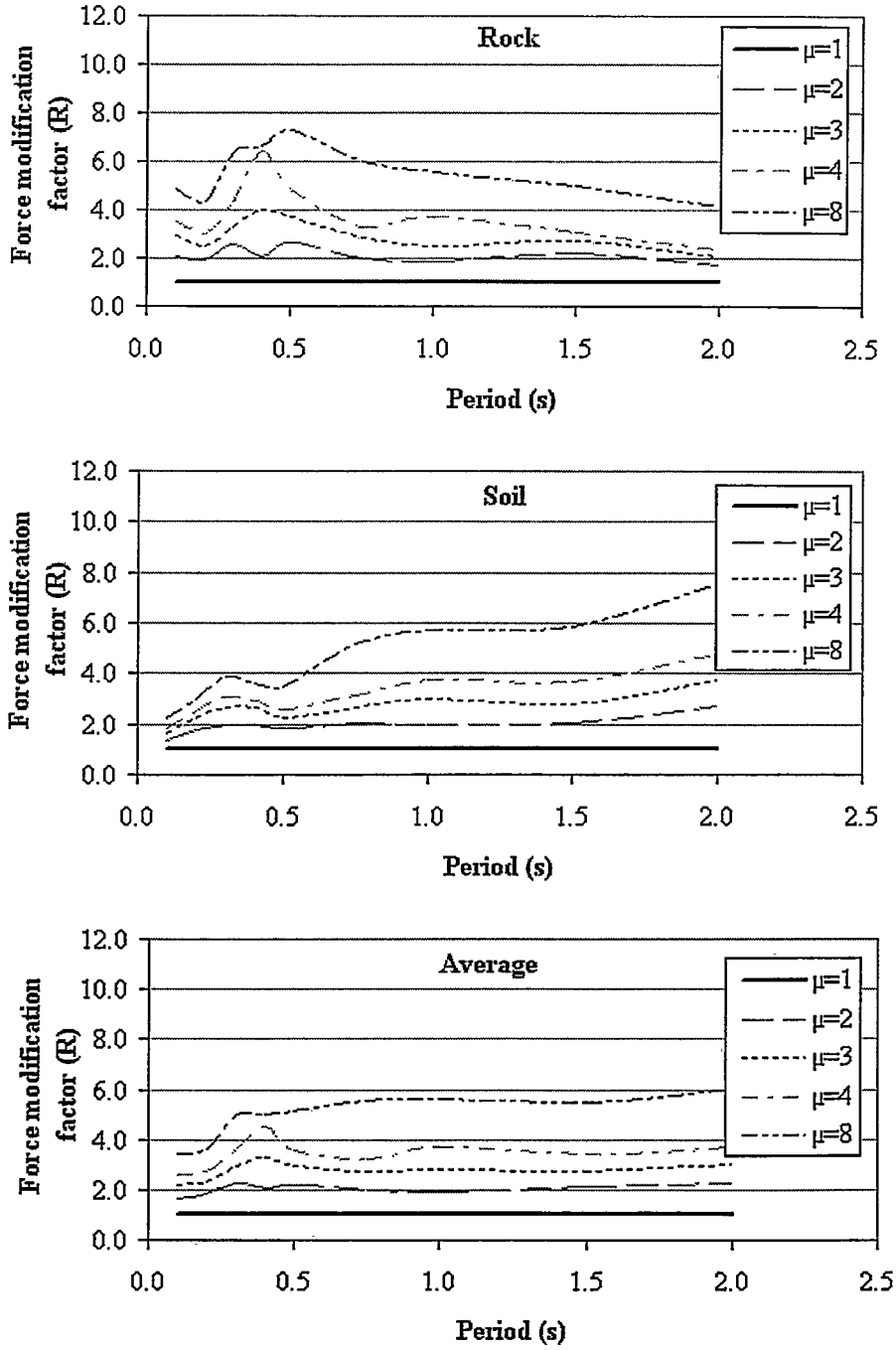

Figure 4.6 Force modification factor variation with period for NFE with magnitude >6 with PGA = 0.3g

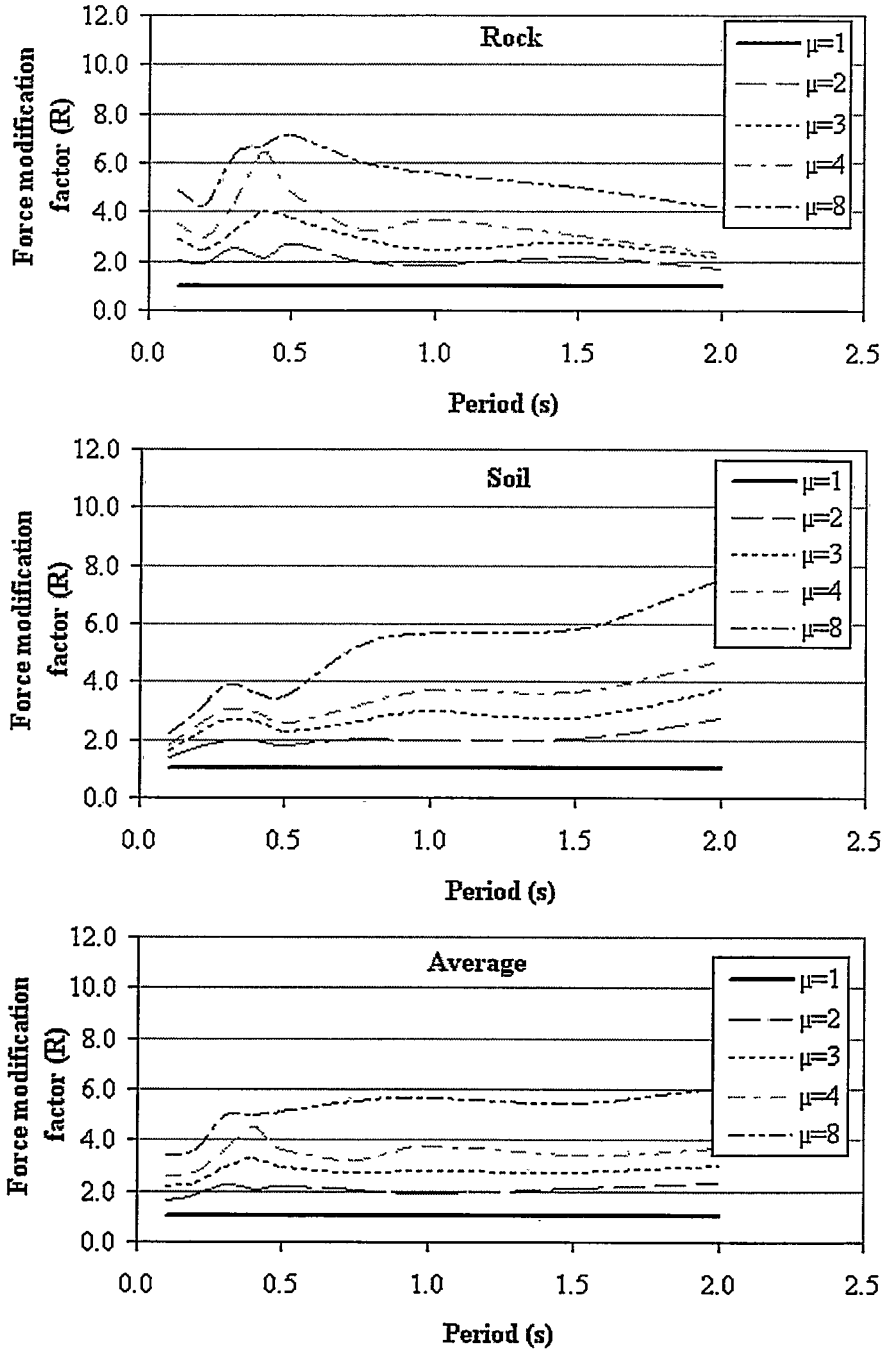

Figure 4.7 Force modification factor variation with period for NFE with magnitude >6 with PGA = 0.4g

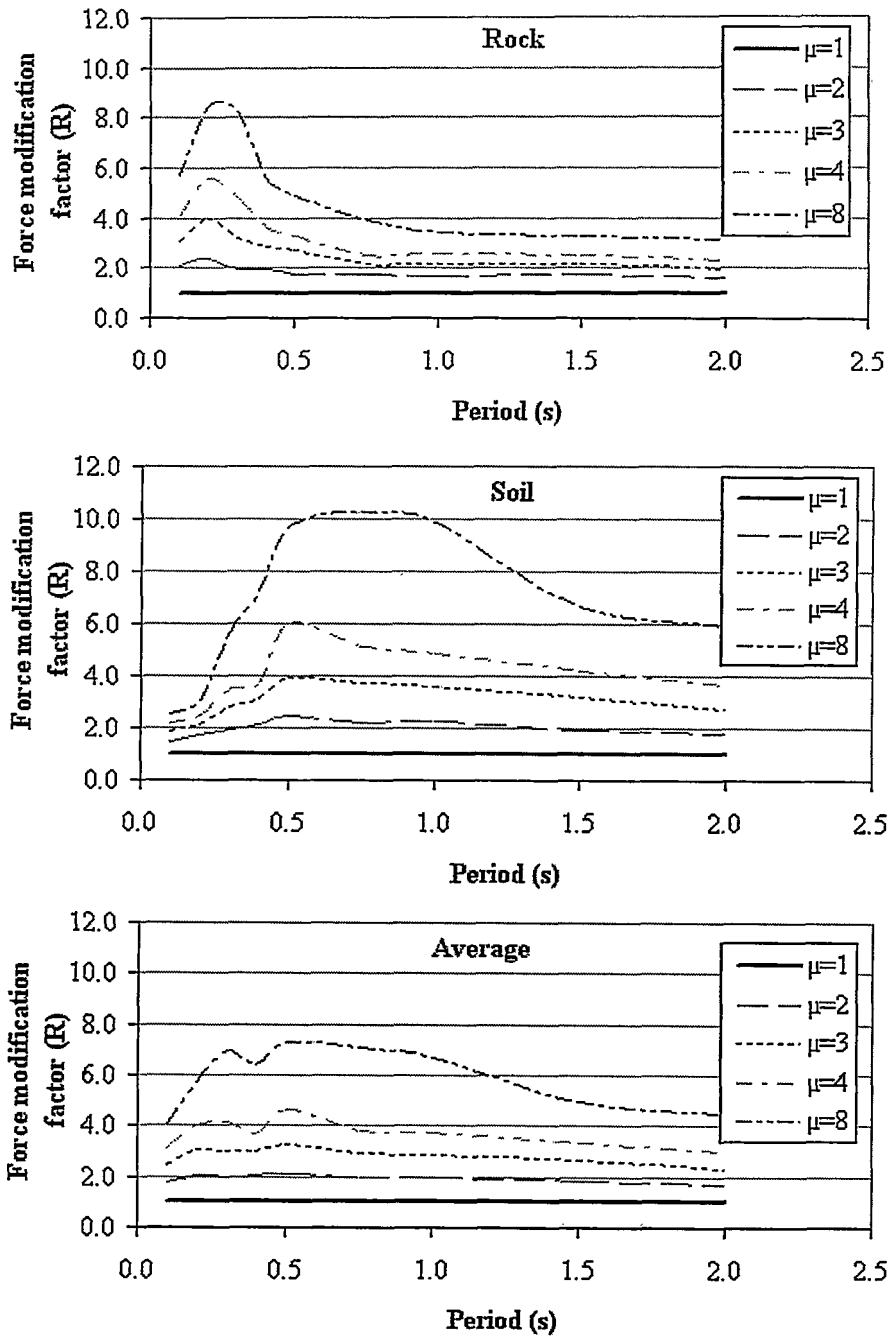

Figure 4.8 Force modification factor variation with period for NFE with magnitude <6 with PGA = 0.2g

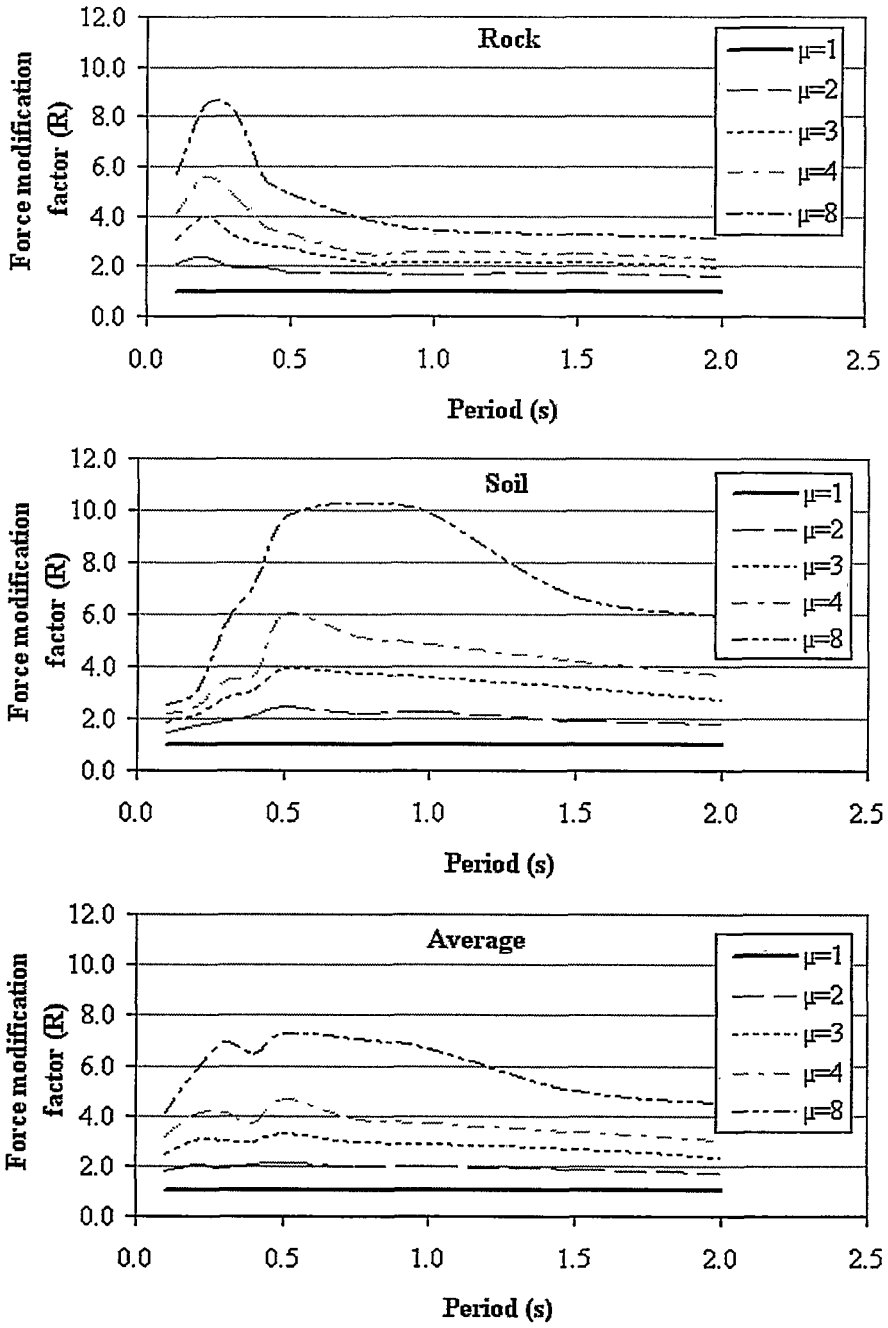

Figure 4.9 Force modification factor variation with period for NFE with magnitude <6 with PGA = 0.3g

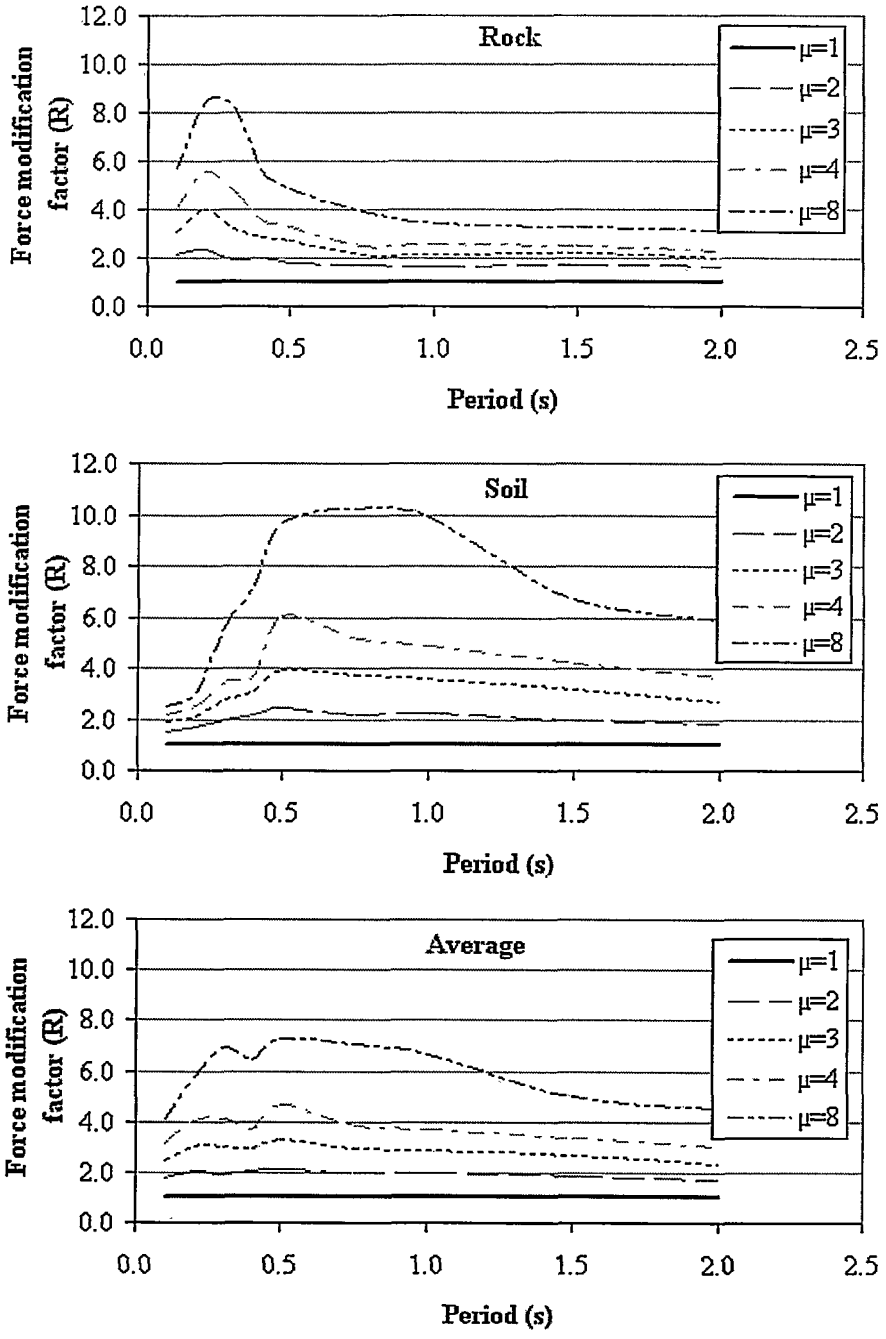

Figure 4.10 Force modification factor variation with period for NFE with magnitude <6 with PGA = 0.4g

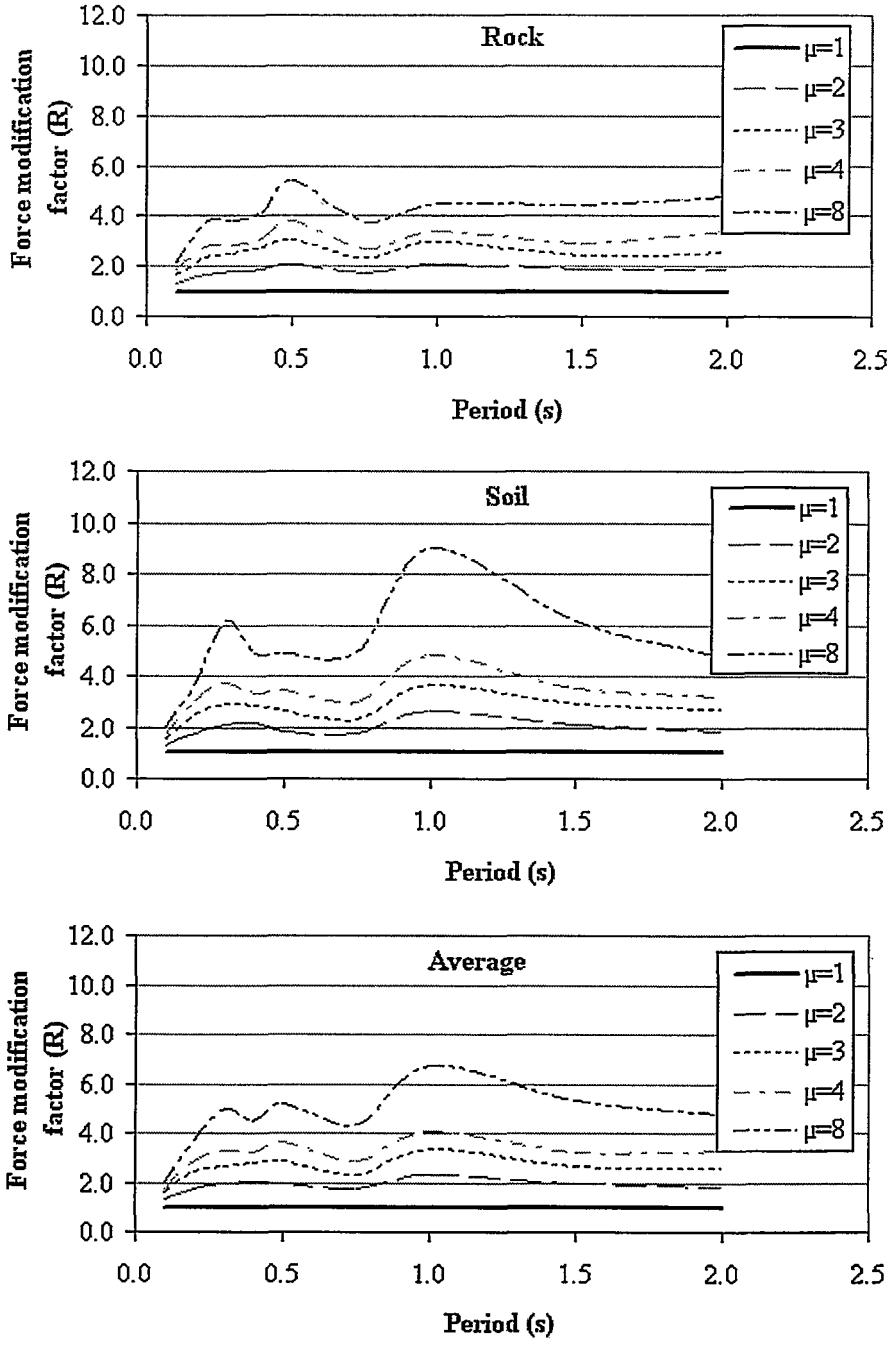

Figure 4.11 Force modification factor variation with period for FFE with PGA = 0.2g

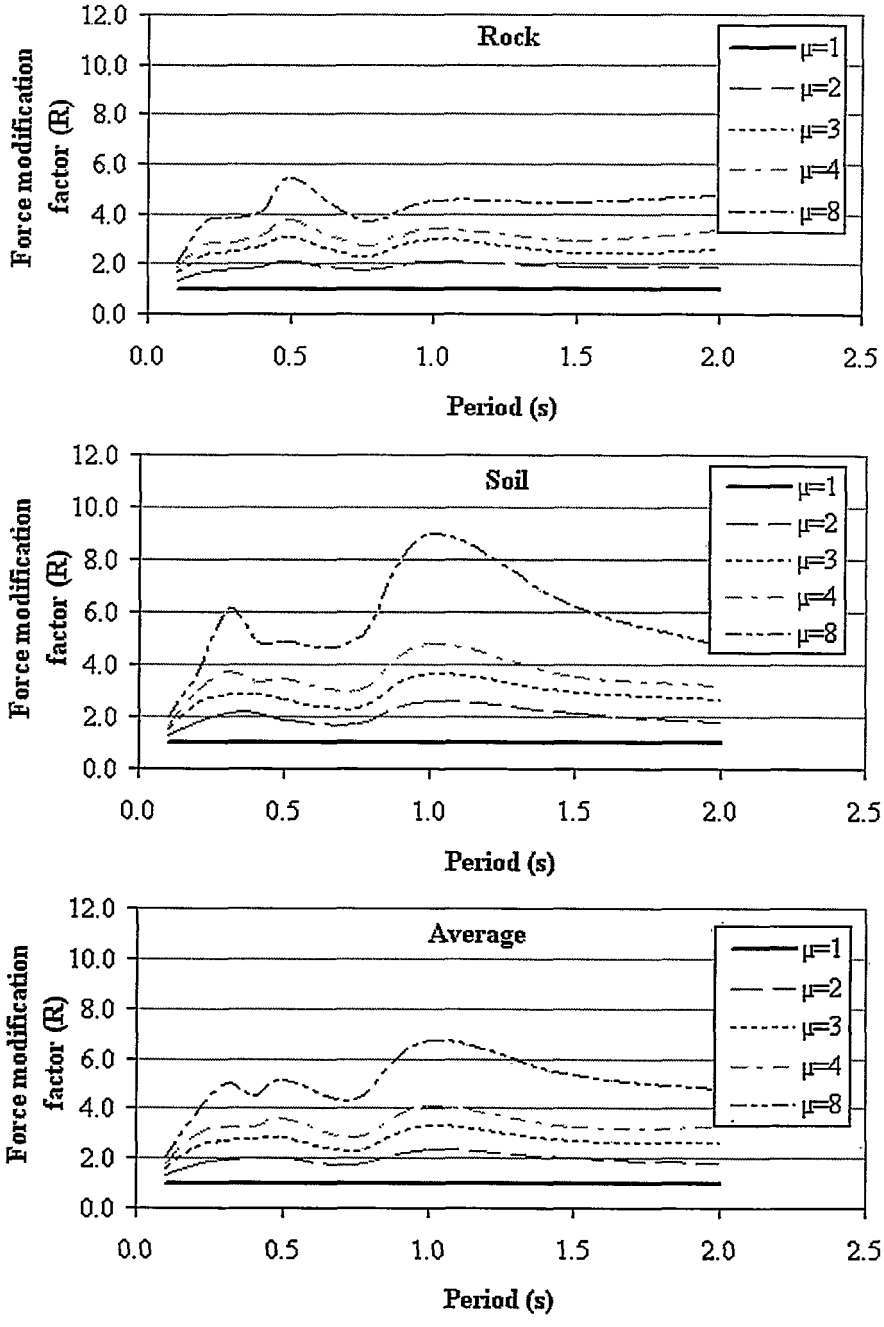

Figure 4.12 Force modification factor variation with period for FFE with PGA = 0.3g

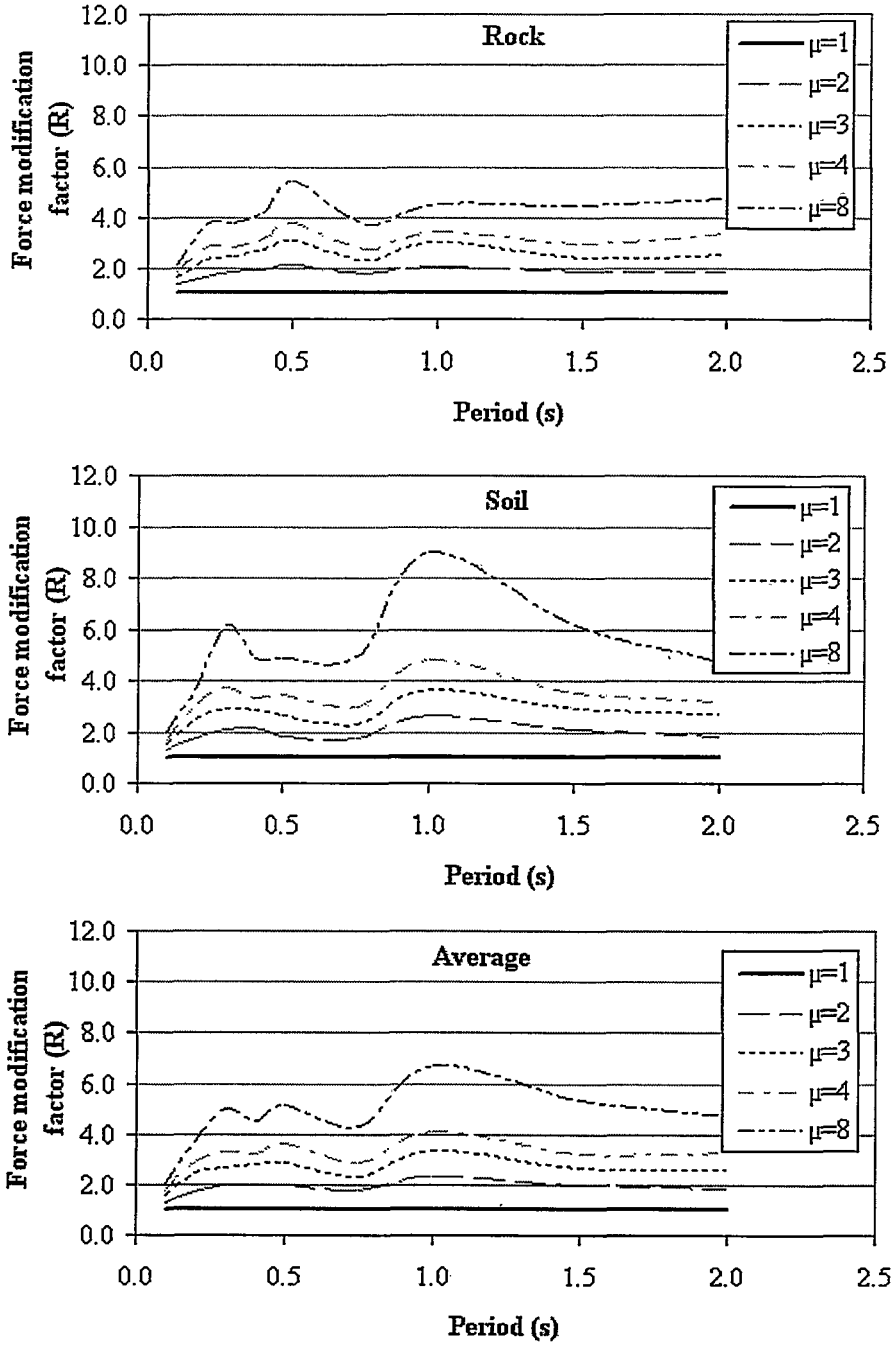

Figure 4.13 Force modification factor variation with period for FFE with PGA = 0.4g

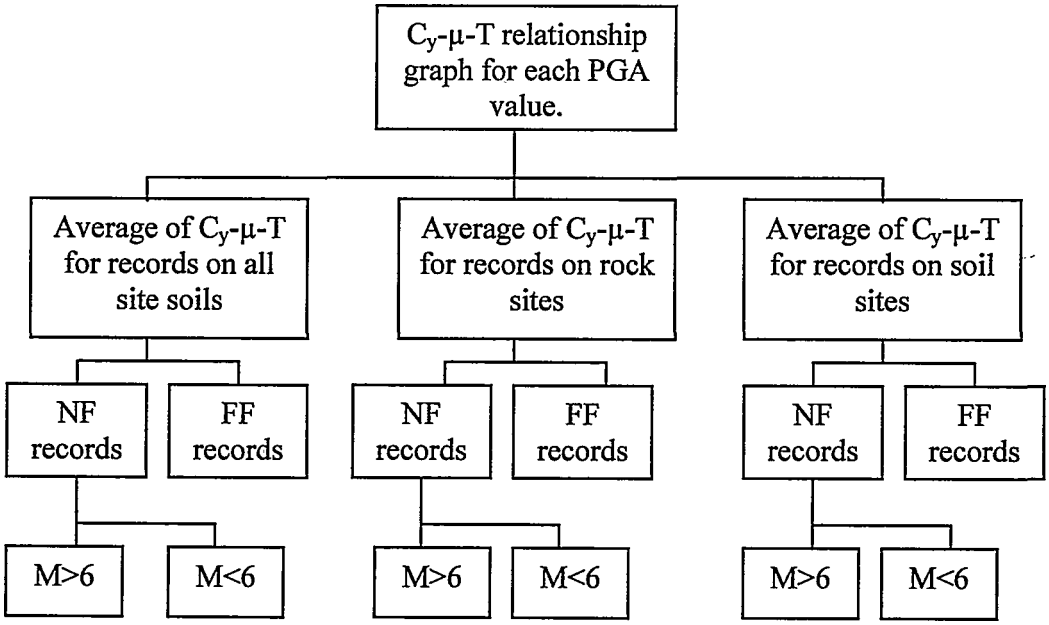

Figure 4.14 Classification of the C_y-μ-T relationship graph

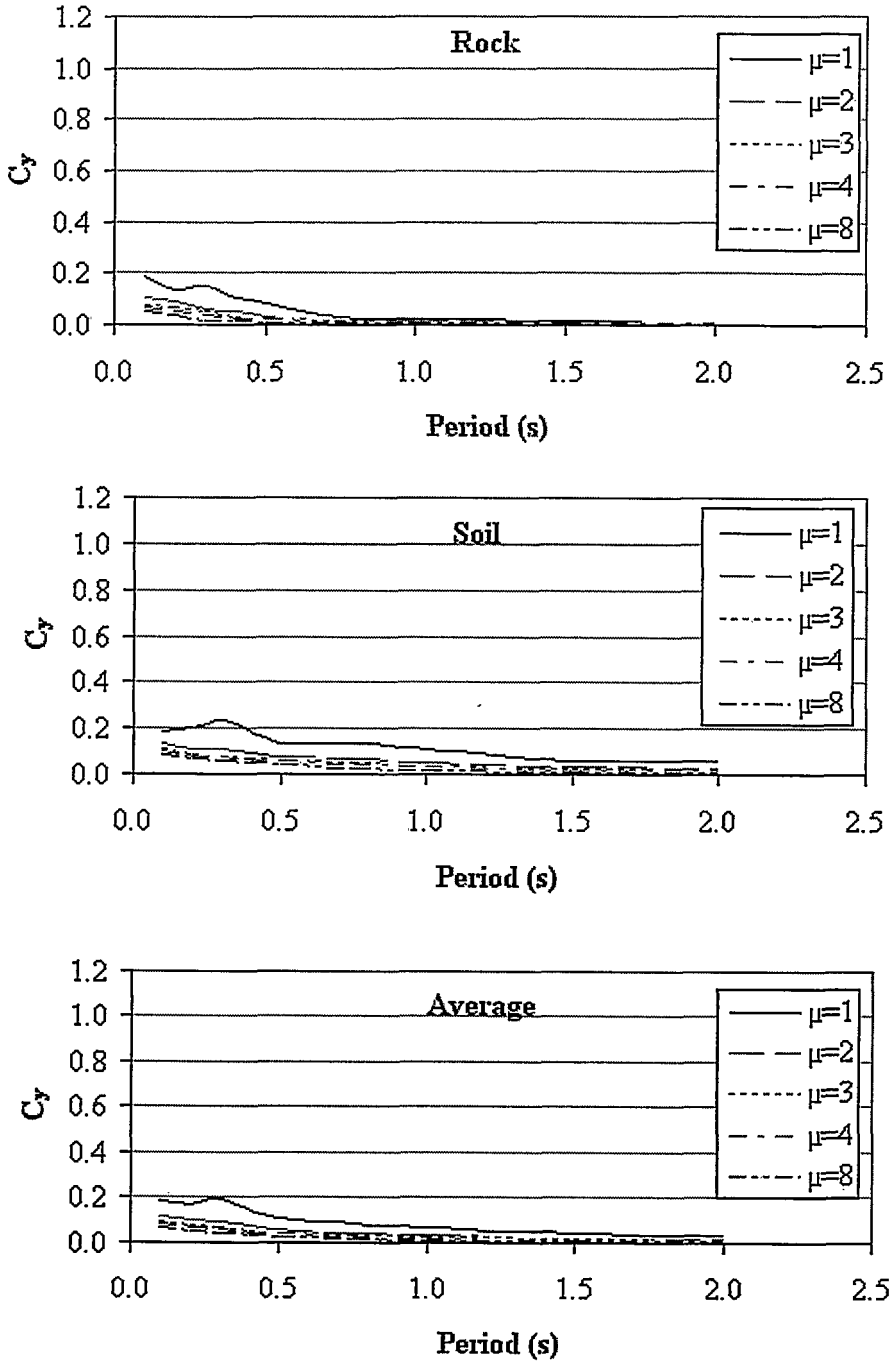

Figure 4.15 C_y factor variation with period for NFE with magnitude >6 with PGA = 0.1g

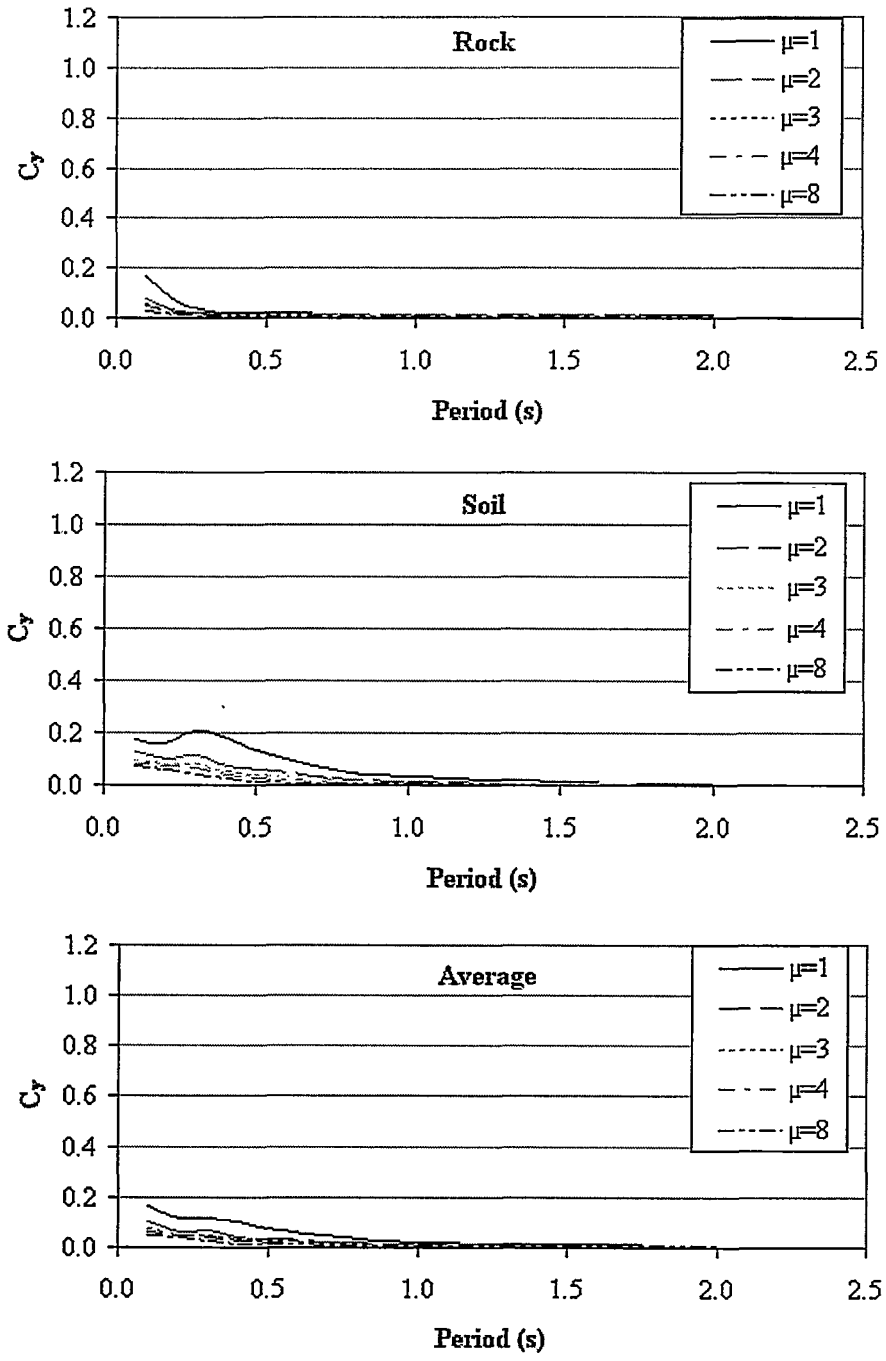

Figure 4.16 C_y factor variation with period for NFE with magnitude <6 with PGA = 0.1g

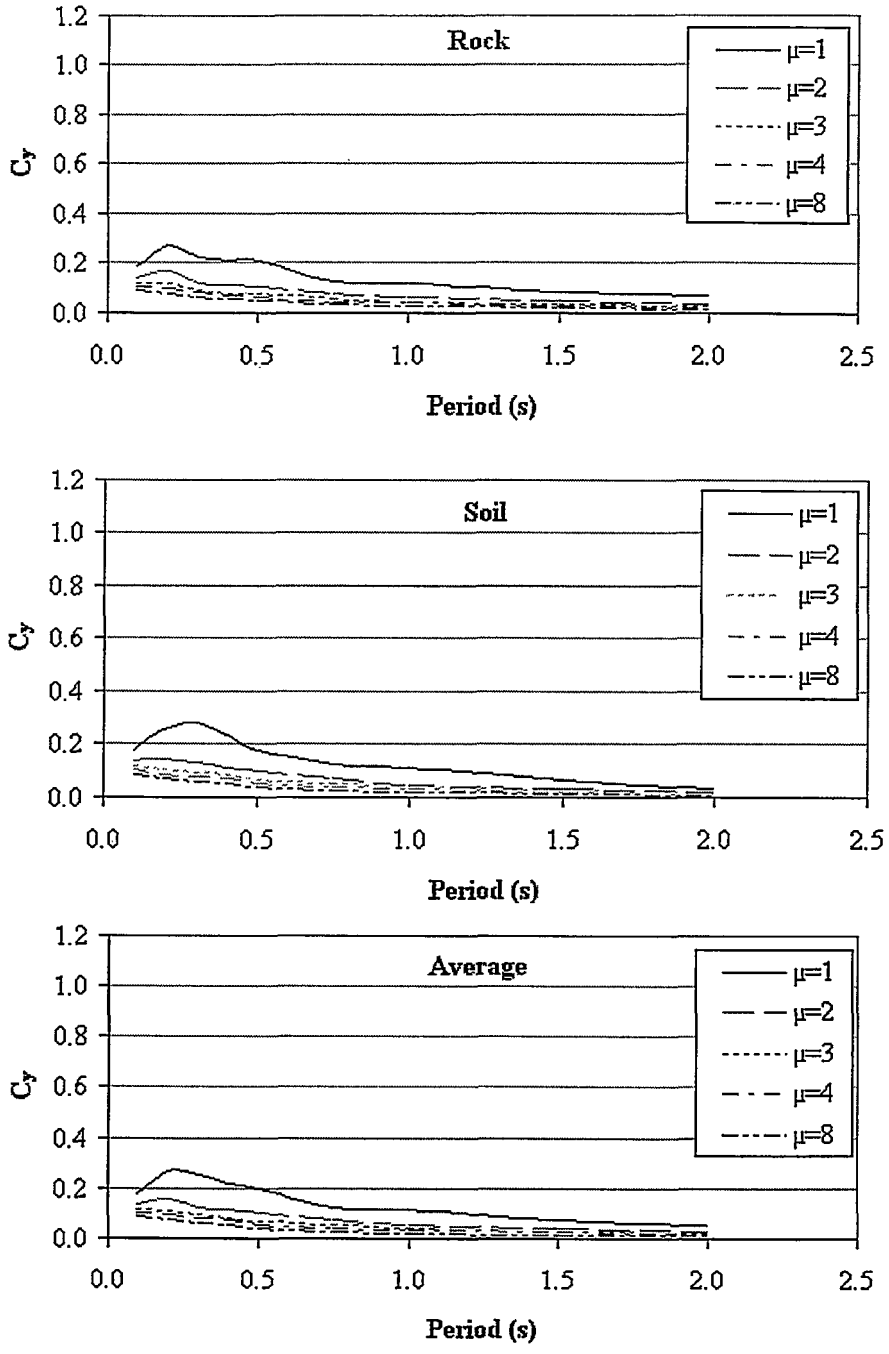

Figure 4.17 C_y factor variation with period for FFE with PGA = 0.1g

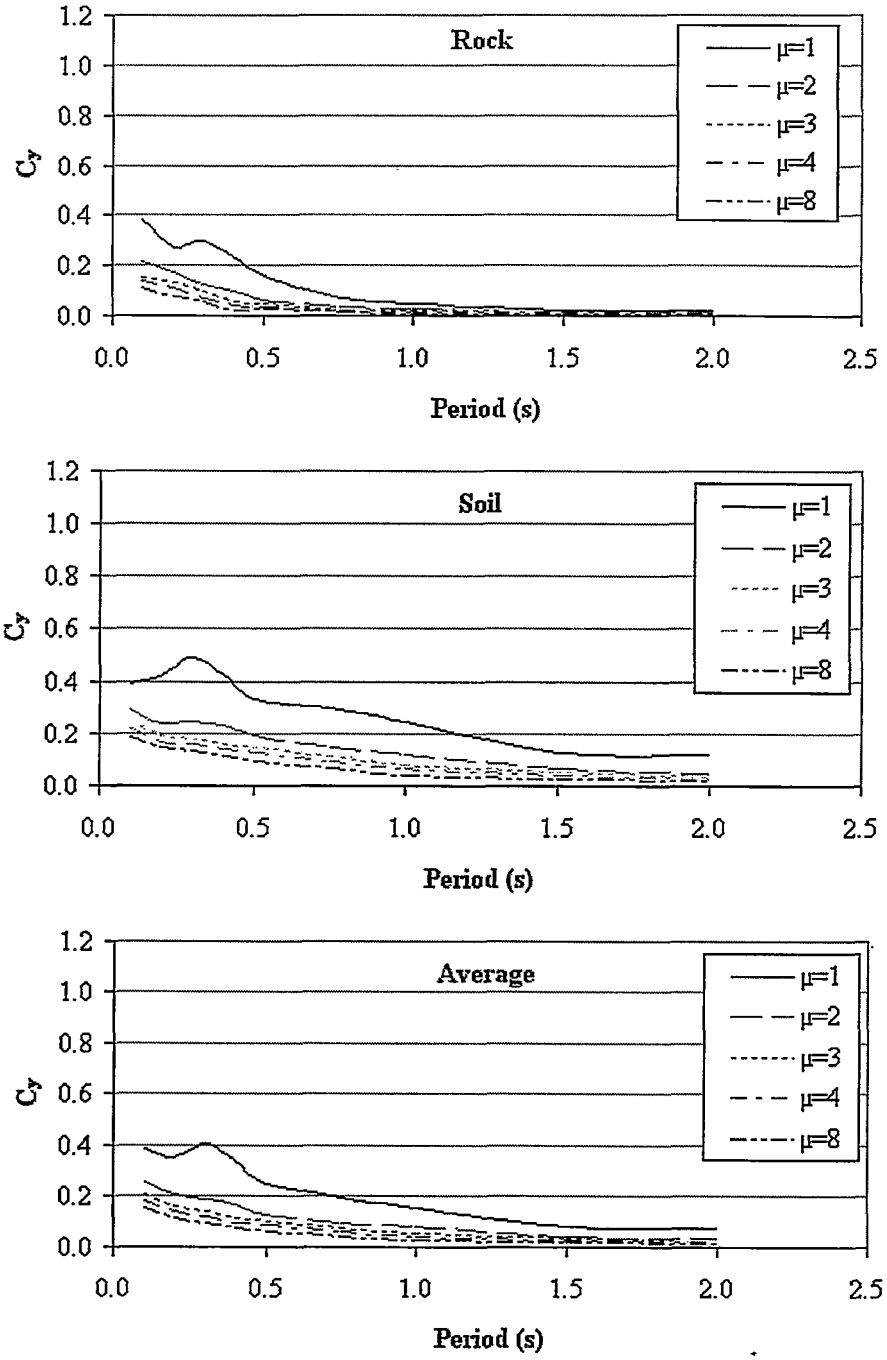

Figure 4.18 C_y factor variation with period for NFE with magnitude >6 with PGA = 0.2g

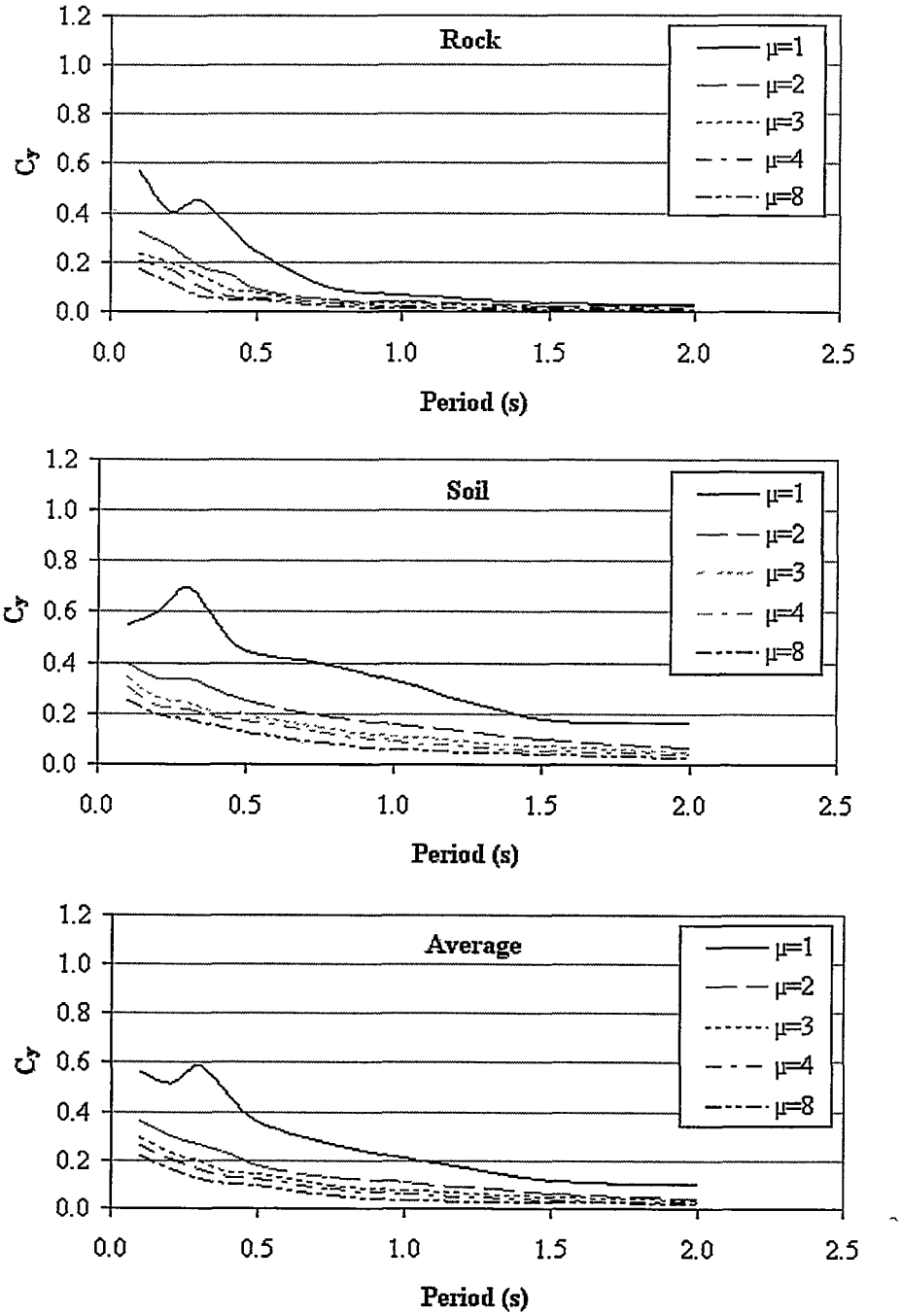

Figure 4.19C_y factor variation with period for NFE with magnitude >6 with PGA = 0.3g

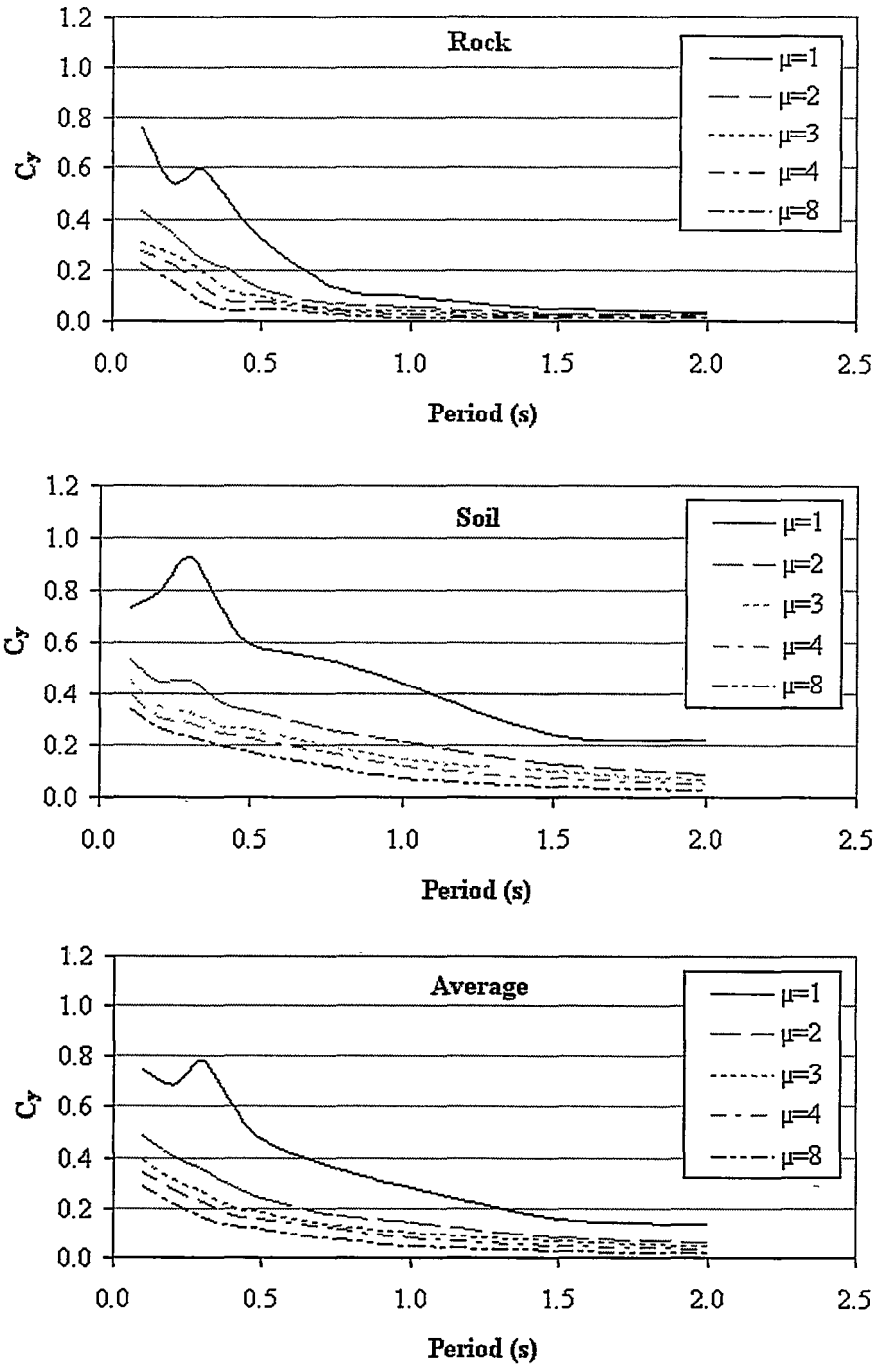

Figure 4.20 C_y factor variation with period for NFE with magnitude >6 with PGA = 0.4g

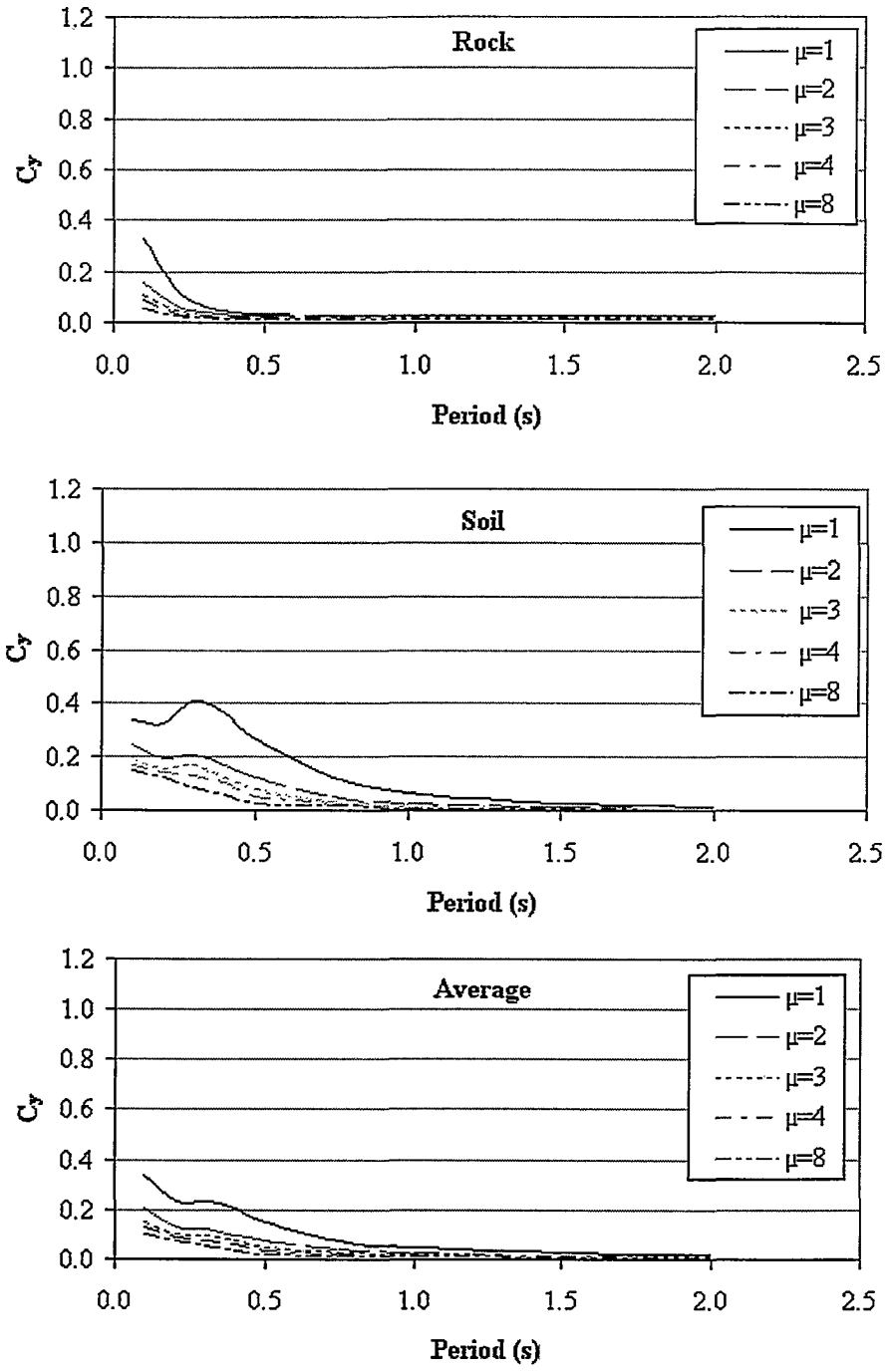

Figure 4.21 C_y factor variation with period for NFE with magnitude <6 with PGA = 0.2g

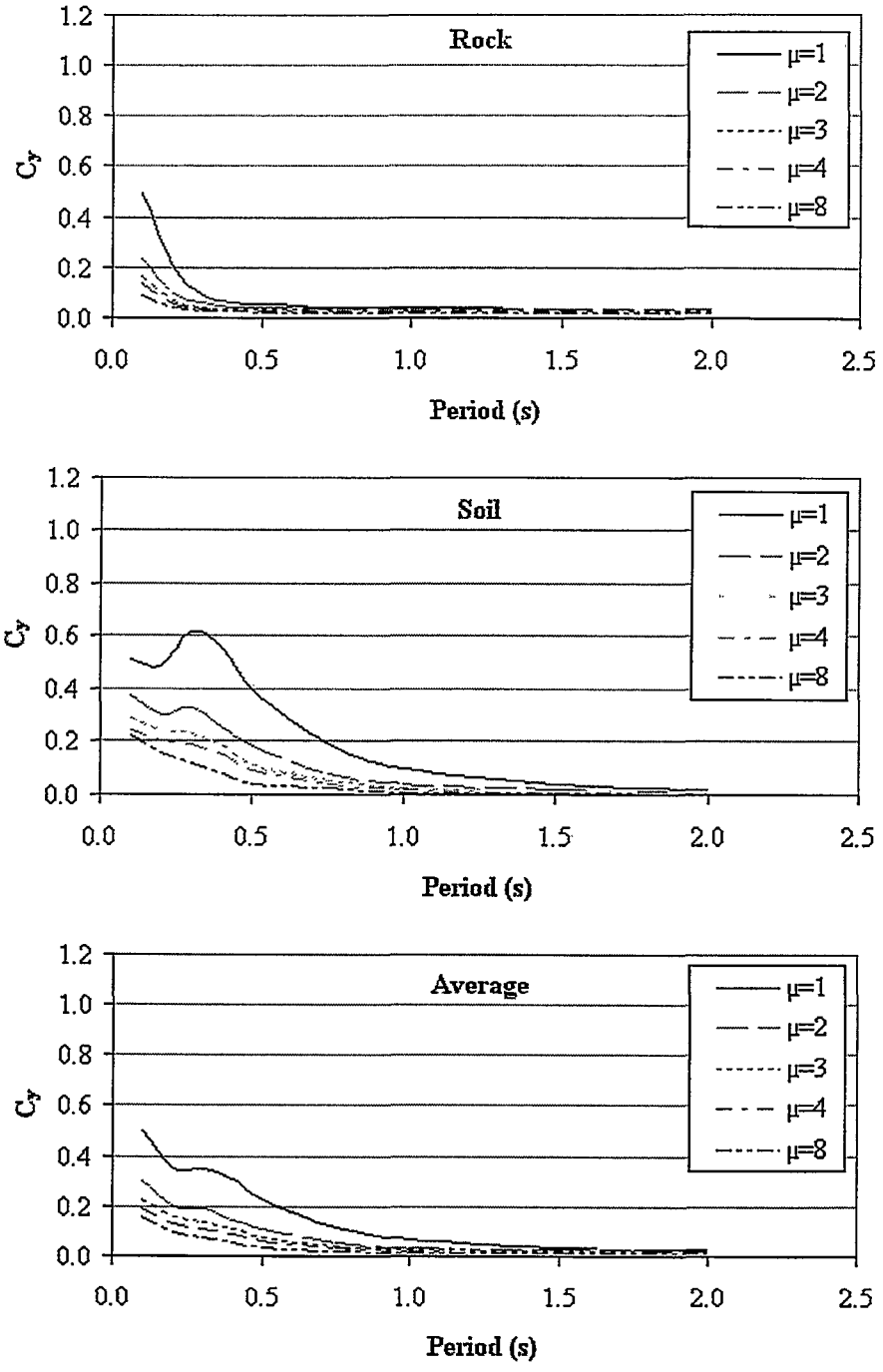

Figure 4.22 C_y factor variation with period for NFE with magnitude <6 with PGA = 0.3g

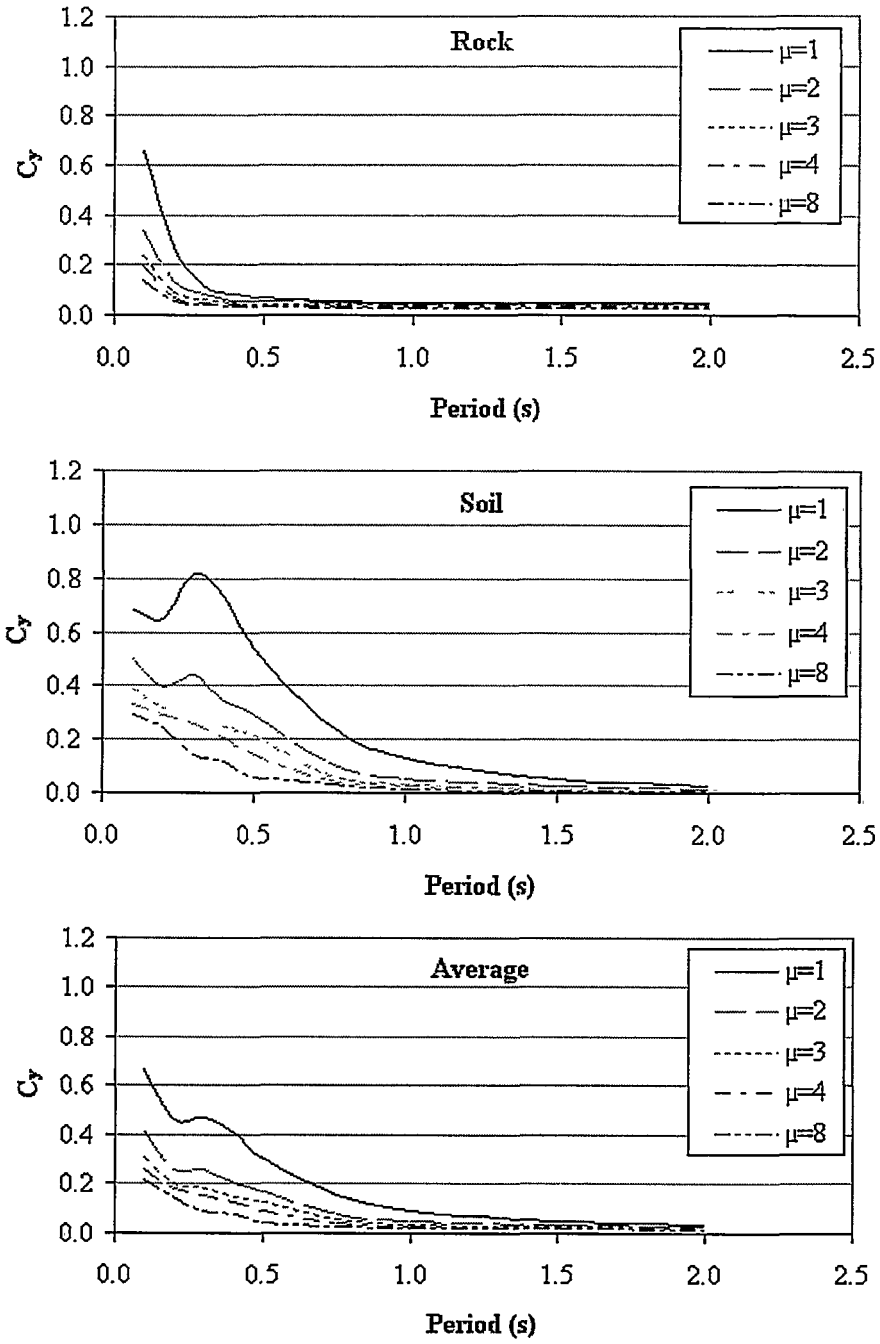

Figure 4.23 Cy factor variation with period for NFE with magnitude <6 with PGA = 0.4g

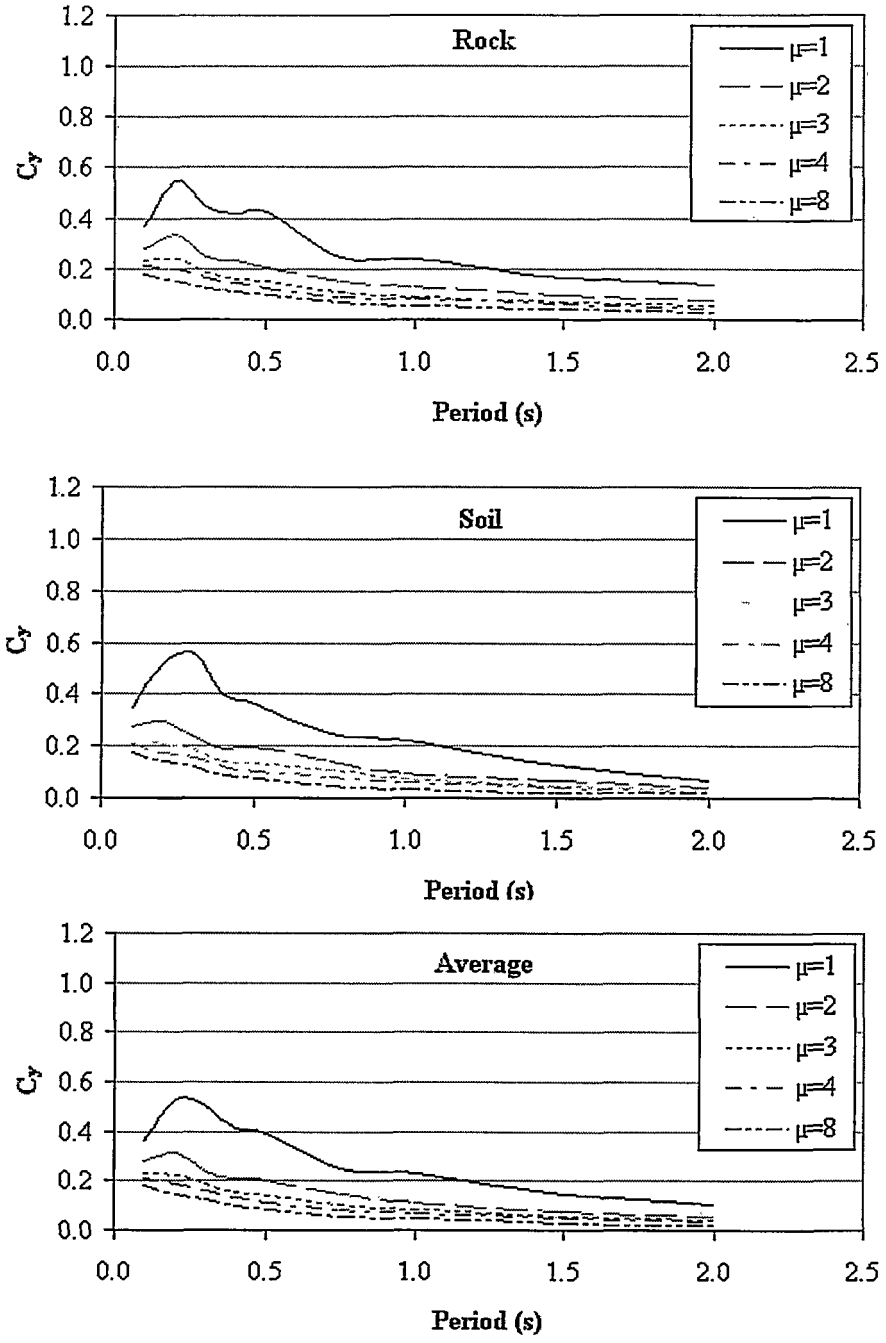

Figure 4.24 C_y factor variation with period for FFE with PGA = 0.2g

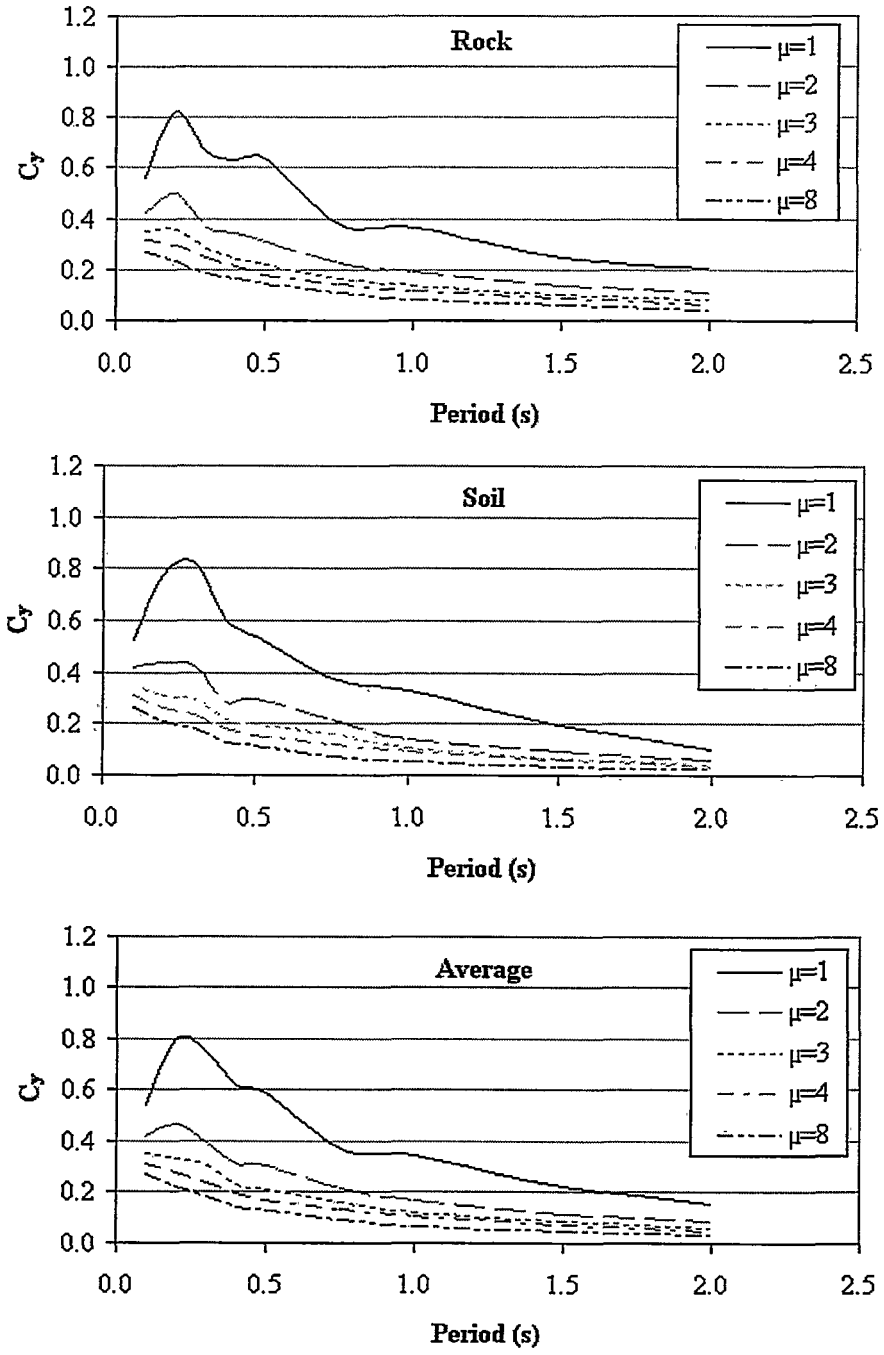

Figure 4.25 C_y factor variation with period for FFE with PGA = 0.3g

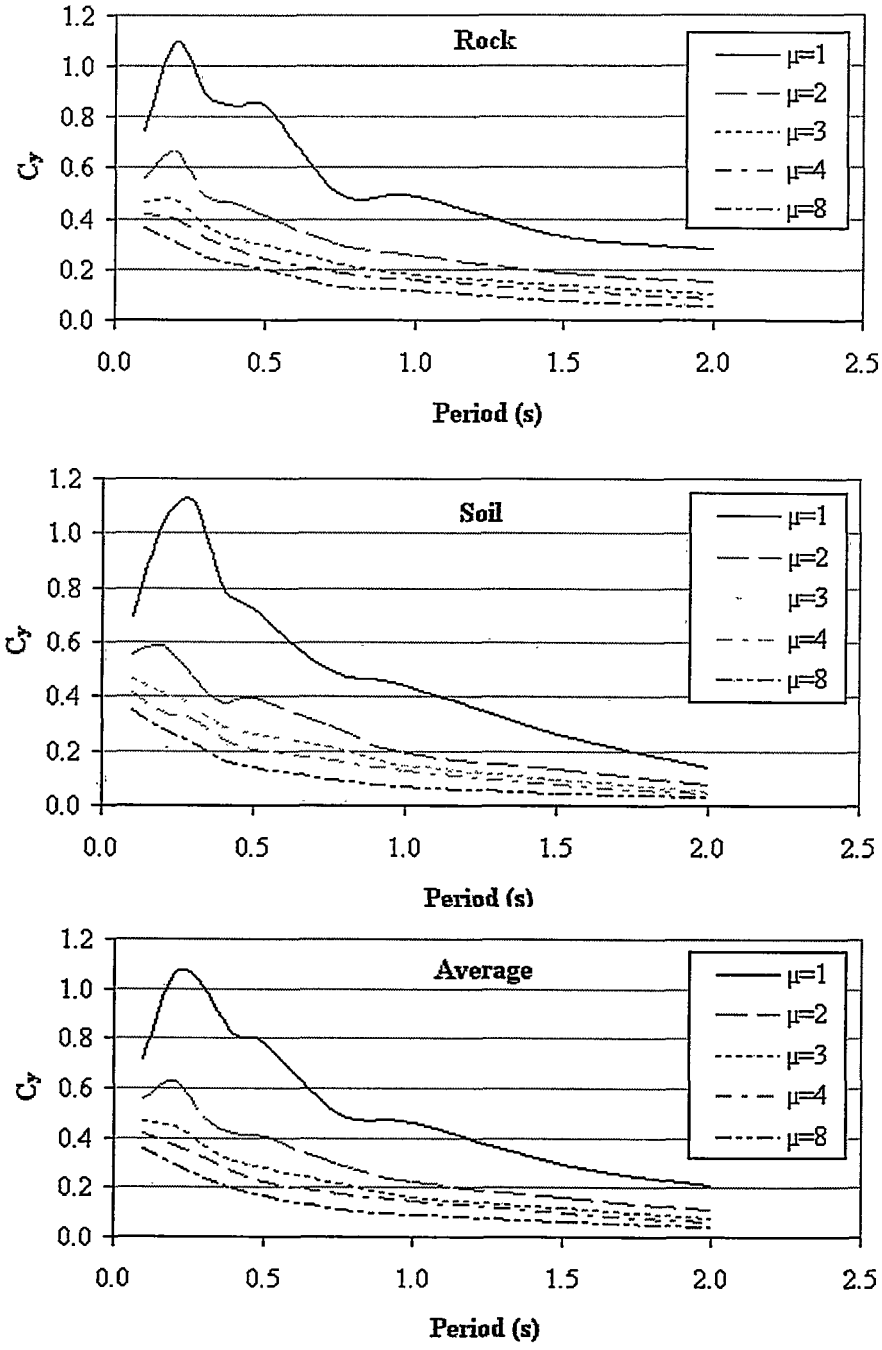

Figure 4.26 C_y factor variation with period for FFE with PGA = 0.4g

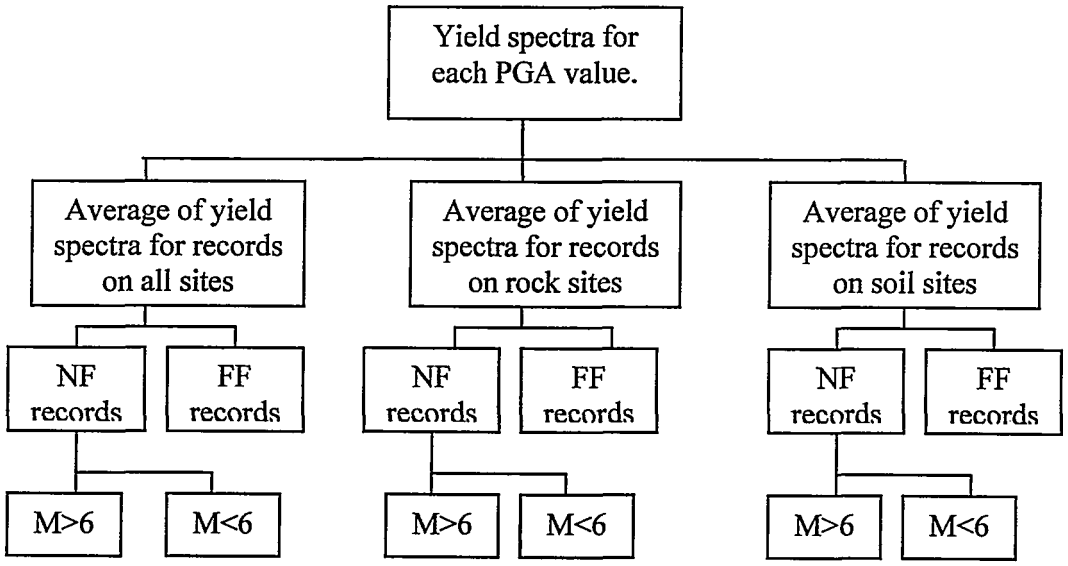

Figure 4.27 Classification of the yield spectra

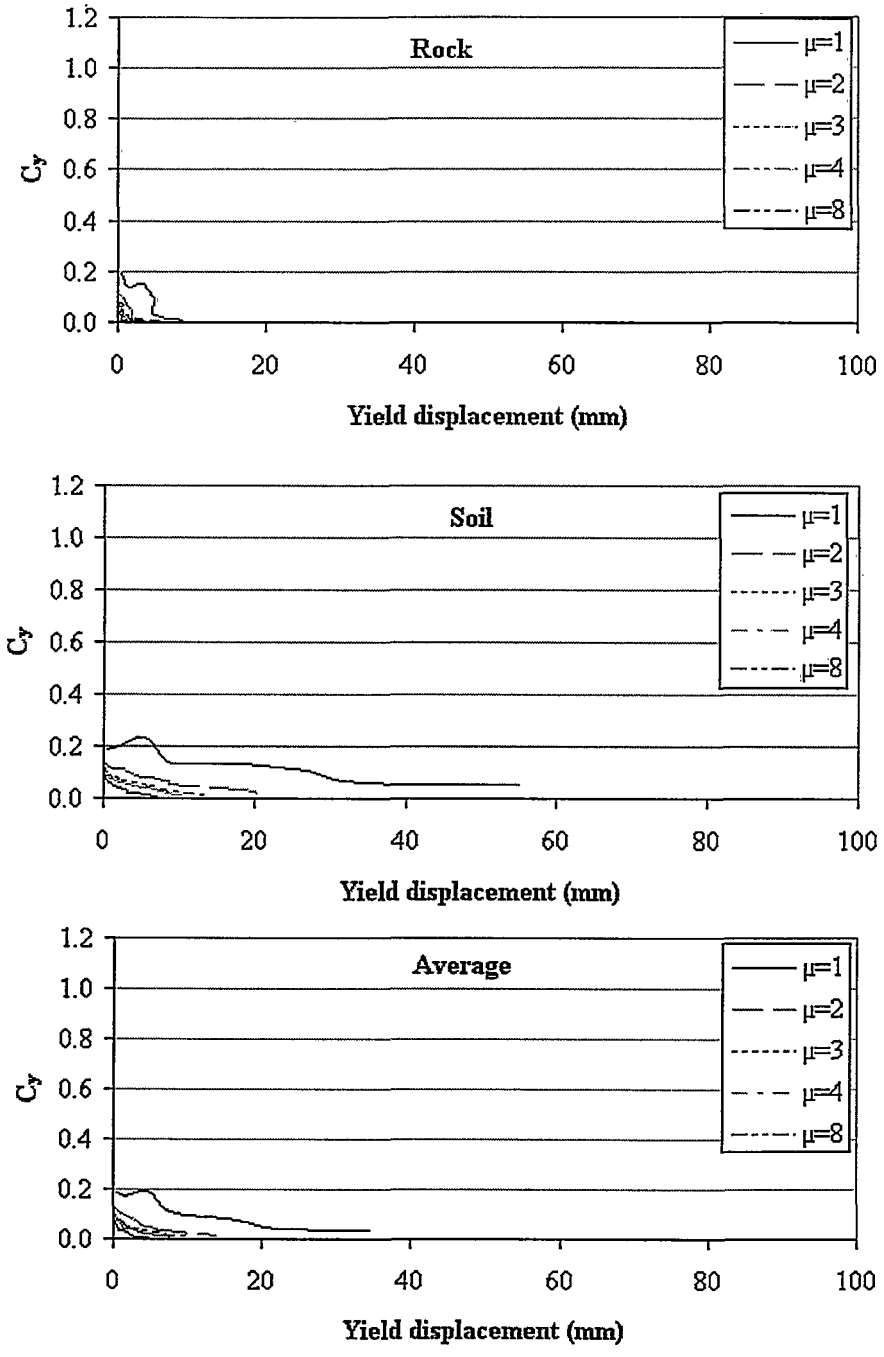

Figure 4.28 Yield spectra for NFE with magnitude >6 with PGA = 0.1g

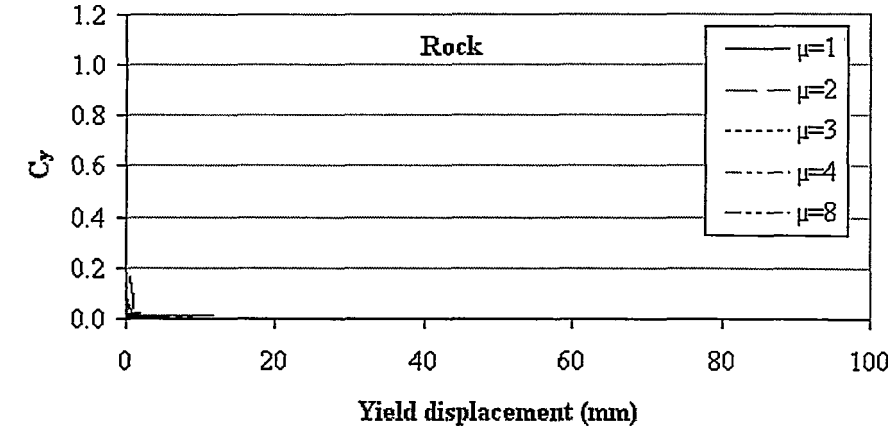

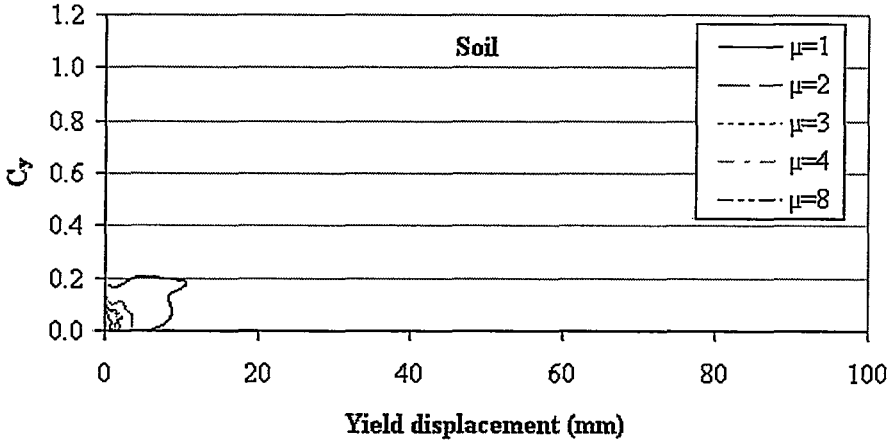

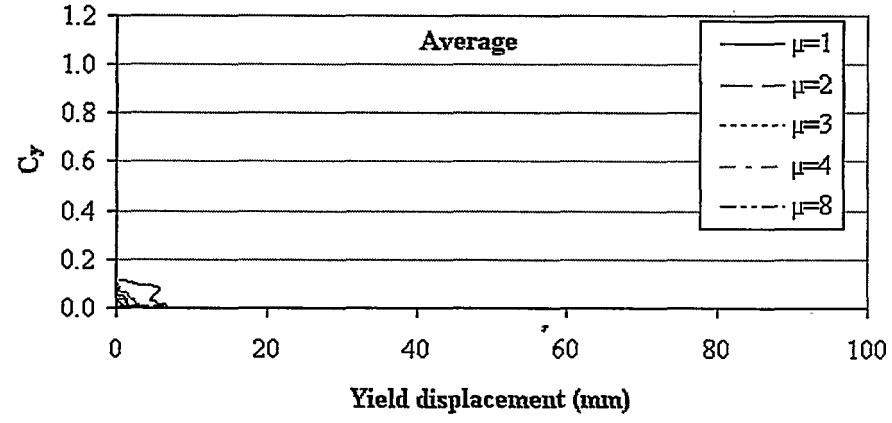

Figure 4.29 Yield spectra for NFE with magnitude <6 with PGA = 0.1g

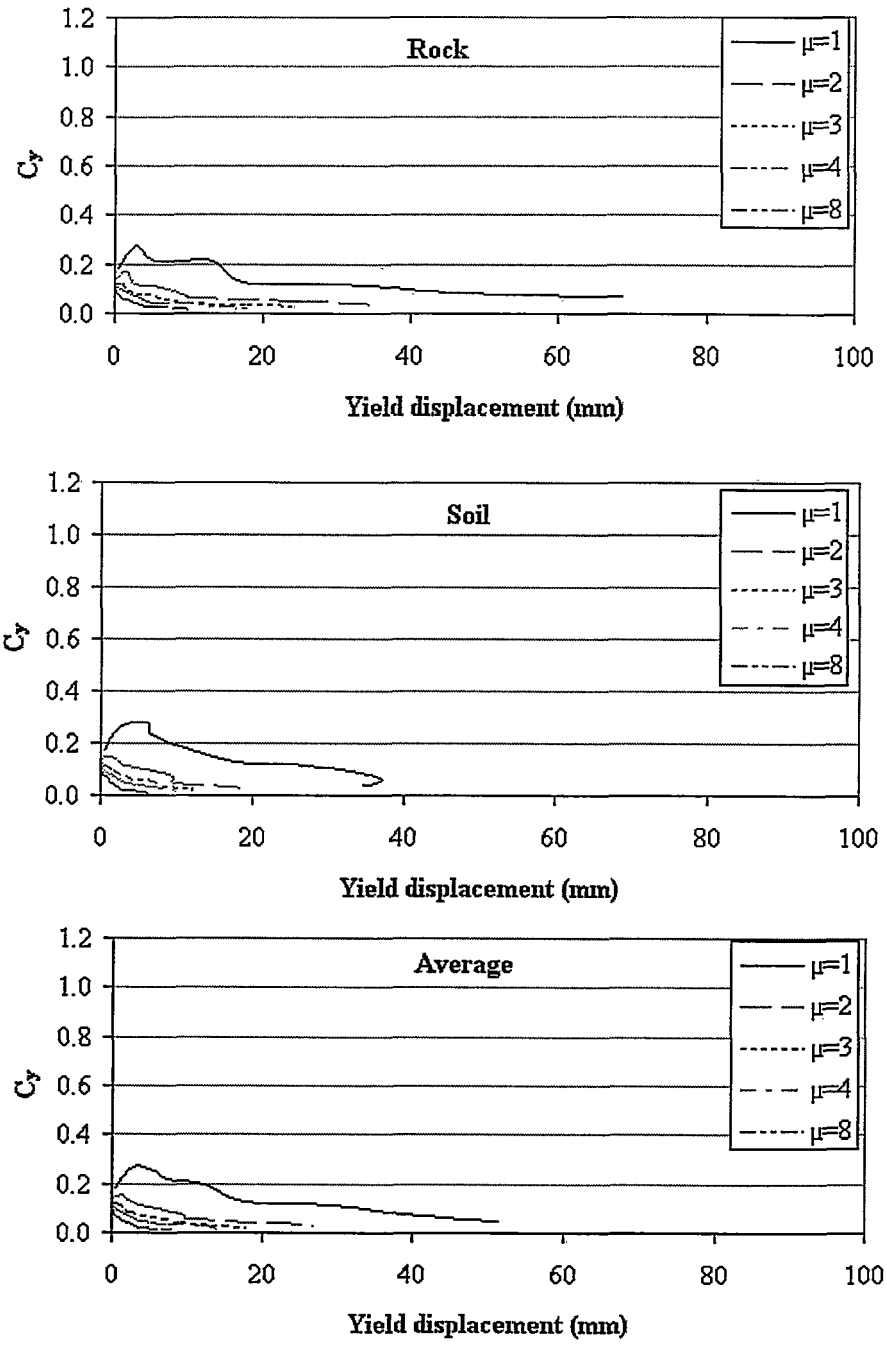

Figure 4.30 Yield spectra for FFE with PGA = 0.1g

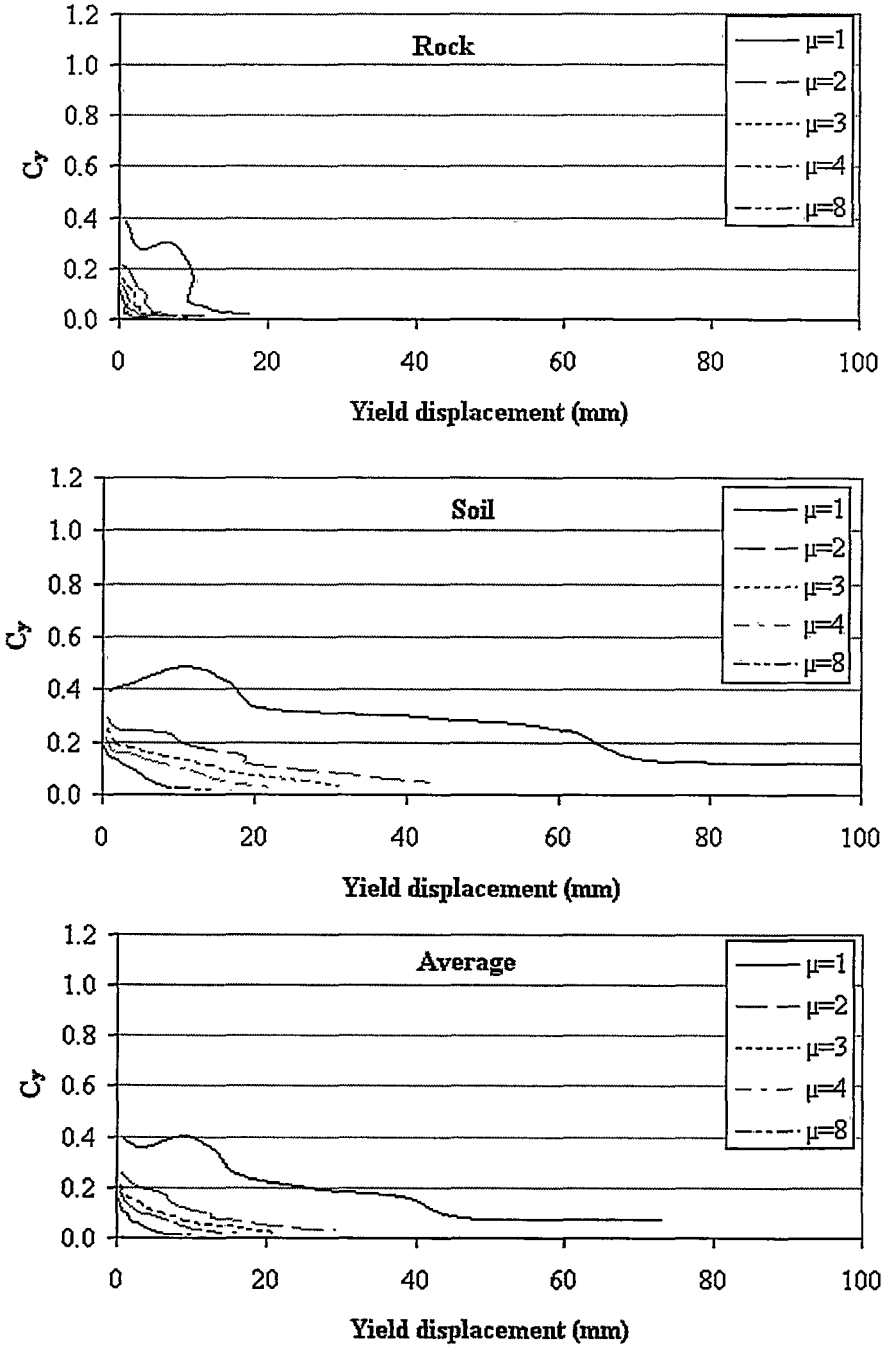

Figure 4.31 Yield spectra for NFE with magnitude >6 with PGA = 0.2g

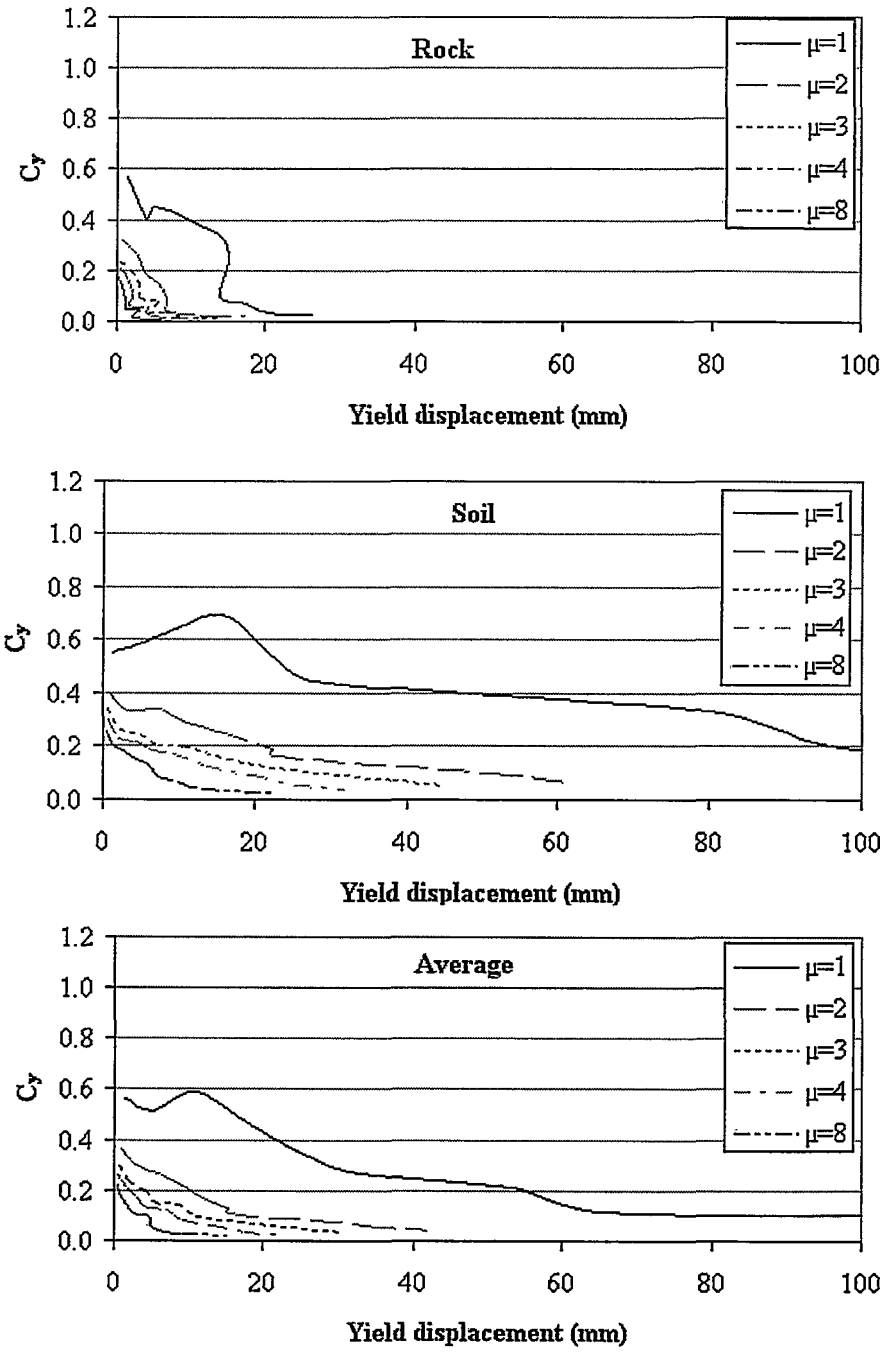

Figure 4.32 Yield spectra for NFE with magnitude >6 with PGA = 0.3g

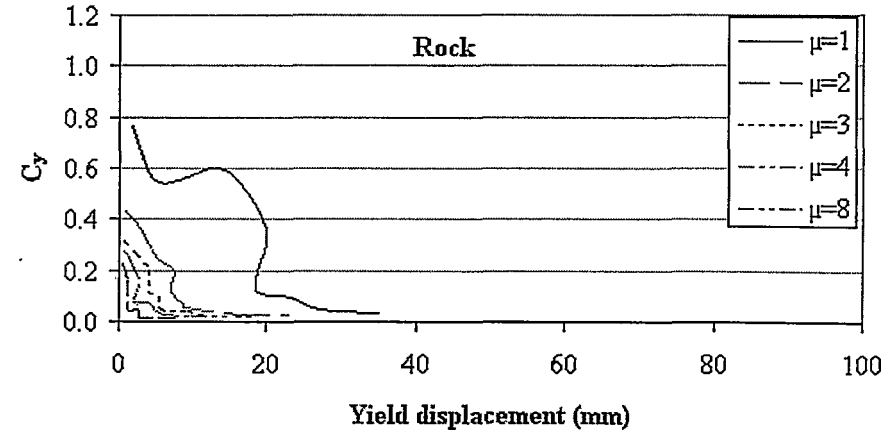

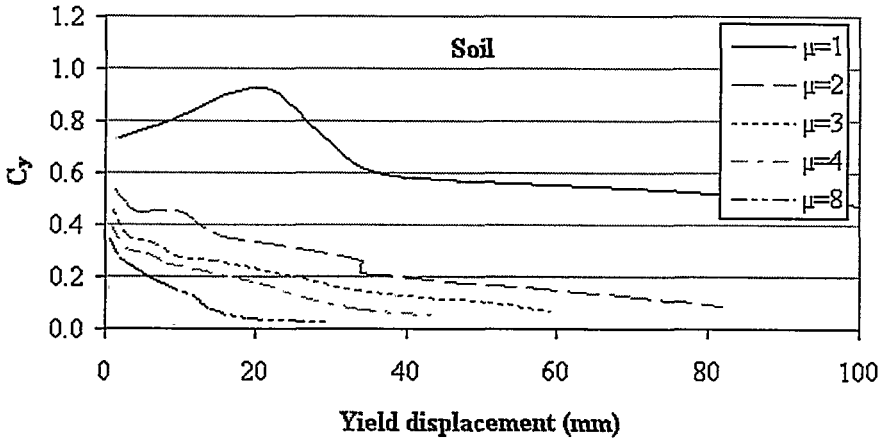

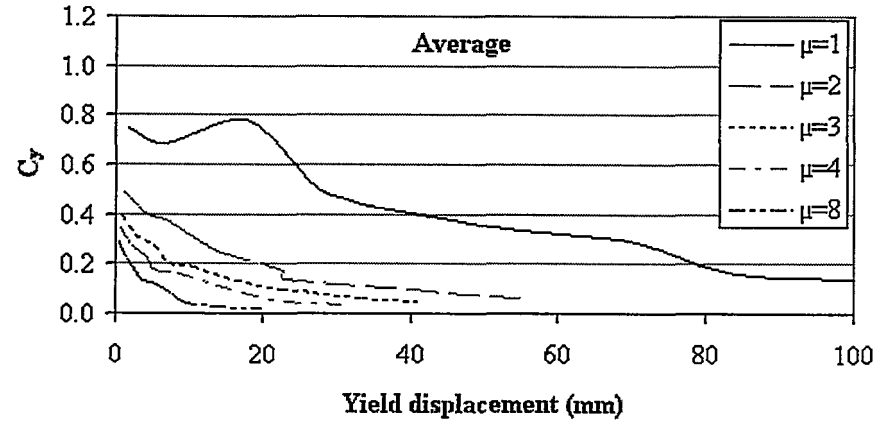

Figure 4.33 Yield spectra for NFE with magnitude >6with PGA = 0.4g

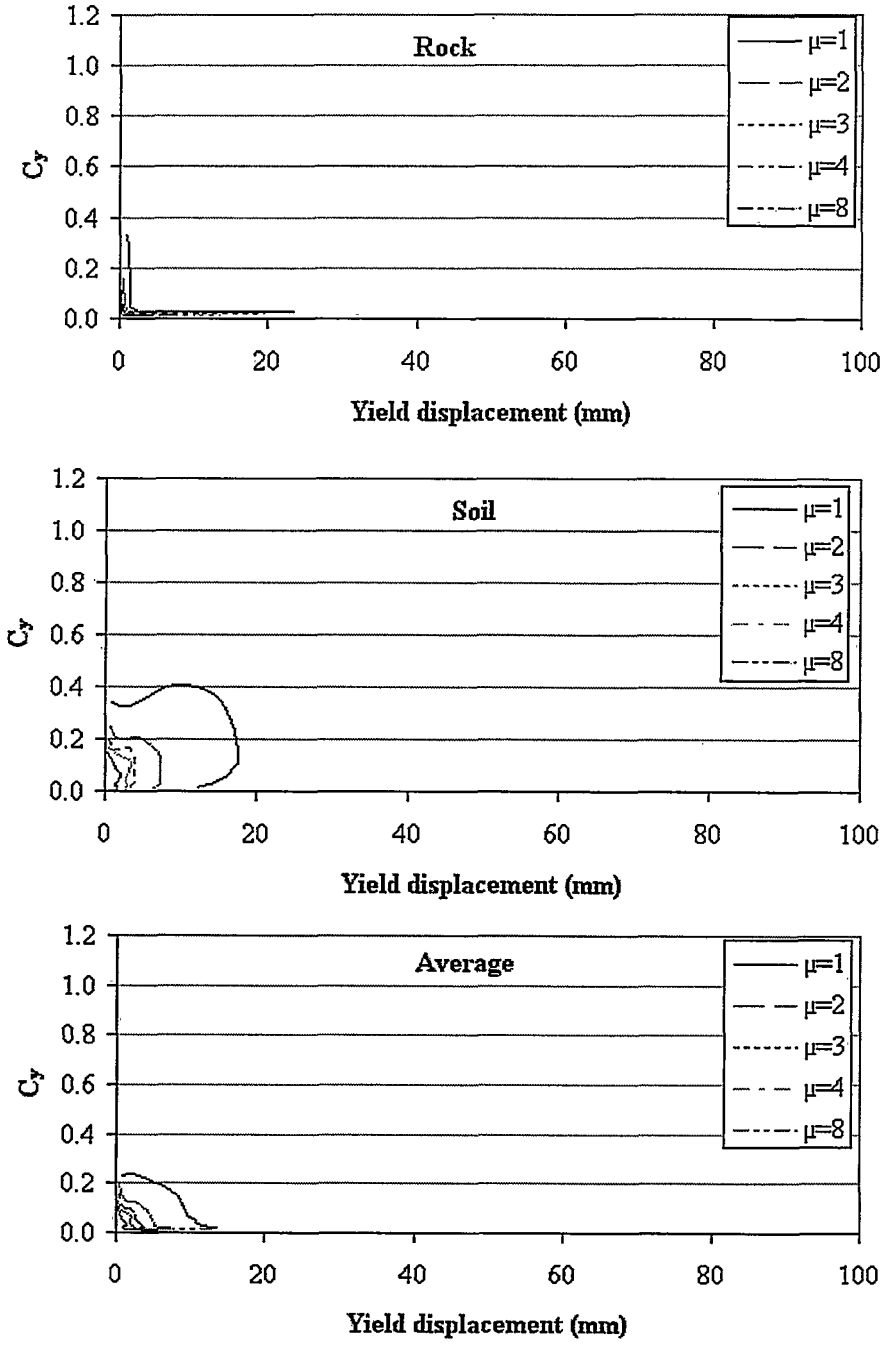

Figure 4.34 Yield spectra for NFE with magnitude <6 with PGA = 0.2g

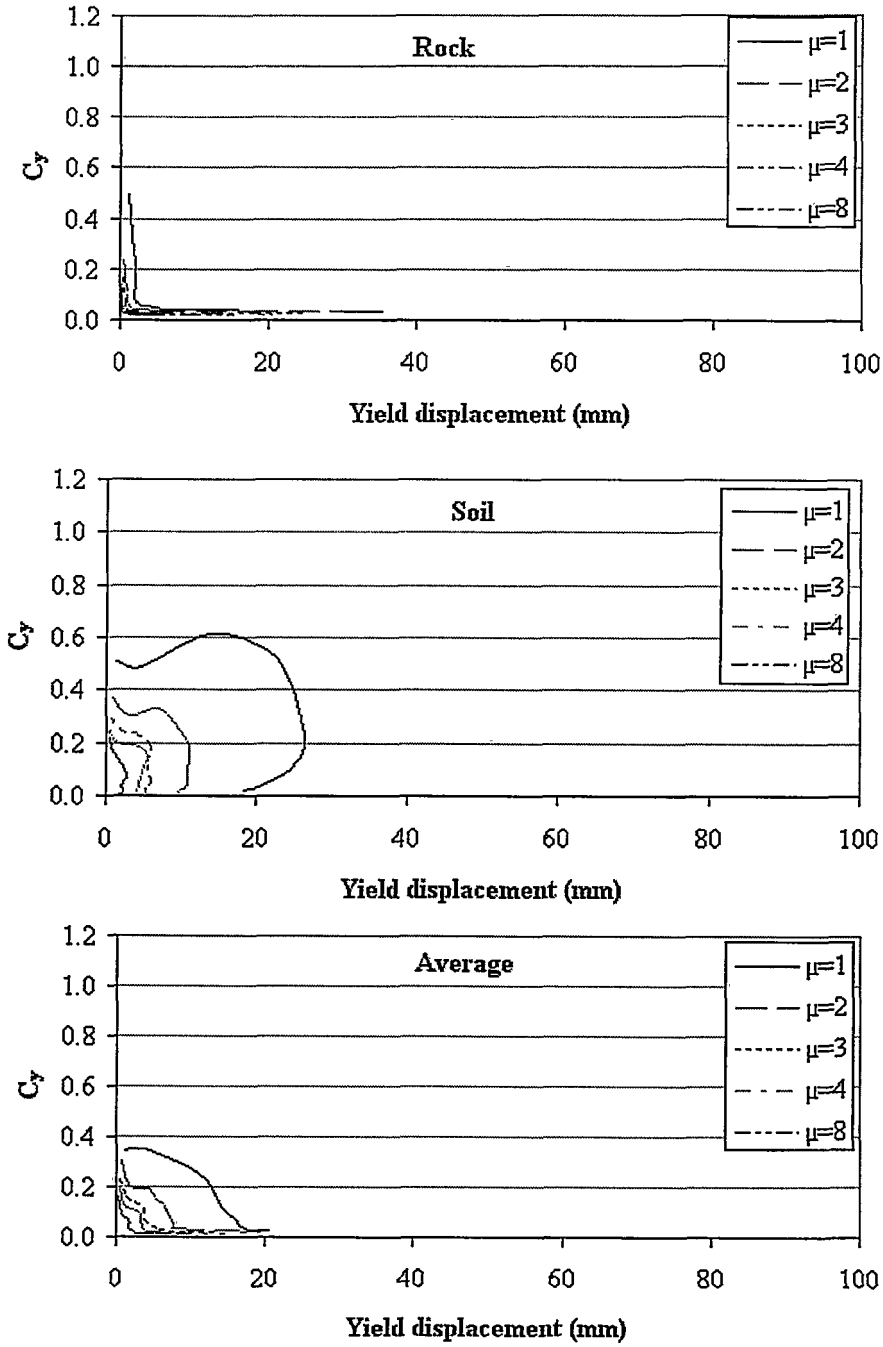

Figure 4.35 Yield spectra for NFE with magnitude <6 with PGA = 0.3g

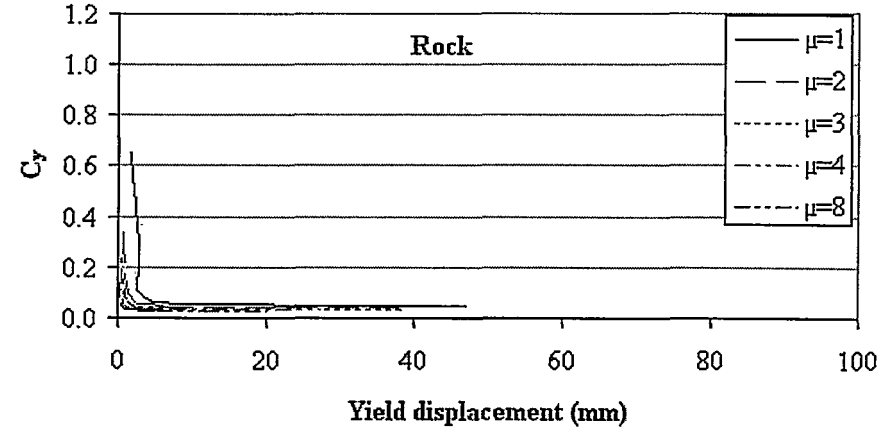

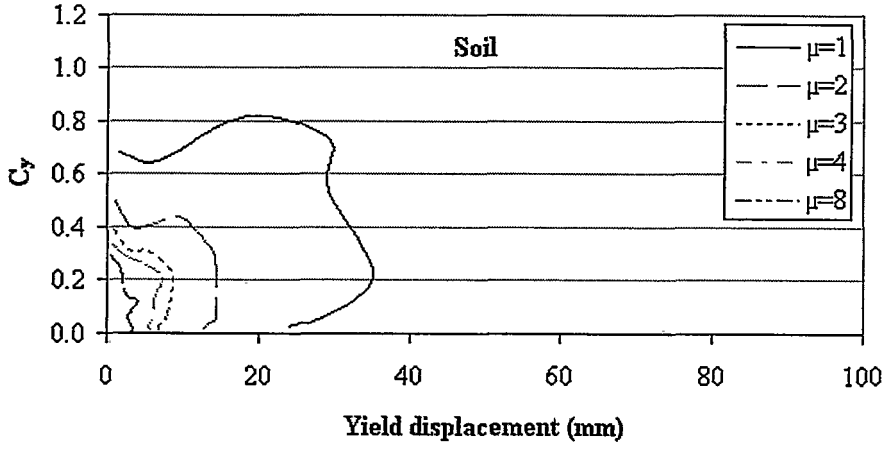

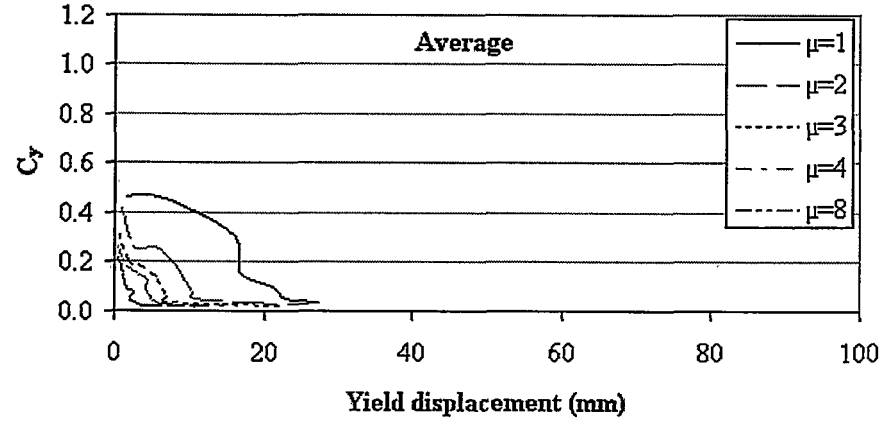

Figure 4.36 Yield spectra for NFE with magnitude <6 with PGA = 0.4g

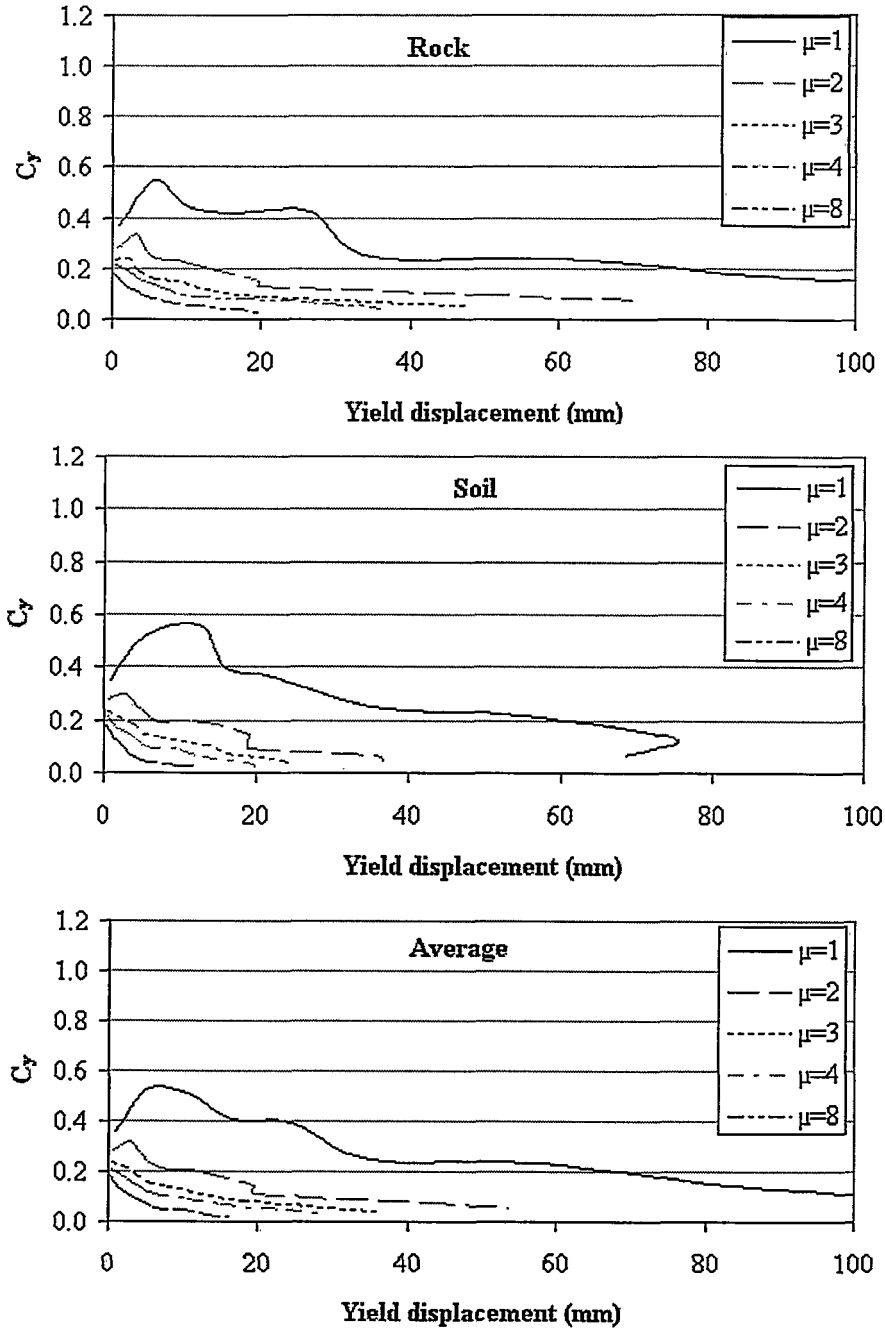

Figure 4.37 Yield spectra for FFE with PGA = 0.2g

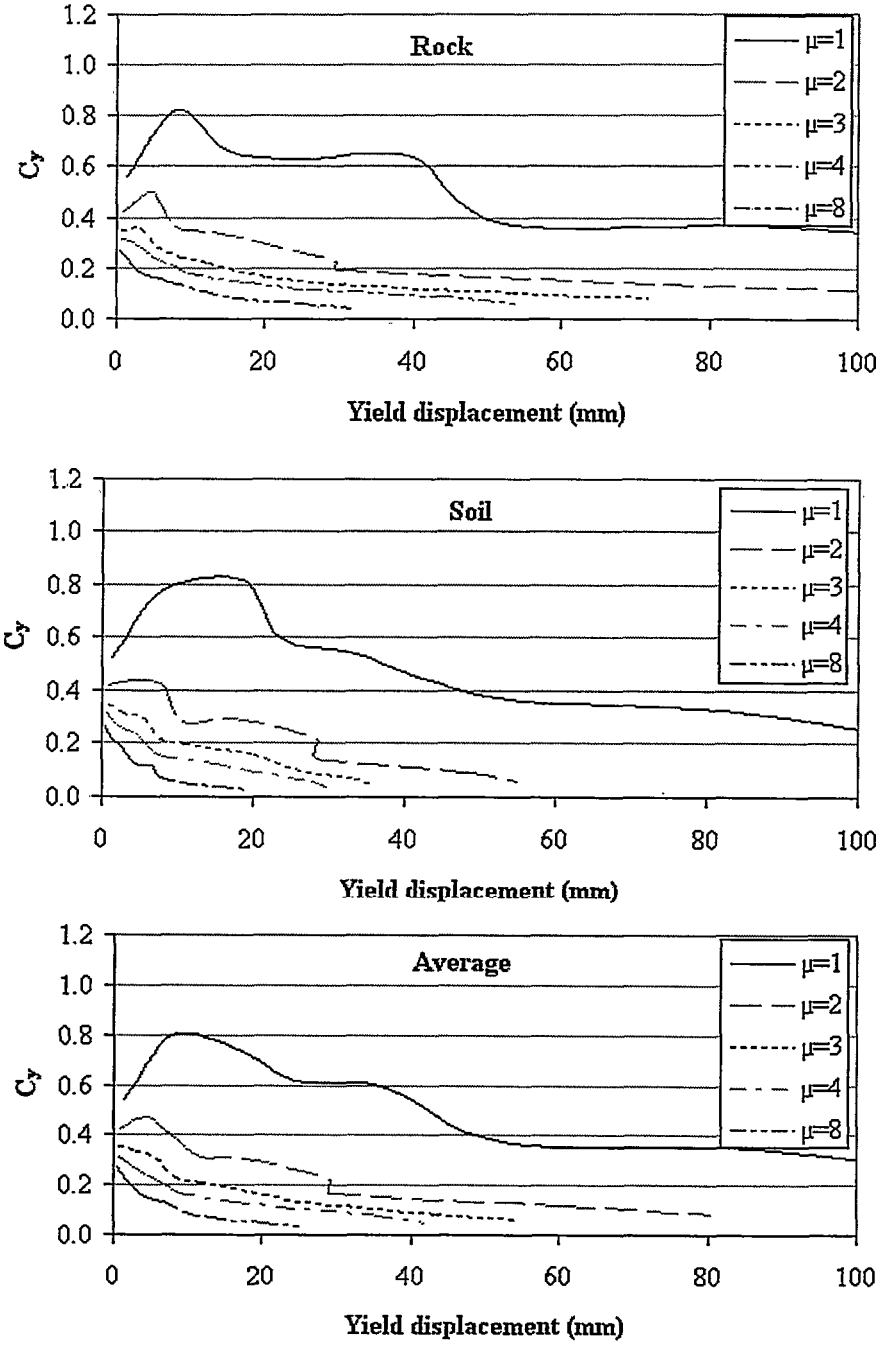

Figure 4.38 Yield spectra for FFE with PGA = 0.3g

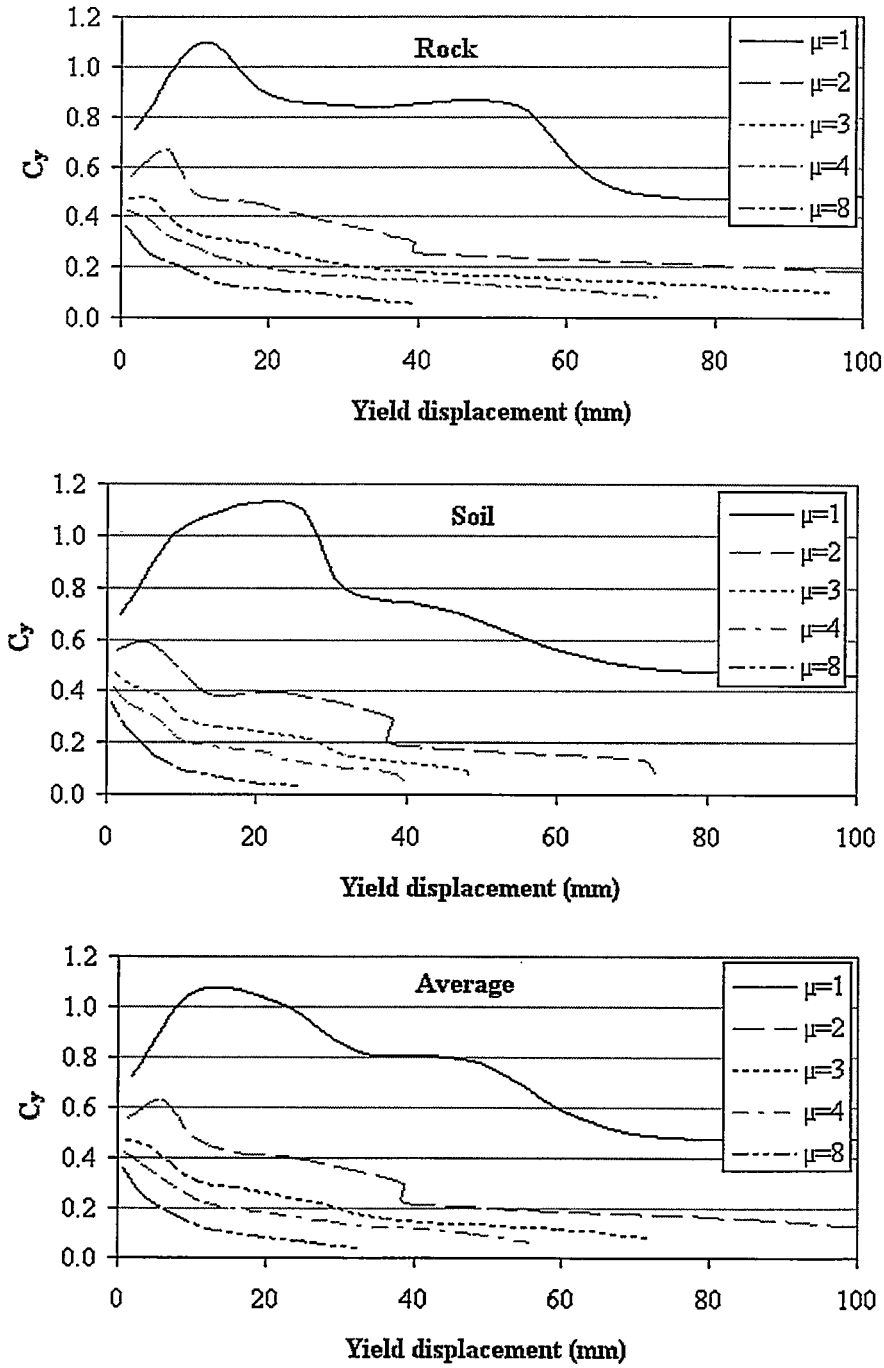

Figure 4.39 Yield spectra for FFE with PGA = 0.4g

5. DESIGN FOR MULTIPLE PERFORMANCE OBJECTIVES

CHAPTER 5

DESIGN FOR MULTIPLE PERFORMANCE OBJECTIVES

5.1 INTRODUCTION

Current trend in seismic design procedures is to achieve multiple performance objectives. The structure is required to meet stated levels of performance when subjected to various defined earthquake hazard levels. Examples of multiple performance objectives include ensuring safety in a major seismic event and minimize economic losses due to damage from moderate earthquakes.

Ghobarah (2001) defined the structural characteristics that correspond to various performance levels for structures. Figure 5.1 illustrates the typical performance curve for the structure. Three performance levels are indicated. These are serviceability, damage control and life safety or collapse prevention. The corresponding structural characteristics are the stiffness, strength and deformation capacity. To address the life safety and damage control in minor and moderate earthquakes, and prevent collapse in major earthquakes, several performance objectives need to be satisfied by the design process which forms a balance between the strength and stiffness of the structure without compromising its safety.

To attain multiple performance objectives in the yield spectra method, a graphical procedure is used to constrain the combinations of strength and stiffness that serve these objectives. In this chapter, the development of the design tools is illustrated for 3 and 12 storey buildings. The admissible design regions in the form of a plot that serve the

performance target are demonstrated. These graphs are superimposed on the yield spectra to show the use of the yield spectra in conjunction with the admissible design region graph. An example is presented to illustrate the design procedure.

5.2 ADMISSIBLE DESIGN REGION

Some of the parameters that quantify the performance objectives are those relating to damage. The roof drift and interstorey drift are indices related to the response of the structure and the damage to the non-structural components. Another quantity that expresses the structural damage associated with the inelastic response is the ductility. Controlling both drift and ductility should be sufficient to control the seismic performance of the structure, thus, achieve the required target performance objectives.

The admissible design region graph presents a quick and effective method for defining the boundary of an admissible region representing the effective combinations between the strength and stiffness. The development of the admissible design region graph requires several steps. The general performance objectives should be first selected. Thus, the allowable drift limits are chosen corresponding to the defined performance levels. The ductility limit is selected to correspond to the given level of structural damage. The admissible region has two boundaries. The first boundary is a curve passing through the points with combinations of strength and stiffness that result in the chosen peak roof drift. The second boundary is the ductility limit chosen for the required performance levels. Combinations resulting in excessive drifts and ductility demands that are larger than the allowable fall in the inadmissible design region.

Superimposing the admissible design region on the yield spectra increases the advantages and effectiveness of the design procedure. Thus, knowing the yield displacement of the structure, the designer can check whether it falls within the admissible design region or not. The design process can proceed knowing the yield strength coefficient that satisfies the required multiple performance levels. The effect of any change in the strength or stiffness of the structure during the design process can be quickly checked to make sure that they are still a safe combination.

a) PERFORMANCE LEVELS

For this study, a three and twelve storey concrete frame buildings are designed for three performance levels. The suggested performance levels are minor damage, repairable damage and irreparable damage of the structure. These levels roughly correspond to the immediate occupancy, operational and life-safety performance levels in Vision 2000. The minor and repairable damage are within the elastic behaviour of the structure, while the irreparable damage is associated with the inelastic behaviour of the structure. Figure 5.2 presents the suggested performance levels relating to the damage level and the performance levels of Vision 2000 superimposed on the lateral load-drift curve.

b) PEAK DRIFT LIMITS

The maximum interstorey or roof drift limits are chosen to represent the damage level corresponding to the defined earthquake hazard level. The drift values are selected from Table 1.1 presented in Chapter 1, which introduces the performance levels, corresponding damage state, and the drift limits (Ghobarah 2001).

c) DUCTILITY LIMITS

The ductility limits are chosen to represent the allowable levels of structural damage corresponding to the stated performance levels. A general estimate for the ductility values in relation to the damage state of the structure is presented in Figure 5.2.

d) EQUIVALENT SDOF SYSTEM

Response spectra based methods are formulated and are applicable to structures that respond predominantly in the first mode. For multi-degree of freedom structures, an equivalent single degree of freedom (SDOF) can be created where displacement and shear correspond to the roof drift and base shear in multi-degree of freedom structures. The modal participation factor (Γ_1) is significant for the calculation of the peak response of the equivalent SDOF system used in the development of the design graphs. The mass participation factor (α_1) is important for the calculation of the required base shear coefficient for the building in the design process. These modal parameters can be calculated from formulas or tables provided in ATC-40 or by Black and Aschheim (2000). For this study, the values given by ATC-40 are used. For the three-storey building, the values used are $\Gamma_1 = 1.3$ and $\alpha_1 = 0.86$. For the twelve-storey building, the values used are $\Gamma_1 = 1.4$ and $\alpha_1 = 0.78$.

e) PERFORMANCE OBJECTIVES

The minor damage performance level is selected for a frequent earthquake hazard level defined as having a 50% probability of exceedance in 30 years (or a 43-year return period). A peak drift limit if 0.2% of the height of the structure is selected for this

performance level. A system ductility value of <1 is chosen for this performance objective.

The repairable damage performance level is selected for an occasional earthquake corresponding to 50% probability of exceedance in 50 years (or 72-year return period). The drift limit for this performance level is 0.5%. The system ductility is chosen to be <1 similar to the minor damage performance level since for both performance levels the structure behaves elastically as shown in Figure 5.2.

The irreparable damage performance level is chosen for an infrequent earthquake, which corresponds to 10% probability of exceedance in 50 years (or 475-year return period). A maximum drift of 1.5% is selected for the performance level. A system ductility of <2 is chosen to correspond to the acceptable damage level. Table 5.1 identifies selected performance levels and the corresponding peak drifts, earthquake hazard levels and system ductilities for this study.

The earthquake characteristics that correspond to various seismic hazard levels are a function of several parameters including the specific site. For the purpose of the illustrative design example earthquakes with PGA of 0.1g, 0.2g and 0.3g are assumed to correspond to the three hazard levels given in Table 5.1. These PGA values are reasonable for a high seismicity zone in Canada.

5.3 YIELD SPECTRA FOR MULTIPLE OBJECTIVES

5.3.1 THREE-STOREY CONCRETE FRAME

To illustrate the technique of forming the graph, the three-storey concrete frame building is studied. To illustrate plotting the admissible design region, the YS of

NFE with magnitude greater than 6 are used. First, consider the irreparable damage performance level. Assuming the storey height is 3m and a peak drift of 1.5%. The peak roof displacement is: (0.015) (3) (3) = 0.135 m = 135 mm. Taking the value of the modal participation factor for the first mode Γ_1 to be 1.3. Hence, the peak displacement of the analogous SDOF system is 135/1.3 = 103.8 mm.

For this performance level, the YS for the earthquake records with PGA of value 0.3g are used as shown in Figure 5.3. A family of points is plotted on each YS, each point has the property that when multiplying its yield displacement by the displacement ductility gives the peak displacement. Thus, point A corresponds to a SDOF system with yield displacement of 103.8 mm. Point B corresponds to a ductility of 2 and a yield displacement of value 103.8/2 = 51.9 mm. Points C, D and E correspond to ductilities 3, 4 and 8 respectively. The curve passing through these points identifies the combinations of strength and stiffness that result in a peak roof drift of 1.5%. Thus, this curve defines the first boundary.

The μ=2 curve defines the second boundary of the combinations of strength and stiffness that has acceptable ductility responses. The two boundaries define the admissible design region. The region form a "V" shape curve, with the left side determined by the ductility considerations and the right side determined by the drift limits. The base of the admissible design region is defined with point B which presents the intersection between the ductility dominated curve and the drift dominated curve. The V curve resulting from this performance level can be called 'Irreparable damage demand

curve'. This curve is illustrated in Figure 5.3 for the records on rock, soil and the average site soils to present the soil effect investigation of this study.

Similar steps are followed when considering the repairable damage performance level. Peak drift of 0.5% is used and the YS for the earthquake records with PGA of 0.2g are used to represent this performance level. A family of points is plotted that results in a peak drift of the oscillator of 34.6 mm when multiplying its yield displacement by the displacement ductility. The ductility μ=1 defines the other boundary of this region as well. Another V-shaped curve results with its base at point F that presents the intersection between the ductility dominated and drift dominated boundaries. The curve of this performance level is called 'Irreparable damage demand curve'. This curve is illustrated in Figure 5.4 for different graphs that present the soil effect.

Now consider the minor damage performance level. The peak roof drift limit is 0.2% of the height of the building. Thus, the peak roof displacement of the structure will be equal to (0.002) (3) (3) = 0.018 m = 18 mm and the peak displacement of the equivalent SDOF system will be 18/1.3 = 13.8 mm. The YS for the earthquake records with PGA of value 0.1g are used to represent this performance level. Another family of points is plotted on the YS to present the combinations of strength and stiffness that result in a peak roof drift of value 0.2%. Point F corresponds to a SDOF system with yield displacement 13.8 mm. Thus, the radial line passing through point F presents the first boundary of the admissible design region. The ductility μ=1 defines the other boundary of the region. Hence, a "V" shaped curve represents this performance level with its base

at point G. This V curve is called 'Minor damage demand curve'. This curve is illustrated in Figure 5.5 for different graphs that present the soil effect.

While plotting the right side of the admissible design curve, which is determined by the drift limits, it may occur that none of the oscillator responses reach the level of the displacement calculated. Thus, the ductility curve restrains the admissible design region. This is shown when studying the rock graphs in Figures 5.3, 5.4 and 5.5. In the figures, the peak displacements are 103.8 mm, 34.6 mm and 13.8 mm representing the roof displacements of the equivalent SDOF systems for the cases of irreparable, repairable damage and minor damage performance levels, respectively. In these figures, none of the SDOF responses reaches the value of the roof displacement calculated for the different ductility levels. Thus, only the ductility limit curve defines the boundary of the admissible design region.

The areas above the V-shaped demand curves represent the admissible design region for that particular performance level. The areas under the curves defines the inadmissible design region in which combinations of strength and stiffness result in drift that exceeds the drift limits and/or result in unacceptable ductility responses. Superimposing the three performance levels demand curves help to satisfy multiple performance objectives. By overlaying the admissible design regions of the target performance levels, combination of the demand curves that satisfies the multiple performance objectives required are obtained. Figure 5.6 represents the superposition of the minor damage, repairable and irreparable demand curves for the earthquake records over rock, soil and both rock and soil sites for NFE with magnitude greater than 6.

In the combinations of multiple performance objectives, the performance objective with the dominating curve controls the boundary of the admissible design region. In the rock graph in Figure 5.6, the repairable damage demand curve controls over the minor damage and the irreparable damage demand curves for small yield displacements <10 mm. The irreparable damage demand curve dominates the minor damage demand curve, thus it controls the combination for large yield displacements >10 mm. The area above the dominating curve defines the admissible design region and the area under the curve represents the inadmissible design region.

In the soil graph in Figure 5.6, the repairable damage demand curve controls the combinations with the minor damage and the irreparable damage performance levels for both ductility dominated and drift dominated branches of the curve. In the absence of repairable damage criteria, the irreparable damage demand curve controls over the minor damage demand curve for SDOF yield displacements less than 21 mm represented by point H. While, the minor damage demand curve controls over yield displacements greater than 21 mm. The area above the controlling demand curve defines the admissible design region for the multiple performance objective combination.

For the graph showing the average of rock and soil sites in Figure 5.6, the same concept applies. The repairable damage controls over the irreparable damage demand curve for both the ductility dominated and drift dominated branches. For the combination between the minor damage and the repairable damage performance levels, the first performance level controls for the SDOF with yield displacements greater than approximately 29 mm. The second performance level controls for yield displacement less

than 29 mm. Point I represents the point of intersection of the two performance levels; point I has yield displacement of 29 mm.

Similarly, for the combination of the minor damage and the irreparable damage performance levels, the first performance level controls for yield displacements greater than approximately 19 mm. The second performance level controls for yield displacement less than 19 mm. The point of intersection between the two performance objectives is denoted with point K. Thus, Figure 5.6 can be used to represent the demand curve for each performance level separately, or can be used for developing the combinations of the multiple performance objectives.

The same method of defining the admissible design region of the YS of NFE with magnitude greater than 6 is applied for the YS of NFE with magnitude less than 6 and for FFE. While defining the admissible design region for the YS of NFE with magnitude less than 6, none of the oscillator responses reaches the level of displacement required. Thus, the admissible design regions are restrained by the ductility curves. This is true for the rock, soil and both rock and soil site graphs. The superposition of the minor damage, repairable and irreparable demand curves for the earthquake records over rock, soil and both rock and soil sites for NFE with magnitude less than 6 is illustrated in Figure 5.7 and that for the FFE YS is illustrated in Figure 5.8.

From studying Figures 5.6 to 5.8, for designing a three-storey building subjected to a NFE of magnitude <6, the design is ductility dominated on both rock and soil sites. This means that the only requirement of the design is to have combinations of strength

and stiffness that does not exceed the ductility limits of the required performance objectives.

For designing a similar structure subjected to a NFE with magnitude >6 on rock site, the design is controlled by the required performance objective ductility limit only. On the other hand, if the structure is built in soil site, then the design is controlled by both the ductility and drift limits. Similarly, when designing a structure subjected to FFE on rock or soil sites, the combinations of strength and stiffness of the design should not exceed either the drift or the ductility limits of the multiple performance objectives. Thus, the use of the admissible design region plot becomes significant in showing the limits of the multiple performance objectives.

5.3.2 TWELVE-STOREY CONCRETE FRAME

Same methodology for determining the admissible design region graph for each performance level is followed for the twelve-storey concrete frame building. For the irreparable damage performance level, the peak roof displacement is (0.015) (12) (3) = 0.54 m = 540 mm. Taking the value of the modal participation factor for the first mode to be 1.4. Hence, the peak displacement of the analogous SDOF system is 540/1.4 = 385.7 mm. For the minor damage performance level the peak roof displacement of the structure will be equal to (0.002) (12) (3) = 0.072 m = 72 mm and the peak displacement of the equivalent SDOF system will be 72/1.4 = 51.4 mm. For the repairable damage performance level, the peak roof displacement of the equivalent SDOF is equal to 0.128 m = 128 mm.

The superposition of the minor damage, repairable and irreparable demand curves for the earthquake records over rock, soil and both rock and soil sites for NFE greater than 6 is illustrated in Figure 5.9. For the twelve-storey building, the admissible design region is now bounded by the ductility dominated curve branch only. For the case of NFE with magnitude less than 6, the admissible design region graph will be typical to that in Figure 5.7. Similar to the three-storey building, the ductility limits controlled the design as shown in Figure 5.10. Thus, for any higher number of storeys, the same behaviour is expected. The superposition of the demand curves for the FFE earthquake records are presented in Figure 5.11. The admissible design region is ductility controlled as well. This behaviour is expected as the twelve-storey buildings have relatively large peak roof displacements. Thus, the only issue of concern would be to make sure that the building ductility is within allowable limits, which would thus control the allowable design region.

Thus, from Figures 5.9, 5.10 and 5.11, for designing a twelve-storey building for NFE with magnitude <6, NFE with magnitude >6 and FFE, only the ductility limits controls the design under the multiple performance objectives.

5.4 SEISMIC DESIGN USING YS AND ADMISSIBLE DESIGN REGION GRAPH

5.4.1 DESIGN PROCEDURE

The proposed seismic design procedure is a combination between a new displacement-based design procedure (YS method) and traditional provisions of the code. This proposed method lies in an advanced place within the spectrum of available methods. The investigation of the epicentral distance, site soil effect and earthquake

magnitude effect on the formation of the spectra and in turn on the admissible design plot increased the simplicity and the clarity of the proposed method. The design base-shear strength is determined using the YS method, and the rest of the design can follow the current design code provisions. The minimum required combinations of strength and stiffness that satisfy the allowable ductility and drift limits can be checked using the admissible design region graph. The steps are as follows:

Step 1: Estimate the yield displacement of the structure. The estimate of the yield displacement can be based on experience, a previous analysis of similar structure, or by using available formulas.

Step 2: Determine the required performance objectives. Thus, determine the allowable ductility limits for the system.

Step 3: Estimate the values of the participation factors (modal participation factor Γ_1, mass participation factor α_1) based on the assumed mode shape and distribution of mass. In this study, a simple straight-line deflected shape representing an estimate of the predominant mode shape is used, with distributed lumped masses over the height of the structures. These assumptions allow the use of the participation factors of the ATC-40 or the values presented by Aschheim and Black (2000).

Step 4: Estimate the yield displacement of the equivalent SDOF system. The ESDOF yield displacement Δ_{ye} equals Δ_y / Γ_1.

Step 5: Enter the YS with the ESDOF yield displacement and the allowable ductility limits determined in steps 2 and 4.

Step 6: Read off the corresponding yield strength coefficient C_y.

Step 7: Check that the combination of the yield displacement and the C_y lies within the admissible design region that satisfy the performance objective or multiple objectives required. This is using the admissible design region graph.

Step 8: Determine the required base shear coefficient for the structure, which equals $\alpha_1 C_y$.

Step 9: Calculate the base shear force. It is equal to the multiplication of the required base shear coefficient for the structure, determined in step 8, by the weight of the structure W.

Step 10: Distribute the base shear over the height of the building according to the equivalent static lateral force procedure of a modern building code.

The steps of the design procedure are illustrated in the flowchart presented in Figure 5.12.

5.4.2 DESIGN EXAMPLE

As an example to illustrate the effectiveness of the YS design procedure, a three-storey building is designed twice. The building is designed once using the force-based design procedure and another time using the proposed method. The yield spectra obtained in Chapter 4 are used as design spectra. The structure is designed to achieve the irreparable damage (life-safety) performance objective. The floor to floor height of the storey is 3.6 m.

a) USING FORCE-BASED PROCEDURE

Step 1: The period of the structure is calculated using the equation $T=0.075\ H^{0.75}$, this gives a value of 0.44 s, where H is the height of the structure.

Step 2: using the C_y-μ-T graph for PGA 0.3g, we get a $C_y = 0.4$

b) USING YIELD SPECTRA PROCEDURE

The steps of the design procedure are followed:

Step 1: The yield displacement is estimated to be 1.2% of the structure height. Thus, it is equal to (0.012) (3) (3.6) = 0.1296 m = 129.6 mm.

Step 2: The allowable ductility of the system is taken $\mu = 2$.

Step 3: The modal participation factor is taken to be $\Gamma_1 = 4$

Step 4: The equivalent SDOF yield displacement Δ_{ye} is calculated to be 129.6/(4)(2) =16.2 mm.

Step 5, 6: Use the YS that presents the case of NFE with magnitude greater than 6 and allowable ductility μ=2. For Δ_{ye} = 16.2 mm, the corresponding C_y value is approximately 0.2.

Step 7: Use figure 5.3 to check whether the Δ_{ye} and the C_y values satisfy the performance objective. It is found that it satisfy the drift limits of the assigned performance objective. Thus, the Cy value 0.2 will satisfy the irreparable performance objective same as the force-based design. However, the ratio between the obtained value for the YS procedure to that of the force based procedure equals 0.4/0.2. This shows that the yield spectra design will obtain half the obtained base shear forces using the force-based design procedure to satisfy the same performance level.

This example illustrates that the use of the YS graphs with the admissible design region graphs is a simple graphical construction that allows the designer to constrain the combinations of the strength and stiffness that satisfy multiple performance objectives in a few simple steps. In addition, the procedure allows the design of the structural members using the conventional methods of the code. Thus, the method can be easily understood and applied in short time by practicing professionals.

Table 5.1 Performance objectives selected for the study

Item	Performance level			
	Minor damage	Repairable damage	Irreparable damage	Extreme damage
Earthquake hazard level	50% exceedance in 30 years	50% exceedance in 50 years	10% exceedance in 50 years	10% exceedance in 100 years
Peak drift	0.2%	0.5%	1.5%	2.5%
System ductility	1	1	2	4

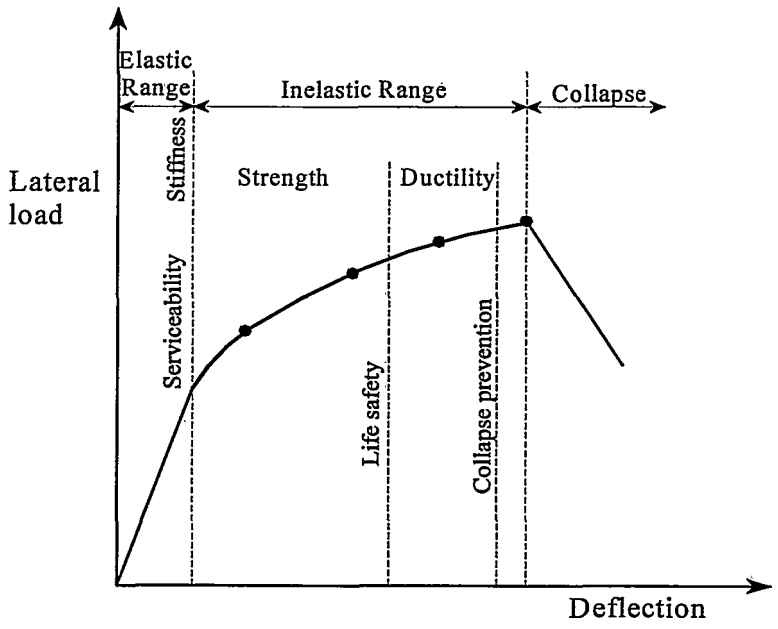

Figure 5.1 Typical performance curve for the structure (Ghobarah 2001)

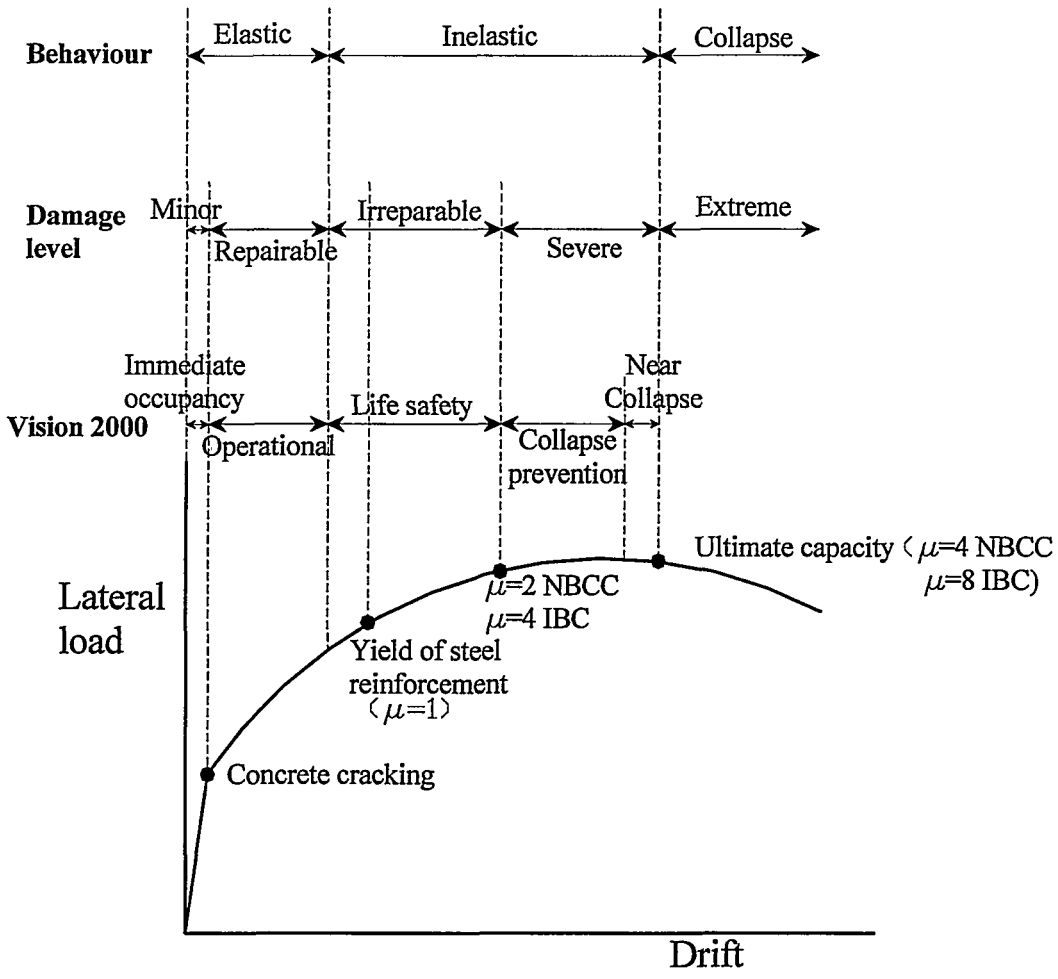

Figure 5.2 Performance levels proposed for the Canadian code and Vision 2000 (Ghobarah 2004)

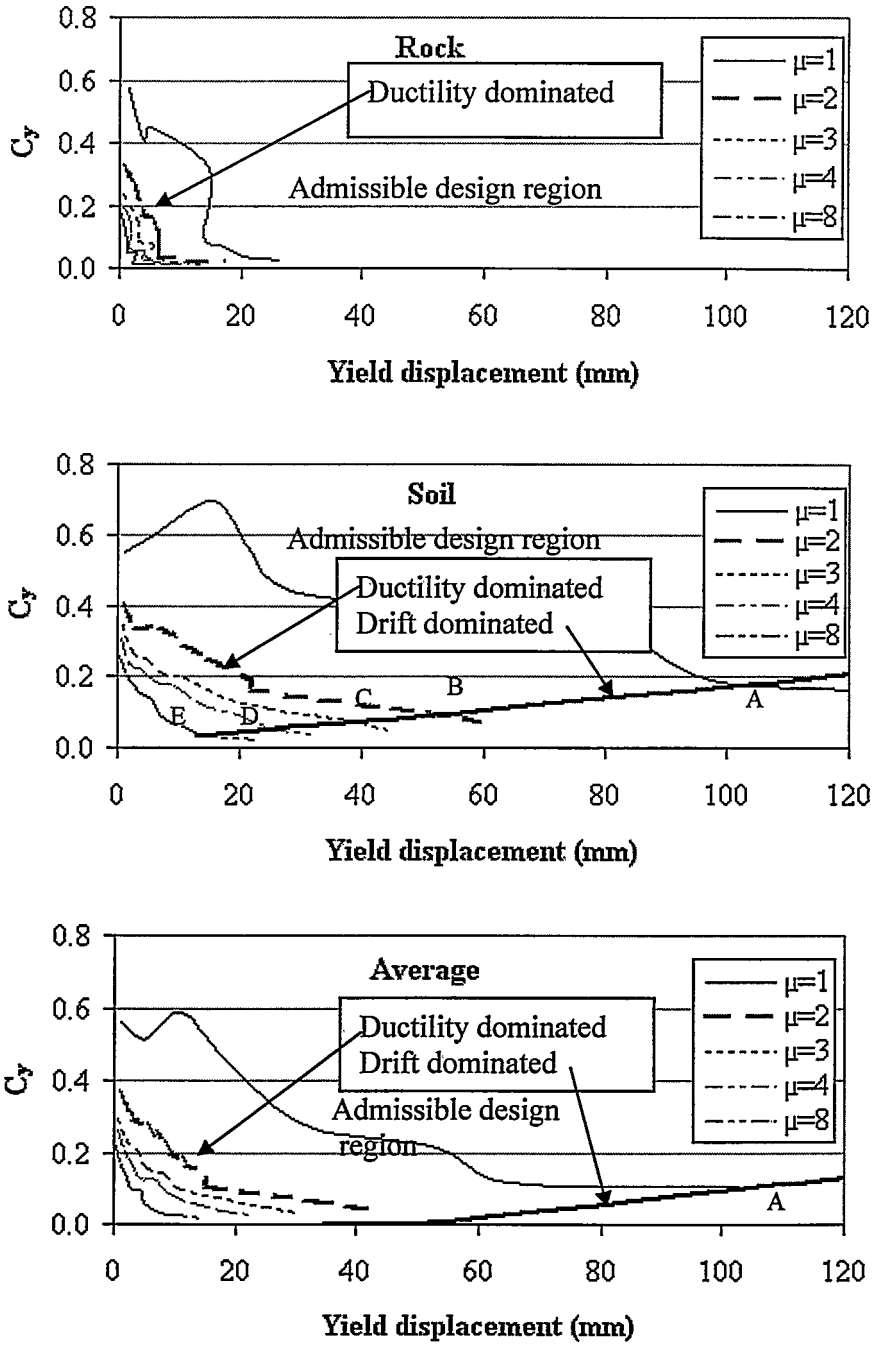

Figure 5.3 Admissible design regions for the irreparable damage performance level, for a three-storey building using YS for NFE with magnitude greater than 6, and having PGA 0.3g

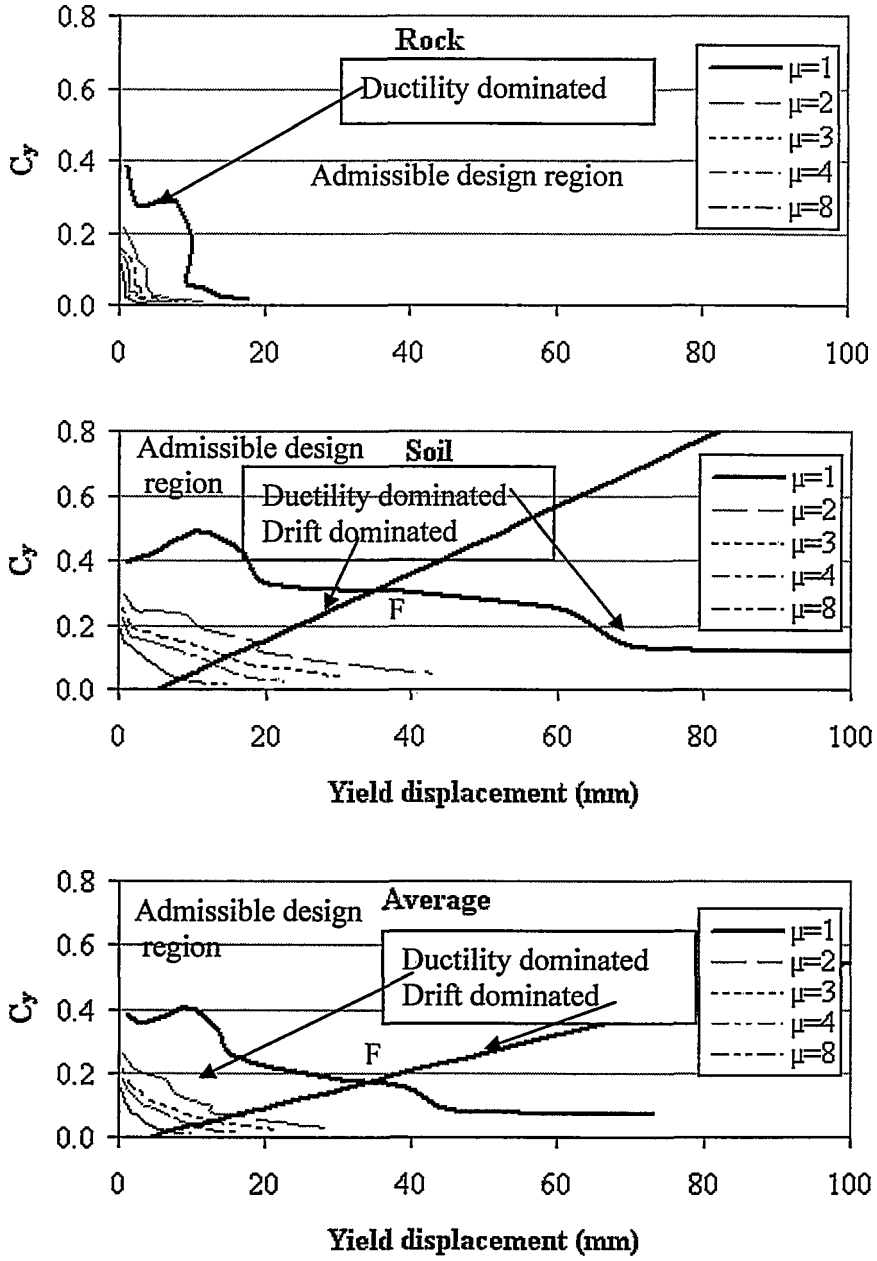

Figure 5.4 Admissible design regions for the repairable damage performance level, for a three-storey building using YS for NFE with magnitude greater than 6, and having PGA 0.2g

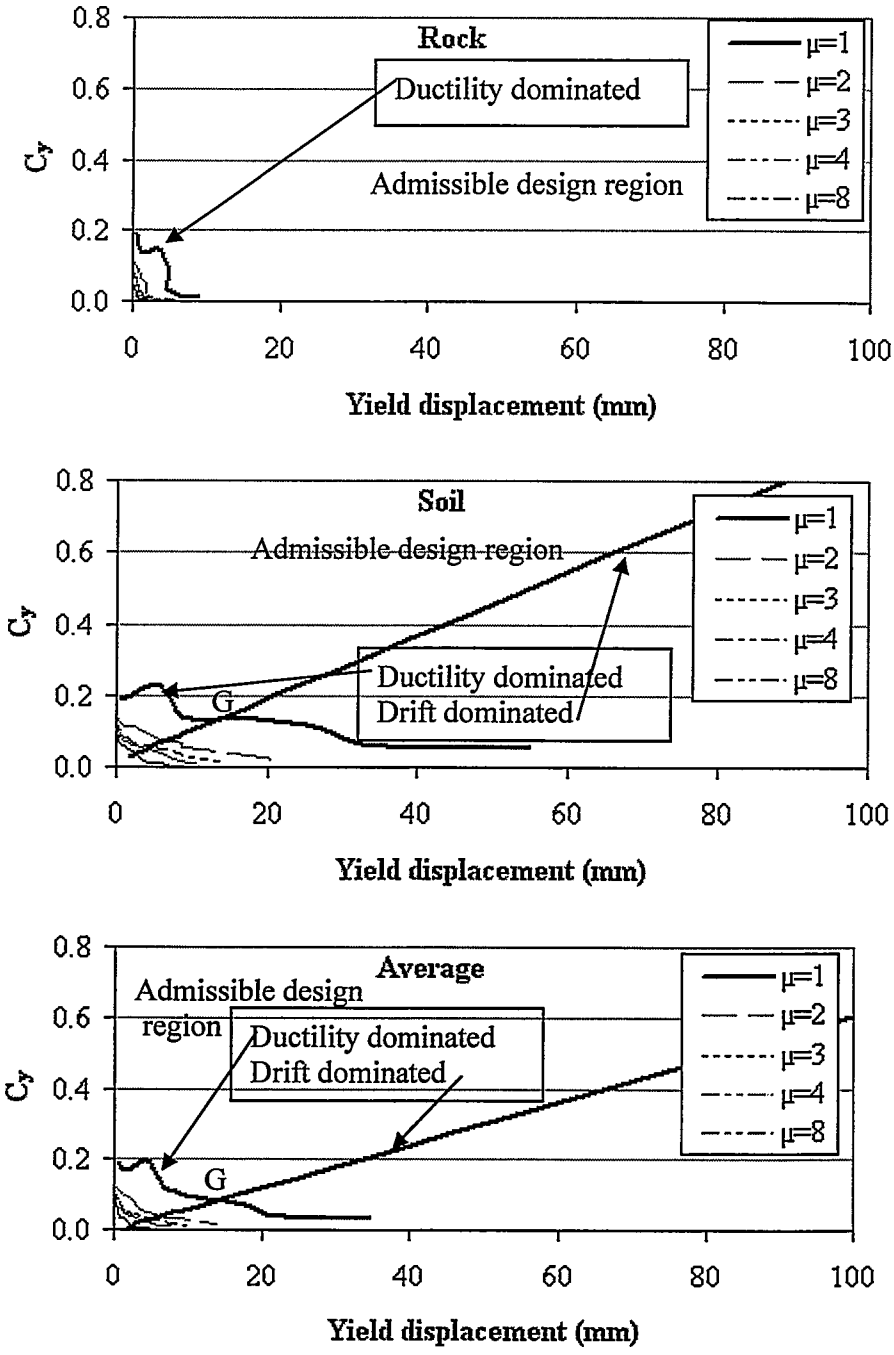

Figure 5.5 Admissible design regions for the minor damage performance level, for a three-storey building using YS for NFE with magnitude greater than 6, and having PGA 0.1g

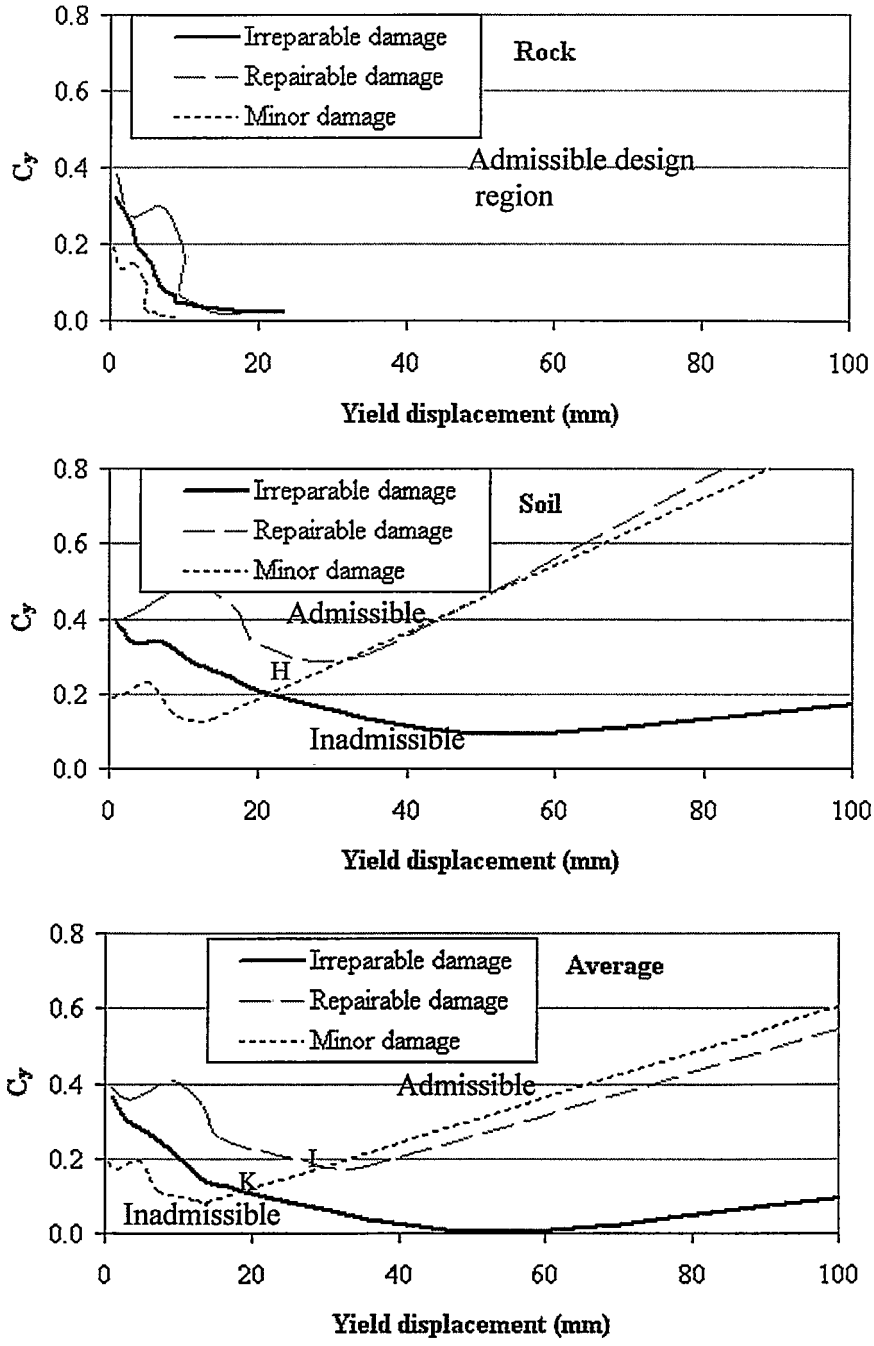

Figure 5.6 Combination of admissible design regions to satisfy multiple performance objectives of a three-storey building for the rock, soil and average of both soils for NFE with magnitude greater than 6

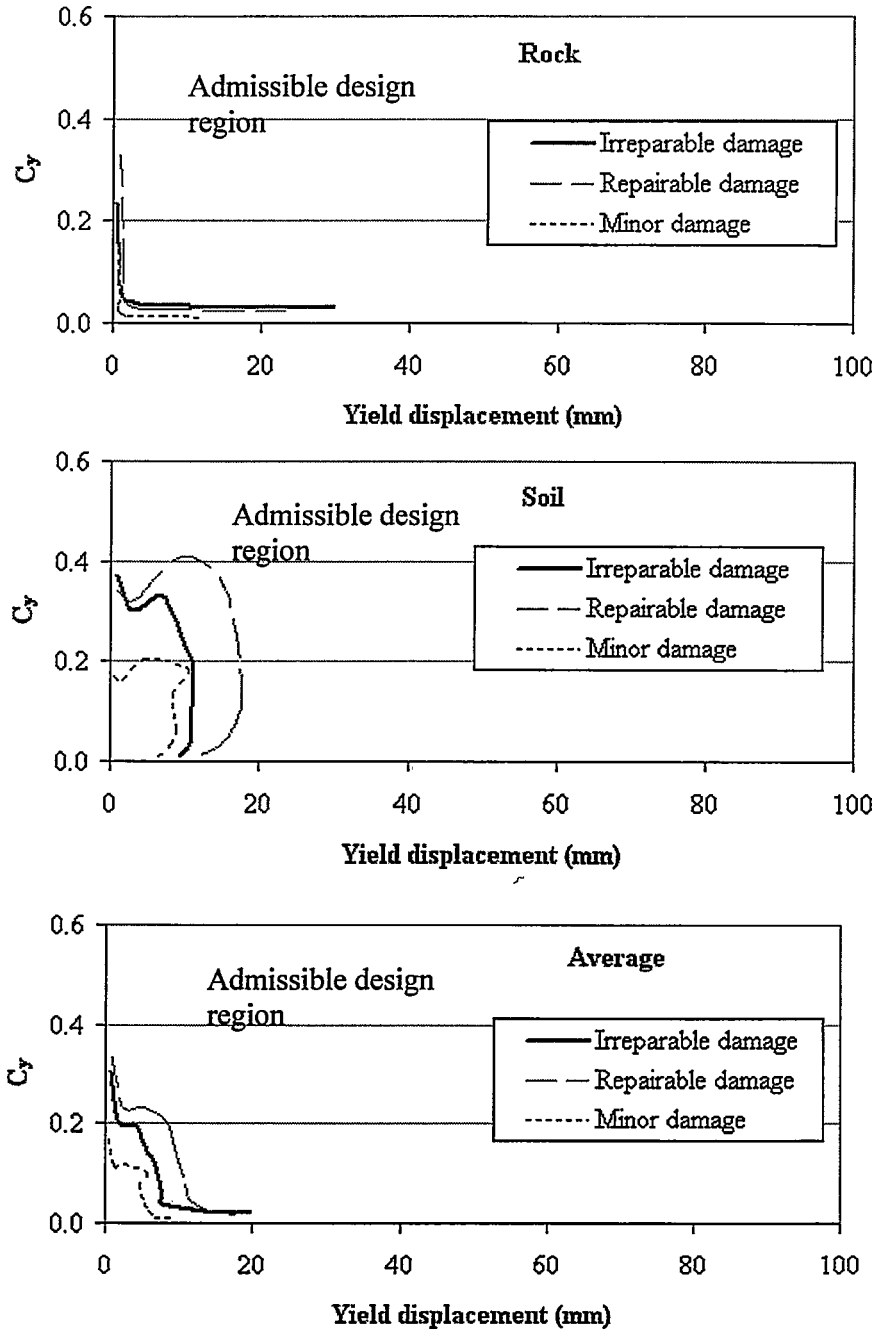

Figure 5.7 Combination of admissible design regions to satisfy multiple performance objectives of a three-storey building for the rock, soil and average of both soils for NFE with magnitude less than 6

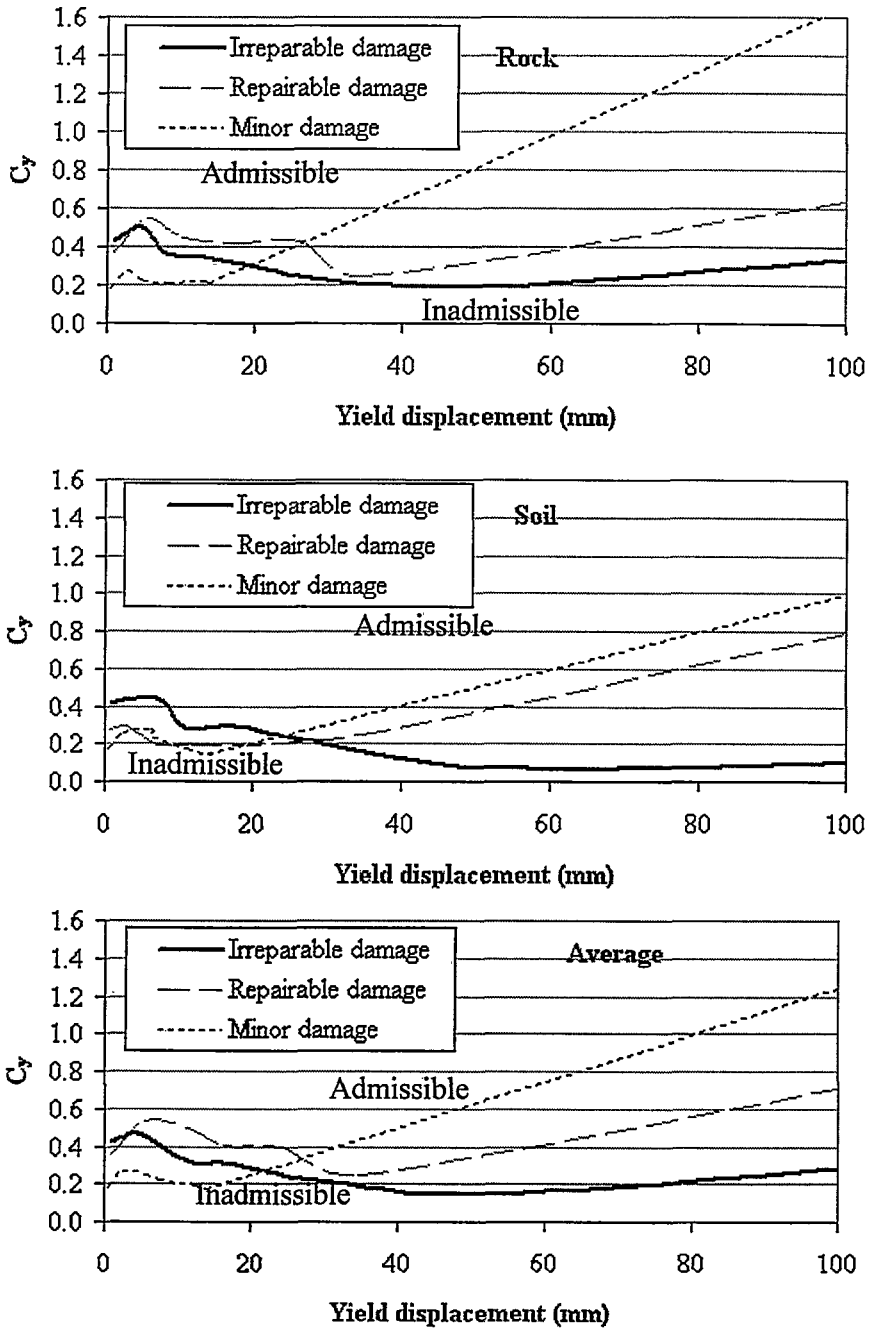

Figure 5.8 Combination of admissible design regions to satisfy multiple performance objectives of a three-storey building for the rock, soil and average of both soils for FFE

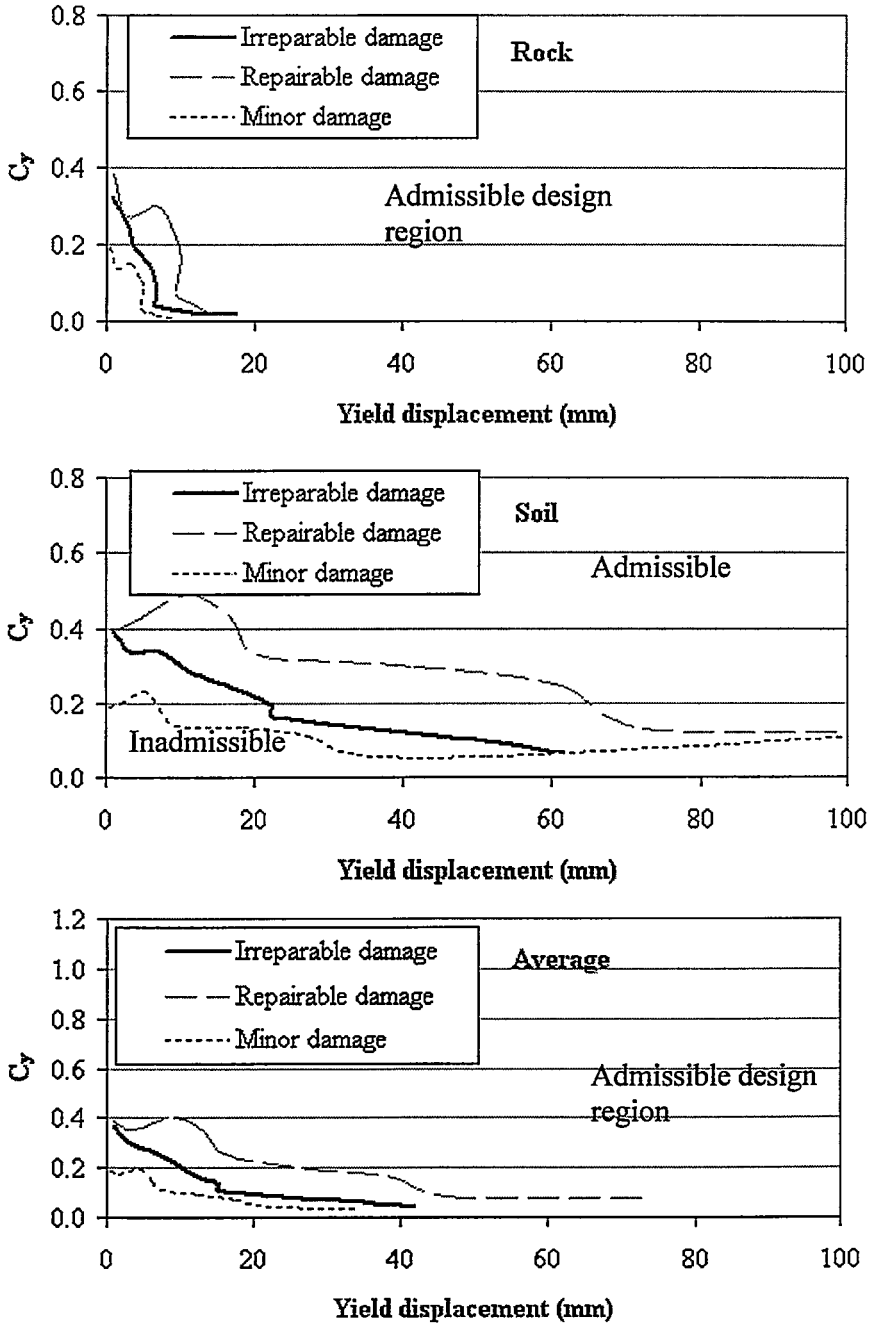

Figure 5.9 Combination of admissible design regions to satisfy multiple performance objectives of a twelve-storey building for the rock, soil and average of both soils for NFE with magnitude greater than 6

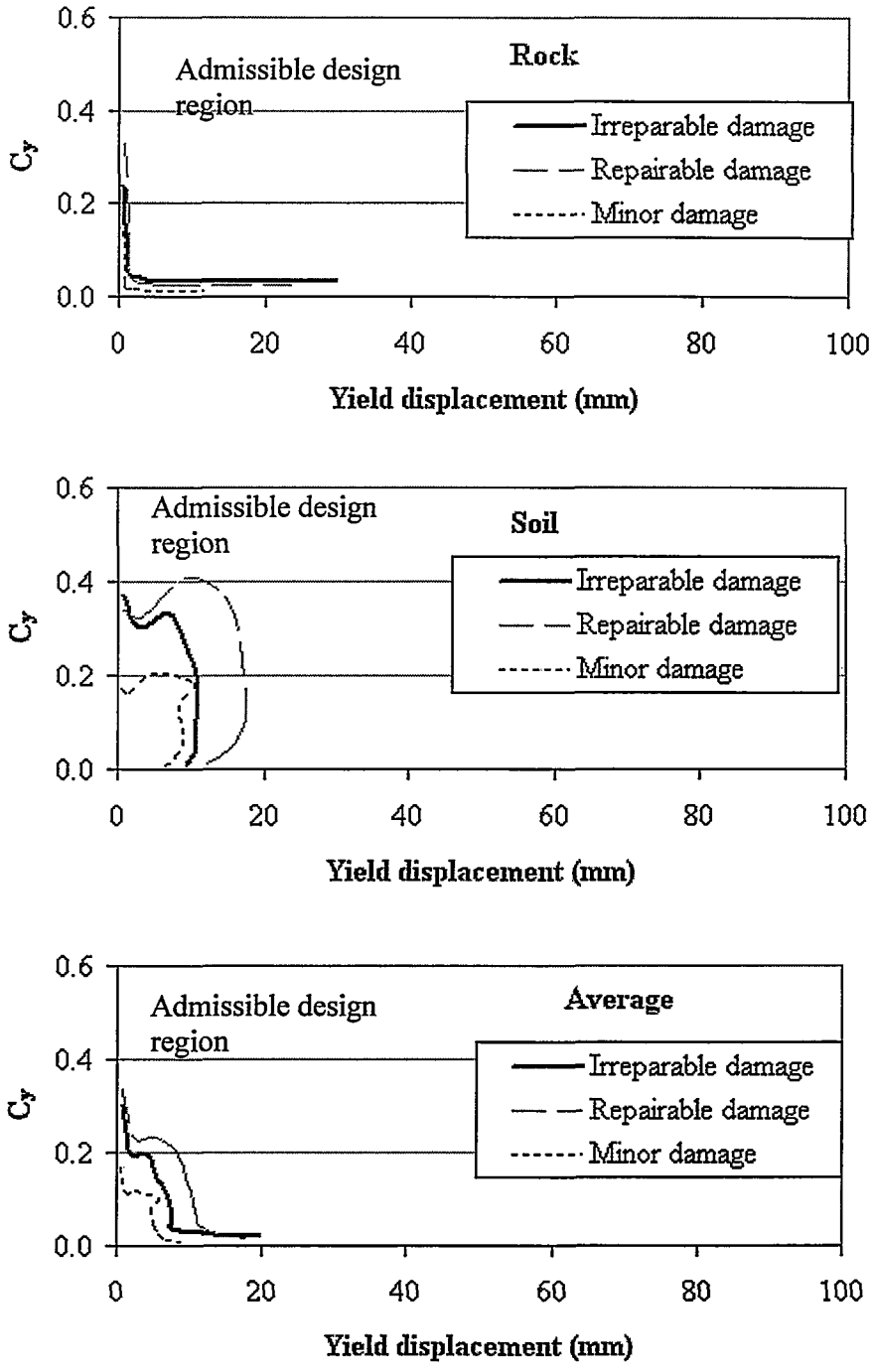

Figure 5.10 Combination of admissible design regions to satisfy multiple performance objectives of a twelve-storey building for the rock, soil and average of both soils for NFE with magnitude less than 6

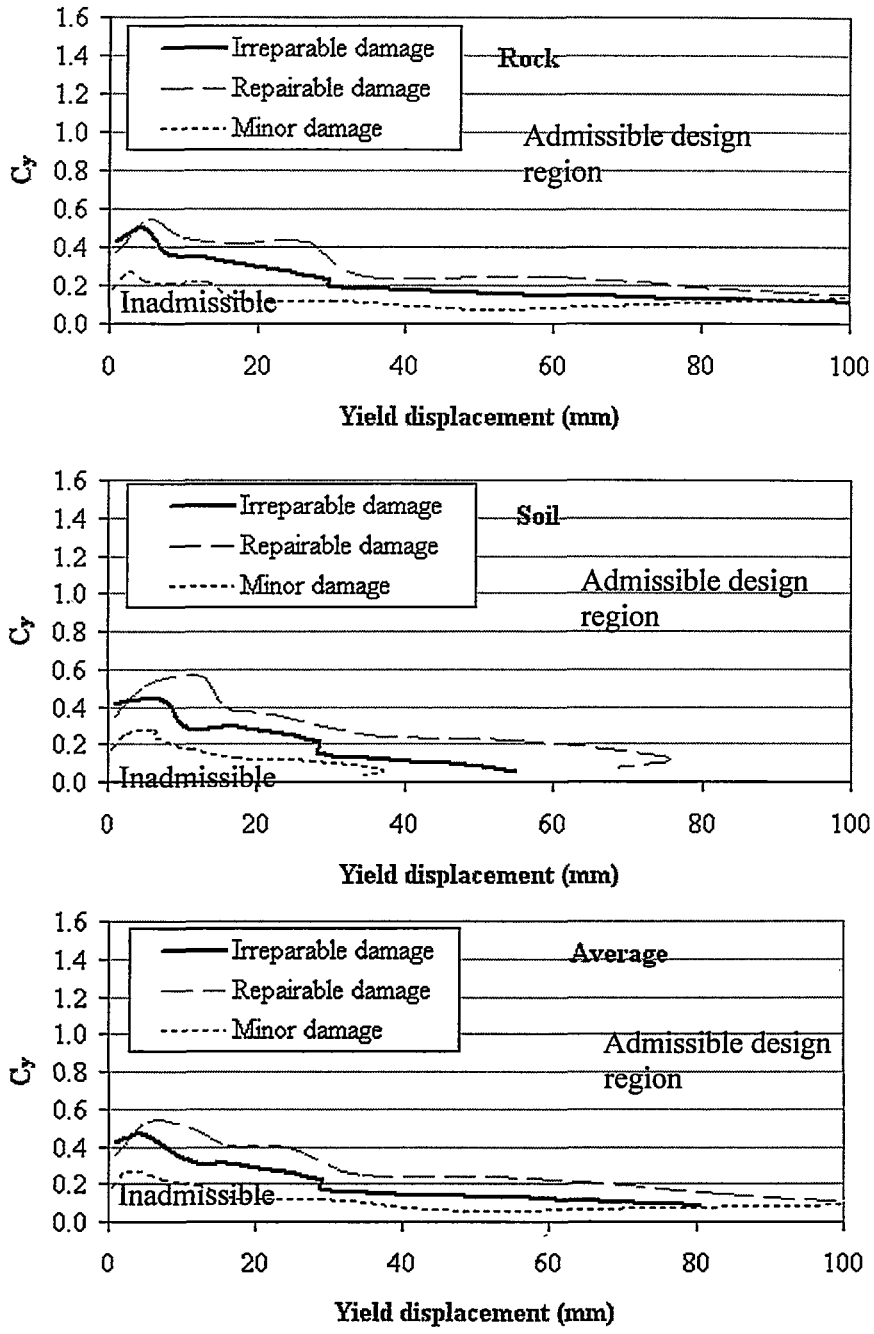

Figure 5.11 Combination of admissible design regions to satisfy multiple performance objectives of a twelve-storey building for the rock, soil and average of both soils for FFE

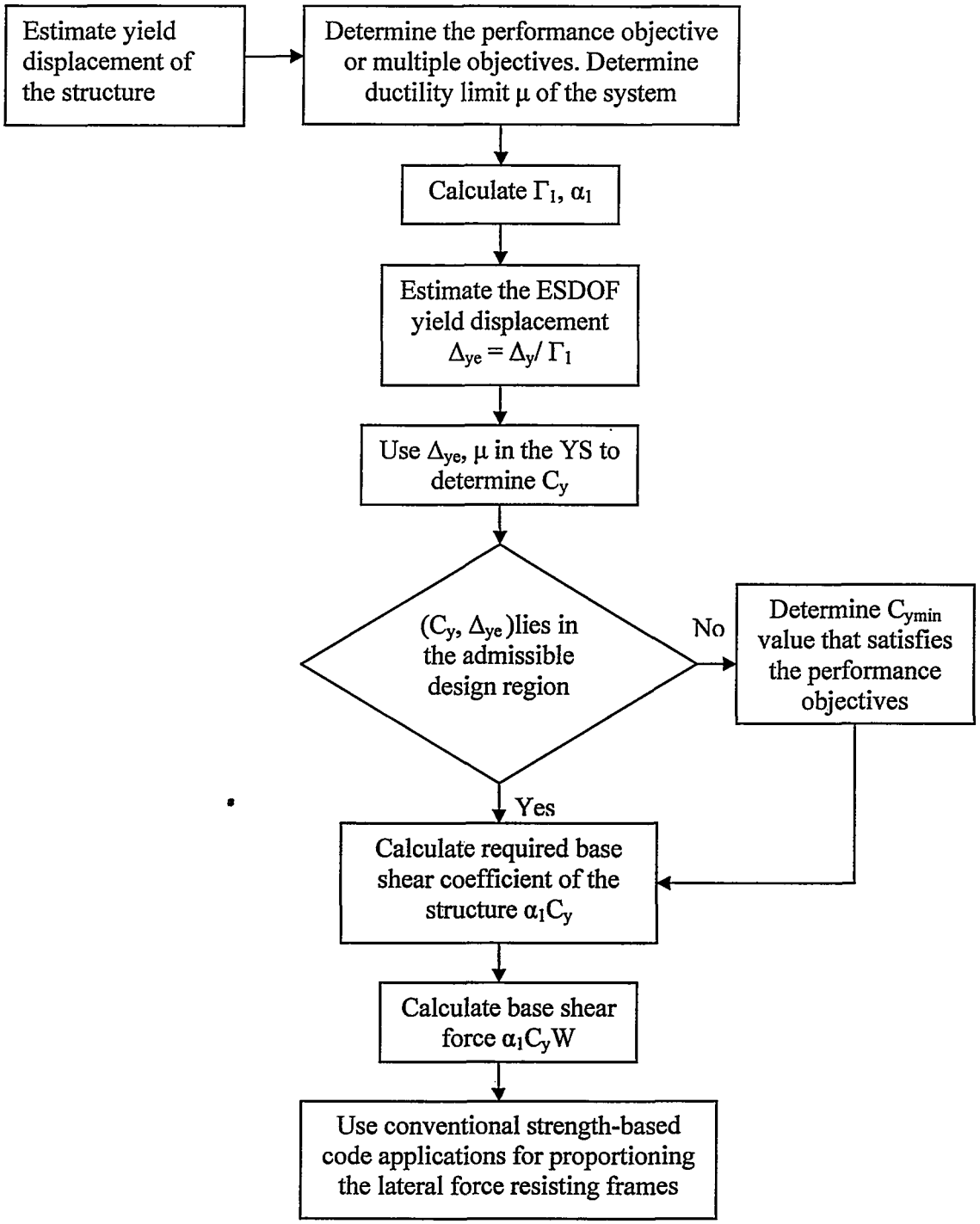

Figure 5.12 Flowchart of the proposed seismic design procedure

6. CONCLUSIONS AND RECOMMENDATIONS

CHAPTER 6

CONCLUSIONS AND RECOMMENDATIONS

6.1 SUMMARY

This chapter summarizes the results obtained during the study in relation to two principle objectives. The first objective of this study is to investigate the effect of earthquake characteristics on the development of the yield spectra. The second objective is to form a graphical plot that defines the allowable design region that satisfies multiple performance objectives.

For developing the yield spectra, actual earthquake records were obtained and categorized according to epicentral distance (whether the earthquakes are near-fault or far-field earthquakes), the directivity factor (forward or backward directivity), the magnitude of the earthquake (greater or less than M=6) and the different type of site soils (rock or soil sites). A SDOF system is subjected to the chosen set of earthquakes scaled to different levels of PGA (0.1g, 0.2g, 0.3g and 0.4g). Linear and nonlinear analyses were conducted using Nonlin version 6.01 program. Using the analyses results, the relationship between the force modification factor and the period for constant ductility values, the relationship between the shear strength coefficient and the period for constant ductility values and the yield spectra were established.

The admissible design region graph was developed by studying each performance level individually. By defining the ductility limit and the drift limit that represent a given performance level, a V-shaped curve defining the admissible design region for the

studied level was obtained. Overlaying the admissible design region for the performance objectives lead to achieving a multiple performance objectives graph which identify the admissible design region that satisfies multiple performance objectives.

The Yield spectra design procedure was introduced. A comprehensive application of the procedure to the design of a three-storey building was conducted, using the yield spectra in conjunction with the admissible design region graph.

6.2 CONCLUSIONS

The current design code does not account for some of the effects of ground motion characteristics in the design of structures. Based on the analysis formed in this study representing the various categories of the investigation, the following conclusions are arrived at:

- The use of the yield displacement as a primary design parameter is more reliable than using the period of the structure. The yield displacement is relatively stable as the base shear strength of the structure is modified. This makes it easy to determine the base shear strength required to satisfy the multiple performance objectives without affecting the design calculations. On the other hand, the period of the structure is seen to be a consequence of the choices made in the design process to satisfy the performance objective. Thus, the period may vary significantly if changes in the strength and/or stiffness of the structure are made during the design process.
- Responses of long period structures in the near-fault and far-field regions varied. Structures in the near-fault regions have higher responses relative to those in the far-field region for the same site soil category.

- Earthquake responses in the near-fault region varied remarkably depending on the site soil type. Structures on soil sites should be designed for higher base shear forces compared to structures on rock sites.
- Structures on rock sites have a sharp short peak response range. While, structures on the soil sites have shown a wide peak response range. This indicates that further sub-categorization of the site soils is required, due to its lack in the available literature, (example: stiff soil, soft soil, alluvium). This sub-categorization will allow identifying more specific response range for the structures on different soil sites.
- In siting of critical facilities as nuclear power plant studies, locations where near faults can cause possible earthquakes with magnitudes 6 or larger are avoided. However, it is likely that existing facilities may be subjected to near-fault earthquakes of magnitude less than 6. The structures may suffer significant damage due to the lack of incorporation of the near-fault effect in the design process.
- The yield spectra of earthquake records scaled to the various levels of PGA (0.1g, 0.2g, 0.3g and 0.4g) show that the ratio between the responses at the different PGA is directly proportional to the ratio between the PGA values.
- The calculated force modification factors have smaller values relative to the initial force modification factor values used in the calculations. The calculated force modification factors do not vary with the scaling of the records to the different PGA.
- The proposed design procedure achieved lower base-shear forces compared to the values obtained using the code design procedure.

- The proposed method proved its effectiveness in achieving the multiple performance objectives target. The graphical procedure shows the admissible design region that limits the strength and stiffness combinations to satisfy several performance objectives in the same time.

The above conclusions were reached based on limited number of analysis cases using the specific selected ground motions.

6.3 RECOMMENDATIONS FOR FUTURE RESEARCH

This research is a step forward towards achieving a method for multiple performance design that is suitable for code applications. This study investigated some of the unresolved issues concerning the design procedure; however, there are still several issues that should be addressed. Some of these issues are:

a) FURTHER SOIL CATEGORIZATION

In this study, the site soils were categorized into rock and soil sites. However, the soil behaviour is still not entirely clear. Thus, further sub-categorization of the soil is required, for example, soft soil, stiff soil, alluvium soil.

b) EFFECT OF MODE SHAPE AND MASS DISTRIBUTION

For using the equivalent SDOF system methodology, the values of the modal participation factor and mass participation factor are based on the assumption of the mode shape and the distribution of the mass. In this study, a simple straight-line deflected shape representing an estimate of the predominant mode shape is used, with distributed lumped masses over the height of the structures. Thus, further investigation

of the effect of other assumptions of the mode shape and mass distribution on the results is required.

c) BACKWARD DIRECTIVITY EFFECT

Based on general observation, backward directivity earthquakes should have the same response as far-field earthquakes. However, this study did not investigate this behaviour. This research was more interested in the forward directivity earthquake. Thus, investigating the effect of the backward directivity earthquake should be studied.

d) IRREGULAR BUILDINGS

The YS method is expected to be effective in the design of regular frame buildings. However, the effect of irregular buildings and irregular mass distribution on the design procedure should be addressed.

e) SOIL-STRUCTURE INTERACTION EFFECTS

The soil-structure interaction has not been incorporated in the available design procedures. Thus, its investigation is significant for the design of stiff massive structures.

REFERENCES

ATC, 1996, "Seismic evaluation and retrofit of concrete buildings", vol. 1, report no, *ATC-40*, Applied Technology Council, Redwood City, CA, November.

Aschheim M.A. (2002), "Seismic design based on yield displacement", *Earthquake Spectra*, vol. 18, No. 4, pp. 581-600.

Aschheim M.A. and Black E.F. (2000), "Yield point spectra for seismic design and rehabilitation", *Earthquake Spectra*, vol. 16, No. 2, pp. 317-336.

Ambraseys N., Smith P., Berardi R., Rinaldis D., Cotton F. and Berge-Theiry C. (2000): Dissemination of European strong-motion data. CD-Rom collection. European Council, Environment and Climate Research Program, *Institute de protection et de sureté nucléaire, Paris, France.*

Black E.F. and Aschheim M.A. (2000), "Seismic design and evaluation of multistory buildings using yield point spectra", CD release 00-04, *Mid-America Earthquake Center, University of Illinois, Urbana*, July.

Browning J.P. (2001), "Proportioning of earthquake-resistant RC building structures", *Journal of the structural division*, ASCE, vol. 127, No. 2, 145-151.

Bommer J.J. and Elnashai A.S. (1998), "Displacement spectra for seismic design", *Journal of Earthquake Engineering*, vol. 3, No. 1, pp 1-32.

Celebi M., Akkar S., Gulerce U., Sanli A., Bundock H. and Salkin A. (2001), "Main shock and aftershock records of the 1999 Izmit & Duzce, Turkey earthquakes." Report 01-163, V-1.0. USGS/OFDA project [USGS project no: 1-7460-63170], California, U.S.

Chopra A.K. and Chintanapakdee C. (2001), "Comparing responses of SDF systems to near-fault earthquake motions in the context of spectral regions", *Earthquake Engineering and Structural Dynamics*; 30:1769-1789.

Chopra A.K. and Goel R.K. (2001), "Direct displacement-based design: use of inelastic vs. elastic design spectra", *Earthquake Spectra*, vol. 17, No.1, pp. 47-64.

Earthquake research institute, university of Tokyo (2003)[http://www.eri.u-tokyo.ac.jp/], accessed June 2003.

Earthquake information at the Kanto Tokai district (2003), Japan [http://www.bosai.go.jp/center/Kanto-tokai/index_e.html], accessed June 2003.

Elsheikh A. (2002), "Response of RC structures to near-fault earthquake records". Master thesis, McMaster University, Canada.

EQE (2003) EQE International Incorporation [http://www.eqecat.com//japancat.htm], accessed December 2003.

FEMA (2002), "Nonlinear Dynamic Time History Analysis of Single Degree of Freedom Systems" [http://training.fema.gov/EMIWeb/nonlin.asp], accessed December 2002.

Freeman S.A. (1998). "The Capacity Spectrum method as a tool for seismic design", *Proceedings of the 11th European Conference on Earthquake Engineering*, Paris, France. Balkema Publishers, Rotterdam, Netherlands.

Fnet (2003) Full-range seismograph network [http://www.Fnet.bosai.go.jp/freesia/index.html], accessed June 2003.

Ghobarah A. (2001), "Performance-based design in earthquake engineering: state of development", *Engineering Structures,* vol. 23, pp. 878-884.

Kappos A.J. and Manafpour A. (2000), "Seismic design of R/C buildings with the aid of advanced analytical techniques", *Engineering Structures*, vol. 23, pp. 319-332.

Kik-net (2003) KIBAN Kyoshin network [http://www.kik.bosai.go.jp/], accessed June 2003.

Knet (2003) Kyoshin network [http:// www.k-net.bosai.go.jp/], accessed June 2003.

Liao W.I, Wan S. and Loh C.H. (2001), "Earthquake responses of RC moment frames subjected to near-fault ground motions." *Structural Design of Tall Buildings* 10: pp. 219-229.

Malhotra P.K. (1999), "Response of buildings to near-field pulse-like ground motions", *Earthquake Engineering and Structural Dynamics;* 28:1309-1326.

Mollaioli F., Bruno S. and Decanini L.D. (2002), "Damage potential of severe long duration acceleration pulses in near-fault records". Proceedings on CD, *12th European Conference on Earthquake Engineering.* Paper reference 155. Elsevier, UK.

National geological survey of Canada (2003) [http://www.seismo.nrcan.gc.ca/index_e.php], accessed June 2003.

PGC (2003) Pacific Geoscience Center, Geological Survey of Canada, accessed November 2003. [http://www.pgc.nrcan.gc.ca]

Panagiotakos T.B. and Fardis M.N. (1999), "Deformation-controlled earthquake resistant design of RC buildings", *Journal of Earthquake Engineering*, vol. 3, No. 4, pp. 495-518.

Priestley M.J.N. and Kowalsky M.J. (2000), "Direct displacement-based seismic design of concrete buildings", *Bulletin of the New Zealand Society for Earthquake Engineering*, vol. 33, No. 4, pp. 421-444.

SCEC (2003) Southern California Earthquake Center [http://www.scec.org], accessed June 2003.

SEAOC (1995), "Vision 2000: Performance based seismic engineering of buildings", Structural Engineers Association of California, Sacramento, CA.

SEAOC (1999), "Recommended Lateral Force Requirements and Commentary", 7th Ed. Structural Engineers Association of California, Sacramento, CA.

Singh J.P. (2003) "Characterization of ground motion for severity and damage potential" [http://nisee.berkeley.edu/lessons/singh.html], accessed November 2003.

Somerville, P.G., N.F. Smith, R.W. Graves, and N.A. Abrahamson (1997), "Modification of empirical strong ground motion attenuation relations to include the amplitude and duration effects of rupture directivity", *Seismological Research Letters*, vol. 68, pp.180-203

Sullivan T. (2002), "The current limitations of performance based design". Master thesis, European school of advanced studies in reduction of seismic risk, University of Pavia, Pavia, Italy.

USGS (2003) United States Geological Survey [http://www.USGS.com], accessed June 2003.

Xue Q. and Chen C. (2003), "Performance-based seismic design of structures: a direct displacement-based approach", *Engineering Structures*, vol. 25, pp. 1803-1813.

A. AVERAGE TABLES FOR EARTHQUAKES

SCALED TO PGA 0.1g

Table A.1 Near-fault earthquakes with magnitude greater than 6 on rock sites for PGA 0.1g

Factor	T (s)	μ=1				Average
		ChiChi	Izumi	Northridge	Tsuwano	
R	0.10	1.00	1.00	1.00	1.00	1.00
	0.20	1.00	1.00	1.00	1.00	1.00
	0.30	1.00	1.00	1.00	1.00	1.00
	0.40	1.00	1.00	1.00	1.00	1.00
	0.50	1.00	1.00	1.00	1.00	1.00
	0.75	1.00	1.00	1.00	1.00	1.00
	1.00	1.00	1.00	1.00	1.00	1.00
	1.50	1.00	1.00	1.00	1.00	1.00
	2.00	1.00	1.00	1.00	1.00	1.00
C_y	0.10	0.195	0.154	0.164	0.249	0.19
	0.20	0.220	0.046	0.190	0.088	0.136
	0.30	0.322	0.027	0.204	0.044	0.149
	0.40	0.226	0.017	0.152	0.026	0.105
	0.50	0.140	0.013	0.144	0.025	0.081
	0.75	0.040	0.006	0.064	0.018	0.032
	1.00	0.039	0.004	0.036	0.015	0.024
	1.50	0.022	0.002	0.013	0.012	0.012
	2.00	0.018	0.001	0.005	0.012	0.009
Δ_y (mm)	0.10	0.490	0.380	0.410	0.620	0.475
	0.20	2.180	0.450	1.890	0.880	1.350
	0.30	7.190	0.600	4.600	0.990	3.345
	0.40	10.600	0.670	6.040	1.050	4.590
	0.50	8.720	0.810	8.910	1.520	4.990
	0.75	6.200	0.830	8.920	2.510	4.615
	1.00	9.590	0.920	8.900	3.640	5.763
	1.50	12.100	0.860	7.490	6.830	6.820
	2.00	17.500	0.710	4.940	12.100	8.813

Table A.1 continued

Factor	T (s)	μ=2				Average
		ChiChi	Izumi	Northridge	Tsuwano	
R	0.10	1.390	3.160	1.600	2.050	2.050
	0.20	1.430	2.880	1.570	1.760	1.910
	0.30	2.240	3.150	2.980	1.850	2.555
	0.40	2.990	2.200	1.940	1.250	2.095
	0.50	2.880	3.600	2.930	1.300	2.678
	0.75	1.890	2.170	2.480	1.440	1.995
	1.00	2.280	2.190	1.700	1.290	1.865
	1.50	2.280	3.480	1.830	1.140	2.183
	2.00	1.840	2.350	1.480	1.170	1.710
C_y	0.10	0.151	0.050	0.108	0.121	0.107
	0.20	0.163	0.016	0.124	0.051	0.088
	0.30	0.144	0.008	0.069	0.024	0.061
	0.40	0.089	0.006	0.078	0.022	0.049
	0.50	0.049	0.003	0.049	0.020	0.030
	0.75	0.023	0.003	0.026	0.014	0.016
	1.00	0.017	0.002	0.021	0.013	0.013
	1.50	0.010	0.001	0.007	0.011	0.007
	2.00	0.009	0.000	0.004	0.011	0.006
Δ_y (mm)	0.10	0.367	0.116	0.258	0.286	0.257
	0.20	1.550	0.150	1.170	0.479	0.837
	0.30	3.050	0.183	1.480	0.513	1.307
	0.40	3.360	0.227	2.990	0.858	1.859
	0.50	2.900	0.211	2.900	1.200	1.803
	0.75	3.120	0.360	3.420	1.820	2.180
	1.00	3.120	0.360	3.420	1.820	2.180
	1.50	5.070	0.235	5.070	6.040	4.104
	2.00	9.070	0.290	3.350	10.500	5.803

Table A.1 continued

Factor	T (s)	μ=3				Average
		ChiChi	Izumi	Northridge	Tsuwano	
R	0.10	1.700	4.730	1.930	3.270	2.908
	0.20	1.770	3.730	2.140	2.230	2.468
	0.30	2.770	4.470	3.530	2.250	3.255
	0.40	6.100	5.310	3.190	1.480	4.020
	0.50	3.090	5.350	4.860	1.560	3.715
	0.75	3.410	3.290	3.030	1.760	2.873
	1.00	2.820	3.470	2.080	1.560	2.483
	1.50	2.900	4.090	2.640	1.280	2.728
	2.00	2.310	2.820	1.870	1.350	2.088
C_y	0.10	0.116	0.033	0.085	0.076	0.078
	0.20	0.125	0.012	0.088	0.040	0.066
	0.30	0.116	0.006	0.058	0.020	0.050
	0.40	0.045	0.006	0.048	0.019	0.030
	0.50	0.047	0.002	0.031	0.016	0.024
	0.75	0.014	0.002	0.021	0.010	0.012
	1.00	0.014	0.001	0.017	0.010	0.011
	1.50	0.008	0.000	0.005	0.010	0.006
	2.00	0.008	0.000	0.003	0.010	0.005
Δ_y (mm)	0.10	0.268	0.075	0.193	0.172	0.177
	0.20	1.120	0.111	0.802	0.357	0.598
	0.30	0.350	0.126	1.180	0.401	0.514
	0.40	1.640	0.221	1.760	0.685	1.077
	0.50	2.800	0.136	1.730	0.924	1.398
	0.75	1.630	0.227	2.660	1.310	1.457
	1.00	3.090	0.240	3.920	2.280	2.383
	1.50	3.750	0.193	2.580	5.260	2.946
	2.00	6.850	0.229	2.400	8.910	4.597

Table A.1 continued

Factor	T (s)	μ=4				Average
		ChiChi	Izumi	Northridge	Tsuwano	
R	0.10	1.790	5.960	2.120	4.220	3.523
	0.20	2.000	4.700	2.680	2.560	2.985
	0.30	5.320	5.520	4.110	2.510	4.365
	0.40	13.100	6.690	4.380	1.650	6.455
	0.50	4.800	6.700	6.060	1.740	4.825
	0.75	3.680	4.200	3.400	1.840	3.280
	1.00	4.310	5.230	3.550	1.710	3.700
	1.50	3.170	4.560	3.080	1.400	3.053
	2.00	2.710	3.050	2.130	1.490	2.345
C_y	0.10	0.109	0.026	0.078	0.060	0.068
	0.20	0.110	0.009	0.070	0.034	0.056
	0.30	0.067	0.005	0.051	0.017	0.035
	0.40	0.020	0.004	0.034	0.017	0.019
	0.50	0.035	0.002	0.024	0.014	0.019
	0.75	0.013	0.002	0.018	0.010	0.011
	1.00	0.009	0.001	0.010	0.009	0.007
	1.50	0.007	0.000	0.004	0.009	0.005
	2.00	0.007	0.000	0.002	0.009	0.004
Δ_y (mm)	0.10	0.235	0.055	0.167	0.131	0.147
	0.20	0.946	0.084	0.611	0.297	0.485
	0.30	1.290	0.095	0.980	0.344	0.677
	0.40	0.890	0.168	1.190	0.560	0.702
	0.50	2.010	0.102	1.290	0.761	1.041
	0.75	1.480	0.174	2.280	1.170	1.276
	1.00	2.000	0.147	2.190	1.860	1.549
	1.50	3.290	0.166	2.100	4.540	2.524
	2.00	5.600	0.202	2.010	7.500	3.828

Table A.1 continued

Factor	T (s)	μ=8				Average
		ChiChi	Izumi	Northridge	Tsuwano	
R	0.10	1.890	9.000	2.510	6.120	4.880
	0.20	2.870	7.000	4.030	3.470	4.343
	0.30	8.000	8.000	6.450	2.850	6.325
	0.40	3.440	13.000	8.410	1.860	6.678
	0.50	9.500	8.500	9.000	2.060	7.265
	0.75	4.910	10.000	7.050	2.020	5.995
	1.00	5.890	9.500	5.160	1.740	5.573
	1.50	4.480	5.590	8.420	1.570	5.015
	2.00	6.930	3.460	4.560	1.610	4.140
C_y	0.10	0.103	0.010	0.065	0.042	0.055
	0.20	0.077	0.007	0.048	0.026	0.039
	0.30	0.020	0.004	0.034	0.015	0.018
	0.40	0.010	0.002	0.020	0.014	0.012
	0.50	0.015	0.001	0.010	0.012	0.010
	0.75	0.009	0.001	0.008	0.009	0.007
	1.00	0.006	0.001	0.001	0.008	0.004
	1.50	0.004	0.000	0.001	0.008	0.003
	2.00	0.003	0.000	0.002	0.008	0.003
Δ_y (mm)	0.10	0.187	0.030	0.121	0.082	0.105
	0.20	0.563	0.069	0.352	0.190	0.294
	0.30	0.900	0.075	0.591	0.257	0.456
	0.40	0.500	0.090	1.000	0.413	0.501
	0.50	1.500	0.100	1.000	0.547	0.787
	0.75	0.902	0.100	0.892	0.913	0.702
	1.00	1.280	0.100	0.094	1.490	0.741
	1.50	1.980	0.111	0.425	3.200	1.429
	2.00	1.690	0.155	0.777	5.500	2.031

Table A.2 Near-fault earthquakes with magnitude greater than 6 on soil sites for PGA 0.1g

Factor	T (s)	μ=1					Average
		Kobe	Duzce	Erzican	Imperial Val.	Loma Prieta	
R	0.10	1.00	1.00	1.00	1.00	1.00	1.00
	0.20	1.00	1.00	1.00	1.00	1.00	1.00
	0.30	1.00	1.00	1.00	1.00	1.00	1.00
	0.40	1.00	1.00	1.00	1.00	1.00	1.00
	0.50	1.00	1.00	1.00	1.00	1.00	1.00
	0.75	1.00	1.00	1.00	1.00	1.00	1.00
	1.00	1.00	1.00	1.00	1.00	1.00	1.00
	1.50	1.00	1.00	1.00	1.00	1.00	1.00
	2.00	1.00	1.00	1.00	1.00	1.00	1.00
C_y	0.10	0.166	0.129	0.131	0.354	0.163	0.189
	0.20	0.340	0.112	0.247	0.134	0.159	0.198
	0.30	0.350	0.127	0.278	0.068	0.337	0.232
	0.40	0.315	0.169	0.123	0.049	0.258	0.183
	0.50	0.118	0.159	0.150	0.032	0.224	0.137
	0.75	0.164	0.159	0.155	0.027	0.160	0.133
	1.00	0.230	0.141	0.093	0.023	0.061	0.110
	1.50	0.158	0.044	0.050	0.021	0.028	0.060
	2.00	0.140	0.038	0.060	0.013	0.026	0.055
Δ_y (mm)	0.10	0.41	0.32	0.32	0.88	0.34	0.454
	0.20	3.38	1.11	2.46	1.33	1.58	1.972
	0.30	7.81	2.85	6.20	1.52	7.53	5.182
	0.40	12.50	6.70	4.87	1.96	10.30	7.266
	0.50	11.00	9.89	9.29	2.00	13.90	9.216
	0.75	22.80	22.20	21.70	3.76	22.40	18.572
	1.00	57.00	34.90	23.10	5.74	15.10	27.168
	1.50	88.60	24.70	27.70	11.70	15.90	33.720
	2.00	139.00	37.60	59.60	13.40	25.50	55.020

Table A.2 continued

Factor	T (s)	μ=2					Average
		Kobe	Duzce	Erzican	Imperial Val.	Loma Prieta	
R	0.10	1.29	1.12	1.13	2.14	1.15	1.37
	0.20	2.20	1.40	2.18	1.73	1.33	1.77
	0.30	1.86	1.45	2.60	1.51	2.60	2.00
	0.40	2.48	1.58	1.54	2.36	1.87	1.97
	0.50	1.47	1.59	1.97	1.69	2.40	1.82
	0.75	1.47	2.31	2.31	1.68	2.40	2.03
	1.00	2.39	1.94	1.70	1.90	1.92	1.97
	1.50	1.92	3.13	1.25	2.35	1.69	2.07
	2.00	2.25	3.37	2.89	2.07	3.16	2.75
C_y	0.10	0.14	0.12	0.12	0.16	0.12	0.13
	0.20	0.16	0.09	0.11	0.08	0.13	0.11
	0.30	0.19	0.09	0.11	0.05	0.13	0.11
	0.40	0.13	0.11	0.08	0.02	0.14	0.10
	0.50	0.10	0.10	0.08	0.02	0.09	0.08
	0.75	0.11	0.07	0.07	0.02	0.06	0.06
	1.00	0.10	0.07	0.06	0.01	0.03	0.05
	1.50	0.08	0.01	0.04	0.01	0.02	0.03
	2.00	0.06	0.01	0.02	0.01	0.01	0.02
Δ_y (mm)	0.10	0.33	0.29	0.29	0.39	0.30	0.32
	0.20	1.46	0.83	1.07	0.75	1.21	1.06
	0.30	3.97	2.03	2.27	1.00	2.75	2.40
	0.40	4.80	4.23	3.20	0.79	5.25	3.65
	0.50	8.60	6.17	4.51	1.17	5.51	5.19
	0.75	14.10	9.16	8.97	2.19	8.35	8.55
	1.00	14.10	9.16	8.97	2.19	8.35	8.55
	1.50	43.80	7.49	24.40	4.74	9.05	17.90
	2.00	58.50	10.60	19.60	6.15	7.71	20.51

Table A.2 continued

Factor	T (s)	μ=3					Average
		Kobe	Duzce	Erzican	Imperial Val.	Loma Prieta	
R	0.10	1.55	1.24	1.26	2.70	1.31	1.612
	0.20	2.74	1.71	2.80	2.27	1.61	2.226
	0.30	3.02	1.77	3.11	1.94	3.56	2.680
	0.40	3.28	1.98	1.89	2.78	3.32	2.650
	0.50	1.83	2.01	2.39	2.04	3.15	2.284
	0.75	1.83	2.80	3.06	2.14	3.50	2.666
	1.00	2.92	5.14	2.11	2.31	2.62	3.020
	1.50	2.31	4.55	1.81	2.88	2.29	2.768
	2.00	2.86	4.98	4.16	2.67	4.17	3.768
C_y	0.10	0.11	0.11	0.10	0.13	0.11	0.112
	0.20	0.12	0.07	0.08	0.06	0.10	0.086
	0.30	0.12	0.07	0.08	0.04	0.09	0.080
	0.40	0.10	0.09	0.06	0.02	0.08	0.067
	0.50	0.08	0.08	0.06	0.02	0.07	0.061
	0.75	0.08	0.06	0.05	0.01	0.05	0.049
	1.00	0.08	0.03	0.04	0.01	0.02	0.036
	1.50	0.07	0.01	0.02	0.01	0.01	0.023
	2.00	0.05	0.01	0.01	0.01	0.01	0.016
Δ_y (mm)	0.10	0.26	0.25	0.22	0.29	0.26	0.255
	0.20	1.12	0.61	0.69	0.53	0.92	0.773
	0.30	2.34	1.47	1.57	0.71	1.92	1.602
	0.40	3.48	3.08	2.00	0.64	2.79	2.398
	0.50	6.57	4.48	3.02	0.89	3.97	3.786
	0.75	10.40	7.19	5.44	1.60	5.79	6.084
	1.00	17.70	6.56	8.35	2.25	5.22	8.016
	1.50	34.60	5.09	7.46	3.70	6.28	11.426
	2.00	43.90	6.90	9.89	4.56	5.63	14.176

Table A.2 continued

Factor	T (s)	μ=4					Average
		Kobe	Duzce	Erzican	Imperial Val.	Loma Prieta	
R	0.10	1.71	1.34	1.38	3.24	1.45	1.824
	0.20	3.18	1.79	3.11	2.70	1.80	2.516
	0.30	3.47	1.91	3.44	2.30	4.08	3.040
	0.40	3.60	2.26	2.11	3.02	3.64	2.926
	0.50	2.10	2.29	2.67	2.26	3.65	2.594
	0.75	2.10	3.14	3.47	2.47	4.57	3.150
	1.00	3.38	6.94	2.40	2.60	3.41	3.746
	1.50	3.27	5.60	3.28	3.36	2.88	3.678
	2.00	3.85	6.36	5.21	3.17	5.20	4.758
C_y	0.10	0.10	0.10	0.10	0.11	0.10	0.101
	0.20	0.11	0.06	0.08	0.05	0.09	0.077
	0.30	0.10	0.07	0.08	0.03	0.08	0.072
	0.40	0.09	0.07	0.06	0.02	0.07	0.062
	0.50	0.07	0.07	0.06	0.01	0.06	0.055
	0.75	0.07	0.05	0.05	0.01	0.03	0.043
	1.00	0.07	0.02	0.04	0.01	0.02	0.031
	1.50	0.05	0.01	0.02	0.01	0.01	0.018
	2.00	0.04	0.01	0.01	0.00	0.00	0.013
Δ_y (mm)	0.10	0.21	0.22	0.22	0.23	0.22	0.220
	0.20	0.93	0.54	0.69	0.43	0.76	0.668
	0.30	1.96	1.29	1.57	0.57	1.64	1.407
	0.40	3.03	2.57	2.00	0.56	2.47	2.126
	0.50	5.46	3.74	3.02	0.77	3.30	3.257
	0.75	8.73	6.10	5.44	1.32	4.24	5.166
	1.00	14.60	4.37	8.35	1.92	3.83	6.614
	1.50	23.30	3.90	7.46	3.02	4.77	8.490
	2.00	31.50	4.91	9.89	3.65	4.16	10.822

Table A.2 continued

Factor	T (s)	μ=8					Average
		Kobe	Duzce	Erzican	Imperial Val.	Loma Prieta	
R	0.10	1.72	1.56	1.55	4.82	1.59	2.248
	0.20	3.42	1.89	3.50	4.04	2.21	3.012
	0.30	3.96	2.19	4.39	3.56	5.46	3.912
	0.40	3.98	3.02	2.60	3.52	4.93	3.610
	0.50	2.53	3.28	3.38	2.79	5.47	3.490
	0.75	2.53	6.27	4.88	3.13	9.18	5.198
	1.00	5.51	8.50	4.27	3.32	7.01	5.722
	1.50	9.97	4.47	3.66	4.73	6.41	5.848
	2.00	11.60	7.07	6.54	4.61	7.96	7.556
C_y	0.10	0.10	0.08	0.08	0.07	0.09	0.085
	0.20	0.10	0.06	0.07	0.03	0.07	0.067
	0.30	0.09	0.06	0.06	0.02	0.06	0.059
	0.40	0.08	0.06	0.05	0.01	0.05	0.050
	0.50	0.07	0.05	0.04	0.01	0.04	0.042
	0.75	0.06	0.03	0.03	0.01	0.02	0.028
	1.00	0.04	0.01	0.02	0.01	0.01	0.018
	1.50	0.02	0.01	0.02	0.00	0.01	0.010
	2.00	0.02	0.00	0.01	0.00	0.00	0.008
Δ_y (mm)	0.10	0.17	0.15	0.15	0.13	0.16	0.153
	0.20	0.72	0.42	0.52	0.24	0.53	0.487
	0.30	1.44	0.96	1.05	0.32	1.00	0.954
	0.40	2.26	1.65	1.38	0.42	1.50	1.442
	0.50	4.02	2.26	2.06	0.53	1.79	2.132
	0.75	5.85	2.58	3.15	0.90	3.00	3.095
	1.00	7.44	2.50	4.29	1.30	2.05	3.516
	1.50	15.00	2.70	5.00	1.79	1.90	5.278
	2.00	21.00	2.00	8.00	2.10	3.00	7.220

Table A.3 Near-fault earthquakes with magnitude less than 6 on rock sites for PGA 0.1g

Factor	T (s)	μ=1					Average
		Atami	Massena(1)	Massena(2)	Miramichi	New Madrid	
R	0.10	1.00	1.00	1.00	1.00	1.00	1.00
	0.20	1.00	1.00	1.00	1.00	1.00	1.00
	0.30	1.00	1.00	1.00	1.00	1.00	1.00
	0.40	1.00	1.00	1.00	1.00	1.00	1.00
	0.50	1.00	1.00	1.00	1.00	1.00	1.00
	0.75	1.00	1.00	1.00	1.00	1.00	1.00
	1.00	1.00	1.00	1.00	1.00	1.00	1.00
	1.50	1.00	1.00	1.00	1.00	1.00	1.00
	2.00	1.00	1.00	1.00	1.00	1.00	1.00
C_y	0.10	0.16	0.11	0.16	0.17	0.22	0.164
	0.20	0.05	0.06	0.05	0.07	0.10	0.065
	0.30	0.05	0.02	0.01	0.02	0.04	0.029
	0.40	0.05	0.01	0.01	0.01	0.02	0.021
	0.50	0.05	0.01	0.01	0.01	0.01	0.017
	0.75	0.05	0.00	0.01	0.00	0.01	0.014
	1.00	0.05	0.00	0.01	0.00	0.00	0.013
	1.50	0.05	0.00	0.00	0.00	0.00	0.012
	2.00	0.05	0.00	0.00	0.00	0.00	0.012
Δ_y (mm)	0.10	0.39	0.27	0.41	0.43	0.53	0.406
	0.20	1.46	0.63	0.46	0.67	1.00	0.844
	0.30	1.21	0.51	0.23	0.51	0.82	0.656
	0.40	2.15	0.41	0.27	0.48	0.92	0.846
	0.50	3.35	0.36	0.48	0.45	0.73	1.074
	0.75	7.53	0.51	0.78	0.41	0.66	1.978
	1.00	13.40	0.39	2.86	0.38	0.63	3.532
	1.50	30.20	0.90	1.93	0.47	0.59	6.818
	2.00	53.60	1.29	3.07	0.38	0.86	11.840

Table A.3 continued

Factor	T (s)	μ=2					Average
		Atami	Massena(1)	Massena(2)	Miramichi	New Madrid	
R	0.10	1.89	2.12	2.53	1.77	2.27	2.12
	0.20	1.33	2.49	2.31	3.47	2.26	2.37
	0.30	2.76	1.96	1.66	1.77	1.56	1.94
	0.40	1.18	2.42	1.86	2.55	1.88	1.98
	0.50	1.18	2.20	1.46	1.85	2.07	1.75
	0.75	1.18	1.86	1.84	1.78	1.97	1.73
	1.00	1.18	1.48	2.12	1.53	2.01	1.66
	1.50	1.18	2.03	1.33	2.53	1.56	1.73
	2.00	1.18	2.04	1.61	1.86	1.48	1.63
C_y	0.10	0.08	0.05	0.06	0.10	0.10	0.08
	0.20	0.04	0.03	0.02	0.02	0.04	0.03
	0.30	0.05	0.01	0.01	0.01	0.02	0.02
	0.40	0.05	0.00	0.00	0.00	0.01	0.01
	0.50	0.05	0.00	0.01	0.00	0.01	0.01
	0.75	0.05	0.00	0.00	0.00	0.00	0.01
	1.00	0.05	0.00	0.00	0.00	0.00	0.01
	1.50	0.05	0.00	0.00	0.00	0.00	0.01
	2.00	0.05	0.00	0.00	0.00	0.00	0.01
Δ_y (mm)	0.10	0.20	0.12	0.15	0.23	0.22	0.19
	0.20	1.12	0.24	0.18	0.18	0.42	0.43
	0.30	1.06	0.25	0.14	0.28	0.50	0.45
	0.40	1.86	0.16	0.14	0.18	0.47	0.56
	0.50	2.88	0.16	0.32	0.23	0.34	0.79
	0.75	6.48	0.22	0.41	0.22	0.32	1.53
	1.00	6.48	0.22	0.41	0.22	0.32	1.53
	1.50	26.00	0.42	1.47	0.18	0.39	5.69
	2.00	46.20	0.60	1.88	0.20	0.60	9.90

Table A.3 continued

Factor	T (s)	μ=3					Average
		Atami	Massena(1)	Massena(2)	Miramichi	New Madrid	
R	0.10	2.24	2.49	4.30	3.70	2.75	3.096
	0.20	1.61	3.26	5.04	6.91	3.07	3.978
	0.30	4.49	3.57	2.09	3.25	2.68	3.216
	0.40	1.36	3.82	2.22	3.41	3.43	2.848
	0.50	1.37	3.42	1.91	2.99	3.75	2.688
	0.75	1.37	2.25	2.23	2.37	2.58	2.160
	1.00	1.37	1.81	2.46	2.41	2.59	2.128
	1.50	1.37	2.63	1.62	3.46	1.86	2.188
	2.00	1.37	2.40	2.04	2.27	1.80	1.976
C_y	0.10	0.07	0.04	0.04	0.05	0.08	0.055
	0.20	0.04	0.02	0.01	0.01	0.03	0.022
	0.30	0.04	0.01	0.01	0.01	0.01	0.015
	0.40	0.04	0.00	0.00	0.00	0.01	0.012
	0.50	0.04	0.00	0.00	0.00	0.00	0.011
	0.75	0.04	0.00	0.00	0.00	0.00	0.010
	1.00	0.04	0.00	0.00	0.00	0.00	0.009
	1.50	0.04	0.00	0.00	0.00	0.00	0.009
	2.00	0.04	0.00	0.00	0.00	0.00	0.009
Δ_y (mm)	0.10	0.20	0.10	0.09	0.11	0.18	0.132
	0.20	1.12	0.18	0.08	0.09	0.29	0.352
	0.30	1.06	0.13	0.10	0.15	0.28	0.344
	0.40	1.86	0.10	0.11	0.13	0.24	0.487
	0.50	2.88	0.09	0.23	0.14	0.18	0.704
	0.75	6.48	0.13	0.32	0.16	0.23	1.464
	1.00	6.48	0.20	0.68	0.14	0.22	1.543
	1.50	26.00	0.31	1.11	0.12	0.29	5.566
	2.00	46.20	0.49	1.36	0.14	0.44	9.724

Table A.3 continued

Factor	T (s)	μ=4					Average
		Atami	Massena(1)	Massena(2)	Miramichi	New Madrid	
R	0.10	2.47	2.86	5.73	6.22	3.13	4.082
	0.20	1.74	4.14	7.24	10.90	3.94	5.592
	0.30	6.12	5.48	2.39	6.13	3.89	4.802
	0.40	1.51	5.00	2.45	4.44	4.58	3.596
	0.50	1.52	3.99	2.35	3.67	4.76	3.258
	0.75	1.52	2.55	2.48	2.99	3.09	2.526
	1.00	1.52	1.98	2.77	3.80	2.94	2.602
	1.50	1.52	2.83	1.84	4.30	1.98	2.494
	2.00	1.52	2.58	2.35	3.15	1.88	2.296
C_y	0.10	0.06	0.04	0.03	0.03	0.07	0.045
	0.20	0.04	0.02	0.01	0.01	0.03	0.019
	0.30	0.04	0.00	0.00	0.00	0.01	0.012
	0.40	0.04	0.00	0.00	0.00	0.01	0.010
	0.50	0.04	0.00	0.00	0.00	0.00	0.009
	0.75	0.04	0.00	0.00	0.00	0.00	0.008
	1.00	0.04	0.00	0.00	0.00	0.00	0.008
	1.50	0.04	0.00	0.00	0.00	0.00	0.008
	2.00	0.04	0.00	0.00	0.00	0.00	0.008
Δ_y (mm)	0.10	0.14	0.08	0.06	0.06	0.15	0.097
	0.20	0.71	0.14	0.06	0.07	0.22	0.240
	0.30	0.77	0.08	0.08	0.07	0.19	0.238
	0.40	1.31	0.07	0.10	0.10	0.18	0.350
	0.50	2.02	0.08	0.18	0.11	0.14	0.505
	0.75	4.55	0.11	0.27	0.12	0.18	1.047
	1.00	8.09	0.17	0.55	0.09	0.19	1.816
	1.50	18.20	0.28	0.91	0.10	0.26	3.948
	2.00	32.40	0.43	1.13	0.10	0.39	6.892

Table A.3 continued

Factor	T (s)	μ=8					Average
		Atami	Massena(1)	Massena(2)	Miramichi	New Madrid	
R	0.10	2.93	4.33	7.00	9.00	5.47	5.746
	0.20	1.78	9.48	12.00	12.00	6.79	8.410
	0.30	12.20	8.00	3.90	10.00	6.95	8.210
	0.40	1.62	8.37	3.14	9.00	5.90	5.606
	0.50	1.62	5.14	3.46	8.14	5.89	4.850
	0.75	1.62	3.90	3.25	6.50	4.40	3.934
	1.00	1.62	2.32	3.89	5.92	3.51	3.452
	1.50	1.62	3.07	2.59	6.93	2.21	3.284
	2.00	1.62	2.88	3.51	5.50	2.05	3.112
C_y	0.10	0.05	0.03	0.01	0.01	0.04	0.028
	0.20	0.04	0.01	0.00	0.01	0.02	0.015
	0.30	0.03	0.00	0.00	0.00	0.01	0.009
	0.40	0.03	0.00	0.00	0.00	0.00	0.008
	0.50	0.03	0.00	0.00	0.00	0.00	0.008
	0.75	0.03	0.00	0.00	0.00	0.00	0.008
	1.00	0.03	0.00	0.00	0.00	0.00	0.007
	1.50	0.03	0.00	0.00	0.00	0.00	0.007
	2.00	0.03	0.00	0.00	0.00	0.00	0.007
Δ_y (mm)	0.10	0.10	0.05	0.03	0.03	0.07	0.055
	0.20	0.53	0.09	0.03	0.00	0.14	0.158
	0.30	0.56	0.05	0.04	0.05	0.14	0.167
	0.40	0.97	0.06	0.06	0.05	0.15	0.258
	0.50	1.50	0.05	0.10	0.05	0.10	0.361
	0.75	3.38	0.07	0.18	0.04	0.11	0.757
	1.00	6.02	0.12	0.41	0.05	0.13	1.348
	1.50	13.60	0.22	0.55	0.07	0.20	2.928
	2.00	24.10	0.33	0.66	0.05	0.31	5.090

Table A.4 Near-fault earthquakes with magnitude less than 6 on soil sites for PGA 0.1g

Factor	T (s)	μ=1					Average
		Japanese	Livermore	Chalfant Valley	Duzce(1)	Duzce (2)	
R	0.10	1.00	1.00	1.00	1.00	1.00	1.00
	0.20	1.00	1.00	1.00	1.00	1.00	1.00
	0.30	1.00	1.00	1.00	1.00	1.00	1.00
	0.40	1.00	1.00	1.00	1.00	1.00	1.00
	0.50	1.00	1.00	1.00	1.00	1.00	1.00
	0.75	1.00	1.00	1.00	1.00	1.00	1.00
	1.00	1.00	1.00	1.00	1.00	1.00	1.00
	1.50	1.00	1.00	1.00	1.00	1.00	1.00
	2.00	1.00	1.00	1.00	1.00	1.00	1.00
C_y	0.10	0.181	0.113	0.245	0.156	0.156	0.170
	0.20	0.113	0.168	0.236	0.147	0.147	0.162
	0.30	0.105	0.186	0.203	0.225	0.305	0.205
	0.40	0.092	0.189	0.096	0.131	0.408	0.183
	0.50	0.070	0.166	0.159	0.078	0.195	0.134
	0.75	0.033	0.140	0.072	0.026	0.043	0.063
	1.00	0.016	0.081	0.029	0.013	0.026	0.033
	1.50	0.007	0.027	0.015	0.005	0.008	0.012
	2.00	0.004	0.013	0.007	0.002	0.004	0.006
Δ_y (mm)	0.10	0.450	0.280	0.610	0.390	0.390	0.424
	0.20	1.120	1.670	2.350	1.460	1.460	1.612
	0.30	2.350	4.150	4.530	5.040	6.820	4.578
	0.40	3.680	7.500	3.800	5.200	32.400	10.516
	0.50	4.370	10.300	9.870	4.860	12.100	8.300
	0.75	4.560	19.600	9.990	3.690	5.960	8.760
	1.00	3.940	20.200	7.220	3.200	6.340	8.180
	1.50	4.010	15.400	8.640	2.520	4.210	6.956
	2.00	4.410	12.800	6.900	2.140	3.770	6.004

Table A.4 continued

Factor	T (s)	μ=2					Average
		Japanese	Livermore	Chalfant Valley	Duzce(1)	Duzce (2)	
R	0.10	2.290	1.030	1.330	1.400	1.260	1.46
	0.20	2.030	1.180	2.220	1.910	1.260	1.72
	0.30	1.580	1.550	1.580	2.990	2.070	1.95
	0.40	1.900	1.780	1.050	2.580	3.400	2.14
	0.50	1.870	1.860	3.500	2.270	2.790	2.46
	0.75	1.810	2.560	2.270	1.810	2.560	2.20
	1.00	2.240	2.920	2.590	1.910	1.660	2.26
	1.50	1.440	2.340	2.470	2.160	1.400	1.96
	2.00	1.640	1.930	2.220	1.950	1.340	1.82
C_y	0.10	0.080	0.110	0.181	0.118	0.132	0.12
	0.20	0.056	0.127	0.108	0.077	0.124	0.10
	0.30	0.069	0.126	0.133	0.076	0.147	0.11
	0.40	0.049	0.107	0.092	0.051	0.057	0.07
	0.50	0.038	0.090	0.079	0.034	0.070	0.06
	0.75	0.018	0.055	0.031	0.015	0.017	0.03
	1.00	0.007	0.028	0.011	0.007	0.016	0.01
	1.50	0.005	0.012	0.006	0.002	0.005	0.01
	2.00	0.002	0.007	0.004	0.001	0.003	0.00
Δ_y (mm)	0.10	0.187	0.264	0.429	0.283	0.320	0.30
	0.20	0.526	1.220	1.020	0.727	1.190	0.94
	0.30	1.460	2.690	2.840	1.600	3.130	2.34
	0.40	1.840	4.060	3.580	1.920	4.050	3.09
	0.50	2.230	5.290	4.700	2.040	4.140	3.68
	0.75	2.440	7.280	4.180	1.950	2.210	3.61
	1.00	2.440	7.280	4.180	1.950	2.210	3.61
	1.50	2.660	6.230	3.320	1.110	2.940	3.25
	2.00	2.590	6.300	2.940	1.050	2.710	3.12

Table A.4 continued

Factor	T (s)	μ=3					Average
		Japanese	Livermore	Chalfant Valley	Duzce(1)	Duzce (2)	
R	0.10	2.850	1.070	2.220	1.720	1.510	1.874
	0.20	2.440	1.620	2.750	2.320	1.490	2.124
	0.30	2.100	1.920	2.020	4.610	3.410	2.812
	0.40	2.410	2.230	1.230	3.460	6.240	3.114
	0.50	2.690	2.340	5.910	2.990	5.660	3.918
	0.75	4.180	3.540	4.750	2.870	3.440	3.756
	1.00	3.070	4.270	4.230	3.270	3.070	3.582
	1.50	2.720	3.570	4.440	3.380	1.860	3.194
	2.00	2.640	2.970	3.330	2.770	1.800	2.702
C_y	0.10	0.064	0.107	0.112	0.091	0.109	0.097
	0.20	0.047	0.098	0.086	0.063	0.103	0.079
	0.30	0.050	0.098	0.100	0.051	0.089	0.077
	0.40	0.039	0.085	0.080	0.037	0.030	0.054
	0.50	0.026	0.071	0.029	0.026	0.036	0.038
	0.75	0.008	0.040	0.015	0.009	0.013	0.017
	1.00	0.005	0.019	0.007	0.004	0.008	0.009
	1.50	0.003	0.008	0.003	0.001	0.004	0.004
	2.00	0.002	0.004	0.002	0.001	0.002	0.002
Δ_y (mm)	0.10	0.143	0.248	0.253	0.207	0.253	0.221
	0.20	0.143	0.889	0.783	0.567	0.946	0.666
	0.30	0.143	1.970	2.030	1.030	1.810	1.397
	0.40	0.143	3.050	3.010	1.360	3.200	2.153
	0.50	0.143	3.990	1.590	1.480	2.030	1.847
	0.75	0.143	5.020	1.950	1.170	1.560	1.969
	1.00	0.143	4.340	1.570	0.883	1.870	1.761
	1.50	0.143	3.910	1.820	0.676	2.060	1.722
	2.00	0.143	3.900	1.870	0.703	1.910	1.705

Table A.4 continued

Factor	T (s)	μ=4					Average
		Japanese	Livermore	Chalfant Valley	Duzce(1)	Duzce (2)	
R	0.10	3.050	1.100	3.250	1.930	1.670	2.200
	0.20	2.690	2.730	2.750	2.670	1.660	2.500
	0.30	2.580	2.150	2.370	5.610	4.530	3.448
	0.40	3.150	2.550	1.580	4.280	7.150	3.742
	0.50	4.340	2.750	6.850	3.700	12.500	6.028
	0.75	5.350	5.260	6.630	4.300	4.220	5.152
	1.00	3.800	6.120	6.080	4.570	3.730	4.860
	1.50	3.510	4.800	6.010	4.350	2.370	4.208
	2.00	3.730	3.900	4.870	3.520	2.390	3.682
C_y	0.10	0.059	0.104	0.076	0.081	0.094	0.083
	0.20	0.042	0.090	0.086	0.055	0.089	0.072
	0.30	0.041	0.086	0.085	0.041	0.068	0.064
	0.40	0.029	0.074	0.063	0.031	0.020	0.043
	0.50	0.017	0.060	0.024	0.021	0.004	0.025
	0.75	0.006	0.028	0.010	0.006	0.010	0.012
	1.00	0.004	0.013	0.005	0.003	0.007	0.006
	1.50	0.002	0.006	0.002	0.001	0.003	0.003
	2.00	0.001	0.003	0.001	0.001	0.002	0.002
Δ_y (mm)	0.10	0.127	0.233	0.165	0.175	0.206	0.181
	0.20	0.361	0.768	0.782	0.474	0.774	0.632
	0.30	0.795	1.670	1.660	0.791	1.320	1.247
	0.40	1.010	2.550	2.180	1.060	2.500	1.860
	0.50	0.880	3.260	1.270	1.150	0.224	1.357
	0.75	0.758	3.310	1.270	0.752	1.240	1.466
	1.00	0.913	2.820	0.976	0.607	1.490	1.361
	1.50	0.997	2.770	1.230	0.513	1.540	1.410
	2.00	1.040	2.880	1.240	0.531	1.380	1.414

Table A.4 continued

Factor	T (s)	μ=8					Average
		Japanese	Livermore	Chalfant Valley	Duzce(1)	Duzce (2)	
R	0.10	3.320	1.210	3.420	2.850	1.720	2.504
	0.20	3.300	3.000	3.280	3.800	1.880	3.052
	0.30	4.900	2.730	6.320	7.000	7.400	5.670
	0.40	11.200	3.630	4.960	8.250	8.250	7.258
	0.50	10.900	4.640	8.500	10.000	14.500	9.708
	0.75	6.700	19.500	8.200	9.900	6.920	10.244
	1.00	6.130	19.300	8.000	8.990	6.910	9.866
	1.50	5.830	8.300	7.850	6.760	4.690	6.686
	2.00	6.060	6.860	6.030	5.950	4.690	5.918
C_y	0.10	0.055	0.094	0.072	0.054	0.092	0.073
	0.20	0.034	0.076	0.077	0.039	0.079	0.061
	0.30	0.021	0.068	0.031	0.030	0.050	0.040
	0.40	0.014	0.053	0.022	0.026	0.010	0.025
	0.50	0.009	0.036	0.010	0.007	0.002	0.013
	0.75	0.005	0.015	0.009	0.003	0.008	0.008
	1.00	0.003	0.010	0.003	0.001	0.004	0.004
	1.50	0.001	0.004	0.001	0.001	0.001	0.002
	2.00	0.001	0.002	0.009	0.000	0.001	0.003
Δ_y (mm)	0.10	0.101	0.178	0.127	0.102	0.165	0.135
	0.20	0.254	0.559	0.677	0.287	0.573	0.470
	0.30	0.342	1.120	0.507	0.600	1.000	0.714
	0.40	0.437	1.540	0.688	0.842	1.200	0.941
	0.50	0.500	1.620	0.560	0.408	0.100	0.638
	0.75	0.500	2.100	0.950	0.500	0.878	0.986
	1.00	0.497	1.300	0.800	0.450	0.841	0.778
	1.50	0.502	1.500	0.960	0.403	0.636	0.800
	2.00	0.557	1.880	0.860	0.268	0.572	0.827

Table A.5 Far field earthquakes on rock sites for PGA 0.1g

Factor	T (s)	μ=1					Average
		Long beach	Kern County	San Fernando(1)	San Fernando(2)	Monte Negro	
R	0.10	1.00	1.00	1.00	1.00	1.00	1.00
	0.20	1.00	1.00	1.00	1.00	1.00	1.00
	0.30	1.00	1.00	1.00	1.00	1.00	1.00
	0.40	1.00	1.00	1.00	1.00	1.00	1.00
	0.50	1.00	1.00	1.00	1.00	1.00	1.00
	0.75	1.00	1.00	1.00	1.00	1.00	1.00
	1.00	1.00	1.00	1.00	1.00	1.00	1.00
	1.50	1.00	1.00	1.00	1.00	1.00	1.00
	2.00	1.00	1.00	1.00	1.00	1.00	1.00
C_y	0.10	0.141	0.120	0.270	0.207	0.194	0.186
	0.20	0.239	0.239	0.417	0.247	0.227	0.274
	0.30	0.131	0.225	0.132	0.254	0.368	0.222
	0.40	0.230	0.219	0.165	0.179	0.257	0.210
	0.50	0.189	0.193	0.125	0.190	0.371	0.214
	0.75	0.143	0.128	0.083	0.160	0.105	0.124
	1.00	0.186	0.088	0.081	0.143	0.108	0.121
	1.50	0.144	0.073	0.039	0.079	0.076	0.082
	2.00	0.173	0.048	0.019	0.048	0.059	0.069
Δ_y (mm)	0.10	0.350	0.300	0.670	0.510	0.480	0.462
	0.20	2.370	2.370	4.140	2.460	2.260	2.720
	0.30	2.930	5.030	2.950	5.670	8.210	4.958
	0.40	9.140	8.710	6.570	7.140	10.200	8.352
	0.50	11.700	12.000	7.800	11.800	23.000	13.260
	0.75	20.000	17.800	11.600	22.300	14.600	17.260
	1.00	46.200	21.900	20.200	35.600	26.800	30.140
	1.50	80.500	40.800	21.600	44.400	42.400	45.940
	2.00	172.000	47.400	19.300	47.800	58.200	68.940

Table A.5 continued

Factor	T (s)	μ=2					Average
		Long beach	Kern County	San Fernando(1)	San Fernando(2)	Monte Negro	
R	0.10	1.060	1.060	1.830	1.480	1.270	1.34
	0.20	1.450	1.440	2.320	1.750	1.310	1.65
	0.30	1.140	1.600	1.380	2.210	2.780	1.82
	0.40	2.030	1.540	2.250	1.820	1.810	1.89
	0.50	1.690	1.600	2.260	2.460	2.550	2.11
	0.75	1.380	2.080	1.540	2.450	1.370	1.76
	1.00	1.570	1.560	2.510	2.530	2.220	2.08
	1.50	1.630	2.160	1.830	1.880	1.800	1.86
	2.00	2.040	2.320	1.780	1.650	1.460	1.85
C_y	0.10	0.135	0.115	0.148	0.146	0.162	0.14
	0.20	0.172	0.164	0.180	0.143	0.174	0.17
	0.30	0.119	0.146	0.098	0.116	0.132	0.12
	0.40	0.114	0.146	0.073	0.099	0.143	0.12
	0.50	0.116	0.122	0.055	0.077	0.145	0.10
	0.75	0.112	0.061	0.053	0.065	0.079	0.07
	1.00	0.124	0.059	0.033	0.056	0.049	0.06
	1.50	0.091	0.034	0.021	0.043	0.042	0.05
	2.00	0.085	0.021	0.011	0.031	0.039	0.04
Δ_y (mm)	0.10	0.324	0.279	0.350	0.345	0.388	0.34
	0.20	1.640	1.560	1.690	1.360	1.660	1.58
	0.30	2.580	3.140	2.080	2.460	2.810	2.61
	0.40	4.290	5.560	2.770	3.750	5.390	4.35
	0.50	6.910	7.220	3.260	4.540	8.550	6.10
	0.75	15.000	8.160	7.100	8.650	10.500	9.88
	1.00	15.000	8.160	7.100	8.650	10.500	9.88
	1.50	48.800	18.000	11.300	22.500	22.500	24.62
	2.00	80.300	19.500	10.400	29.100	37.800	35.42

Table A.5 continued

Factor	T (s)	μ=3					Average
		Long beach	Kern County	San Fernando(1)	San Fernando(2)	Monte Negro	
R	0.10	1.130	1.110	2.590	1.900	1.500	1.646
	0.20	1.820	2.660	3.290	2.210	1.720	2.340
	0.30	1.290	1.990	1.840	3.190	4.100	2.482
	0.40	2.520	2.050	3.720	2.720	2.760	2.754
	0.50	1.990	2.350	4.120	3.480	3.410	3.070
	0.75	1.680	2.710	2.400	3.110	1.770	2.334
	1.00	1.940	3.020	3.290	3.490	3.210	2.990
	1.50	2.050	2.460	2.450	2.540	2.620	2.424
	2.00	2.840	3.070	2.430	1.980	2.460	2.556
C_y	0.10	0.128	0.110	0.105	0.110	0.135	0.118
	0.20	0.131	0.090	0.126	0.112	0.132	0.118
	0.30	0.107	0.113	0.072	0.080	0.091	0.093
	0.40	0.092	0.107	0.044	0.066	0.094	0.081
	0.50	0.095	0.082	0.032	0.055	0.108	0.074
	0.75	0.087	0.047	0.023	0.052	0.060	0.054
	1.00	0.096	0.029	0.025	0.041	0.033	0.045
	1.50	0.070	0.030	0.015	0.032	0.029	0.035
	2.00	0.061	0.016	0.008	0.025	0.024	0.027
Δ_y (mm)	0.10	0.298	0.258	0.236	0.246	0.307	0.269
	0.20	1.190	0.818	1.140	1.010	1.190	1.070
	0.30	2.240	2.300	1.460	1.610	1.850	1.892
	0.40	3.310	3.870	1.610	2.380	3.420	2.918
	0.50	5.340	4.630	1.760	3.060	6.100	4.178
	0.75	11.100	5.970	2.930	6.600	7.520	6.824
	1.00	21.600	6.520	5.540	9.240	7.550	10.090
	1.50	35.800	15.000	7.990	15.900	14.700	17.878
	2.00	55.100	14.000	7.200	22.000	21.500	23.960

Table A.5 continued

Factor	T (s)	μ=4 Long beach	Kern County	San Fernando(1)	San Fernando(2)	Monte Negro	Average
R	0.10	1.190	1.170	2.880	2.330	1.680	1.850
	0.20	2.130	2.830	4.120	2.590	2.320	2.798
	0.30	1.420	2.250	2.290	3.630	4.590	2.836
	0.40	2.670	2.520	4.400	3.040	3.070	3.140
	0.50	2.170	3.650	4.760	4.100	4.270	3.790
	0.75	1.820	3.220	2.720	3.600	2.190	2.710
	1.00	2.170	3.190	3.860	4.020	3.760	3.400
	1.50	2.330	2.740	3.080	2.890	3.690	2.946
	2.00	3.520	3.730	3.250	2.170	4.240	3.382
C_y	0.10	0.122	0.105	0.094	0.090	0.116	0.105
	0.20	0.113	0.084	0.103	0.096	0.098	0.099
	0.30	0.096	0.100	0.058	0.070	0.082	0.081
	0.40	0.087	0.088	0.039	0.059	0.084	0.071
	0.50	0.087	0.053	0.028	0.048	0.087	0.061
	0.75	0.079	0.039	0.015	0.045	0.048	0.045
	1.00	0.086	0.027	0.021	0.037	0.029	0.040
	1.50	0.061	0.027	0.012	0.028	0.021	0.030
	2.00	0.050	0.013	0.006	0.022	0.014	0.021
Δ_y (mm)	0.10	0.273	0.237	0.202	0.194	0.251	0.231
	0.20	0.975	0.712	0.891	0.831	0.849	0.852
	0.30	1.920	1.940	1.130	1.370	1.570	1.586
	0.40	2.960	3.010	1.330	2.030	2.890	2.444
	0.50	4.680	2.870	1.460	2.550	4.710	3.254
	0.75	9.530	4.790	1.500	5.440	5.800	5.412
	1.00	18.400	5.880	4.590	7.850	6.250	8.594
	1.50	29.900	12.900	6.070	13.300	10.100	14.454
	2.00	42.500	11.200	5.130	19.100	12.300	18.046

Table A.5 continued

Factor	T (s)	μ=8					Average
		Long beach	Kern County	San Fernando(1)	San Fernando(2)	Monte Negro	
R	0.10	1.370	1.340	3.230	2.640	2.040	2.124
	0.20	2.520	3.010	6.140	3.890	3.060	3.724
	0.30	1.570	2.950	3.880	5.060	5.560	3.804
	0.40	2.770	4.180	5.730	4.000	4.070	4.150
	0.50	2.440	5.430	5.800	5.650	7.850	5.434
	0.75	2.040	4.710	3.420	4.990	3.460	3.724
	1.00	3.000	4.600	4.350	5.360	5.220	4.506
	1.50	3.100	5.720	3.560	3.600	6.380	4.472
	2.00	7.100	5.970	3.800	2.570	4.330	4.754
C_y	0.10	0.103	0.091	0.083	0.078	0.096	0.090
	0.20	0.095	0.079	0.070	0.065	0.074	0.077
	0.30	0.083	0.076	0.035	0.050	0.066	0.062
	0.40	0.083	0.052	0.029	0.044	0.063	0.054
	0.50	0.077	0.035	0.022	0.036	0.079	0.050
	0.75	0.070	0.027	0.010	0.033	0.030	0.034
	1.00	0.063	0.019	0.014	0.027	0.021	0.029
	1.50	0.047	0.013	0.003	0.023	0.013	0.020
	2.00	0.026	0.008	0.002	0.019	0.011	0.013
Δ_y (mm)	0.10	0.193	0.169	0.154	0.141	0.175	0.166
	0.20	0.683	0.548	0.529	0.474	0.546	0.556
	0.30	1.370	1.260	0.534	0.809	1.050	1.005
	0.40	2.410	1.540	0.831	2.030	1.820	1.726
	0.50	3.530	1.590	0.980	1.510	3.000	2.122
	0.75	7.200	2.720	0.800	3.380	3.170	3.454
	1.00	11.400	3.600	2.520	4.790	3.720	5.206
	1.50	19.300	5.350	1.540	9.270	5.660	8.224
	2.00	21.500	5.930	1.500	13.700	7.000	9.926

Table A.6 Far field earthquakes on soil sites for PGA 0.1g

Factor	T (s)	μ=1 Imp. Valley	Honshu1	San Fern.3	San Fern.4	Honshu2	Average
R	0.10	1.00	1.00	1.00	1.00	1.00	1.00
	0.20	1.00	1.00	1.00	1.00	1.00	1.00
	0.30	1.00	1.00	1.00	1.00	1.00	1.00
	0.40	1.00	1.00	1.00	1.00	1.00	1.00
	0.50	1.00	1.00	1.00	1.00	1.00	1.00
	0.75	1.00	1.00	1.00	1.00	1.00	1.00
	1.00	1.00	1.00	1.00	1.00	1.00	1.00
	1.50	1.00	1.00	1.00	1.00	1.00	1.00
	2.00	1.00	1.00	1.00	1.00	1.00	1.00
C_y	0.10	0.163	0.154	0.126	0.245	0.183	0.174
	0.20	0.187	0.270	0.227	0.296	0.308	0.258
	0.30	0.203	0.282	0.340	0.253	0.319	0.279
	0.40	0.353	0.246	0.231	0.213	0.129	0.234
	0.50	0.238	0.302	0.155	0.144	0.058	0.179
	0.75	0.167	0.148	0.162	0.102	0.045	0.125
	1.00	0.148	0.114	0.098	0.117	0.074	0.110
	1.50	0.050	0.061	0.095	0.103	0.017	0.065
	2.00	0.051	0.031	0.046	0.037	0.008	0.035
Δ_y (mm)	0.10	0.410	0.380	0.310	0.610	0.460	0.434
	0.20	1.850	2.680	2.250	2.940	3.060	2.556
	0.30	4.530	6.280	7.600	5.640	7.130	6.236
	0.40	0.176	9.770	9.190	8.450	5.110	6.539
	0.50	14.800	18.800	9.600	8.970	3.620	11.158
	0.75	23.300	20.700	22.700	14.300	6.240	17.448
	1.00	36.700	28.200	24.400	29.100	18.500	27.380
	1.50	30.400	33.800	52.900	57.800	9.650	36.910
	2.00	50.600	30.700	45.600	36.900	7.790	34.318

Table A.6 continued

Factor	T (s)	μ=2					Average
		Imp. Valley	Honshu1	San Fern.3	San Fern.4	Honshu2	
R	0.10	1.060	1.060	1.830	1.480	1.270	1.34
	0.20	1.450	1.440	2.320	1.750	1.310	1.65
	0.30	1.140	1.600	1.380	2.210	2.780	1.82
	0.40	2.030	1.540	2.250	1.820	1.810	1.89
	0.50	1.690	1.600	2.260	2.460	2.550	2.11
	0.75	1.380	2.080	1.540	2.450	1.370	1.76
	1.00	1.570	1.560	2.510	2.530	2.220	2.08
	1.50	1.630	2.160	1.830	1.880	1.800	1.86
	2.00	2.040	2.320	1.780	1.650	1.460	1.85
C_y	0.10	0.142	0.133	0.120	0.164	0.137	0.14
	0.20	0.148	0.142	0.171	0.146	0.130	0.15
	0.30	0.150	0.140	0.153	0.107	0.095	0.13
	0.40	0.190	0.123	0.100	0.104	0.053	0.11
	0.50	0.108	0.137	0.118	0.099	0.029	0.10
	0.75	0.073	0.091	0.090	0.071	0.031	0.07
	1.00	0.052	0.079	0.050	0.039	0.020	0.05
	1.50	0.030	0.028	0.047	0.051	0.011	0.03
	2.00	0.026	0.015	0.030	0.022	0.005	0.02
Δ_y (mm)	0.10	0.346	0.318	0.287	0.391	0.331	0.33
	0.20	1.390	1.340	1.620	1.380	1.230	1.39
	0.30	2.050	2.970	3.230	2.260	2.020	2.51
	0.40	0.095	4.680	3.760	3.920	2.000	2.89
	0.50	6.390	8.080	7.030	5.860	1.740	5.82
	0.75	9.670	12.200	12.000	9.510	4.220	9.52
	1.00	9.670	12.200	12.000	9.510	4.220	9.52
	1.50	16.000	15.000	24.700	27.000	6.240	17.79
	2.00	24.100	14.600	27.900	20.300	4.680	18.32

Table A.6 continued

Factor	T (s)	μ=3 Imp. Valley	Honshu1	San Fern.3	San Fern.4	Honshu2	Average
R	0.10	1.130	1.110	2.590	1.900	1.500	1.646
	0.20	1.820	2.660	3.290	2.210	1.720	2.340
	0.30	1.290	1.990	1.840	3.190	4.100	2.482
	0.40	2.520	2.050	3.720	2.720	2.760	2.754
	0.50	1.990	2.350	4.120	3.480	3.410	3.070
	0.75	1.680	2.710	2.400	3.110	1.770	2.334
	1.00	1.940	3.020	3.290	3.490	3.210	2.990
	1.50	2.050	2.460	2.450	2.540	2.620	2.424
	2.00	2.840	3.070	2.430	1.980	2.460	2.556
C_y	0.10	0.122	0.113	0.115	0.128	0.106	0.117
	0.20	0.103	0.096	0.131	0.102	0.091	0.105
	0.30	0.075	0.105	0.127	0.091	0.067	0.093
	0.40	0.150	0.093	0.072	0.080	0.038	0.087
	0.50	0.071	0.083	0.076	0.075	0.026	0.066
	0.75	0.055	0.064	0.067	0.055	0.022	0.053
	1.00	0.041	0.056	0.042	0.032	0.011	0.036
	1.50	0.024	0.020	0.030	0.037	0.008	0.024
	2.00	0.012	0.011	0.023	0.018	0.004	0.013
Δ_y (mm)	0.10	0.284	0.258	0.265	0.289	0.241	0.267
	0.20	0.927	0.858	1.180	0.924	0.822	0.942
	0.30	1.530	2.130	2.590	1.850	1.360	1.892
	0.40	0.075	3.340	2.600	2.920	1.350	2.057
	0.50	4.000	4.700	4.280	4.230	1.440	3.730
	0.75	7.080	8.220	8.510	6.900	2.850	6.712
	1.00	9.190	12.500	9.470	7.130	2.410	8.140
	1.50	12.000	10.200	15.100	18.400	4.200	11.980
	2.00	11.000	9.620	20.600	15.600	3.420	12.048

Table A.6 continued

Factor	T (s)	μ=4					Average
		Imp. Valley	Honshu1	San Fern.3	San Fern.4	Honshu2	
R	0.10	1.190	1.170	2.880	2.330	1.680	1.850
	0.20	2.130	2.830	4.120	2.590	2.320	2.798
	0.30	1.420	2.250	2.290	3.630	4.590	2.836
	0.40	2.670	2.520	4.400	3.040	3.070	3.140
	0.50	2.170	3.650	4.760	4.100	4.270	3.790
	0.75	1.820	3.220	2.720	3.600	2.190	2.710
	1.00	2.170	3.190	3.860	4.020	3.760	3.400
	1.50	2.330	2.740	3.080	2.890	3.690	2.946
	2.00	3.520	3.730	3.250	2.170	4.240	3.382
C_y	0.10	0.106	0.097	0.109	0.116	0.092	0.104
	0.20	0.069	0.087	0.107	0.089	0.080	0.086
	0.30	0.071	0.093	0.094	0.081	0.049	0.078
	0.40	0.130	0.082	0.062	0.066	0.032	0.074
	0.50	0.055	0.065	0.044	0.066	0.024	0.051
	0.75	0.044	0.043	0.056	0.048	0.017	0.042
	1.00	0.033	0.041	0.038	0.029	0.015	0.031
	1.50	0.020	0.016	0.027	0.030	0.007	0.020
	2.00	0.010	0.009	0.020	0.016	0.003	0.012
Δ_y (mm)	0.10	0.235	0.211	0.243	0.250	0.199	0.228
	0.20	0.598	0.739	0.924	0.770	0.693	0.745
	0.30	1.360	1.800	1.830	1.570	0.939	1.500
	0.40	0.065	2.800	2.160	2.280	1.100	1.681
	0.50	2.980	3.520	2.380	3.530	1.280	2.738
	0.75	5.410	5.120	6.710	5.850	2.050	5.028
	1.00	7.140	8.900	8.220	6.310	1.500	6.414
	1.50	9.580	7.820	13.200	14.200	3.110	9.582
	2.00	8.510	7.580	17.400	13.300	2.860	9.930

Table A.6 continued

Factor	T (s)	μ=8					Average
		Imp. Valley	Honshu1	San Fern.3	San Fern.4	Honshu2	
R	0.10	1.370	1.340	3.230	2.640	2.040	2.124
	0.20	2.520	3.010	6.140	3.890	3.060	3.724
	0.30	1.570	2.950	3.880	5.060	5.560	3.804
	0.40	2.770	4.180	5.730	4.000	4.070	4.150
	0.50	2.440	5.430	5.800	5.650	7.850	5.434
	0.75	2.040	4.710	3.420	4.990	3.460	3.724
	1.00	3.000	4.600	4.350	5.360	5.220	4.506
	1.50	3.100	5.720	3.560	3.600	6.380	4.472
	2.00	7.100	5.970	3.800	2.570	4.330	4.754
C_y	0.10	0.096	0.092	0.092	0.086	0.076	0.088
	0.20	0.068	0.083	0.074	0.077	0.053	0.071
	0.30	0.063	0.076	0.069	0.059	0.025	0.058
	0.40	0.091	0.057	0.040	0.046	0.022	0.051
	0.50	0.042	0.047	0.033	0.046	0.020	0.037
	0.75	0.018	0.025	0.036	0.037	0.003	0.024
	1.00	0.026	0.003	0.029	0.024	0.009	0.018
	1.50	0.009	0.010	0.020	0.017	0.003	0.012
	2.00	0.009	0.005	0.015	0.012	0.001	0.008
Δ_y (mm)	0.10	0.174	0.165	0.172	0.159	0.137	0.161
	0.20	0.485	0.629	0.547	0.561	0.385	0.521
	0.30	1.040	1.260	1.270	0.982	0.680	1.046
	0.40	0.045	1.660	2.160	1.330	0.640	1.167
	0.50	2.090	2.500	1.460	2.100	0.883	1.807
	0.75	2.240	2.590	3.650	3.810	0.383	2.535
	1.00	4.500	1.170	5.250	4.180	0.560	3.132
	1.50	4.010	4.480	7.990	7.220	0.919	4.924
	2.00	6.500	3.840	11.300	9.080	0.974	6.339

B. APPENDIX B

C_Y-T GRAPHS AND YIELD SPECTRA AT CONSTANT DUCTILITY
FOR PGA 0.1g, 0.2g, 0.3g AND 0.4g

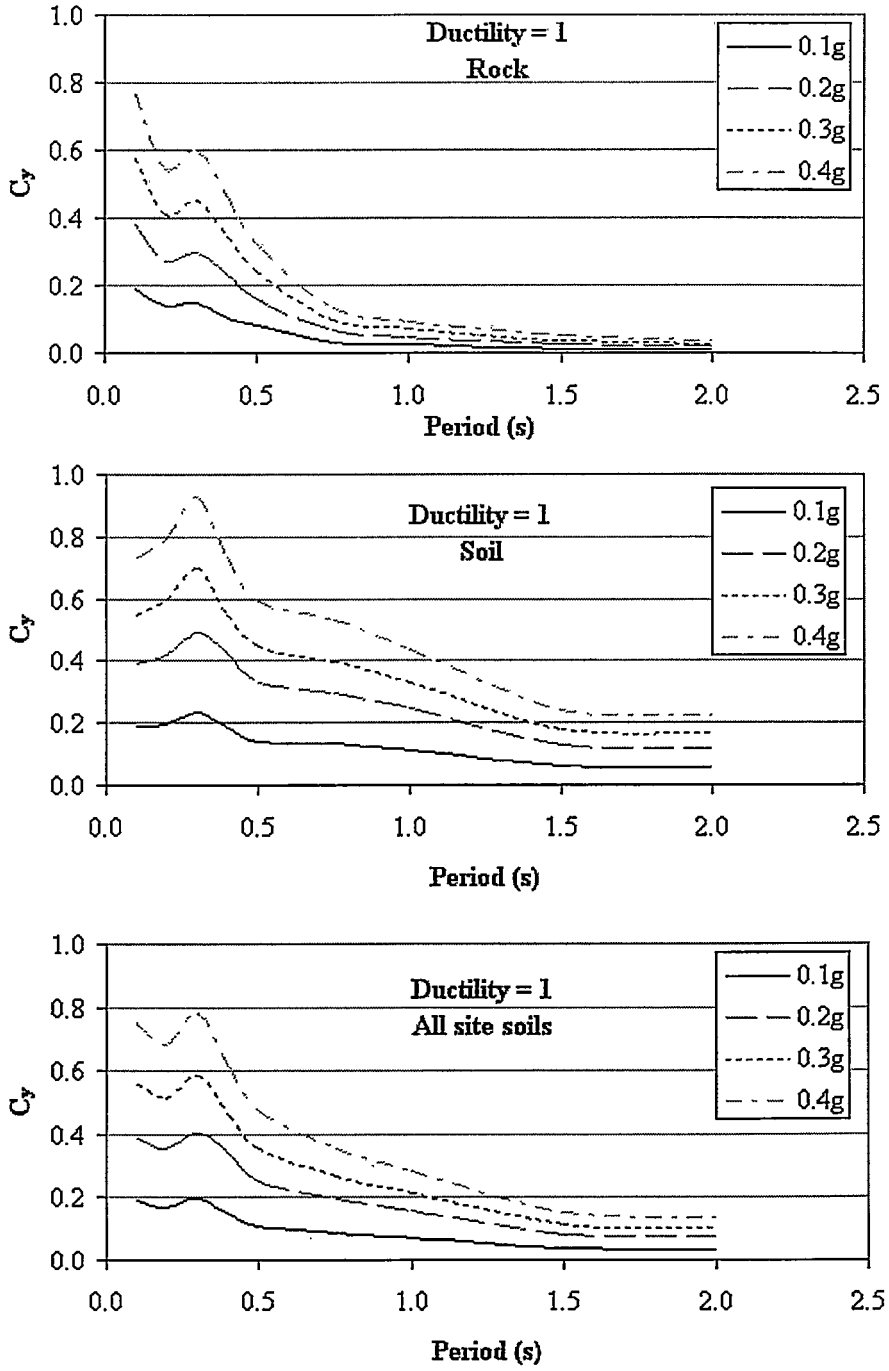

Figure B.1 C_y factor variation with period for NFE with magnitude >6 for ductility level 1

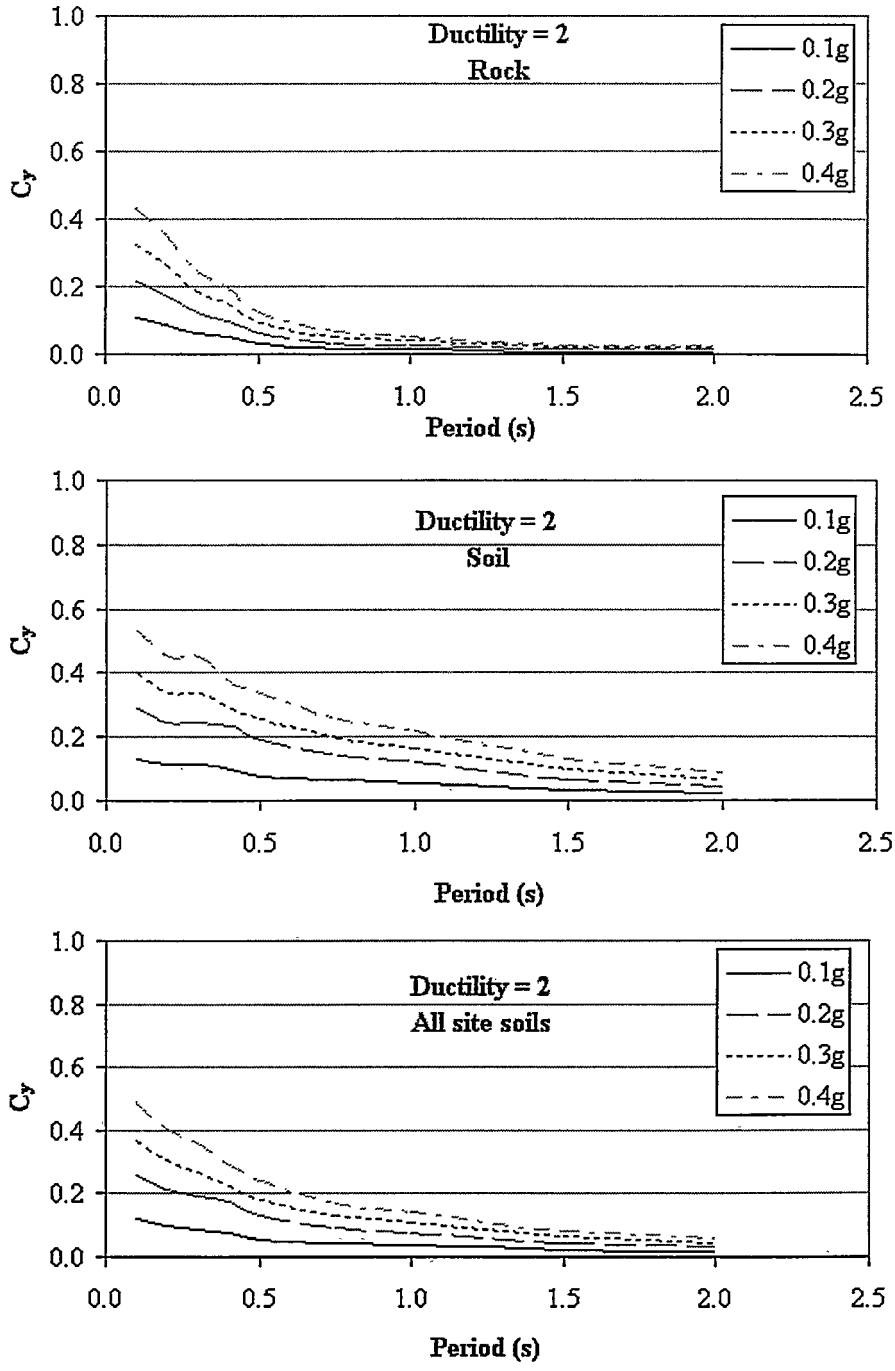

Figure B.2 C_y factor variation with period for NFE with magnitude >6 for ductility level 2

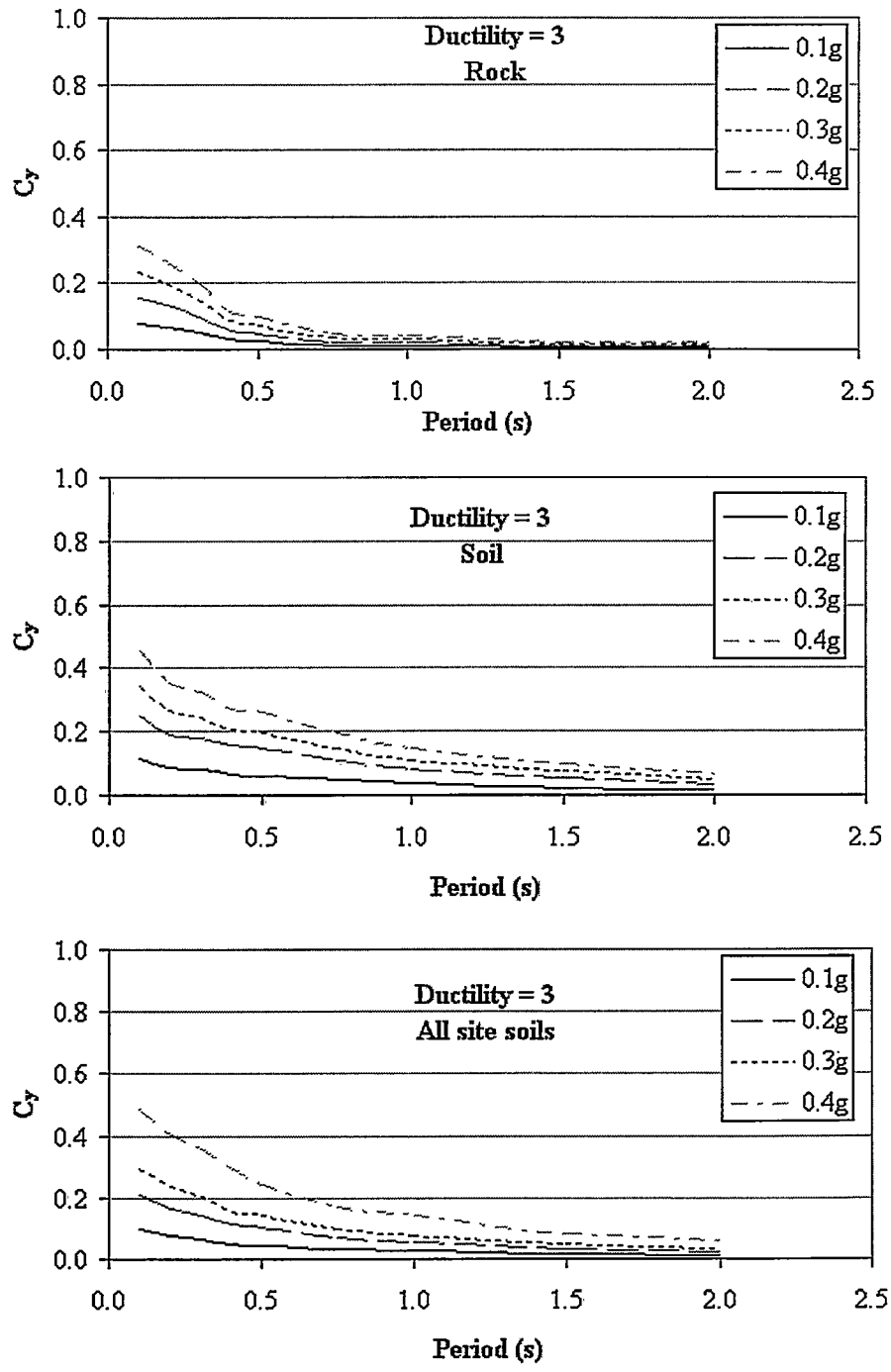

Figure B.3 C_y factor variation with period for NFE with magnitude >6 for ductility level 3

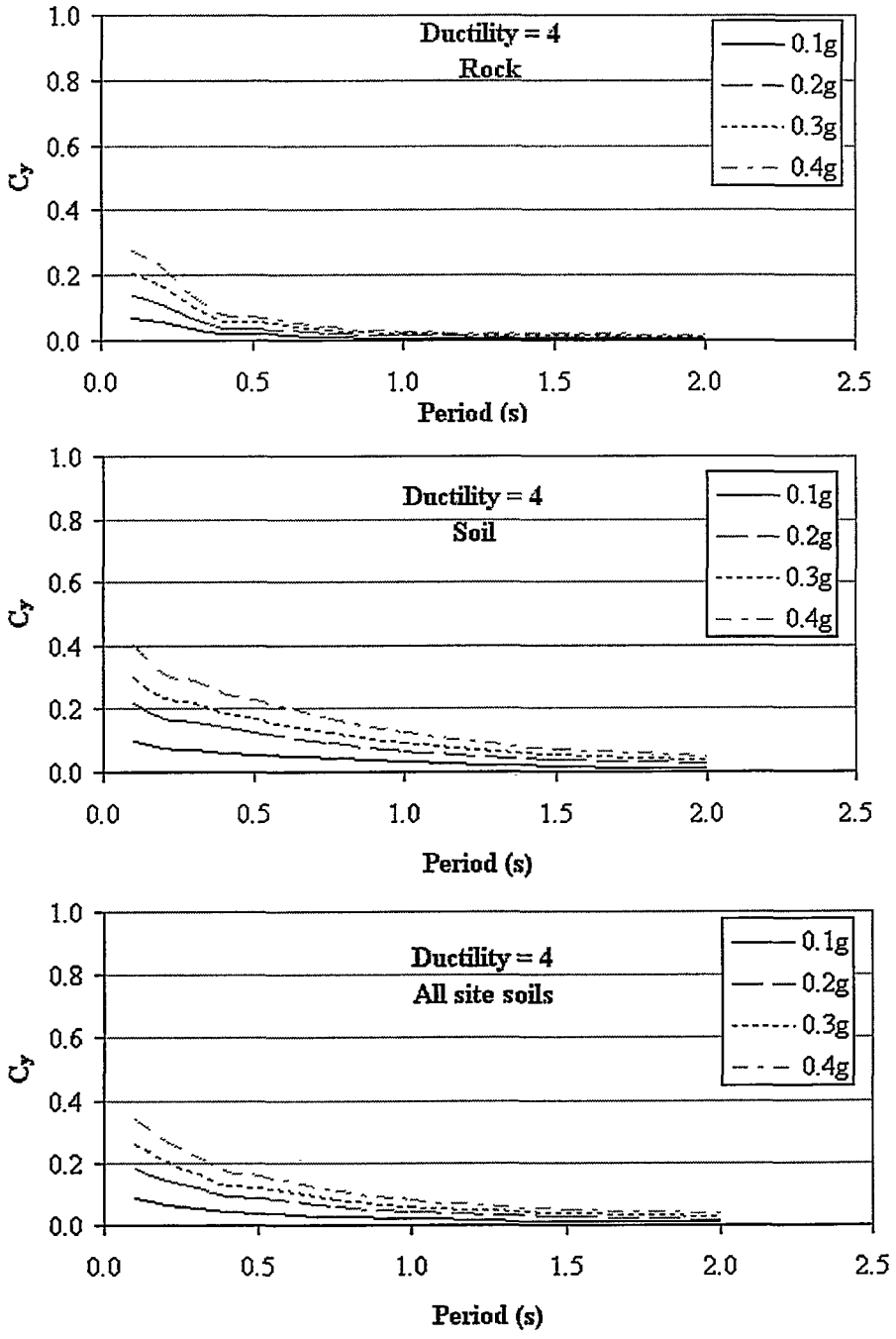

Figure B.4 C_y factor variation with period for NFE with magnitude >6 for ductility level 4

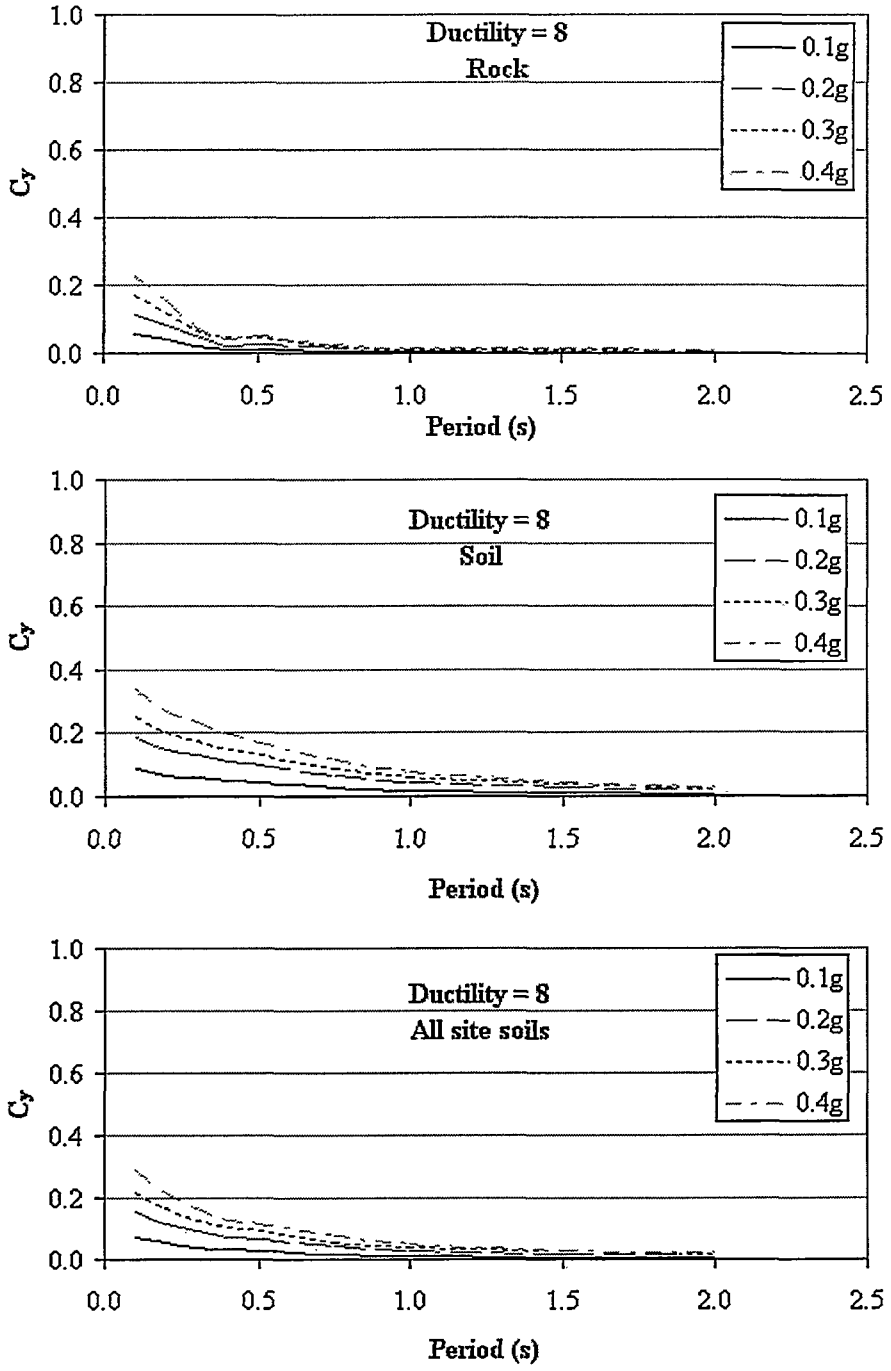

Figure B.5 C_y factor variation with period for NFE with magnitude >6 for ductility level 8

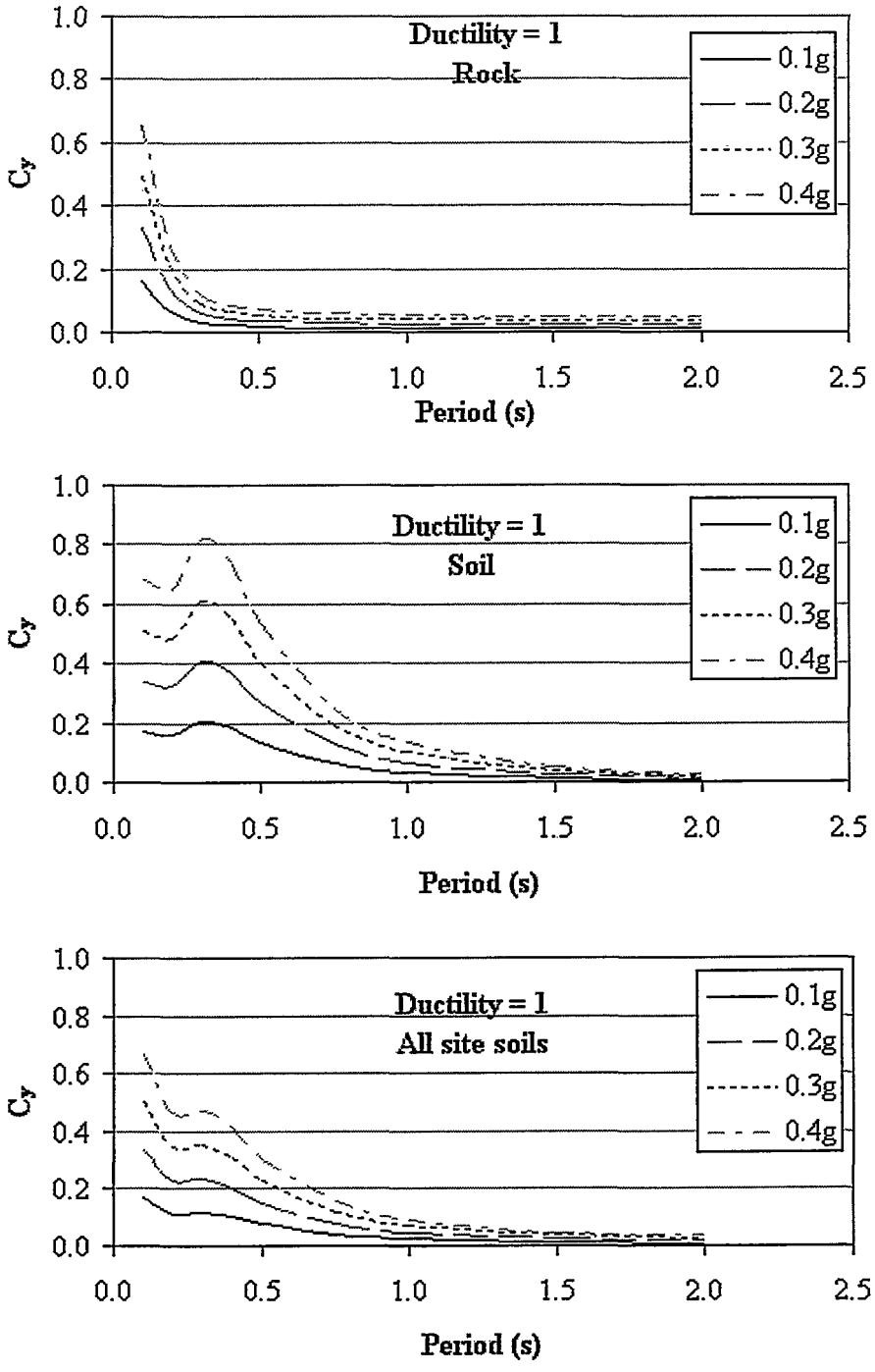

Figure B.6 C_y factor variation with period for NFE with magnitude <6 for ductility level 1

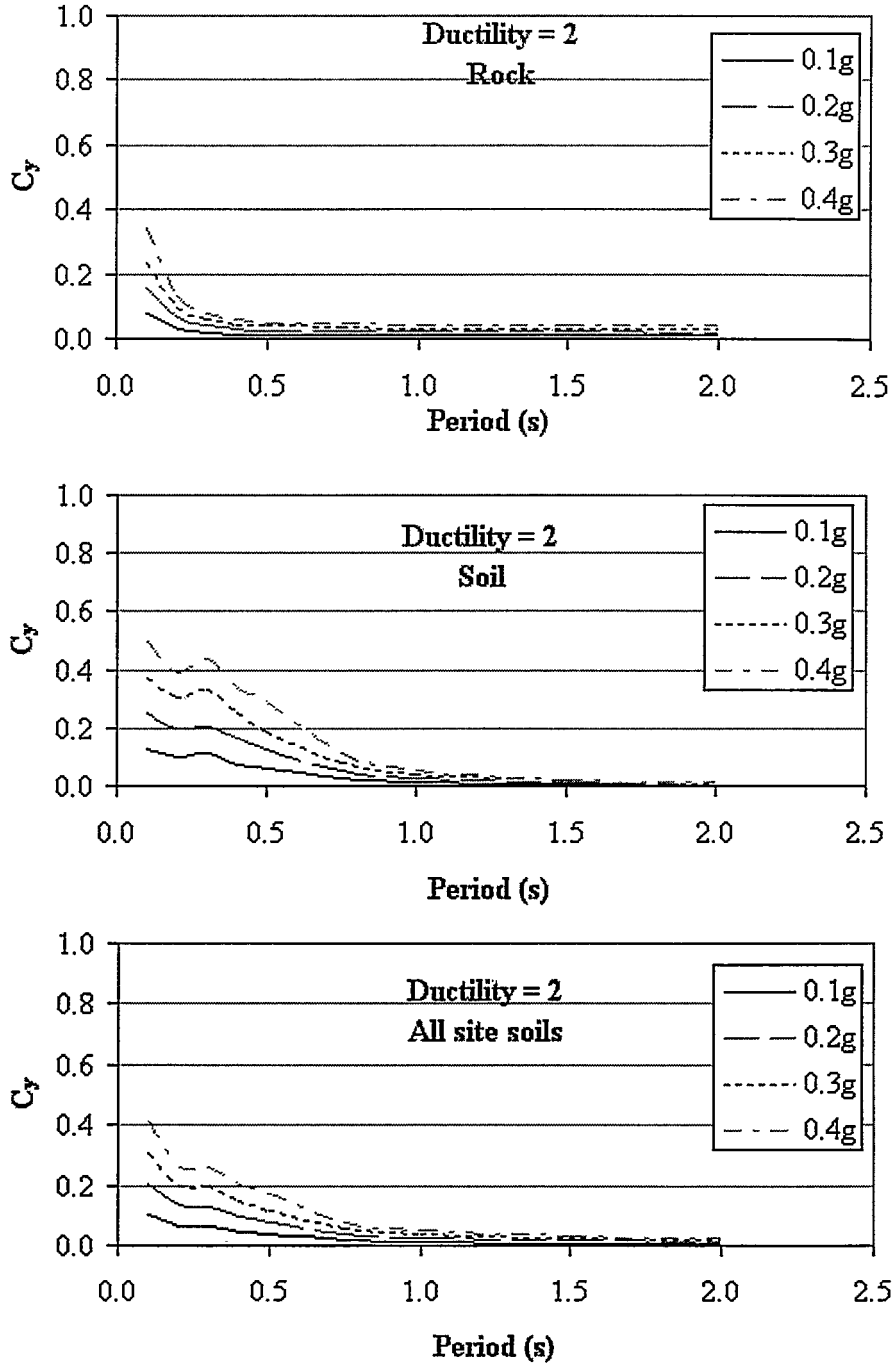

Figure B.7 C_y factor variation with period for NFE with magnitude <6 for ductility level 2

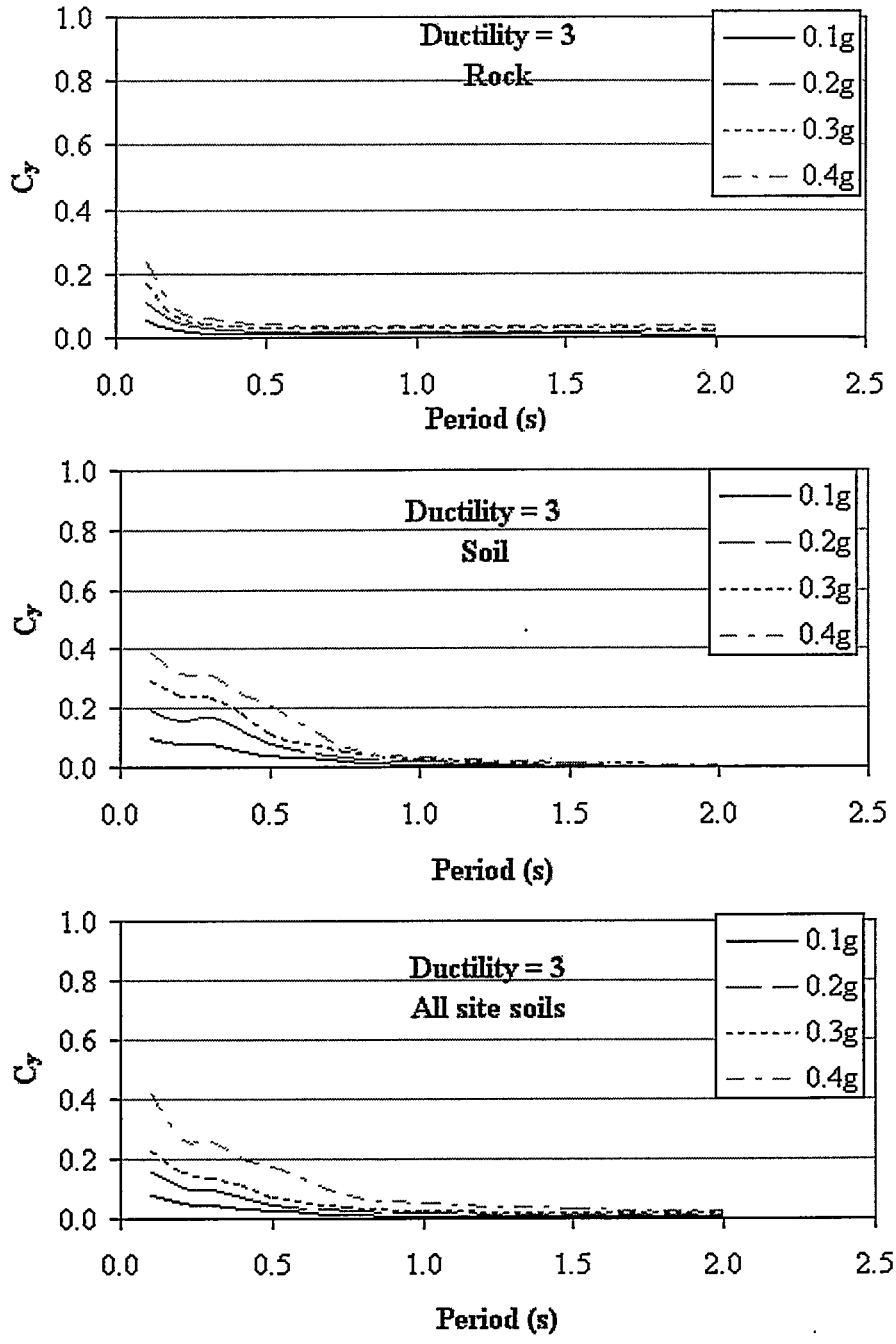

Figure B.8 C_y factor variation with period for NFE with magnitude <6 for ductility level 3

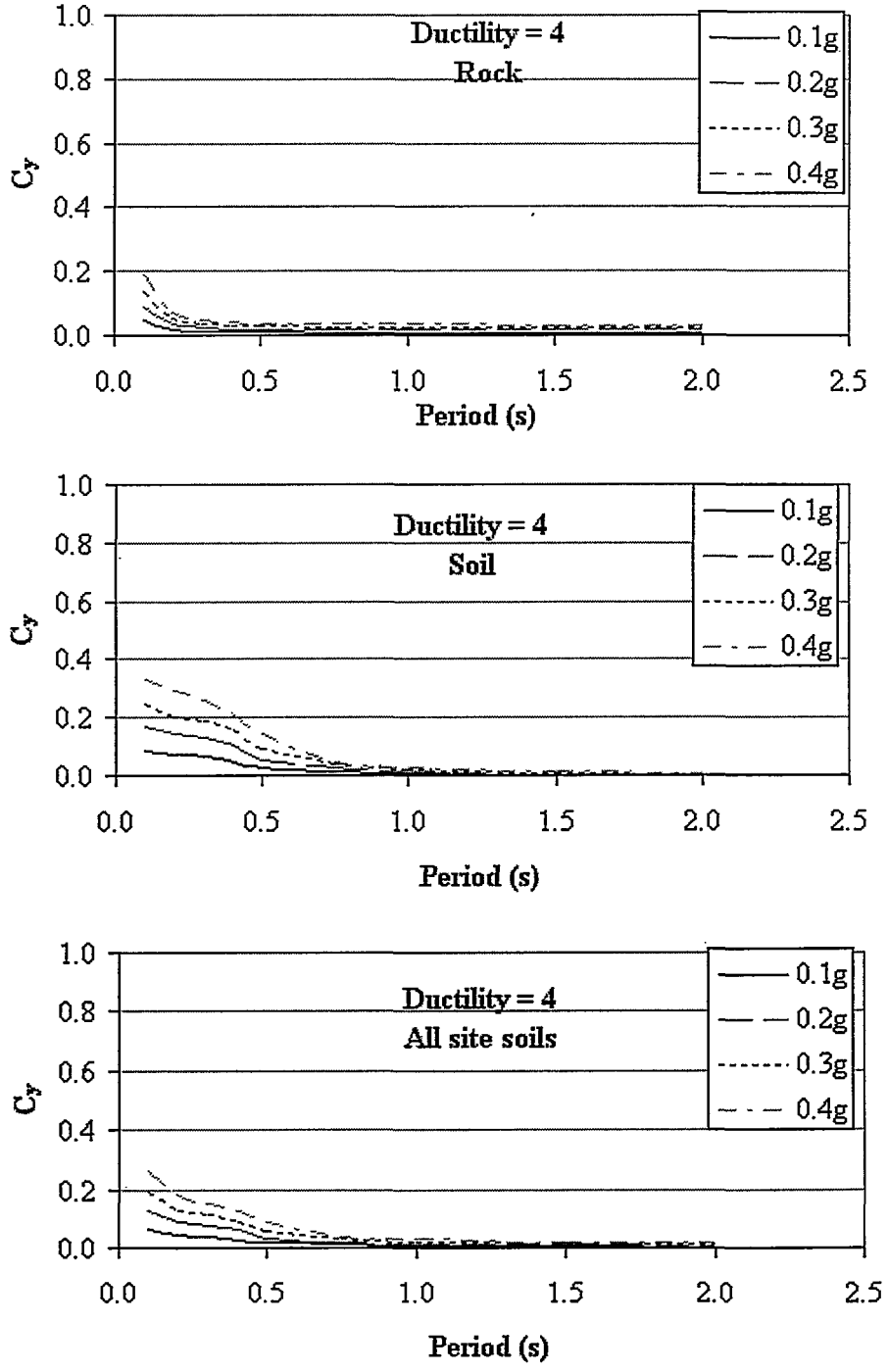

Figure B.9 C_y factor variation with period for NFE with magnitude <6 for ductility level 4

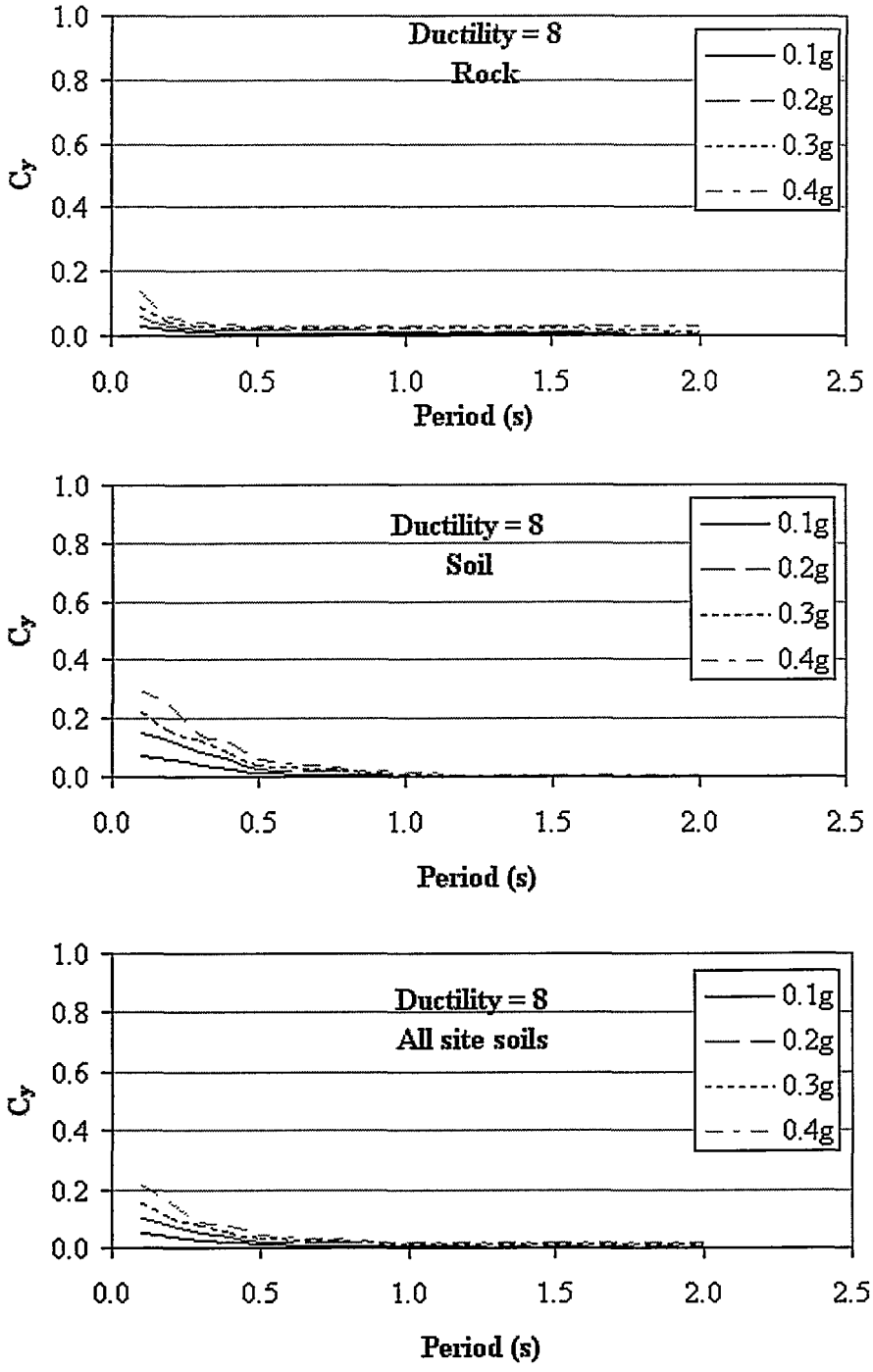

Figure B.10 C_y factor variation with period for NFE with magnitude <6 for ductility level 8

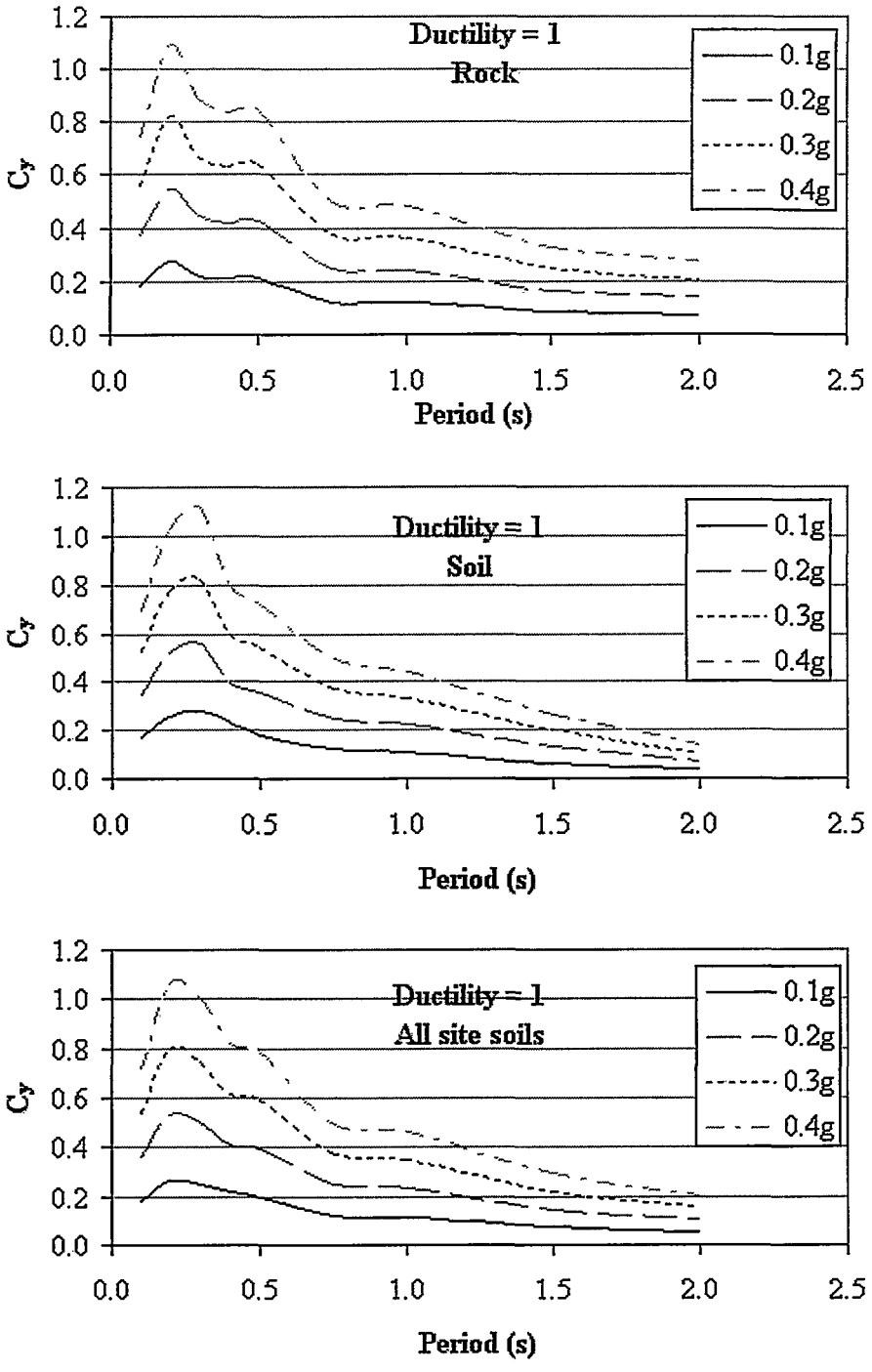

Figure B.11C_y factor variation with period for FFE for ductility level 1

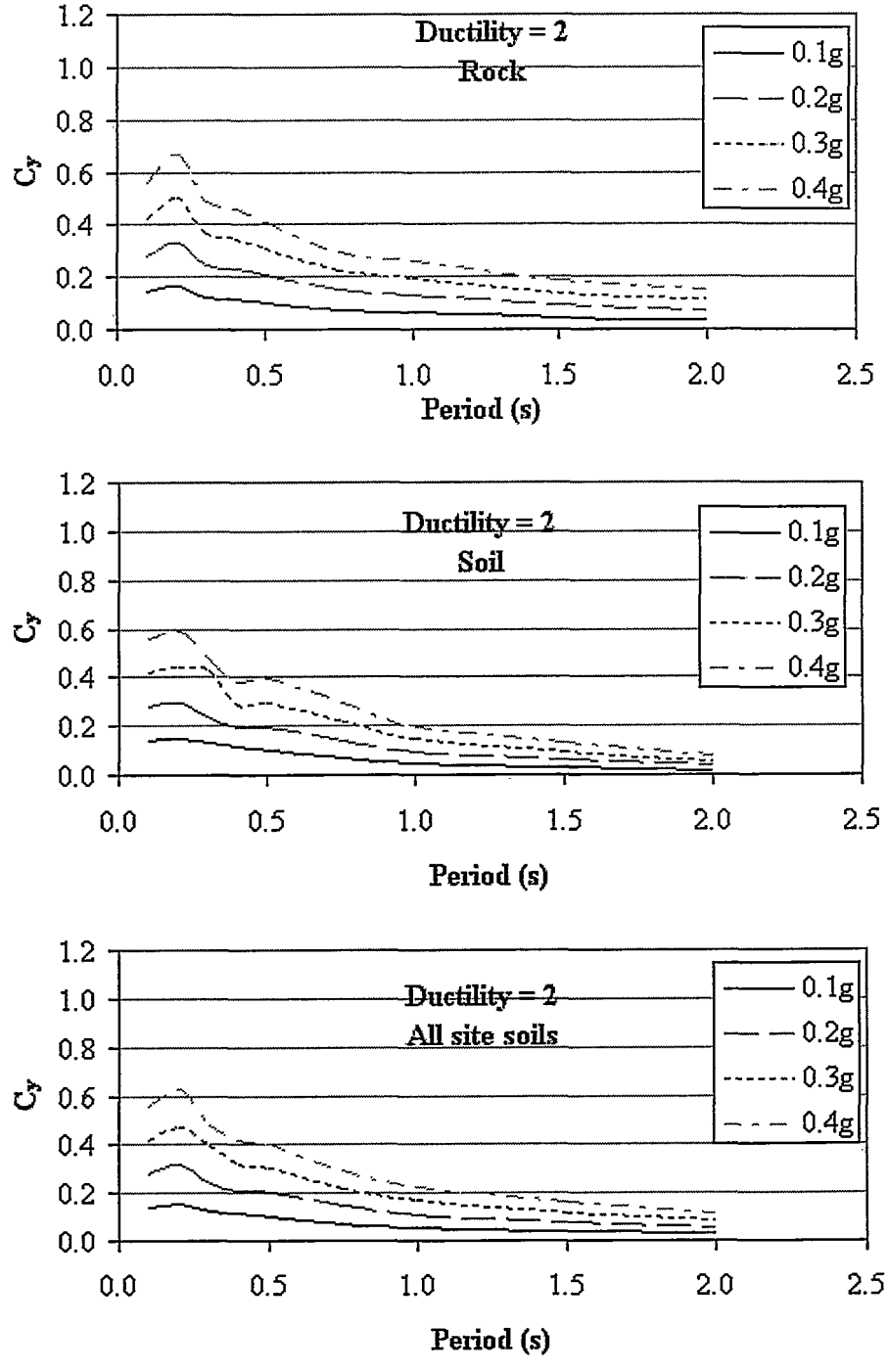

Figure B.12 C_y factor variation with period for FFE for ductility level 2

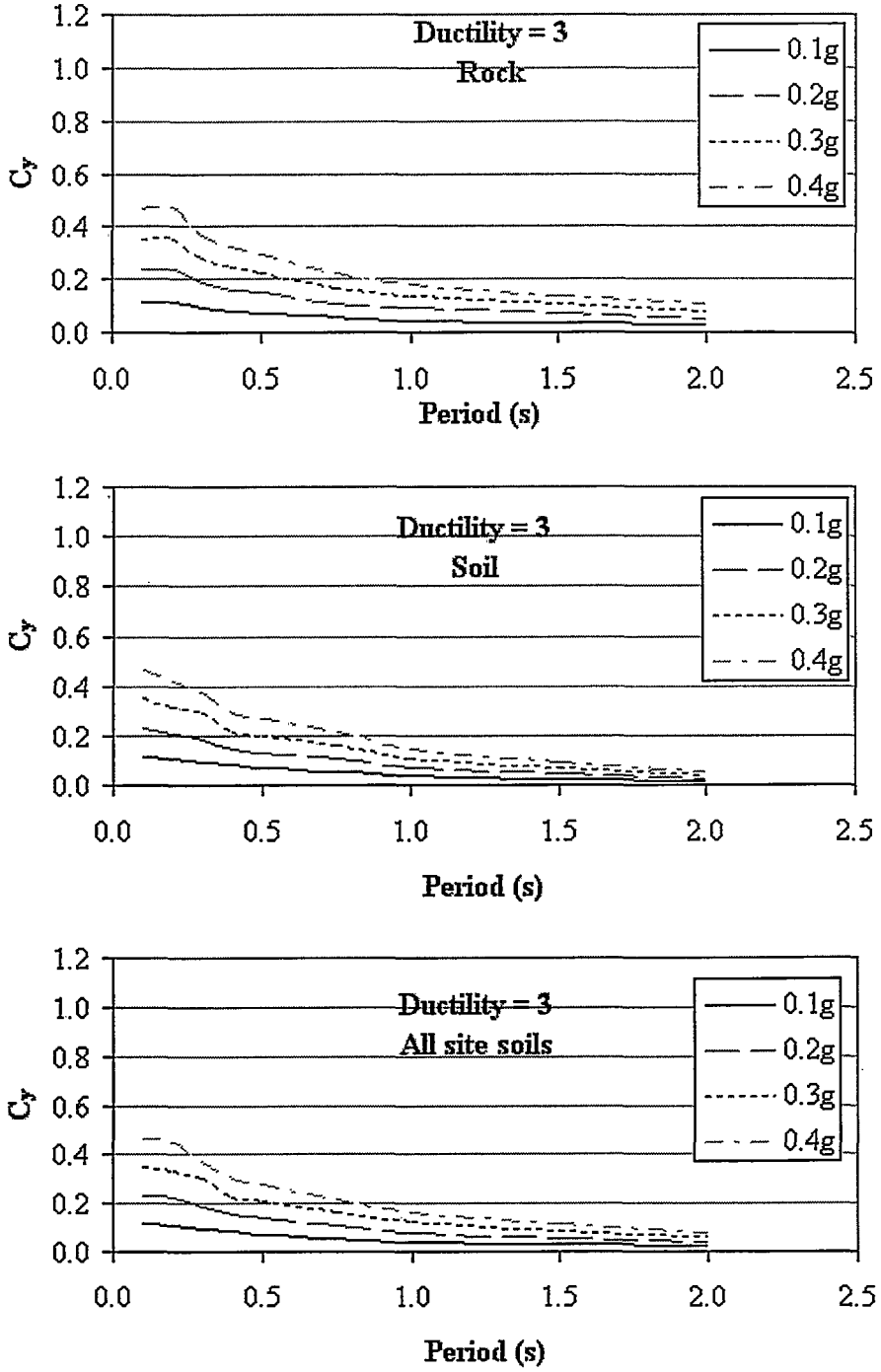

Figure B.13 C_y factor variation with period for FFE for ductility level 3

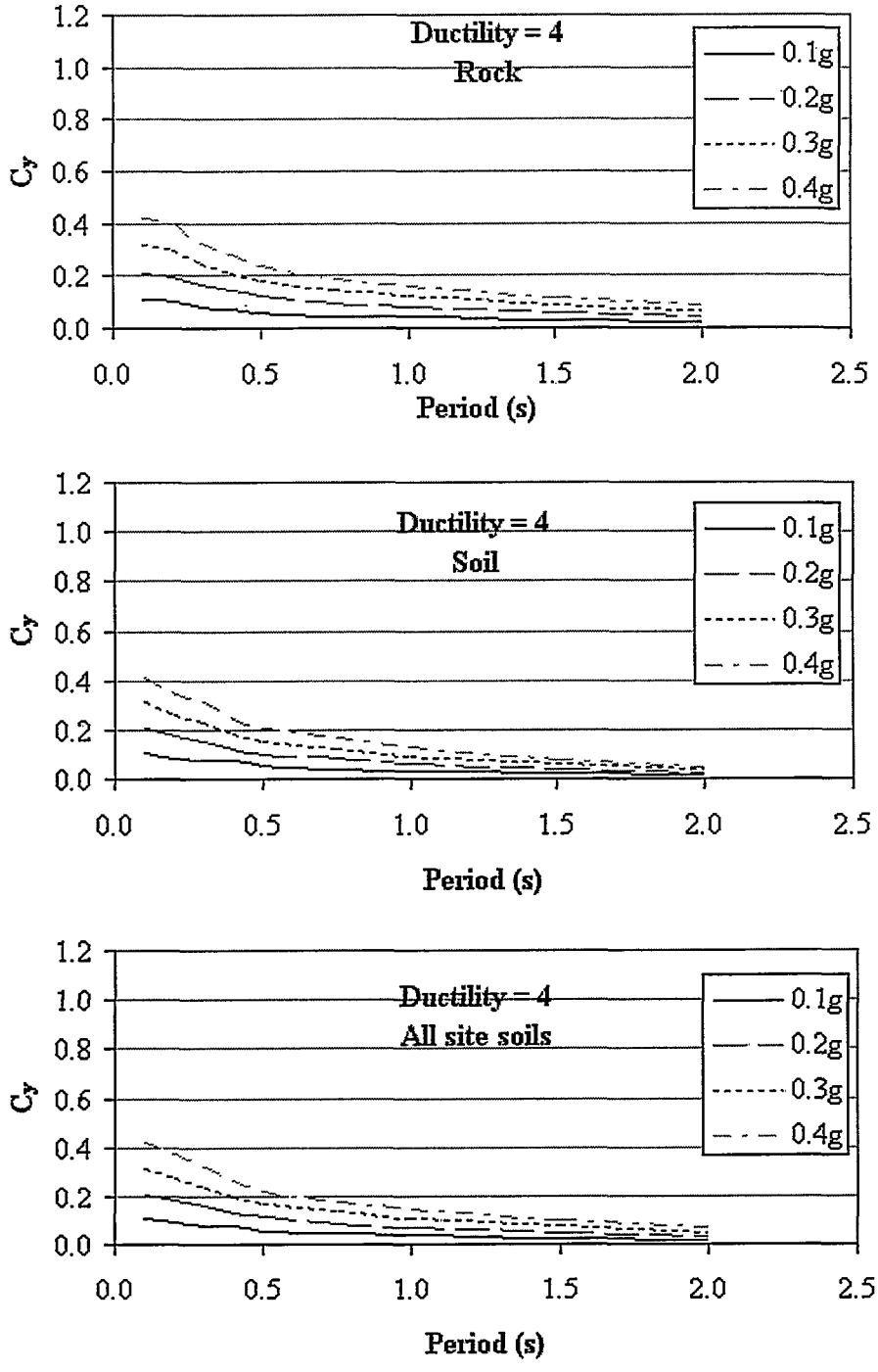

Figure B.14 C_y factor variation with period for FFE for ductility level 4

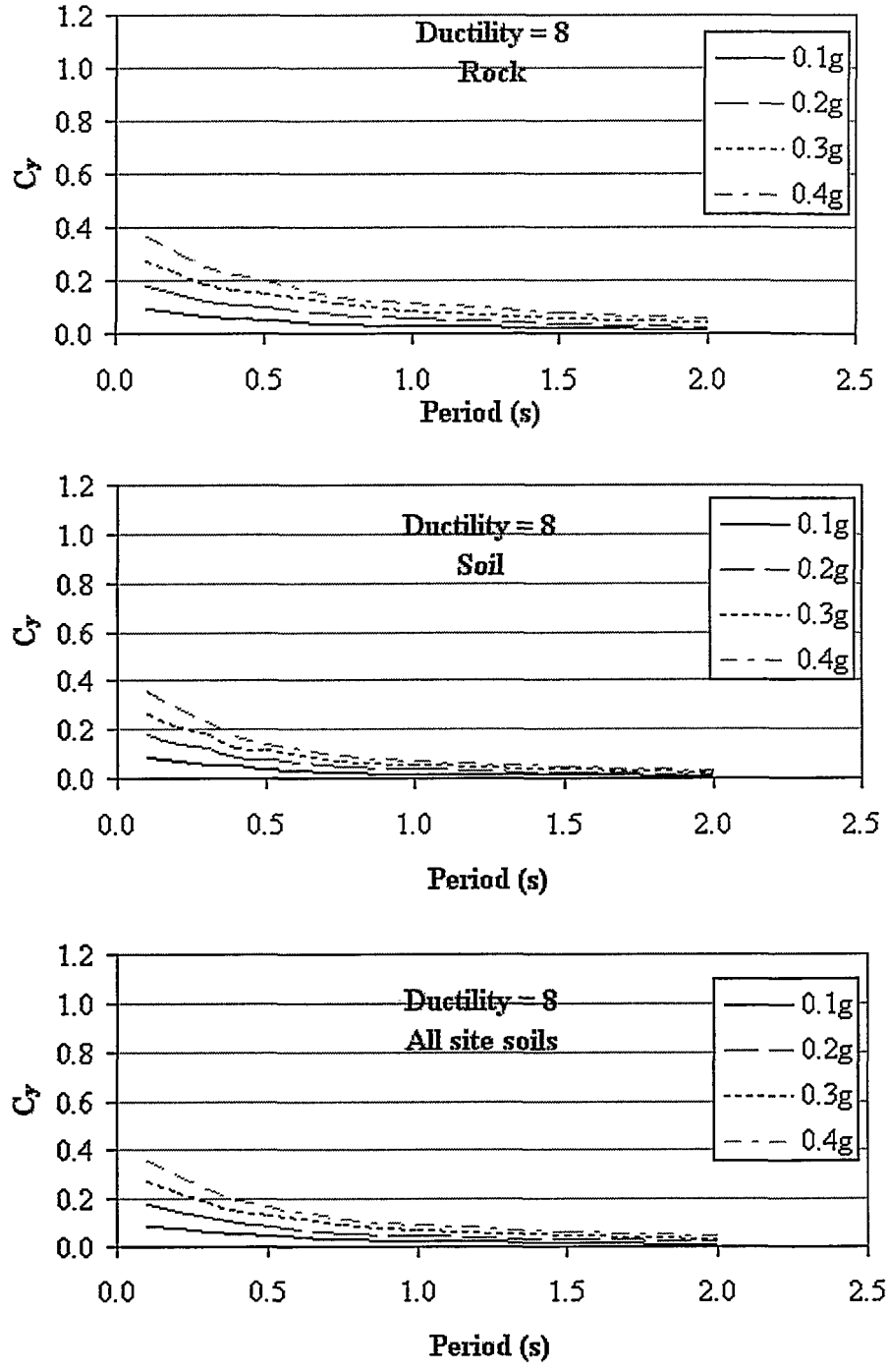

Figure B.15 C_y factor variation with period for FFE for ductility level 8

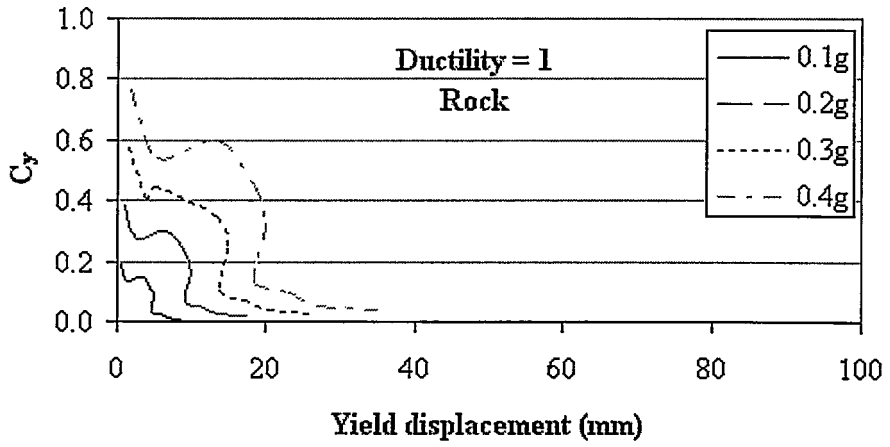

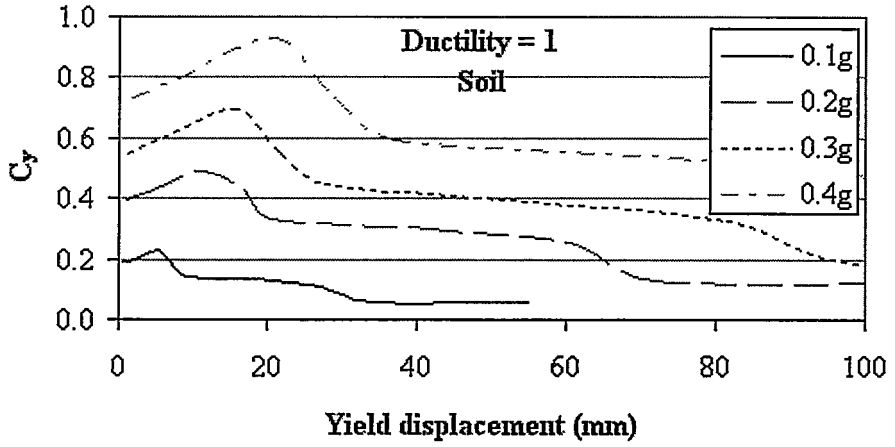

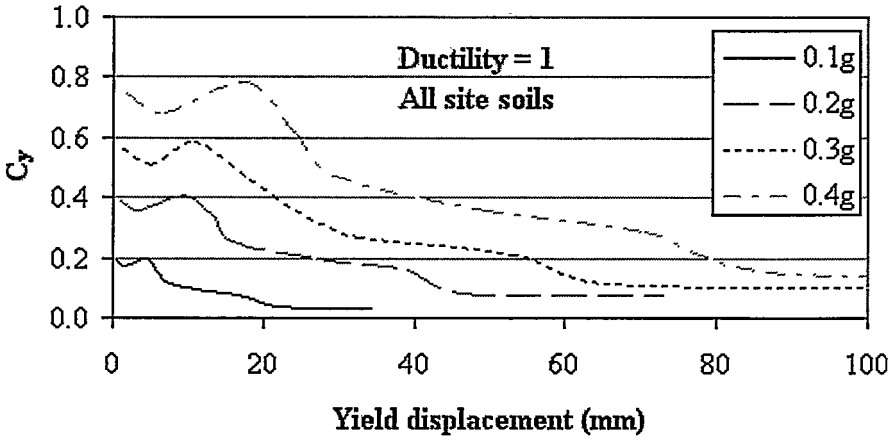

Figure B.16 Yield spectra for NFE with magnitude >6 for ductility level 1

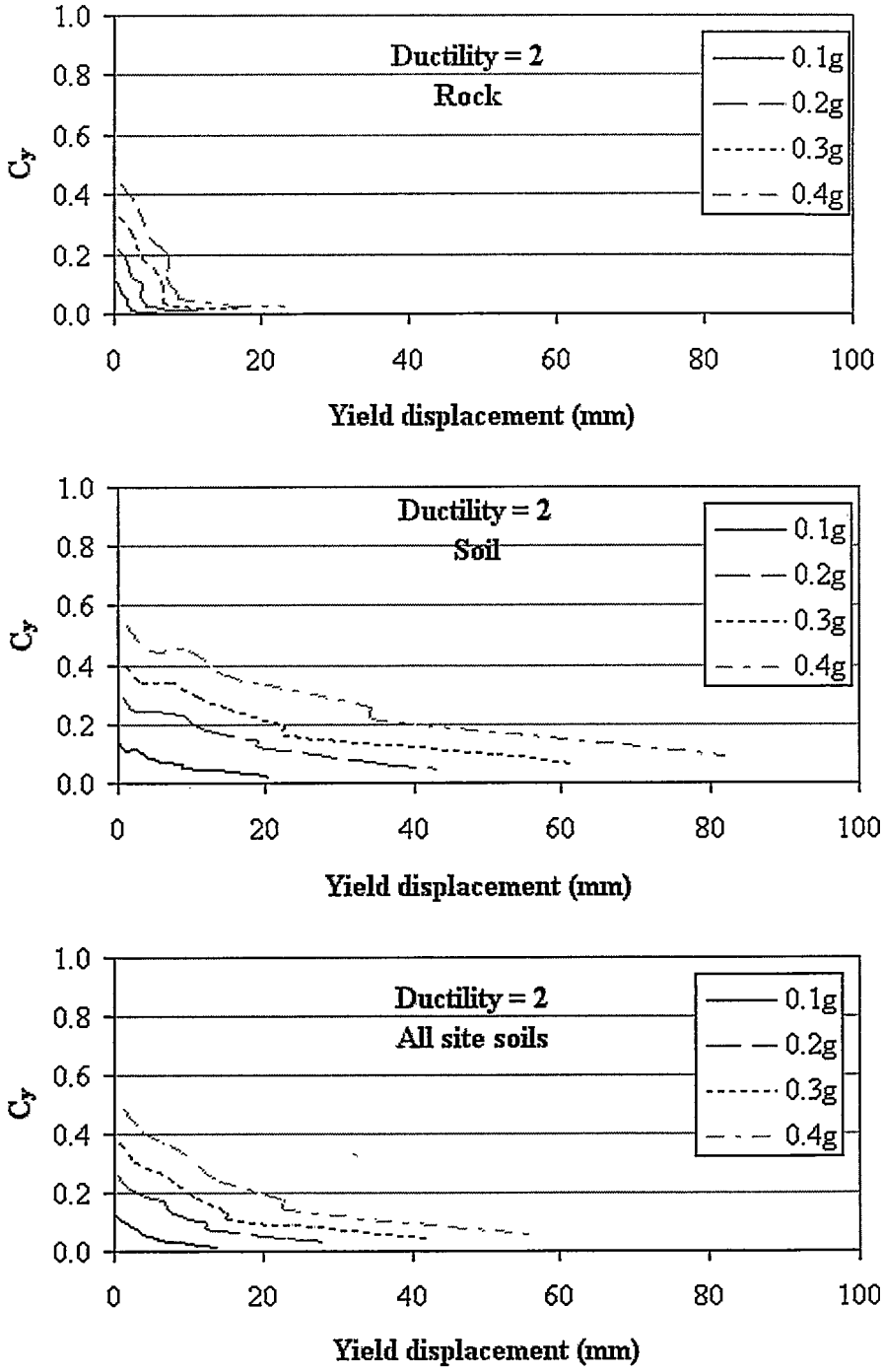

Figure B.17 Yield spectra for NFE with magnitude >6 for ductility level 2

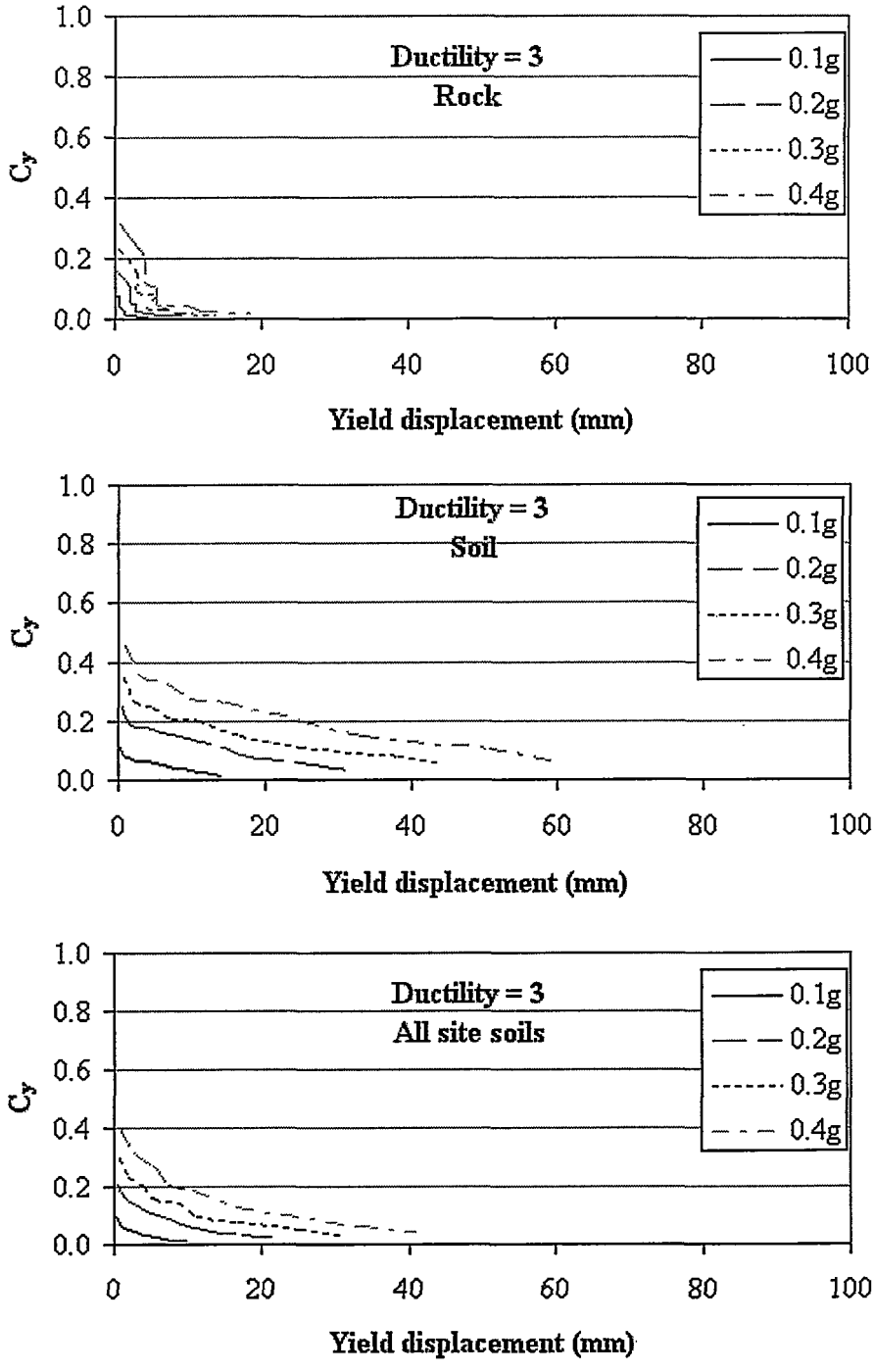

Figure B.18 Yield spectra for NFE with magnitude >6 for ductility level 3

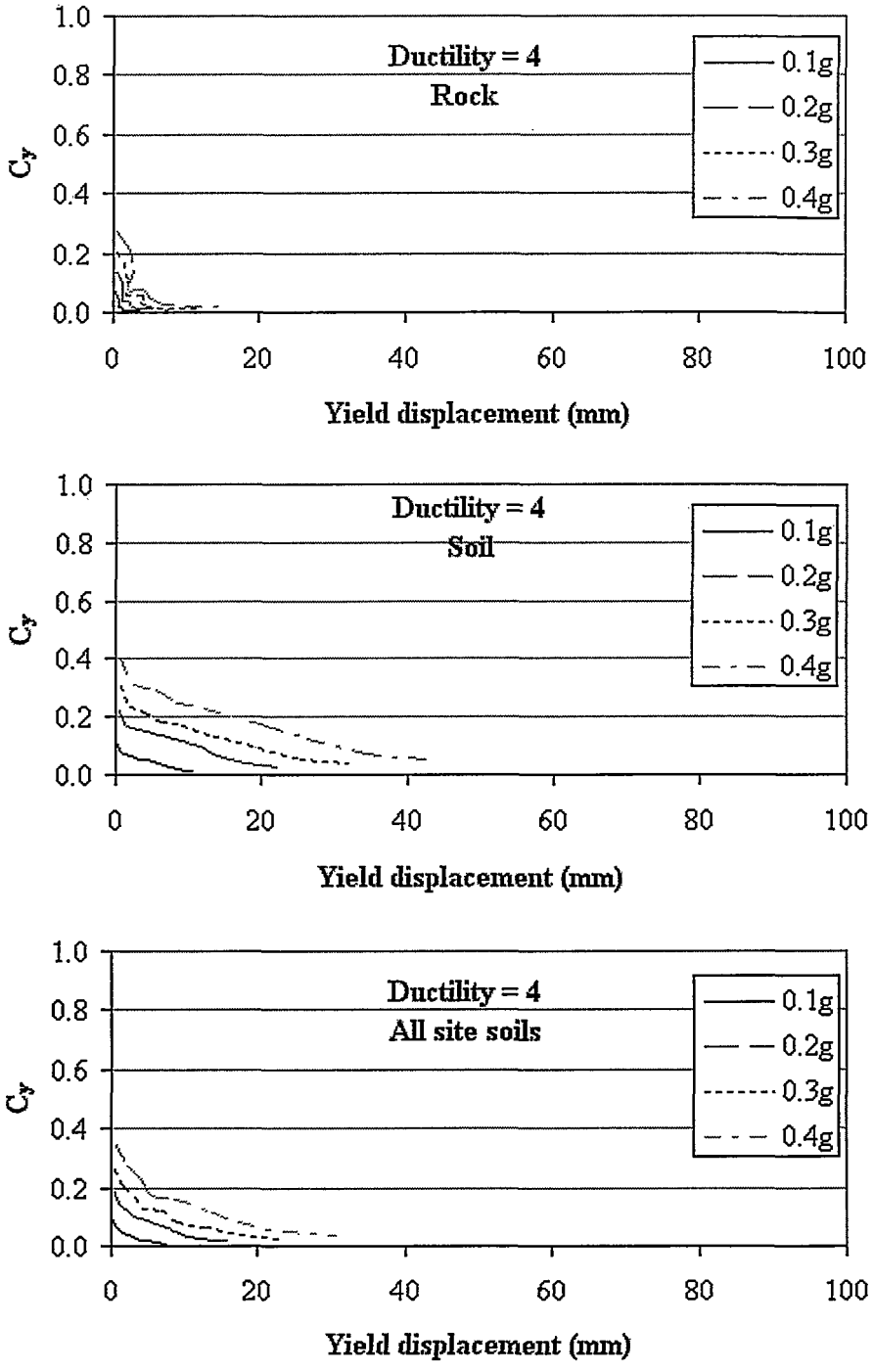

Figure B.19 Yield spectra for NFE with magnitude >6 for ductility level 4

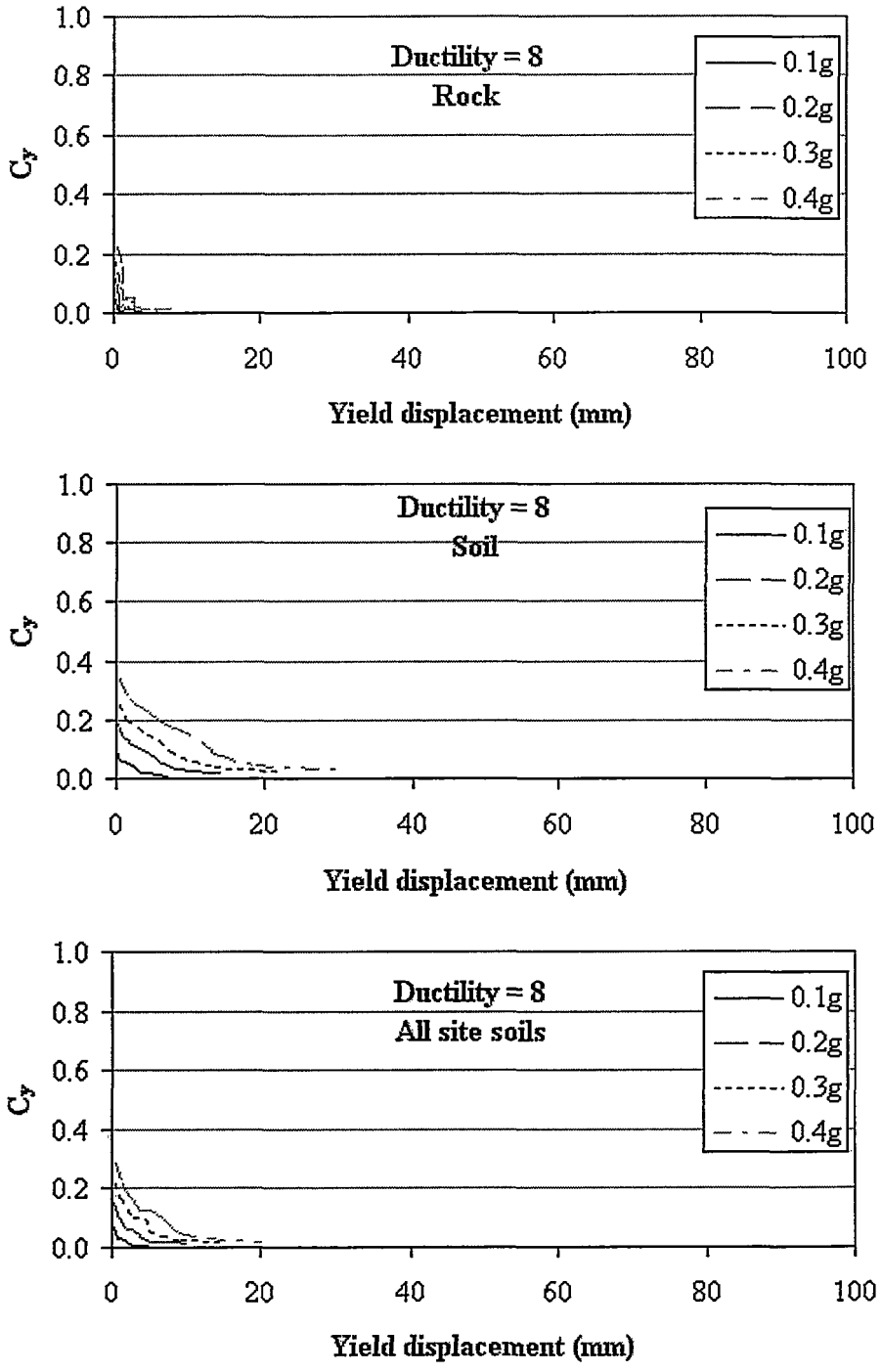

Figure B.20 Yield spectra for NFE with magnitude >6 for ductility level 8

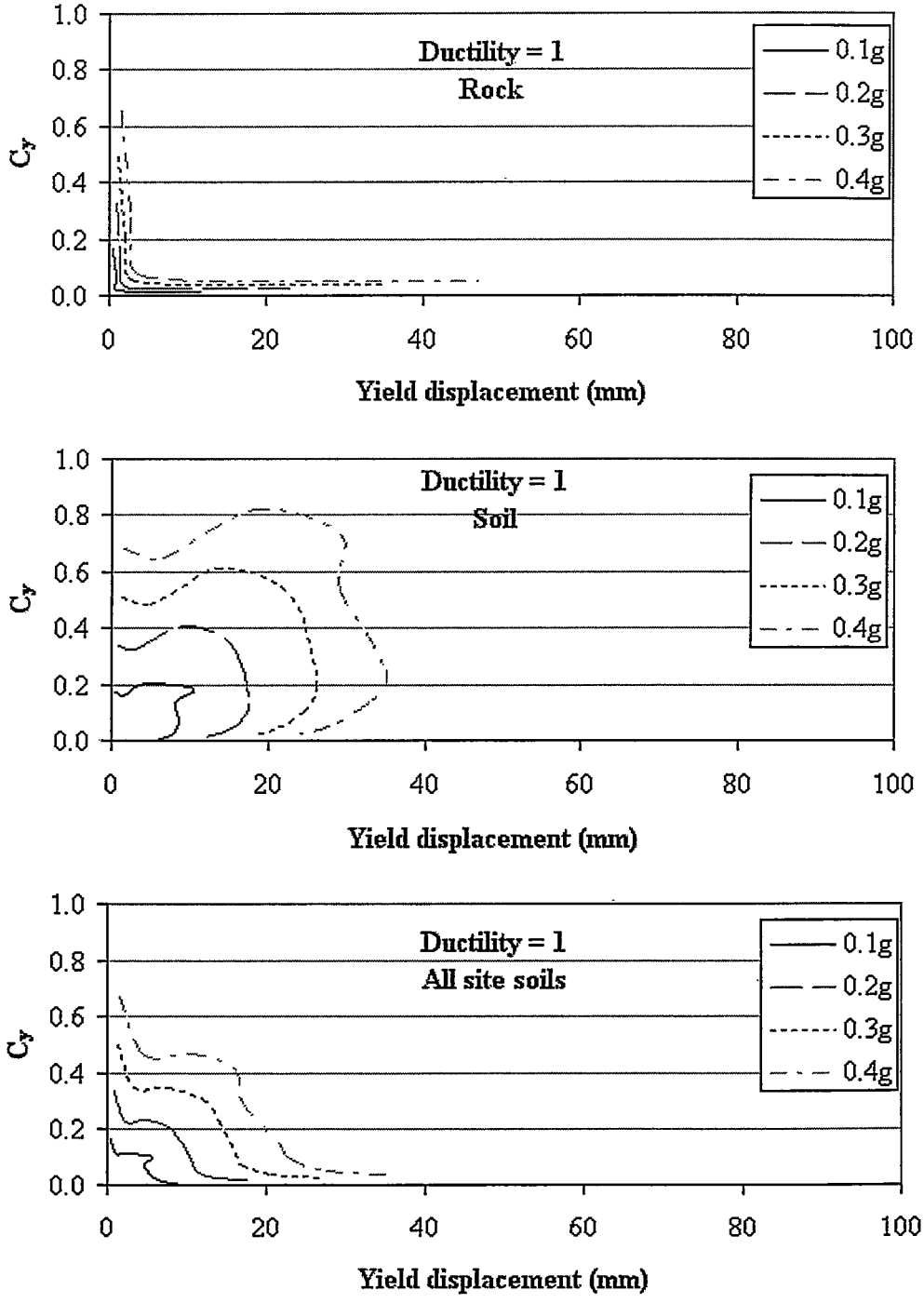

Figure B.21 Yield spectra for NFE with magnitude <6 for ductility level 1

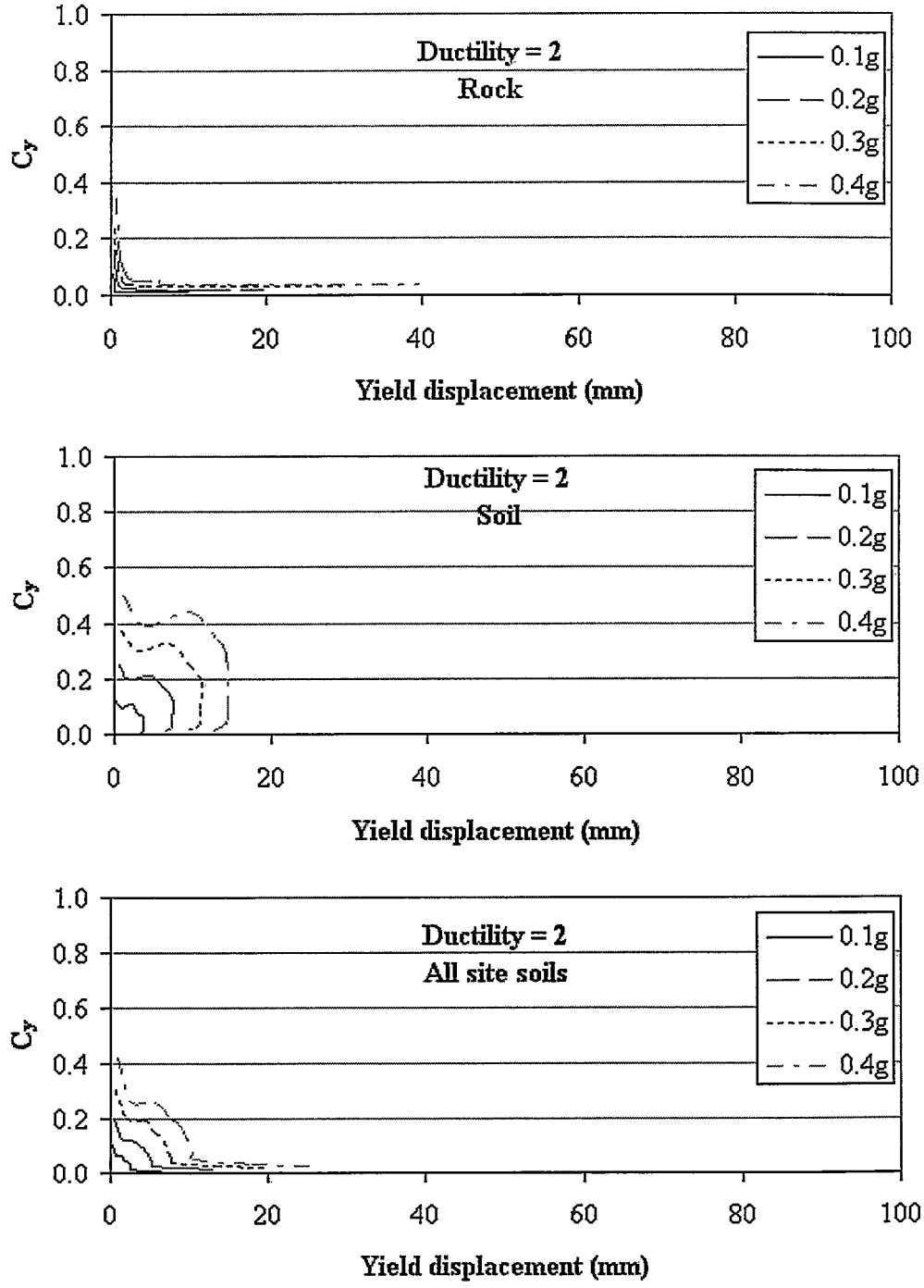

Figure B.22 Yield spectra for NFE with magnitude <6 for ductility level 2

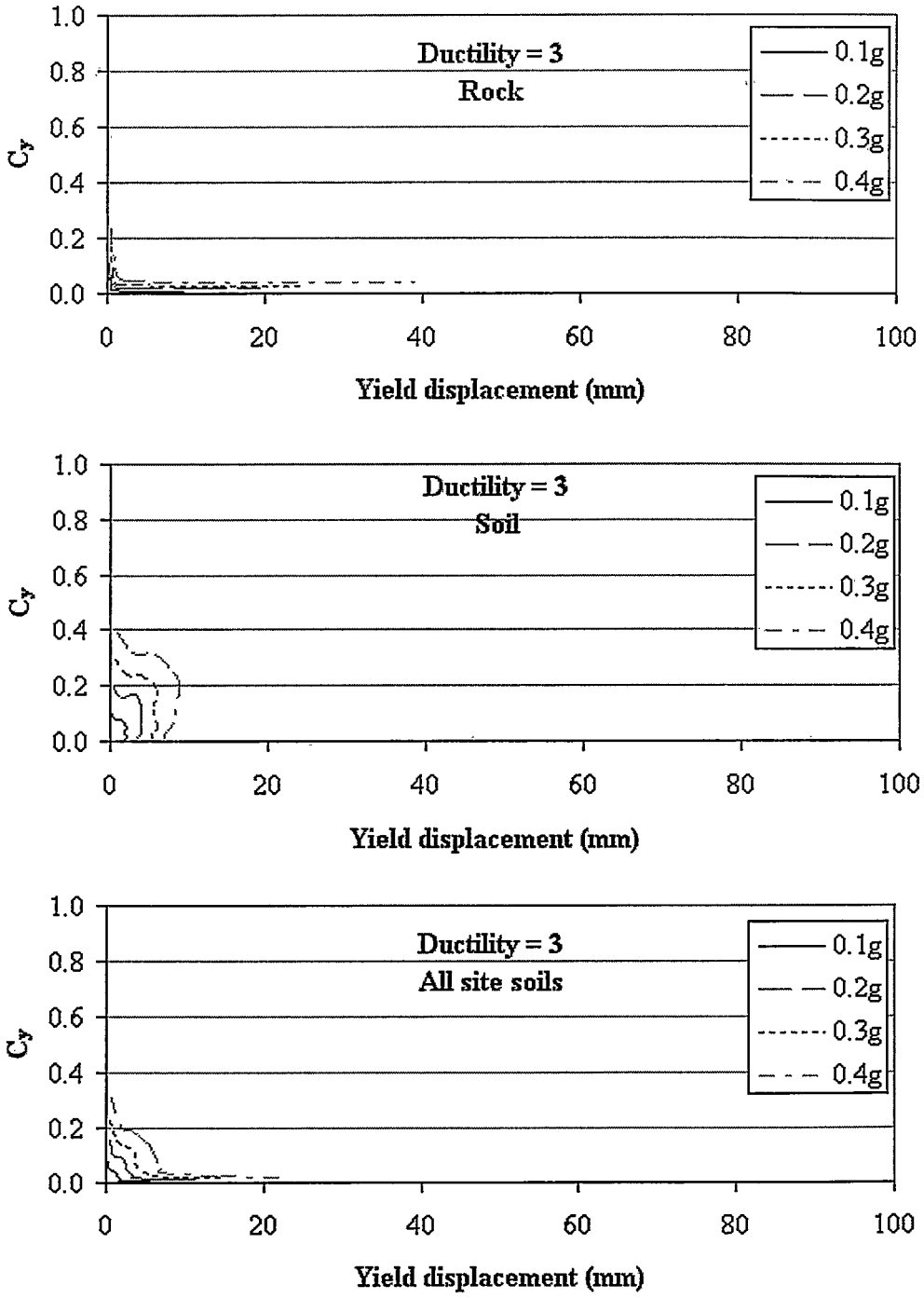

Figure B.23 Yield spectra for NFE with magnitude <6 for ductility level 3

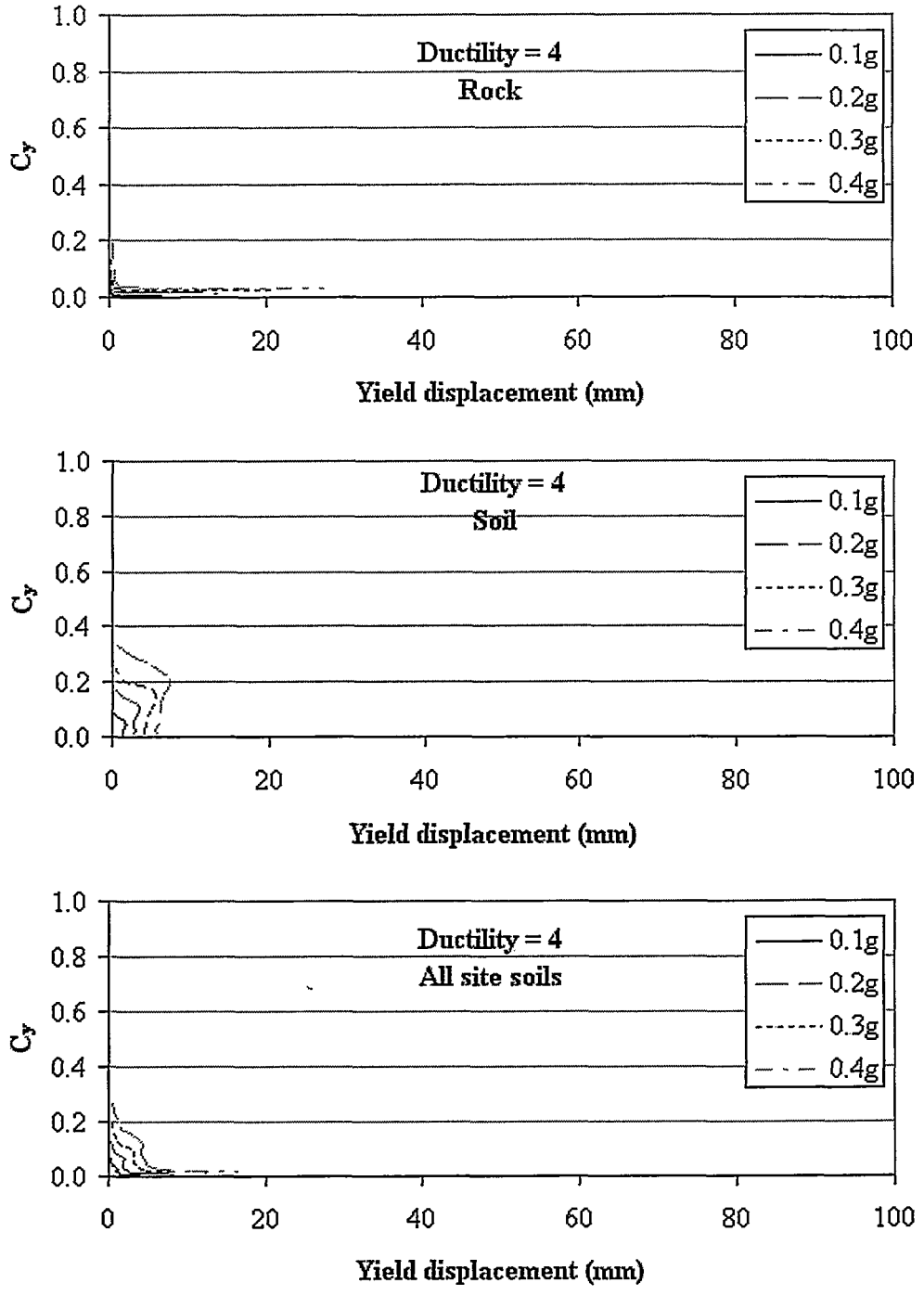

Figure B.24 Yield spectra for NFE with magnitude <6 for ductility level 4

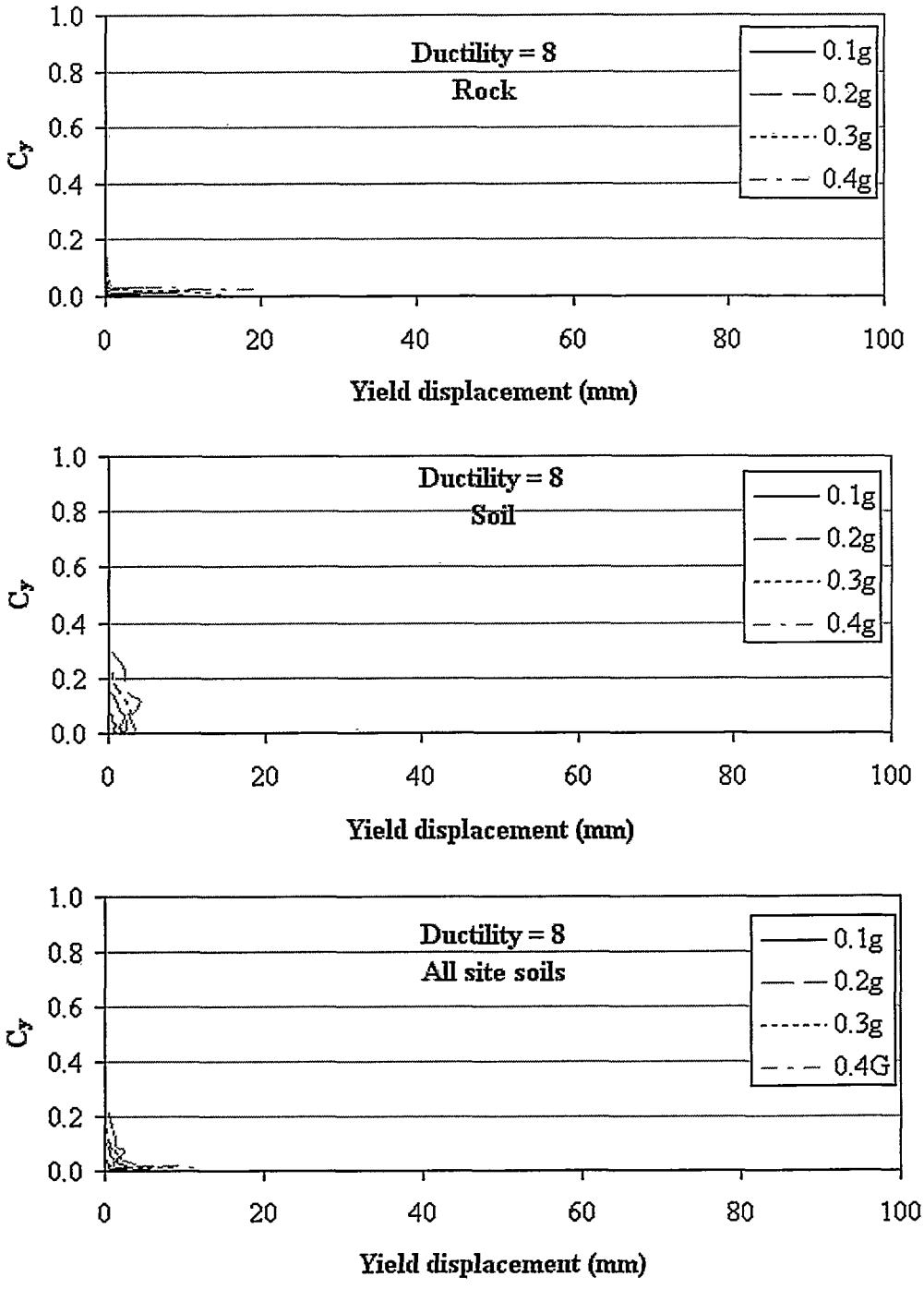

Figure B.25 Yield spectra for NFE with magnitude <6 for ductility level 8

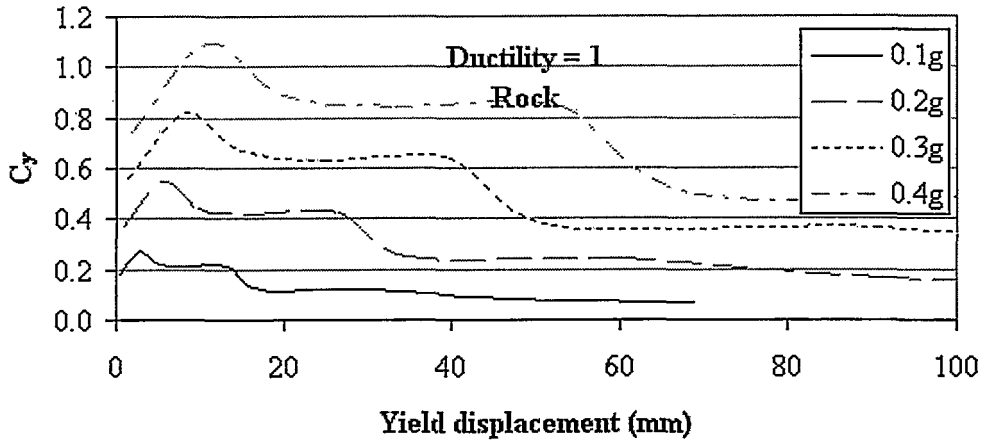

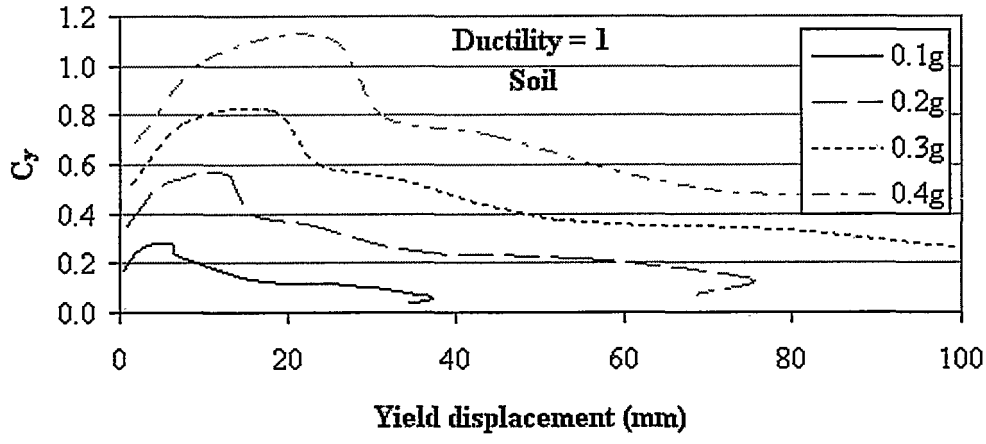

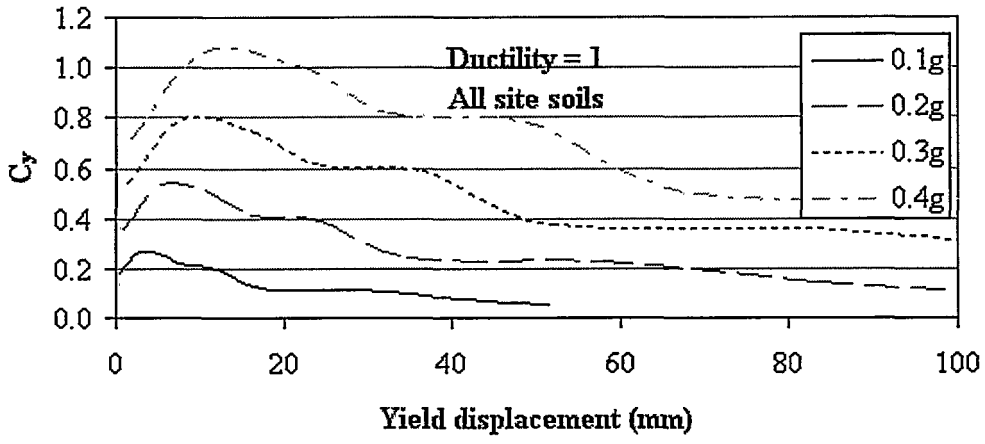

Figure B.26 Yield spectra for FFE for ductility level 1

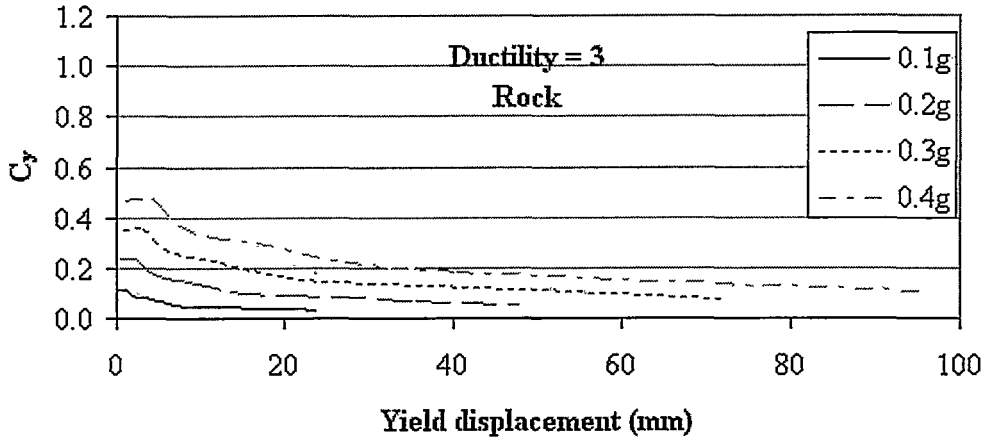

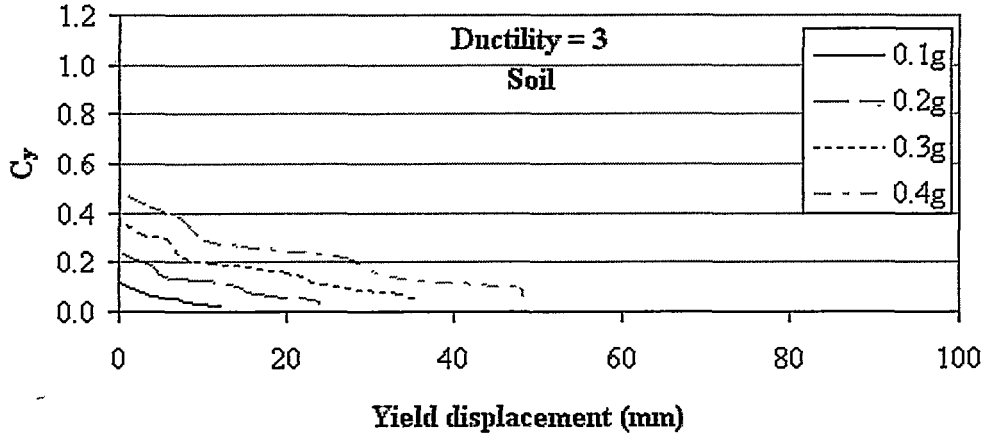

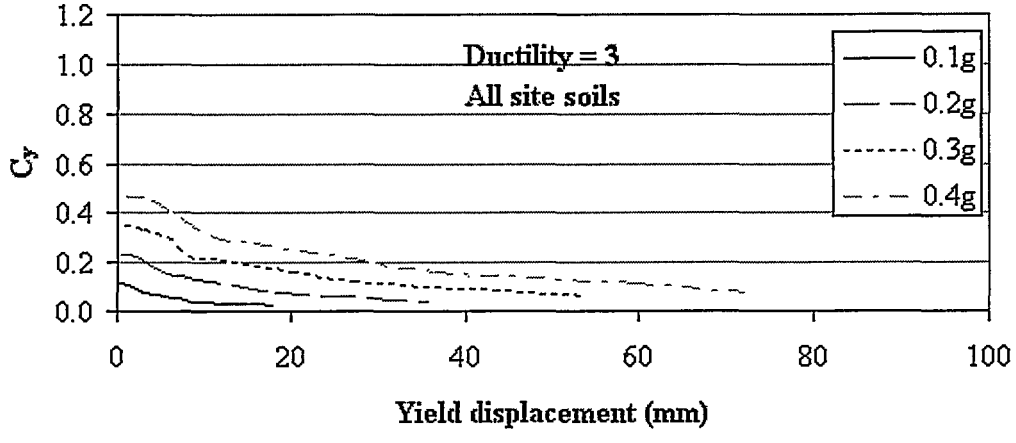

Figure B.28 Yield spectra for FFE for ductility level 3

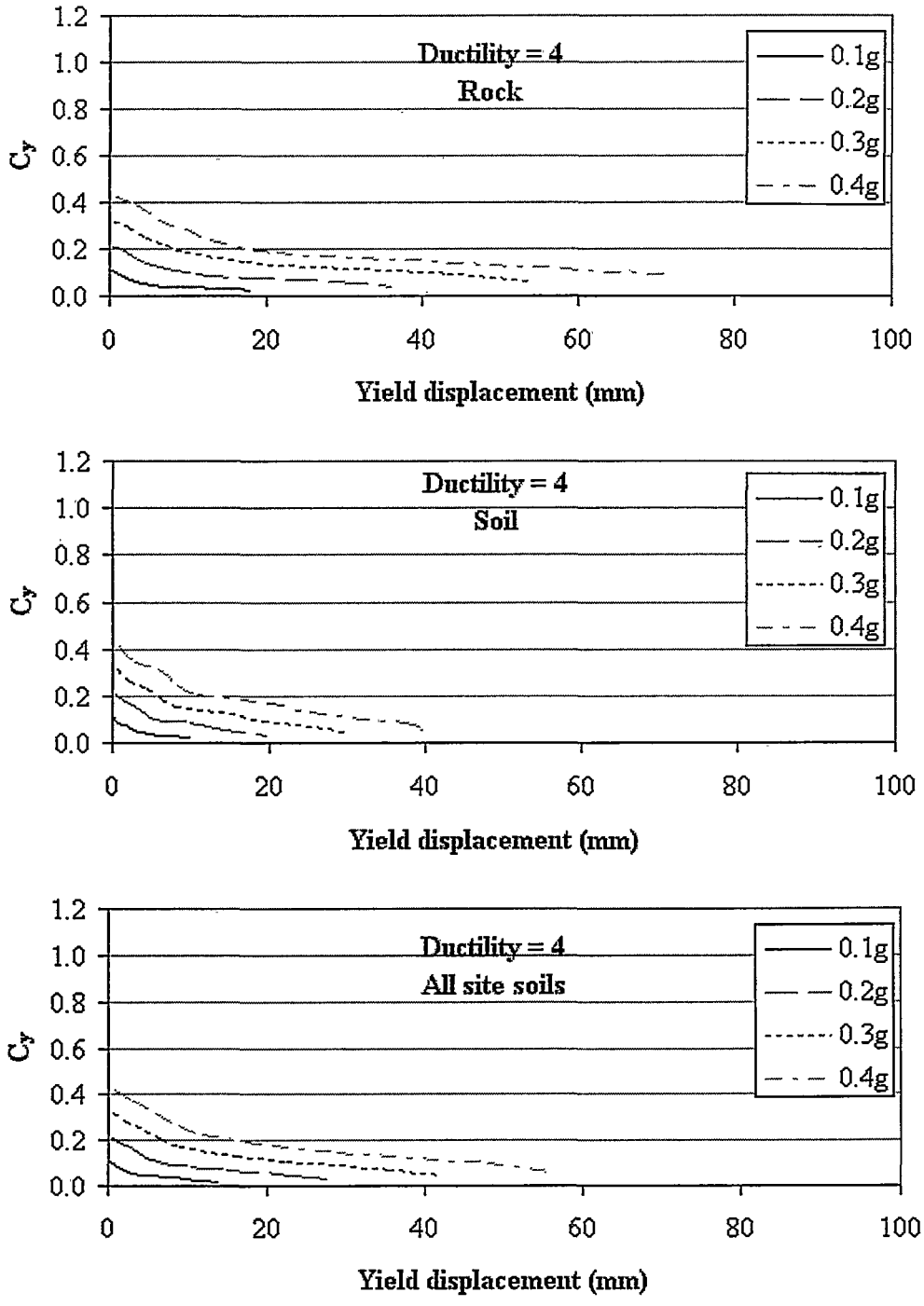

Figure B.29 Yield spectra for FFE for ductility level 4

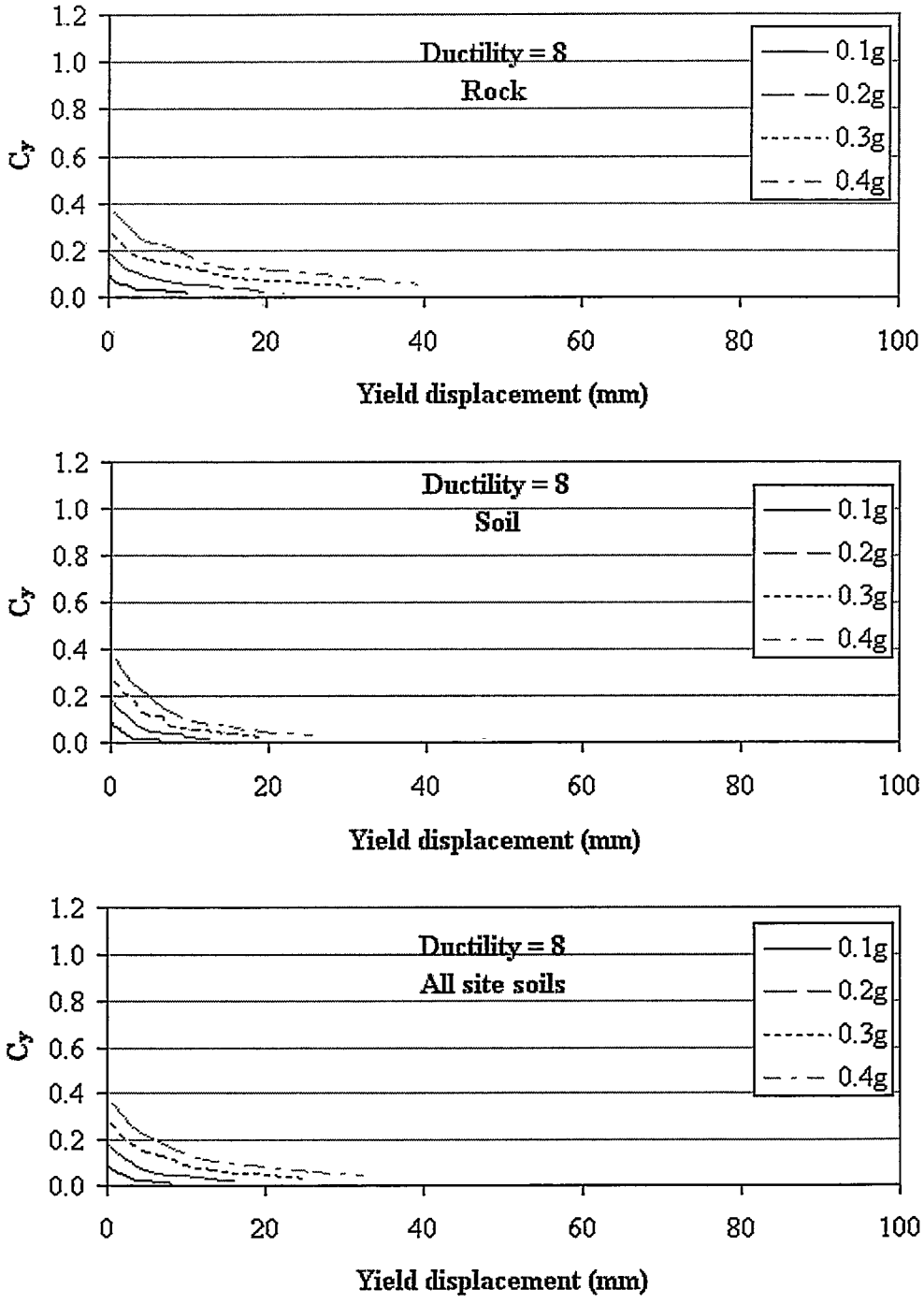

Figure B.30 Yield spectra for FFE for ductility level 8